CHALMERS

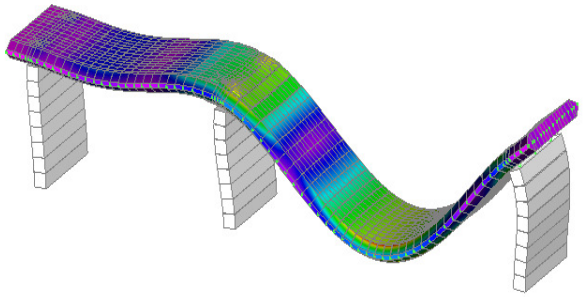

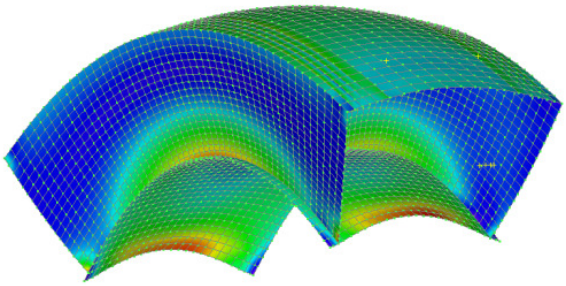

# Concrete Bridge Design with FEM

## A comparative analysis between 3D shell and 2D frame models

*Master of Science Thesis in the Master's Programme Structural Engineering and Building Performance Design*


ADNAN JUKIC
KRISTOFFER EKFELDT

Department of Civil and Environmental Engineering
*Division of Structural Engineering*
*Concrete Structures*
CHALMERS UNIVERSITY OF TECHNOLOGY
Göteborg, Sweden 2012


Master's Thesis 2012:15

MASTER'S THESIS 2012:15

# Concrete Bridge Design with FEM

## A comparative analysis between 3D shell and 2D frame models

*Master of Science Thesis in the Master's Programme Structural Engineering and Building Performance Design*

ADNAN JUKIC

KRISTOFFER EKFELDT

Department of Civil and Environmental Engineering
*Division of Structural Engineering*
*Concrete Structures*
CHALMERS UNIVERSITY OF TECHNOLOGY
Göteborg, Sweden 2012

Concrete Bridge Design with FEM
A comparative analysis between 3D shell and 2D frame models

*Master of Science Thesis in the Master's Programme Structural Engineering and Building Performance Design*

ADNAN JUKIC
KRISTOFFER EKFELDT



Examensarbete / Institutionen för Bygg- och Miljöteknik,
Chalmers tekniska högskola 2012:15

Department of Civil and Environmental Engineering
Division of Structural Engineering
Concrete Structures
Chalmers University of Technology
SE-412 96 Göteborg
Sweden
Telephone: + 46 (0)31-772 1000

Cover:
*Figure shows the principal behaviour of a concrete slab frame bridge under thermal action load and a slab bridge loaded with self-weight displayed as deformed.*

Chalmers Reproservice, Göteborg, Sweden 2012

Concrete Bridge Design with FEM

A comparative analysis between 3D shell and 2D frame models

*Master of Science Thesis in the Master's Programme Structural Engineering and Building Performance Design*

ADNAN JUKIC
KRISTOFFER EKFELDT
Department of Civil and Environmental Engineering
Division of Structural Engineering
Concrete Structures
Chalmers University of Technology

ABSTRACT

For many years, design of concrete bridge structures has been based on two-dimensional (2D) frame analysis. The results from longitudinal frame analysis were assumed to be valid over the entire bridge width except for some adjustments in the support regions. Nevertheless, proper designed structures often remain uncracked under service conditions. For the new generation of design codes, Eurocodes, the Swedish transport administration demands a new approach for analysis of bridge structures. In the new approach, the overall structural behavior shall be accounted for by, for example by a three-dimensional (3D) finite element (FE) analysis based on shell theory. The 2D frame analysis is no longer an acceptable method for analysis of slab bridges. However, it is not clear if the more rigorous demands are necessary for simple types of slab and slab frame bridges.

The aim of this thesis is therefore to investigate the difference in design results when using 3D analysis based on shell theory and 2D frame analysis based on beam theory. Analysis and comparison of bending moments were performed for two types of bridge structures: slab and slab frame bridges. The two bridges were modeled as 3D shell structures in the general FE software Nastran and in the 2D frame software Strip step 2. Based on the results a comparative analysis was performed and conclusions were drawn concerning the difference in design results. The comparative analysis showed that the 3D shell analysis will lead to larger reinforcement amounts to balance the bending moments for the selected bridge structures. One reason for this is that the geometry and, consequently, also the stiffness of the slab sections varies. Another reason is that the transversal direction is taken into account in design, leading to increased reinforcement amounts in this direction. For the 2D frame analysis, the transversal direction was not taken into account and only a minimum reinforcement amount was provided.

Another objective of the thesis was to evaluate different ways to apply thermal actions in the FE model. It was shown that, in order to obtain realistic membrane forces in the integral abutment walls, the thermal actions need to be applied with a linear variation over the height of the walls.

Finally, a study of the maximum traffic load action was done. An envelope of maximum bending moments in the 3D shell analysis was performed with three different methods. A comparison to the envelope of maximum bending moments obtained from the 2D frame analysis showed no large differences between the 3D shell and the 2D frame analysis.

Key words: Reinforced concrete, Bridge design, FEM, finite element method, 3D shell analysis, 2D frame analysis, thermal actions, Nastran, Strip step 2

Dimensionering av betongbroar med FEM

En jämförande analys mellan 3D skal- och 2D rammodeller)

Examensarbete inom masterprogrammet Structural engineering and building performance design

ADNAN JUKIC KRISTOFFER EKFELDT
Institutionen för bygg- och miljöteknik
Avdelningen för Konstruktionsteknik
Betongbyggnad
Chalmers tekniska högskola

## SAMMANFATTNING

Under många år har dimensionering av broar varit baserad på tvådimensionell (2D) ramanalys. Resultaten från den longitudinella ramanalysen ansågs vara giltigaöver hela brobredden med undantag för vissa justeringar i stödregionerna. Trots detta förblev korrekt utformade konstruktioner ospruckna i bruksstadiet. För den nya generationen dimensioneringsbestämmelser, Eurokoderna, krävertrafikverket ett nytt tillvägagångsätt för analys av brokonstruktioner. Med det nya tillvägagångsättet skallkonstruktionens övergripande beteende beaktas genom till exempel en tredimensionell (3D) finita element analys (FE analys), baserad på skalteori. Den tvådimensionella ramanalysen anses inte länge vara en acceptabel metod för analys av plattbroar. Trots detta är det oklart om de mer rigorösa kraven är nödvändiga för enklare typer av platt- och plattrambroar.

Syftet med detta examensarbete är därför att undersöka skillnaden i resultat vid tillämpning av skalteoribaserad 3D-analys och balkteoribaserad 2D ramanalys. Analys och jämförelse av böjande moment genomfördes för två typer av brokonstruktioner: platt- och plattrambroar. De två broarna modellerades som 3D skalmodeller med det generella FE-programmet Nastran och som 2D rammodeller med programmet Strip step 2.

Baserat på resultaten utfördes en jämförande analys och slutsatser drogs rörande skillnaden mellan resultaten. Den jämförande analysen visade att 3D-analysen leder till en större armeringsmängd för att balansera det böjandemomentet för de utvärderade brokonstruktionerna. En anledning till detta är att geometrin och följaktligen också styvheten hos brotvärsnittet varierar. En annan anledning är att den tvärgående riktningen är med i modellen i 3D-analysen vilket leder till ett ökat armeringsbehov i denna riktning. Vid 2D-ramanalysen var inte den tvärgående riktningen med i modellen utan minimiarmeringsmängderhar använts.

Ytterligareett syfte med examensarbetet var att utvärdera olika sätt att applicera temperaturlaster i FE-modellen. Det visade sig att, för att uppnå realistiska membrankrafter i rambenen skall temperaturlasterna appliceras med en linjär variation över höjden av rambenen.

Slutligen utfördes en studie av maximal trafiklasteffekt. En envelop av maximala böjmoment beräknades med tre olika metoder för 3D-analysen. En jämförelse mellan dessa och motsvarande envelop beräknad med 2D-ramanalys, visade inga stora skillnader mellan 3D- och 2D-analyserna.

Nyckelord: Armerad betong, broar, dimensionering, FEM, finita element metoden, 3D skalanalys, 2D ramalalys, temperaturlaster, Nastran, Strip step 2

# Contents

# Preface

In this thesis, an investigation concerning the difference in design results from 3D shell analysis and 2D frame analysis for concrete bridges was performed. Special attention has been put on the comparison of the bending moments from the different analyses. In addition, two sub- tasks were performed concerning thermal action application in FE 3D modeling and determination of maximum traffic load action. This master´s thesis was performed between September 2011 and March 2012 at the Department of Civil and Environmental Engineering at Chalmers University of Technology, Göteborg, Sweden. The project was initiated by Sweco Infrastructure AB where the work also was carried out.

This thesis could not have been performed without the help from certain individuals and we would therefore like to thank everyone who was involved. Firstly, special thanks go to Sweco Infrastructure AB who provided with resources and a good working environment. Here we had a great support from out supervisor; the structural engineer M.Sc. Hristo Sokolov who at all times shared his knowledge with us.

Special appreciation is directed to our supervisor and examiner Associate Professor Mario Plos at the Department of Civil and Environmental Engineering at Chalmers, for his courtesy to advise and improve our performance.

Furthermore, we would like to thank our opponent Poja Shams Hakimi for a good response throughout the work and for an inspiring discussion at the presentation occasion. At last we would like to thank the persons close to us for their support and that they have put up with us during our work.

Göteborg March 2012

Adnan Jukic and Kristoffer Ekfeldt

# Notations

In the notation table, all variables occurring in the report are listed alphabetically.

**Roman upper case letters**

| | |
|---|---|
| $E$ | Young´s modulus |
| $G$ | Shear modulus |

**Roman lower case letters**

| | |
|---|---|
| $b$ | Width of a slab |
| $h$ | Height of a slab |
| $l$ | Length of a slab |
| $l_1$ | Length to support 1 in slab bridge |
| $l_2$ | Length to support 2 in slab bridge |
| $l_3$ | Length to support 3 in slab bridge |
| $m_x$ | Bending moment in a slab around the local x-axis |
| $m_{x.pos}$ | Positive reinforcement moment for bending around the local x-axis |
| $m_{x.neg}$ | Negative reinforcement moment for bending around the local x-axis |
| $m_y$ | Bending moment in a slab around the local y-axis |
| $m_{y.pos}$ | Positive reinforcement moment for bending around the local y-axis |
| $m_{y.neg}$ | Negative reinforcement moment for bending around the local y-axis |
| $m_{xy}$ | Torsional moment in a slab with respect to the local x- and y-axis |
| $q$ | Uniformly distributed load |
| $t$ | Thickness of a slab |
| $u_1$ | Factor with respect to practical considerations, usually set = 1 |
| $u_2$ | Factor with respect to practical considerations, usually set = 1 |
| $v_x$ | Shear force in z-direction acting on a slab cross- section |
| $v_y$ | Shear force in z-direction acting on a slab cross- section |
| $w$ | Width of carriageway |
| $w_1$ | Width of notional lane |
| $x$ | Coordinate in x-direction |
| $y$ | Coordinate in y-direction |
| $z$ | Coordinate in z-direction |

**Greek letters**

| | |
|---|---|
| $\varepsilon$ | Strain |
| $\delta$ | Displacement in vertical direction of slab |
| $\sigma_z$ | Stress in vertical direction of slab |
| $\tau$ | Shear stress |
| ν | Possion´s ratio |

**Abbreviations**

| | |
|---|---|
| *EC* | Eurocode |
| *FE* | Finite Element |
| *FEM* | Finite Element Method |
| HGV | Heavy goods vehicle |

# 1 Introduction

## 1.1 Background

During many years the established engineering practice in Sweden for analysis of concrete bridge structures, comprising slab frame bridges or superstructures of flat slabs, was based on equivalent frame analysis. Bridge structures were divided longitudinally into frames with a width of 1.0m and then analyzed as 2D structures with loads adjusted to the 1.0m width. The obtained results were then assumed to be valid over the entire bridge width with some adjustments over the edge regions. This method of analysis, though non-admitted, is more or less based on theory of plasticity. Nevertheless, in reality, structures, when proper designed, often proved to remain uncracked under service conditions even if the design was carried out according to the above mentioned method.

With introduction of the new generation of design codes, Eurocodes, the Swedish transport administration demands a new approach for analysis of bridge structures where the overall structural behavior shall be accounted for. Furthermore, for bridges with slab superstructures, the Swedish transport administration recommends an analysis based on plate or shell theory. The equivalent frame analysis according to the Swedish transport administration, not anymore an acceptable method for analysis of slab bridges. However the new demands require more comprehensive analysis and it can be questioned if these are motivated for simpler cases. Furthermore, the more comprehensive analyses in combination with design for maximum load effects in all sections may lead to less economical design solutions.

However, it is not clear if the more rigorous demands are necessary for all types of structures where they are demanded. It is also unclear if the more rigorous demands will lead to less economical solutions. Due to these reasons a comparative study was required. The comparative study should focus on analysis of typical bridge structures with the finite element method (FEM) and shell theory and 2D equivalent frame analysis.

## 1.2 Aim of the thesis

The aim of this master thesis was to investigate the difference in design results when using 3D analysis based on shell theory and 2D frame analysis based on beam theory. Analysis and comparison of results were performed for two types of bridge structures, a slab frame concrete bridge and a concrete slab bridge. Structural modeling, loads and load combinations were carried out according to the relevant parts of Eurocode with nationally determined parameters according to Swedish transport administration. Further, a thermal action study was performed in order to evaluate the most suitable way to apply thermal actions in 3D shell FE analysis. Finally, an evaluation of envelopes for maximum load actions was carried out in order to compare the design for one critical load position with design for all possible load positions.

## 1.3 Method and limitations

To reach the aims of the thesis the following methodology was used:

- A literature study was performed on design of concrete structures based on linear analysis with 2D frame and 3D shell theory by using FEM and frame

analysis softwares. The study focused on advantages and disadvantages of the different methods.

- Comparative analyses was performed for a concrete slab bridge and a slab frame concrete bridge with 3D shell and 2D frame models.

- Based on the results from the analyses conclusions was drawn concerning when it is motivated to use the 3D shell analysis instead of 2D frame analysis for the bridge types studied.

- Comparison of design results, both for one critical load position and for all load combinations with all load position was made using envelopes of maximum load actions. This was done for 2D and 3D models for bending moments.

- A thermal action study was performed in order to evaluate the most suitable way to apply thermal actions in a 3D shell FE analysis. Three different load applicationswas evaluated and the evaluation formsa basis for the selection of load application in the 3D shell FE models.

The 3D FE-software used in the project is NX Nastran (2008).For 2D frame analysis the software strip step 2, Ingengöresfirma Åke Bengtsson (2004), was used. Booth programs are commonly used for bridge modeling at Sweco, the consulting company of civil engineering where this study was carried out.

## 1.4 Outline

To get a better overview of this thesis, a short description of the chapters is presented here.

1. **Introduction:** Background information about the issues treated in this thesis are presented together with aim, method and limitations.
2. **Concrete bridge design with FEM:** Design methods for concrete bridges are schematically treated. Some theoretical explanations about the finite element process and finite element modelling is presented. Also, sectional force and moment distribution and redistribution in concrete structures based on 2D frame- and 3D shell analysis is treated.
3. **FE bridge models:** Geometry, support conditions and convergence studies for the 3D shell models of the case study bridges, a slab bridge and a slab frame bridge, are illustrated and explained.
4. **Loads**: Choices and assumptions for the loads used in the analysis are presented.
5. **Investigations:** The studies made with the case study bridges are presented and the results and discussions for the investigated areas are presented in this chapter.
6. **Conclusions:** The conclusions of the study is presented in this chapter

   More extensive calculations and reporting of results are presented in the appendices.

# 2 Concrete Bridge Design with FEM

This chapter treats design methods as well as, force and moment distribution in bridge structures. The chapter also covers an underlying theory of FE modeling and FE modeling of slabs. The chapter is intended to give a background and a greater understanding of the analysis in the forthcoming chapters.

## 2.1 Design methods

Analysis of bridge structures is often performed using FE analysis. The analysis is mainly done with 2D or 3D beam or 3D shell elements. The analysis is usually linear elastic. Nonlinear analyses and analysis with continuum elements are seldom used due to massive work efforts, Davidson (2003).

### 2.1.1 Design according to Eurocode

According to Eurocode 2, CEN (2001) there are four approaches to determine the force distribution in a structure:

- Linear elastic analysis
- Linear elastic analysis with limited redistribution
- Plastic analysis
- Non-linear analysis

For design in serviceability limit state (SLS), linear elastic analysis or non-linear analysis should be used. Eurocode 2, CEN (2001) also state that the geometry and the properties of each part of the structure should be taken into account in the design. According to Engström (2007) cracking can have significant effects on the structure in the service state and can only be analyzed by non-linear analysis.

A linear elastic analysis is valid if the concrete structure is un-cracked or in ultimate limit state (ULS) when the assumed moment distribution is reached after plastic redistribution, Engström (2007). It is however not valid for analysis of a cracked section in service state. A common assumption according to Engström (2007) is that the difference between the real moment distribution in SLS and the distribution from linear elastic analysis is neglectable. Nevertheless, for a continuous beam an underestimation of 25 % of the negative moment at interior support can occur. Hence, non-linear analysis gives the most reliable analysis of concrete structures, which allow for the possibility to follow the redistribution in service state as well as in ultimate state, Engström (2007).

### 2.1.2 Bridge Structures

Most of the existing bridges in Sweden today have been designed using 2D frame analysis. According to earlier Swedish design codes, bridges should be design according to elastic force and moment distribution, except for accident loads where the lower bound theory of plasticity could be used. The main reason for this is to avoid choices of moment and force distributions that require too large plastic redistribution. The elastic theoretical distribution is considered sufficient for design of reinforcement and to avoid too large cracks. A distribution using strictly linear elastic analysis gives an uneconomical solution and is sometimes a practical impossible

solution basis for reinforcement design. For concentrated loads and values extracted over supports, the result can give high peak values which has to be interpreted, Davidson (2003).

The requirements on bridge design in Sweden are stated in the "Technical Requirements for Bridges" (TK Bro) issued by the Swedish transport administration, Vägverket(2009). According to these requirements the design of bridge structures in Sweden should be carried out according to relevant parts of Eurocode 2, CEN (2001)taking into account all nationally determined parameters stated in BVS2011:10 (2009) and TRVFS 2011:12,(2009)as well as the client requirements stated in TK Bro. As a manual for bridge design the Swedish transport administration has issued also the "Technical advises for Bridges" TR Bro, Vägverket(2009). This manual is however not a mandatory document but a guideline which need not to be followed.

TK Bro states translated from Swedish that *"The structural model for system analysis shall with respect to loads, geometry and deformation properties describe the overall response of the structure"*.

In this TR Bro is further intrepreted as: *"A global three dimensional structural model can be considered to describe the overall response of the structures. Two-dimensional structural models do not meet this criterion, except for a structure that with respect to geometry, loads and design conditions have a clear two-dimensional response."*

Furthermore:*"A structural model consisting of three-dimensional beam or truss members cannot be expected to give a good representation of a structure in which the essential elements consist of slabs and walls."*

This has by the Swedish structural engineers designing bridges been interpreted as, more or less, a requirement to perform a 3D shell FEM analysis for basically all bridges, since slab elements occur in almost all bridges

## 2.2 Force and moment distribution in concrete structures

Force and moment distributions in a concrete slab, over the supports and in the span, are dependent on the variations of stiffness across and between the slab cross-sections. A common assumption is that the influence of reinforcement in the uncracked state is small but according to Engström (2007) more than a 20 % increase of stiffness of the section can be gained from the reinforcement for concrete structures. This means that the reinforcement cannot always be disregarded, Engström (2007). A stiffer region attracts moments and forces and, due to this, it will crack before the less stiff regions.

When the region cracks it loses stiffness and the forces and moments will be redistributed to stiffer regions, Engström (2011). The stiffness of a cracked concrete section is mainly dependent on the amount of reinforcement in the section, Davidson (2003). In cracked reinforced concrete, the local effects at the crack result in a drastically decrease of stiffness. The local cracks also affect the global distribution of forces and moments as one or some critical sections can affect the stiffness of the whole section. This means that a fully cracked structure can behave differently compared to an un-cracked structure, Engström (2007).

In SLS, the design load is often significantly higher than the crack load and the whole section is often regarded as cracked in bending. Since the position of critical section of the structure depends on the force and moment distribution, the reinforcement distribution is of great importance. In linear elastic analysis, the moment and force

distribution is only dependent on the concrete cross section. These analyses disregard the redistribution due to cracking and reinforcement, Engström (2003).

During further increase of the load up to the ULS, the material response will become non-linear for concrete in compression and yielding will start in the reinforcement. The stiffer, heavily reinforced areas start to yield before the ultimate limit state is reached. On the other hand, the less stiff sections attracts less of the forces and moments and will therefore start to yield later. The load can still be increased since the reinforcement yields, which leads to increase of deformation. In other words, a plastic redistribution takes place with yielding reinforcement and eventually crushing of concrete. The plastic redistribution continues until the ultimate limit state is reached and the structure collapses. In the ultimate limit state, the force and moment distribution will become equivalent to the linear elastic distribution. This is due to the fact that the moment in a cross-section does not exceed the posted capacity and that it was designed for the same linear distribution, Engström (2003).

According to these facts, reinforced concrete slab structures have a plastic redistribution both in transverse and longitudinal direction even if it is designed for a linear elastic distribution. Design of reinforcement is done with linear elastic analysis with regard to plastic theory principles. In other words, the force and moment distribution are calculated with elastic theory, but, the reinforcement is designed taking into account the plastic material behavior. This requires that the critical cross-sections are not over reinforced. It is important that the reinforcement can handle the forces and moment from a simplified calculation method, Engström (2003).

As earlier stated, concrete structural behavior varies with increasing load due to cracking of concrete, yielding of reinforcement and other non-linear material response. However, the concrete structures will also be affected by other factors than then the external load. For example prestressing, creep, shrinkage, temperature and support settlements will influence the moment and force distribution, Engström (2007).

## 2.3 Finite element modeling and analysis

When performing modeling and analysis with the finite element method (FEM) it is essential to understand the underlying theory, Blaauwendraad (2010). In order to comprehend the examinations and comparisons made in this thesis, it is necessary to have a general understanding of FEM and how it can be used for design of concrete structures. This chapter is intended to give an overview of this area and to describe the FEM modeling process.

### 2.3.1 Background

The finite element method (FEM) is a numerical method which can be used to solve virtually all physical problems. The advantage with FEM is that it allows systematical and accurate calculations on all types of structures. In recent years structural engineers have to a greater extent started using linear elastic FE analysis for structural analysis of bridges. Shell elements are mainly used, if necessary in combination with beam elements. In other industries, shell and volume elements has been used for decades and has dramatically changed the design and product development process.

3D FE analysis gives a more detailed and geometrically more correct distribution of forces and moment in comparison to the traditional 2D frame analysis, Davidson (2003). However, to be able to benefit from the advantages of the third dimension, an accurate analysis is required. The analysis demands knowledge and the results need to be properly evaluated.

Rombach (2004) states that today, graphical input user-friendly software makes it fairly straightforward to produce three-dimensional finite element models with several thousand degrees of freedom. Furthermore, huge structures can be analyzed with a simple computer. This has led to an increased use of finite element analysis. Nevertheless, incorrect application of the method has also increased. It occurs that engineers believe that expensive computer software is free from errors, but this is more or less never the case. It should also be kept in mind that the finite element method is a numerical method based on numerous assumptions and simplifications.

Reinforced concrete is a complex nonlinear material and is very time consuming to analyze in a nonlinear method. This is one of the main reasons why elastic analysis is often chosen for the material modeling. The model disregards the reduction and redistribution of stiffness as a result of cracking of the concrete and yielding of the reinforcement. However, an engineer does not have the time or the experimental data to verify a complicated non-linear analysis. Furthermore, the aim of the engineer is often not to find the correct response of the structure; it is rather to find a safe and economical design for the structure, Rombach (2004).

### 2.3.2 The FE modeling process

In this subchapter, the FE modeling and analysis process is divided into six basic theory steps. The section describes the accuracy and restrictions for each step. The description of FE modeling process below is mainly based on Samuelsson & Wiberg (1998).

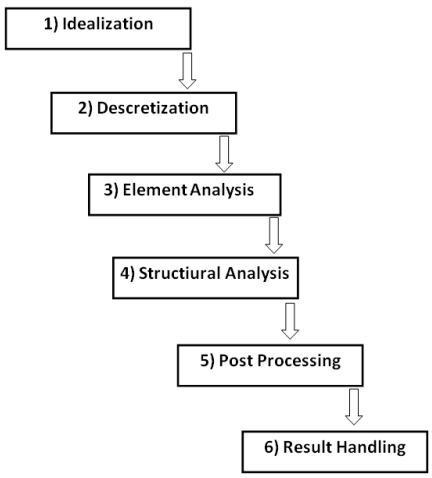


*Figure 2.1- Illustration of the different steps for how to obtain a FE model. Adapted from Samuelsson & Wiberg (1998).*

#### 2.3.2.1 Idealization (Step 1)

In the first step of FE analysis an idealization and simplification of the real structure is done by representing it with a structural model, for example by a 3D Shell model. The model includes geometry, boundary conditions, loads etc. In design of concrete structures it is commonly assumed that the material is linear elastic. Boundary conditions at supports are often simplified as being 100% fixed or not fixed at all even though in reality it is somewhere in-between. In some situations it is important to include the support stiffness to give a good interpretation of reality, Rombach (2004). The designer should have in mind that the interpretation of the reality gives rise to a variety of choices and selections. This puts high demands on the structural engineer since wrong assumptions have a large impact on the resulting outcome.

Two theories that are often used for analyzing linear plates are the Kirchhoff-Germain and the Reissner-Mindlin theories. Both theories can be used for moderate thin plates, where the deflection is less than half of the plate's thickness. According to Blaauwendraad (2010), thin plates should preferably be calculated with Kirchhoff theory. Similar result can be achieved with Mindlin theory but a much finer mesh is required. The required element size in case of Krichhoff theory should not be larger than approximately the plate thickness. However, for very thick plates, the Mindlin theory must be used. For the Mindlin theory, the width of the edge zone is comparable to the thickness of the plate; in this edge area a sufficiently fine mesh should be applied, Blaauwendraad (2010).

In slab structures modeled with linear plates, discontinuity regions may appear under point loads and at pin supports. According to plate theory a point load is acting in a single point in which the shear force and bending moment approaches infinity, Rombach (2004). One way to overcome this is to include the load or support pressure distribution in the model.

#### 2.3.2.2 Discretization (Step 2)

In the second step, the structural model is divided into finite elements. The results, primarily in integration points, depend on the element size, the type and shape, and how the load is applied. Consequently a denser element mesh and less distorted elements lead to a more correct answer.

Higher order elements often lead to a more correct result, Ottosen & Petersson (1992). However, quadric shell and plate elements can lead to a large variation in sectional forces at point loads and pin supports. Shell elements differ from plate element due to that shell element can be curved and can carry both membrane and bending forces , Michigan Tech (2011). Shell element needs larger computer capacity. A lower order element can in this case be favorable , even if the element size need to be smaller.

#### 2.3.2.3 Element Analysis (Step 3)

Element approximation and element stiffness is calculated in this step. The internal element stiffness in the element analysis is approximated with a base function. In FE-analysis, a numerical integration is used to get an accurate integration over the chosen integration points in the elements. This integration is an approximation even if a sufficient amount of integration points is used, due to the fact that integration of rational functions does not give exact solutions, Rombach (2004).

#### 2.3.2.4 Structural Analysis (Step 4)

A calculation of the stiffness matrix is done by paring the single elements´ stiffness matrix with equilibrium conditions and geometry conditions. The equation system can be solved for the whole structure. The computer can only use a certain amount of significant numbers; thereby rounding errors can arise in this step.

#### 2.3.2.5 Post Processing (Step 5)

In this step, the calculations of stress components in all the elements are performed. The stress is calculated in the integration points. These points are generally not situated in the elements nodes, but are situated a distance into the element with for example Gauss integration.

The values in the integration points are the most exact results from the FE analysis. Nevertheless, the results are often showed in the element nodes. The integration point results are extrapolated to the nodes with the element base functions. Generally an element with high order produces a better approximation for a linear elastic analysis, Ottosen & Petersson (1992). Every node is in general connected to more than one element. Due to this, the node result is calculated as a mean value from the single elements contributions. In other words all elements connected to the same node have an effect on the node value. Hence, the results from the post processing as mentioned above are not exact and contains rounding.

#### 2.3.2.6 Result Handling (Step 6)

The results from the FE-analysis has to be further analyzed. This leads to large uncertainties due to considerations of the structure`s real behavior. The analysis is dependent on choices made in Step 1.

For 2D frame analysis the output data is manageable for large models. Due to the increased complexity with 3D shell analysis, it is very hard and sometimes practically impossible to analyze all output data. The use of reviewing all the output from the analysis can also be questioned. Instead a combination of words, numbers and iso colour plots gives a good description of the results, Davidson (2003).

## 2.4 FE modeling of slabs

The definition of a slab is a thin plane spatial surface structure dominantly loaded by forces normal to the plane of the plate, Ottosen. N & Petersson. H (2002). According to Eurocode, a slab is a member for which the minimum panel dimension is not less than five times the overall slab thickness.

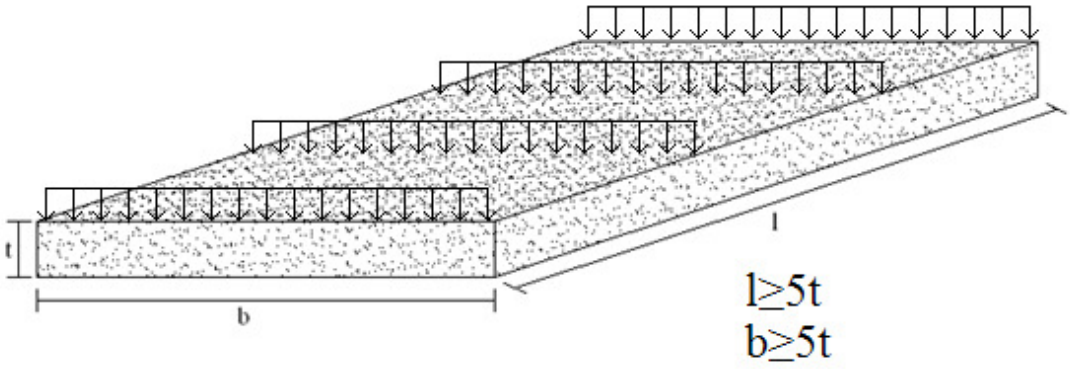


*Figure 2.2- Definition of slab cross-section*

### 2.4.1 General

To be able to understand the mode of action of a slab, a definition of the sectional forces is made. First of all, a co-ordinate system (x, y) is introduced; see Figure 2.3. The bending moment that gives bending around the x- axis is denoted $m_x$ and the bending moment that gives bending around the y- axis $m_y$. The torsional moment that twists the slab is denoted as $m_{xy}$ and the shear forces $v_x$ and $v_y$, Engström (2011). In a shell element there are also membrane forces acting in the plane of the element.

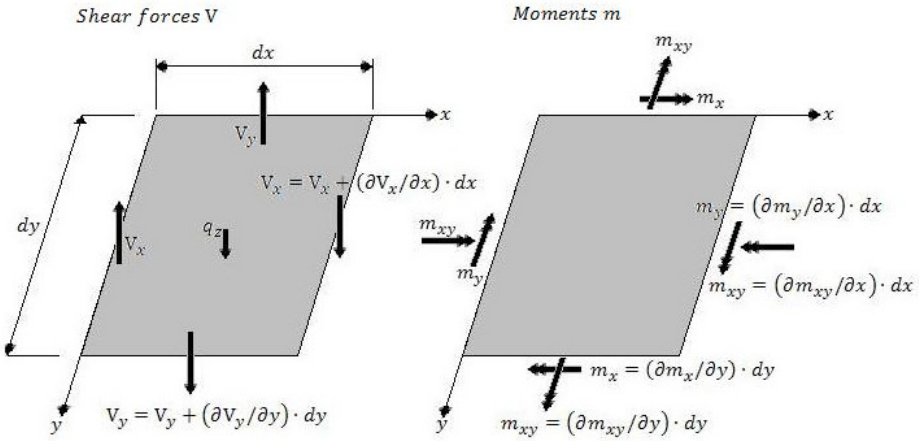


*Figure 2.3- Sectional forces and stresses of a finite plate element*

Some additional assumptions are used together with the definitions. One assumption is that the vertical stress in the slab cross-section $\sigma_z$ is equal to zero. This is considered valid as long as the thickness of the slab t is constant and much smaller than the width, t<<b. Stresses in normal direction can be neglected which means that there are no normal strains in the middle plane. Another assumption is that the displacements in vertical direction are considered to be small, $\delta$<<t. This means that the first order theory can be used. Also, the material is assumed to exhibit a linear strain distribution over the section depth. One further assumption is that the plane sections before loading remain plane after loading (Bernoulli-Euler theory), Rombach (2004).

In FE modeling of slabs, shell elements are often used. In this case, membrane forces are included in the element definition. In this case also horizontal loading can be taken into account. Some of the provided sectional forces from a 3D shell analysis are the

longitudinal- and transversal bending moments $m_x$, $m_y$ and the torsional moment $m_{xy}$. The reinforcement is designed is based on the assumption that the reinforcement in a cracked concrete section cannot resist torsional moments. Instead, the principal moments caused by the elastic moments $m_x$ ,$m_y$ and $m_{xy}$ are resisted by reinforcement moments acting in pure bending in ultimate limit state. The torsional moment will result in increased requirements of both top and bottom reinforcement. Consequently, a positive reinforcement moment and a negative reinforcement moment is derived. The equations for calculating the positive- and negative moments are presented below:

$$m_{x.pos} = m_x + u_1 \cdot |m_{xy}| \quad \text{Eq. (2.1)}$$

$$m_{x.neg} = m_x - u_2 \cdot |m_{xy}| \quad \text{Eq. (2.2)}$$

$$m_{y.pos} = m_y + \frac{1}{u_1} \cdot |m_{xy}| \quad \text{Eq. (2.3)}$$

$$m_{y.neg} = m_y - \frac{1}{u_2} \cdot |m_{xy}| \quad \text{Eq. (2.4)}$$

Here, $u_1$ and $u_2$ are factors that can be chosen with respect to practical considerations, most often they are chosen to 1.

## 2.5 Structural analysis with FEM

This part treats literature recommendations of how to model slab frame bridges and slab bridges in accurate ways. This underlying theory is used as a base for the choices made for the FE-models in this thesis. The first parts about mesh and element types and FE mesh are common for both bridge models.

### 2.5.1 Element types

The choice of element type depends on the requested output. The main element categories are continuum elements, structural elements and special purpose elements. Within each of these categories, there is a range of various types of elements. Structural elements are elements based on e.g. beam and shell theory. In contrast to continuum elements they have rotational degrees of freedom in addition to the translational. Furthermore, their response can be expressed in terms of cross-sectional forces and moments. Due to the aim of the thesis, it is appropriate to use structural elements, more specifically shell elements

### 2.5.2 FE mesh

Proper meshing is essential for obtaining accurate results. This has to do with how finite element programs treat data and calculate the sectional forces. It is clear that for a given type of element, the accuracy increases with decreasing element size. In general, one could say that a denser mesh should be used in regions where the results of the analysis changes rapidly like over the supports, Ottosen. N & Petersson. H (2002).Depending on how the support conditions in the FE model are modeled, singularity problems can be obtained over the supports. In this case, an increase of mesh density will lead to that the values will approach infinity. With triangular elements a denser mesh is needed in order to obtain a more accurate result. Distorted elements also give large errors in the results should be avoided. If distorted elements

still need to be used locally a compensation for the error can be made by a denser mesh, within certain limits.

A common perception is that a good mesh is a uniform mesh with quadratic elements. One reason for this is that the finite elements are derived for this shapes and that this shape will give better approximation of the result in the integration points. Another reason is that finite element programs extrapolate the results calculated in the Gauss points to the nodes. This interpolation becomes more inaccurate for triangular and rectangular elements compared to quadratic elements. In finite element analysis the slab is divided into small elements which are connected by their nodes. By increasing the number of elements and consequently increasing the density of the mesh, a more accurate interpolation of the node displacement is obtained. Increasing the mesh density will lead to a more accurate result, Ottosen. N & Petersson. H (2002). Although it is preferred to aim at a more accurate analysis, it should not be more accurate than required. In chapters 3.1.3 and 3.2.3convergence studies were made to ensure that a further condensing of the mesh for the case study bridges would not lead to a noticeable more accurate result. Despite the benefits with a finite element analysis, one should never underestimate the need of proper understanding of the method. As will be discussed later in this chapter, it is essential that correct modeling of the support conditions is made.

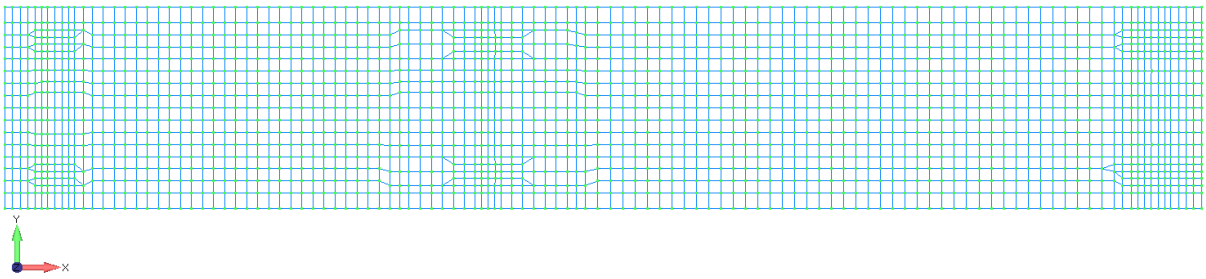


*Figure 2.4- Illustration of the meshing of the slab bridge and also the condensed grid over the support.*

### 2.5.3 Support conditions for slab bridges

Modeling the support conditions for a slab requires a great deal of consideration. Depending on how various restraints are introduced, the properties of the connection will change and the resulting outcome will be considerably influenced. Rombach (2004) recommends to model slab supports as concentrated supports or as line supports. A concentrated support can be interpreted as a pin support on a column, e.g. for a flat slab. The line support can instead be seen as a continuous support of the slab over a wall. A line support can also be discontinuous where the wall ends inside the slab. Both concentrated supports and interrupted line supports causes singularity problems since the shear force and bending moment tend to go to infinity upon mesh refinement, Rombach (2004). However, this is only a numerical problem and the slab should not be designed for the values obtained in the support points. Instead the design should be based on reduced values take in critical sections adjacent to the support points. The following subchapter will present appropriate ways to model support conditions used for the slab bridge and frame slab bridge

#### 2.5.3.1 Pin support of one node

Pin support of one node refers to restraining a single node in the vertical direction; see Figure 2.5 (a). Modeling the support this way will give rise to peak values in the moment distribution which does not exist in reality. A way of treating this phenomena is to use values in adjacent critical sections. Recommendations for this is being developed in a currently ongoing project for the Swedish transport administration.

#### 2.5.3.2 Coupling of nodes

Coupling of nodes builds on the principle that the node in the center of the support is connected to the other nodes representing the support, with infinitely stiff connections. This connection can then be regarded as an infinitely stiff plate connected to the slab, which is allowed to rotate around the center node; see Figure 2.5(b). To couple the nodes provides an advantage of not having to reduce the peak values, in contrast to the pin support of one node.

#### 2.5.3.3 Bedding of the supported elements

This model implies that a spring-system is used to model an elastic support; see Figure 2.5(c). This support condition give a rotation constraint.

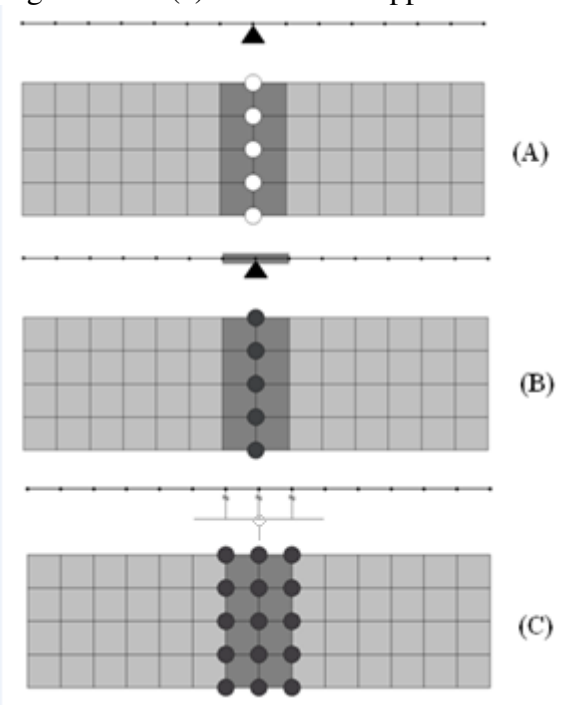


*Figure 2.5- Illustration of the different supports of slabs the meshing of the slab bridge and also the condensed grid over the support., Adapted from Rombach (2004).*

The stiffness of the support and the sub-structure or foundation will also have a great influence on the response in the slab. The supports can be modeled as fully or partially fixed and sometimes the slab can also be free to lift from the support.

The elastic bedding of the foundation should be modeled by individual springs or alternatively with special boundary elements, Rombach (2004). In section 5.1, alternative ways to model the bedding and boundary conditions for the studied slab frame bridge are evaluated more in detail with respect to thermal action.

### 2.5.4 Modeling of frame connections in slab frame bridges

The connection region between an abutment wall and a slab in a slab frame bridge can be modeled similar to a beam-column intersection. Bernoulli hypothesis is assumed for the slab and wall. This means that the model assumes that plane sections remain plane after loading, which in reality is not the case in a disturbed region such as a slab-wall intersection. Due to this, it is only possible to get an approximate value of the cross-sectional forces and moments in the frame corner region, Rombach (2004).

Exact values are often not needed in design calculations. However, a realistic modeling of the stiffness of the frame corners is important because it affects the internal forces and the deformation of the different members. One way to handle this is to add stiff couplings in the corners

Furthermore, it should be considered that the "missing area" in the corner effects the horizontal and vertical loads; see Figure 2.6. The load not accounted for through pressure load on the elements might be necessary to take into account in an alternative way. Another detail is the double contribution of area on the inside of the bridge corner, Rombach (2004).

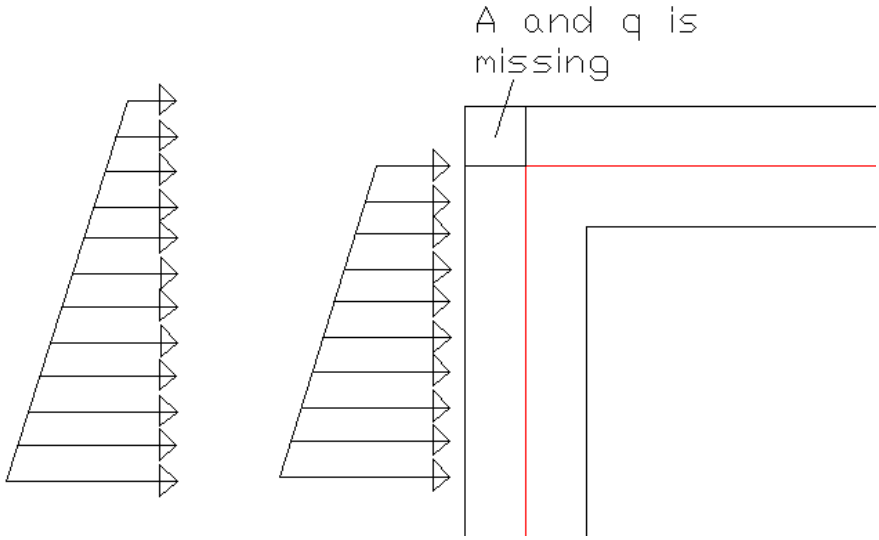


*Figure 2.6 - Detail load problems of framework corner of a frame slab bridge, the red line is the central line. Adapted from Rombach (2004).*

### 2.5.5 Analysis of a one-way slab

An illustrative example to show the difference in results between 2D beam and 3D shell analysis was performed. This was done to show that there is no need for advanced calculations of complex structures to understand that differences between 3D finite element analysis and conventional 2D frame analysis occur. To illustrate how the result can differ between the 2D frame and3D shell analysis, a simple example will be presented. The comparison will be demarcated to bending moment only. The case is based on a simply supported one –way spanning slab on two supports, calculated with 3D shell analysis, a 2D frame analysis and by hand calculations.

The slab was designed according to the following material properties and dimensions:

Concrete C35/45 has been assigned to all sections

| | |
|---|---|
| Young´s modulus | $E = 34\ GPa$ |
| Shear modulus | $G = 14\ GPa$ |
| Poisson´s ratio | $v = 0.2$ |
| Length | $l = 4\ m$ |
| Width | $b = 8\ m$ |
| Thickness | $t = 0.45\ m$ |

The slab was subjected to a uniformly distributed load of $q = 90\text{kN/m}^2$.

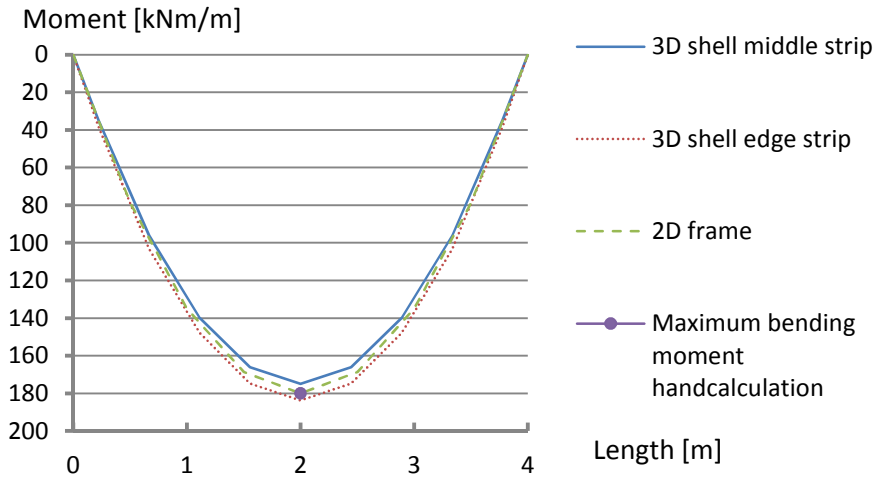


*Figure 2.7- Illustration of the maximum bending moments for 3D shell, 2D frame and hand calculations.*

From the results obtained and presented in Figure 2.7, a small deviation of the maximum bending moment between the different methods can be noticed. The hand calculation and 2D frame analysis exhibit a good correlation for this simple case because both methods are based on beam theory. The 3D FE analysis, on the other hand, is based on shell theory, Here we can see a difference between the edge strip and a strip thought the center of the slab. The results from the middle strip and the edge strip are bounding the results obtained with beam theory.

## 2.6 Structural 2D frame analysis

During many years calculation of forces and moments in bridge design was mainly done with 2D frame analysis. Only if the geometry was extremely complicated other methods where used. Often, one strip in the main longitudinal direction of the bridge was used for design. In the transverse direction a minimum amount reinforcement was used. Hence, 2D frame analysis was used to fulfill equilibrium in an 3D structure. However, the 2D analysis do not fully fulfill the requirements of theory of elasticity for a 3D structure. As a substitute, the lower bound theory of plasticity was used as a basis for design, Sustainable bridges (2007).

In the thesis, separate 2D frame analyses were made for the main directions of the bridges. The linear 2D frame software strip step 2 was used. Strip step 2 has for a long time been one of the most used computer software for designing bridges in Sweden. It has often been used for design of slab frame and slab bridges, mainly due to that the results are easy to analyze.

Strip step 2 is a 2D FE-software which considers a strip with a given width. Often the strip width was chosen to be 1.0 m. In other words, the bridges are analyzed as 2D frame structures with the width of 1m. The results from this analysis are assumed to be valid across the whole width except over the edge regions, where some adjustments are made.

The software uses the theory of elasticity and implies a linear relation between stress and strain (Hookes law), that plane surfaces remain plane (Bernoulli hypothesis) and a rectilinear stress condition (Navier). The calculations are done by the first order theory with small deformations. Due to the assumptions made superposition of results can be used, Ingengöresfirma Åke Bengtsson (2004).

# 3 FE Bridge models

In this thesis, a slab bridge and a slab frame bridge were used to investigate the difference in design results when using 3D shell analysis and 2D frame analysis, respectively. The purpose of this chapter is to give an understanding of how the 3D-shell FE models of the slab bridge and the slab frame bridge were created. Furthermore, an illustration of the assumptions and choices made will be presented.

The bridges were designed using the following material properties:

Concrete C35/45 has been assigned to all sections

Young´s modulus $E = 34\ GPa$

Shear modulus $G = 14\ GPa$

Poisson´s ratio $v = 0.2$

## 3.1 Slab Bridge

### 3.1.1 Geometry

The bridge is a straight continuous slab bridge with the slab supported on three columns. The total length of the bridge deck slab is $l = 45.3$ m and the width is $w = 7.6$ m, see Figure 3.1 and Appendix F. The bridge deck has span widths of 16.4 m and 25.1 m and two cantilevering parts at each end with the same length of 1.9 m. The two bearings on each column are positioned 2.8 m apart, symmetrically with respect to the centerline of the bridge.

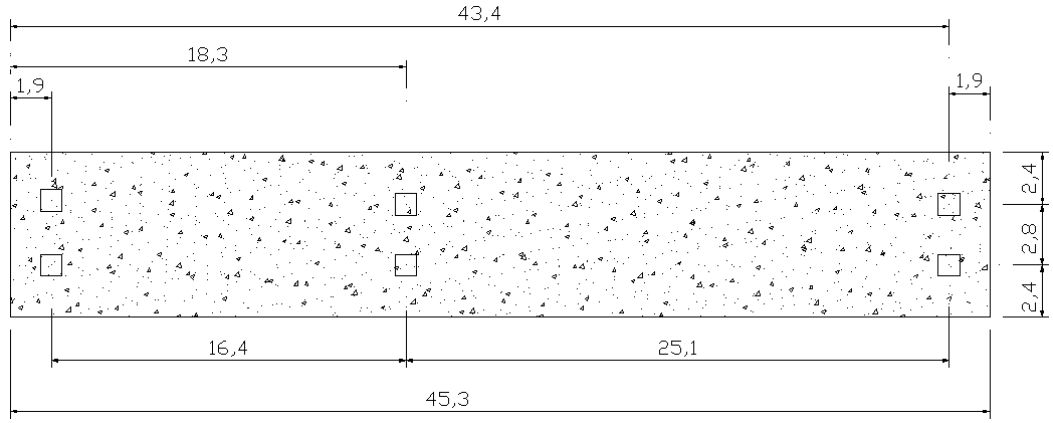


*Figure 3.1- Geometry of the bridge slab.*

The cross-sectional height is reduced towards the longidudinal edges according to the design drawings, see Appendix F. In some parts, the thickness increases in both x-and y-direction simultaneoustly. In these regions the cross-section was modeled with an average height to simplify the modeling. Here, the areas with varying height have been divided into a number of sections.These sections have individually been assigned the mean height of that section. Similarly, for the boundaries along the longitudinal edges, the real geometry has been modeled with a mean inclination; see Figure 3.2. In spite of that the shape of the specific parts does not resemble the real geometry in detail, this simplyfication provides an equivalent representation of the stiffness.

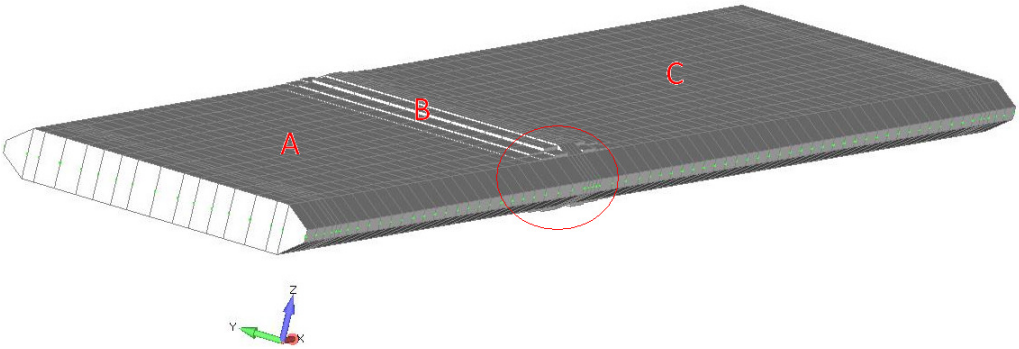


*Figure 3.2- Illustration of the cross-sectional thickness variation of the slab.*

The height in zone A and C is 1.192 m while the maximum height over the mid support,zone B, is 1.592 m; see Figure 3.2. All three zones has the same height along the longitudinal edges, 0.3 m.

### 3.1.2 Support conditions

Constraints were prescribed individually for each support node. The six different supports have different support conditions and are able to translate differently in x- and y-direction in order to avoid constraint forces. Figure 3.3 shows the free translational degrees of freedom at the supports; all other translational degrees of freedom are prevented. The center node of each support is free to rotate in all directions.

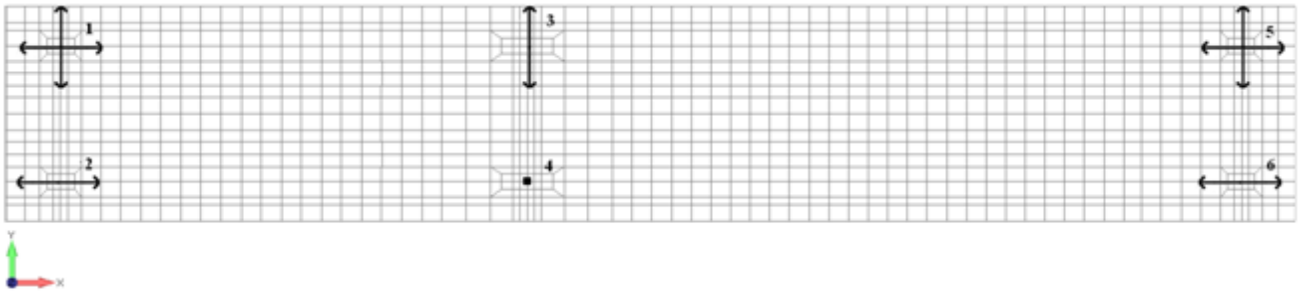


*Figure 3.3- Illustration of the six different supports and their free translational degrees of freedom*

The nodes representing the support area of each support were connected to each other with infinitely stiff elements (rigid links); see Figure 3.4. The main reason to model the supports like this was to avoid high peak values for the results, something that would have been obtained if they were modeled with pin supports, see Figure 2.5 (b).

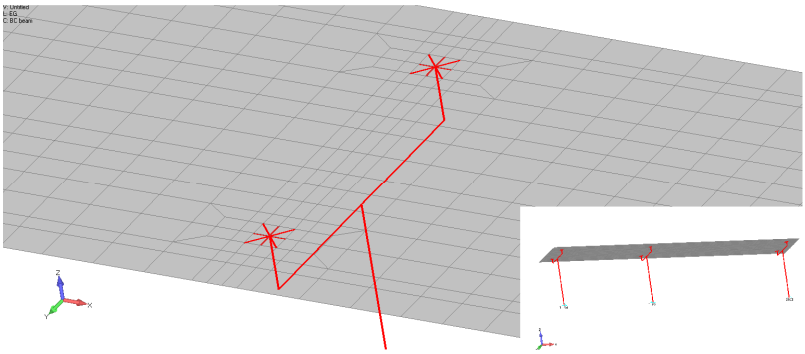

*Figure 3.4 - Illustration of how the supports were modeled in Nastran*

A node was created at the center of the bearing. The node in the center of the supports was connected to the bearing node with an infinitely stiff element. In order not to introduce forces into the support and instead allow the slab angle change, the rotational degrees of freedom for the bearing node are not restrained. Furthermore, the two nodes representing the bearings on the same column were connected to the column top node by infinitely stiff elements; see Figure 3.5. The column was modeled with beam elements with all translations and rotations restrained at the bottom.

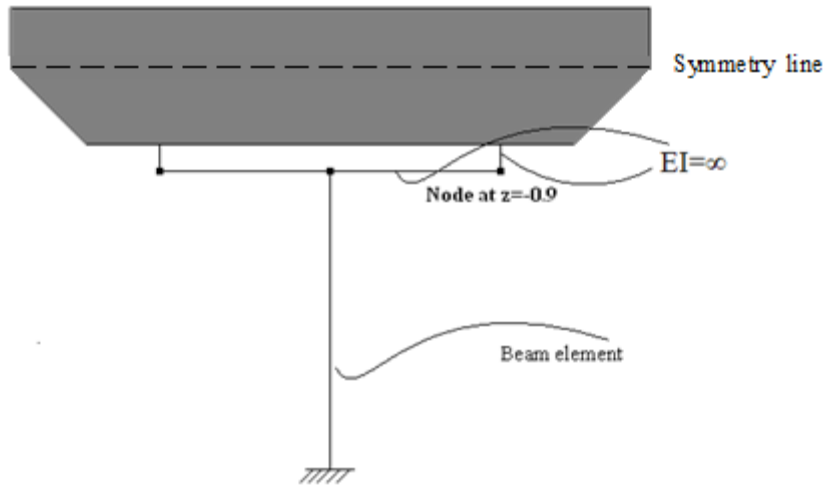


*Figure 3.5- Illustration of the support modeled with infinitely stiff connections and beam elements for the columns.*

### 3.1.3 Convergence study

In order to confirm the reliability of the FE mesh, a convergence study was made. Bending moments $m_y$, around the y- axis, for loading with selfweight were obtained from a row of elements in the center of the slab width and another element row over the bearing supports; see Figure 3.6. The two graphs; Figure 3.7 and 3.8 represent the results obtained with the original mesh density and a doubled mesh density. What can be seen is that, despite a denser mesh, the results remain unchanged. This means that the FE mesh is dense enough.

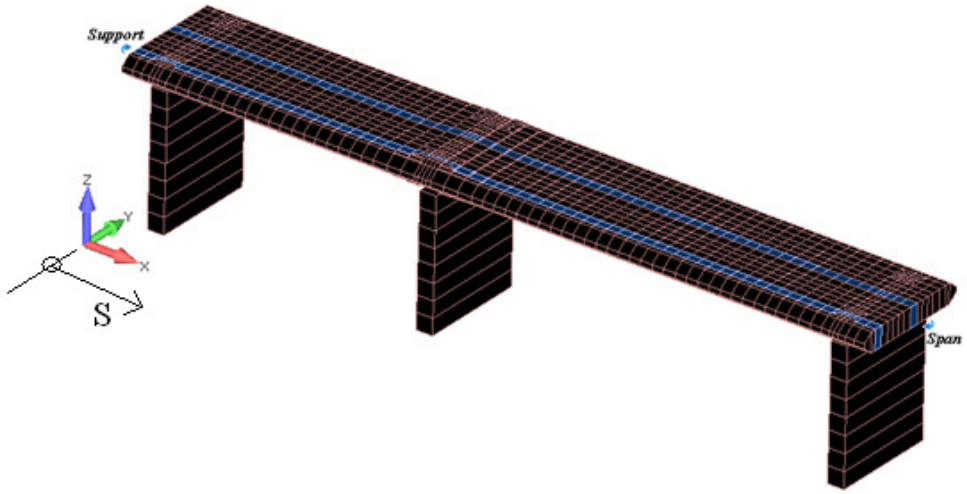


*Figure 3.6- Illustration of where the support strip and span strip are located.*

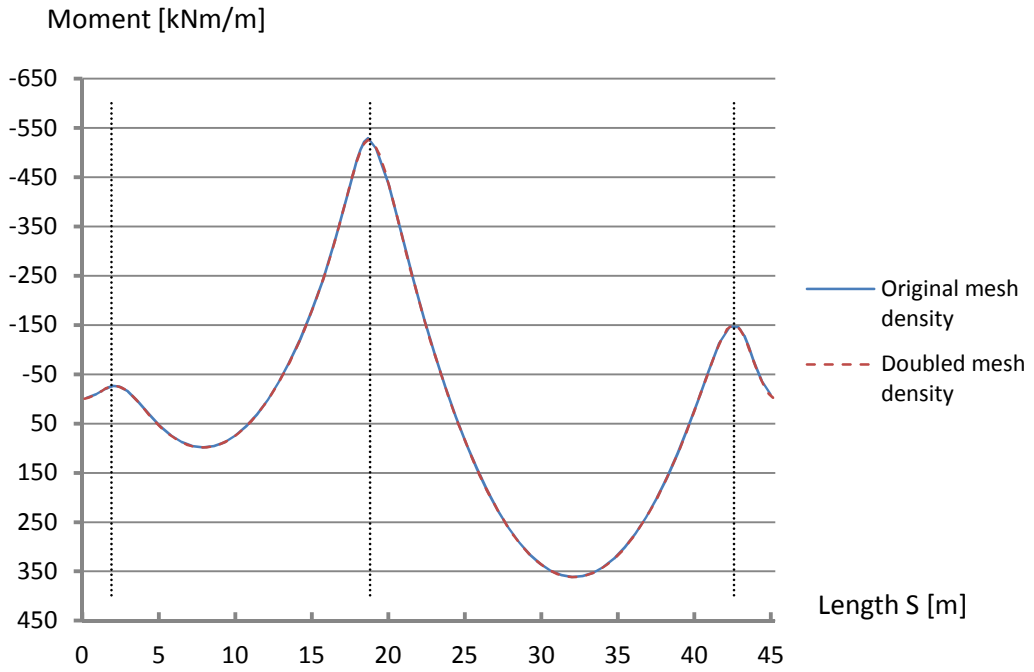


*Figure 3.7- Illustration from the convergence study, showing the bending moments for the 3D shell analysis in the span strip. The vertical lines represent the locations of the supports.*

Both for the span and support strips, the correlation is good except over the end support by the longest span. This discrepancy is due to how the supports were modeled, see section 3.1.2; since the support area is forced to remain undeformed, a certain stress concentration is obtained at the edge of the support. However, since this is a local effect and does not affect the response in the rest of the slab, and moreover is a result of the support modeling rather than the mesh density, this difference is disregarded.

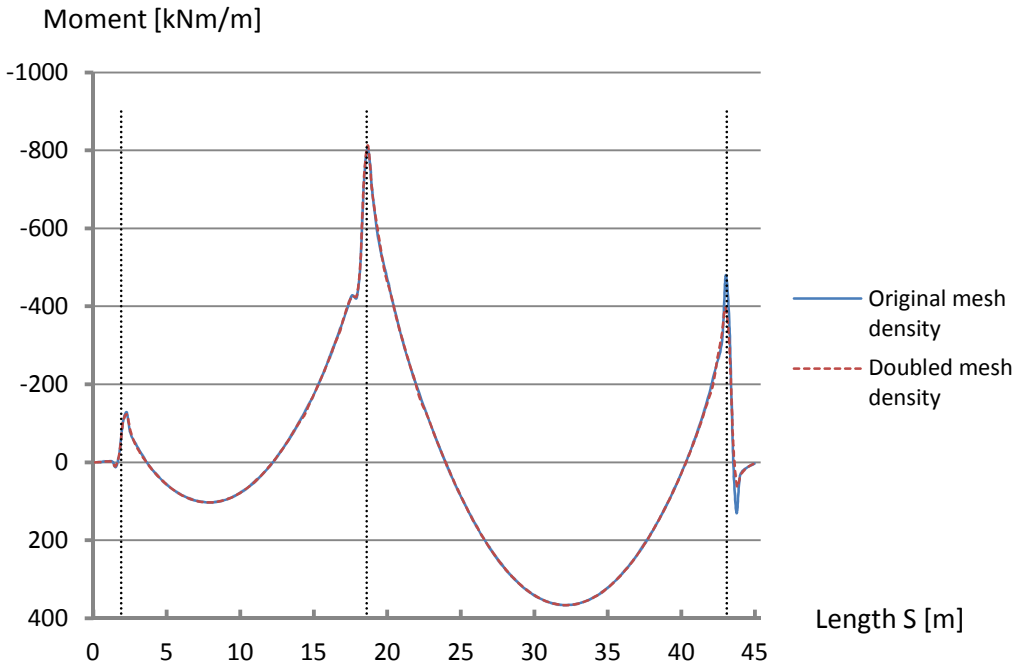


*Figure 3.8- Illustration from the convergence study, showing the bending moment for the 3D shell analysis in the support strip. The vertical lines represent the locations of the supports.*

### 3.1.4 Comparison between 3D shell and 2D frame analysis

In order to verify the 3D shell- and 2D frame model, a comparison of bending moments have been performed for the self-weight. Two strips in the 3D shell model was selected according to figure 3.6. The result from the comparison is presented in figure 3.9.

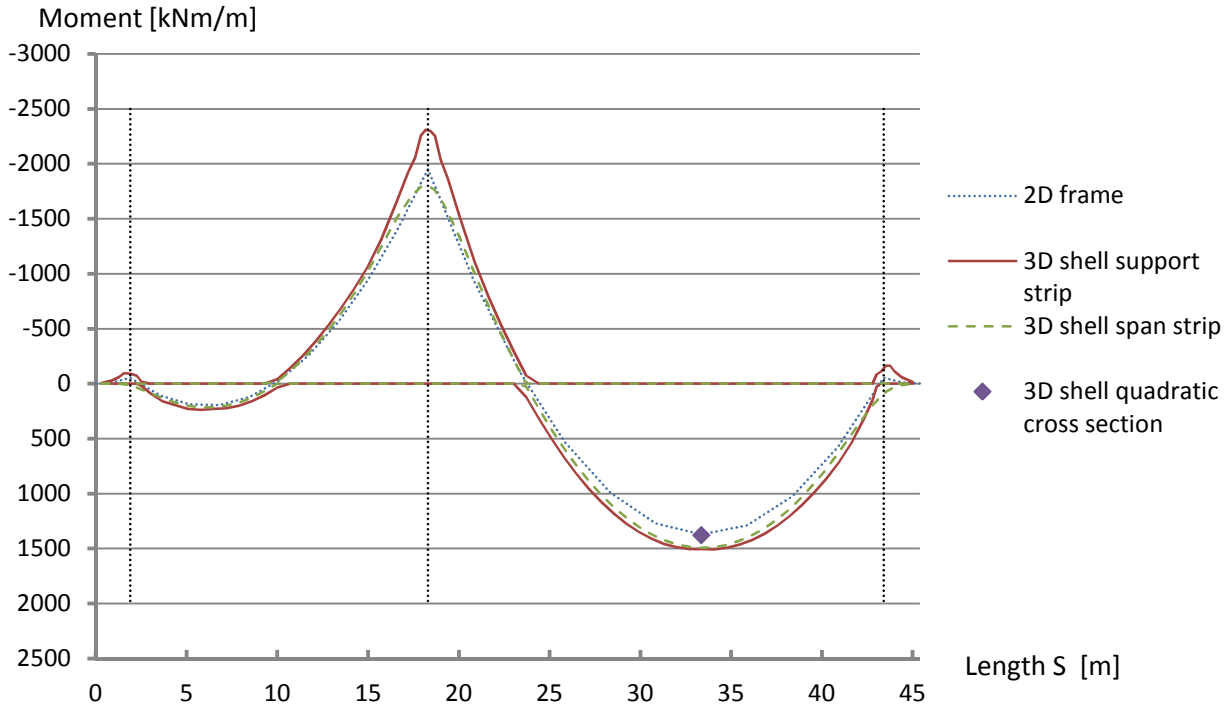


*Figure 3.9 - Comparison between main bending moments from the3D shell and 2D frame analysis for the slab bridge. The vertical lines represent the locations of the supports.*

By comparing the 3D shell- and 2D frame model a major difference in bending moment can be seen, both over the supports and in the main span. The difference over the supports are mainly due to stress concentrations obtained in the 3D shell analysis. The difference in the largest span is depending on that the 2D frame model assumes a constant thickness over the slab width (rectangular cross section) while the 3D shell model has a decreasing height towards the longitudinal edges; see Figure 3.2. Due to redistribution of forces within the cross section, the 3D shell model get an increased maximum bending moment in the strips with full slab thickness. To verify the models, the cross section was changed in the 3D shell model to be rectangular, to resemble the 2D frame model. In this analysis the 3D shell model resemble the 2D frame model in a better way, and a good correlation was obtained; see Figure 3.9.

## 3.2 Slab frame Bridge

### 3.2.1 Geometry

For the frame slab bridge, the deck slab is resting on two integral abutment walls which in turn rest on a bottom slab. The bottom slab and the integral abutment walls have uniform thickness while the deck slab has a variable thickness over the width.

The total length of the bridge is$l = 24.5$ mperpendicular to the span direction and the width is$w = 10.2$ m in the direction of the bridge span. The height of the frame slab bridge is$h = 5.45$ m. The thickness of the abutment walls is $t_1 = 0.65$ m and of the

bottom slab$t_2 = 0.75$ m, while the thickness of the top slab varies between $t_3 = 0.5$ m in midspan to $t_4 = 0.75$ m over the supports; see Appendix F

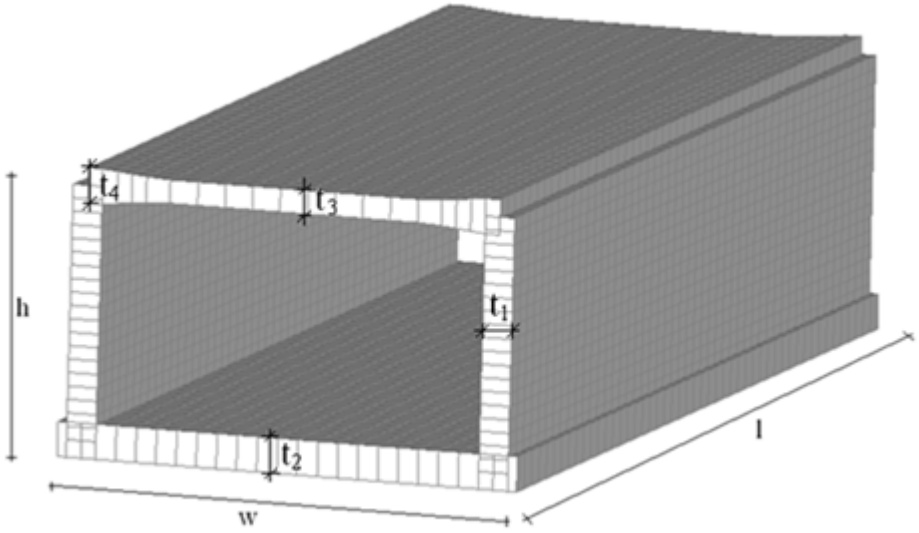


*Figure 3.10- Illustration of the geometry of the frame slab bridge.*

### 3.2.2 Support conditions

The support of the bottom slab was modeled as an elastic bed in vertical direction, under the entire slab horizontal restraint was made by restraining the translations in x- and y- direction respectively, see Figure 3.11. It is of importance to model these boundary conditions in a correct way to avoid unintended restraint actions. When thermal actions are added to the analysis, incorrect restraining will result in secondary forces. In order to avoid this, boundary conditions placed along the x-axis in the center of the bottom slab restricted translations in y-direction and, similarly, boundary conditions placed along the y-axis in the center of the slab restricted translations in x-direction.

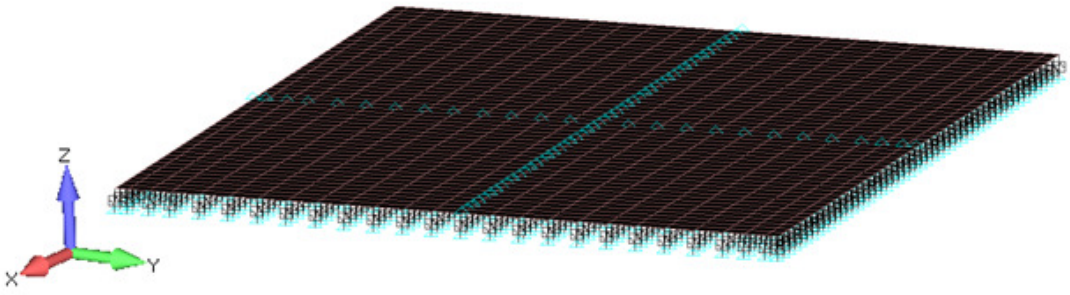


*Figure 3.11 - Illustration of the boundary conditions for the bottom slab of the slab frame bridge, showing the directions of the prescribed restraints.*

### 3.2.3 Convergence study

As for the slab bridge, a convergence study was performed to evaluate whether the mesh density was high enough to give reliable results. Bending moments around the

x-axis was obtained from two strips in y-direction, one in the middle of the bridge and one along the end of the bridge; see Figure 3.12. The two graphs in Figure 3.13 and 3.14 present the results obtained with the original mesh density and with doubled mesh density. It can be seen that, despite doubling of the mesh size, the results give the same maximum moments and that the difference is negligible. This means that the original mesh is sufficiently dense and provides sufficiently correct results.

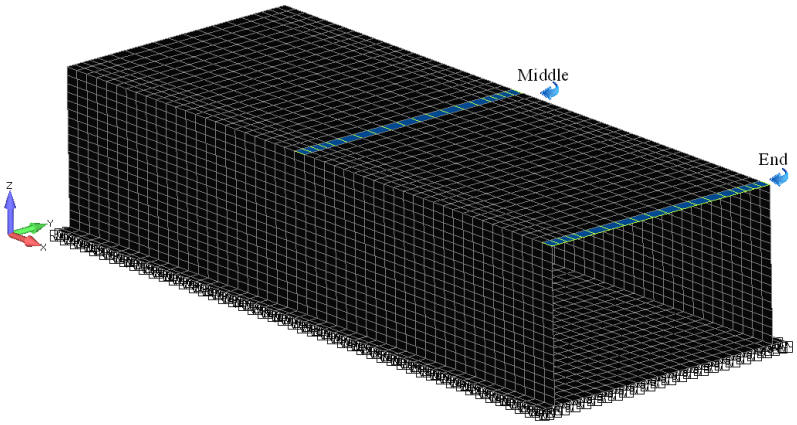


*Figure 3.12- Illustration of where the end- and middle strips are located.*

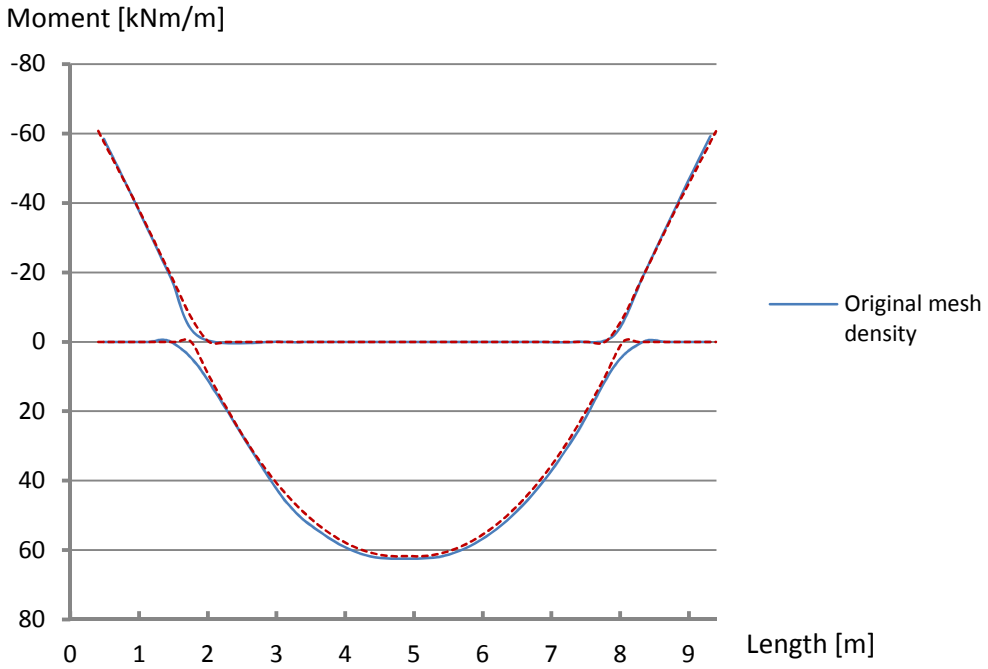


*Figure 3.93 - Illustration from the convergence study, showing the bending moment for 3D shell analysis in the end strip.*

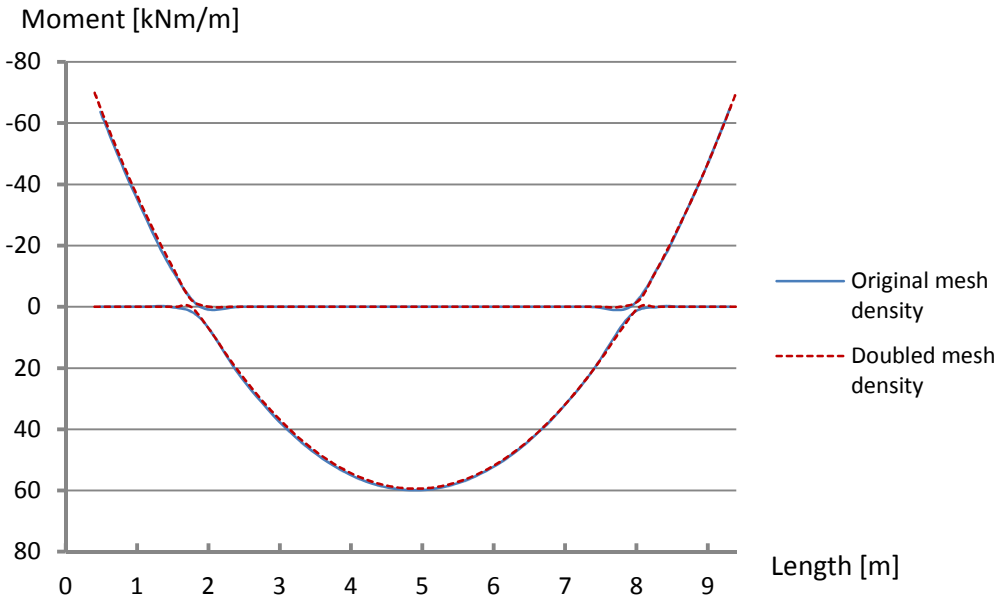


*Figure 3.14- Illustration from the convergence study, showing the bending moment for 3D shell analysis in the middle strip.*

### 3.2.4 Comparison between 3D Fem and 2D frame analysis

In order to verify the 3D shell- and 2D frame models a comparison of the bending moment have been done for the self-weight. Two strips in the 3D shell model have been selected according to figure 3.12. The result from the comparison is presented in figure 3.15 and 3.16.

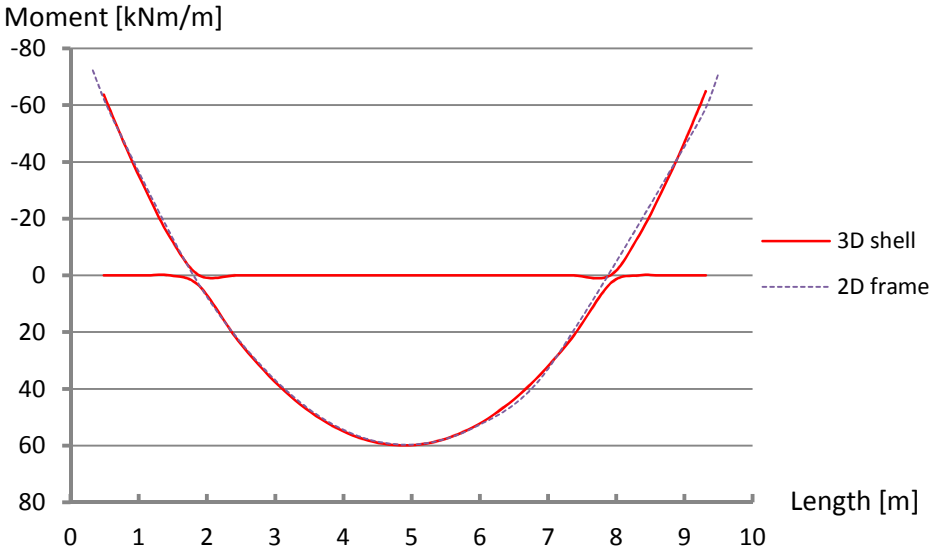


*Figure 3.15- Comparison between the main bending moments from the3D shell and the2D frame analysis for the middle strip, for the slab frame bridge subjected to self-weight*

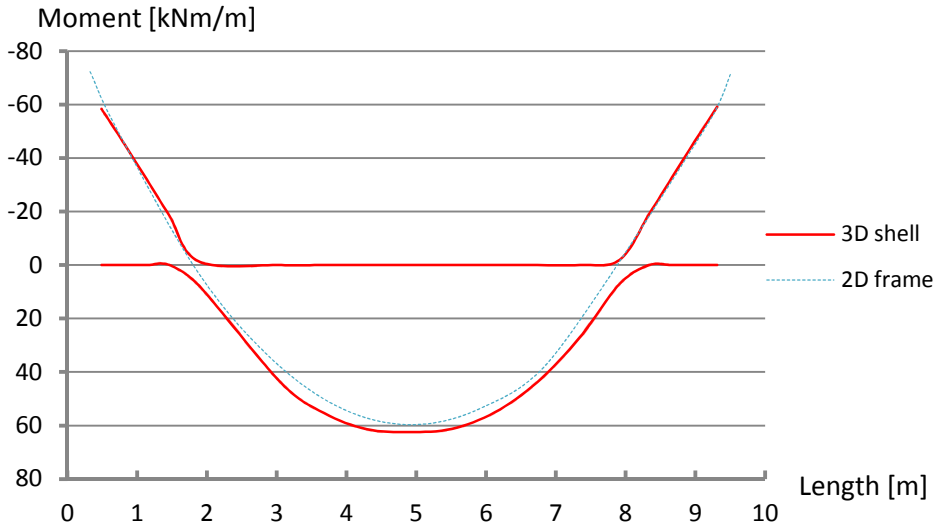


*Figure 3.16- Comparison between the main bending moments from the3D shell and the2D frame analysis for the end strip, for the slab frame bridge subjected to self-weight.*

The correlation for the middle strip is good. For the end strip the values obtained from the 3D shell analysis are larger, which depends on redistribution of load to the edges. This effect is not reflected in the 2D frame analysis.

The reason why the graph obtained from 3D shell analysis does not extend along the length axis as far as the graph obtained from 2D frame analysis is due to how the finite element method produces the results. The computational software Strip step 2is based on two-dimensional beam theory as described in chapter 2.7, which means that the slab is subdivided into a number of beam elements connected by their nodes. This means that the starting- and ending coordinate of the slab will end up in a node, from where the results will be extracted. The results obtained from the finite element software Nastran produces the results by Gauss integration between the nodes. This means that the values are obtained from the middle of the element; it is due to that the results are obtained from half the element size that the graph from the 3D shell analysis is shorter; see Figure 3.17.

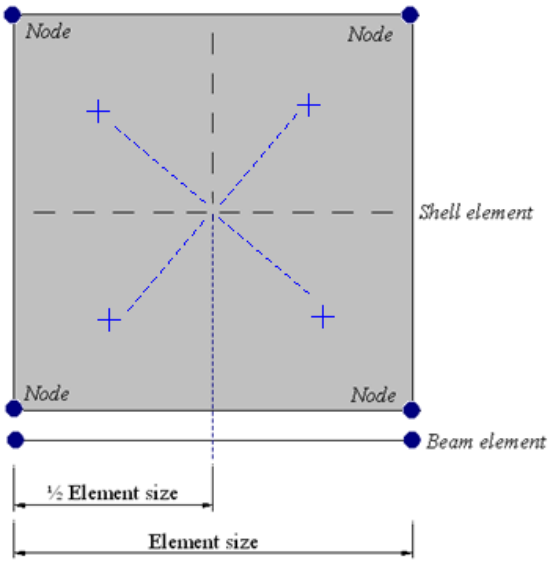


*Figure 3.17 – Results extracted from 3D shell and 2D frame analysis*

# 4 Loads

In reality a structure is loaded with many different loads. In this study, the load types on the bridges studied were limited and a representative amount of loads were selected in order to obtain a credible comparison. The loads included in the analysis are the self-weight of the structure and the pavement, thermal actions, traffic loads, shrinkage, earth pressure and support settlement.

## 4.1 Self-weight and pavement

The self-weight was calculated from the geometry of the bridge section. The density of concrete was assumed to be 25 kN/m$^3$; see Appendix A.

The pavement was assumed to be equal for both the slab bridge and the slab frame bridge. This assumption was made to simplify the calculations of temperature loads which depend on the pavement thickness. Since the purpose was not to design a bridge, but rather to perform a comparison, this assumption will not have any influence. The pavement consisted of a 10 mm bituminous sealing placed in two layers, covered with three layers asphaltic concrete with a total thickness of 140 mm; see Appendix A. The pavement was assumed to have the density of 24 kN/m$^3$.

## 4.2 Thermal Actions

The thermal actions applied on the bridge structures can be subdivided into two types, uniform temperature and temperature gradient. The uniform temperature component of the thermal action determines the expansion and contraction of the bridge, which results in change of length. The temperature gradient does in turn determine the variation of temperature between the superstructure´s upper and lower surfaces, resulting in curvature changes.

In statically determinate structures the need for movement due to thermal actions does not result in sectional forces but only in translations and rotations of the structure.

In statically indeterminate structures, on the other hand, the need for movement due to thermal actions results in translations, rotations and sectional forces. As the magnitude of these sectional forces depends of the stiffness of the structure, the forces will be dramatically reduced when the concrete cracks. This is due to the reduced stiffness of the concrete section in cracked state. Furthermore, in concrete structures the stiffness is influenced by creep, resulting in further reduction of the sectional forces due to thermal actions.

For ultimate limit state design of concrete structures the sectional forces due to thermal actions are of minor importance, provided that the ductility and rotational capacity of the structural elements are sufficient and the vertical stability of members is not compromised. This is due to that concrete structures experience a severe cracking under ultimate loads and, hence, the stiffness is dramatically reduced. Furthermore the reinforcement will yield, leading to plastic deformation and redistribution of internal forces and moments. In serviceability limit state, especially for control of crack widths, the sectional forces due to thermal actions should be taken into account. In this case, a gradual evaluation of cracking should be considered, (Eurocode 1 CEN (2002). This is however a difficult task as the precise solution requires a non-linear analysis. A simplified and more practical approach is to calculate the sectional forces due to thermal actions assuming reduced stiffness corresponding to cracked sections and an effective modulus of elasticity. A common practice in

Sweden is to reduce the stiffness of the structure with about 40% and to employ a creep coefficient of about 1.3 for the calculation of sectional forces due to thermal actions

For the purpose of this thesis, the uniform temperature components are calculated to $\Delta T_{CON} = -27.6 \quad ^{\circ}C$ and $\Delta T_{EXP} = 23.5 \quad ^{\circ}C$; see Appendix A.In the case of the slab frame bridge no thermal actions were applied to the bottom slab, due to the fact that the bottom slab lies protected from outside environmental changes. Because the bottom slab does not expand or contract, thus providing a restraint for the rest of the structure, forces in the integral abutment walls are obtained and not only deformations. In the case of the slab bridge, the boundary conditions are such that the superstructure is statically determined in its own plan; thus no sectional forces arise from the uniform thermal action.

The temperature gradient load is calculated to $\Delta T_{cool} = -6.5C$ and $\Delta T_{heat} = 6.0 \quad ^{\circ}C$; see Appendix A. Due to the fact that mainly the roadway will be exposed to solar heating, application of the temperature gradient load is limited to the bridge deck slab in both models.

## 4.3 Traffic loads

The vehicle traffic can differ between different bridges depending on how the traffic is composed. The differences can include the proportion of heavy goods vehicles (HGV´s), the traffic density accounting for the average number of vehicles over a year and the traffic conditions. The conditions can include a number of different factors where one is the number of congestions, (Eurocode 1991-2:2003). In addition, extremely heavy vehicles and their axel loads need to be taken into account. These differences are taken into consideration by using load models according to Eurocode.

In order to apply the load models, the carriageway needs to be partitioned into a number of notional lanes, with the width$w_1$and a remaining area. This is made according to Table 4.1.

*Table 4.1 –Definition of how the partitioning of the carriageway width is performed, adopted from Eurocode 1, CEN(2002)*

| Carriageway width $w$ | Number of notional lanes | Width of a notional lane $w_1$ | Width of the remaining area |
|---|---|---|---|
| $w<5,4$ m | $n_1 = 1$ | 3 m | $w$ - 3 m |
| 5,4 m $\leq w < 6$ m | $n_1 = 2$ | $\frac{w}{2}$ | 0 |
| 6 m $\leq w$ | $n_1 = Int\left(\frac{w}{3}\right)$ | 3 m | $w - 3 \cdot n_1$ |

The width of one notional lane is defined according to table 4.1. The notional lanes are variously loaded with both uniformly distributed loads and point loads depending on which load model is to be used. The notional lane that provides the most

unfavorable effect will be denoted notional lane 1, the second most unfavorable will be number 2 and so on.

### 4.3.1 Load model 1

In accordance with the limitation of the thesis, only load model 1 will be evaluated where the numbering of lanes in the general case is shown in Figure 4.1. Load model 1 accounts for concentrated and distributed loads which cover most of the effects coming from HGV´s and private cars. It consists of two subsystems, one load group with double axels and one load group with uniformly distributed load, (Eurocode 1991-2:2003).

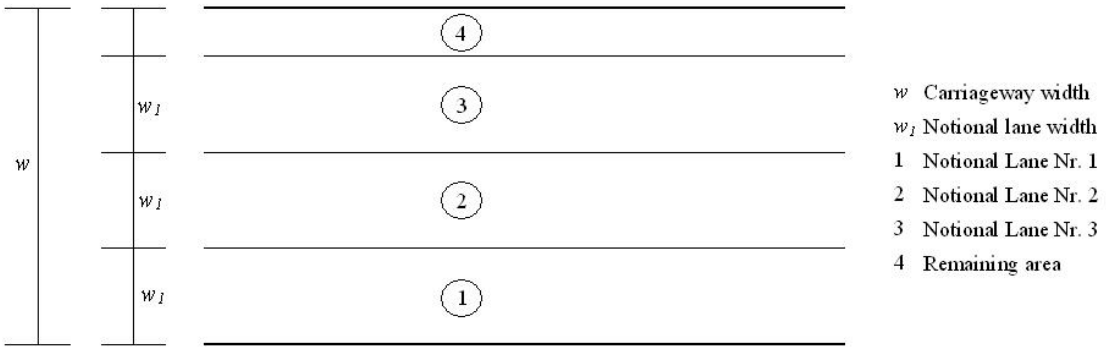


*Figure 4.1 - Illustration of the numbering of notational lanes in the general case, adopted from Eurocode 1, CEN(2002)*

Depending on which notional lane that gives the most unfavorable effect, loads are applied according to Table 4.2.

*Table 4.2 - Defines loads on each notional lane, adopted from Eurocode 1, CEN(2002)*

| Location | Tandem system TS | UDL system |
|---|---|---|
| | Axle Loads $Q_{ik}$ (kN) | $q_{ik}$ (kN/m$^2$) |
| Lane Number 1 | 300 | 9 |
| Lane Number 2 | 200 | 2,5 |
| Lane Number 3 | 0 | 2,5 |
| Other lanes | 0 | 2,5 |
| Remaining area ($q_{rk}$) | 0 | 2,5 |

To determine which of the lanes that is the most unfavorable, an influence line study was performed. In accordance with Figure 4.2 and Table 4.1, the carriageway width was partitioned into notional lanes of 3 meters width and one remaining area. For the point loads representing axle loads, each lane was in turn partitioned into two lines with 2 m distance in between and 0,5 m from the notational lane borders; see Figure 4.2. The point loads will for each lane be placed on these two lines.

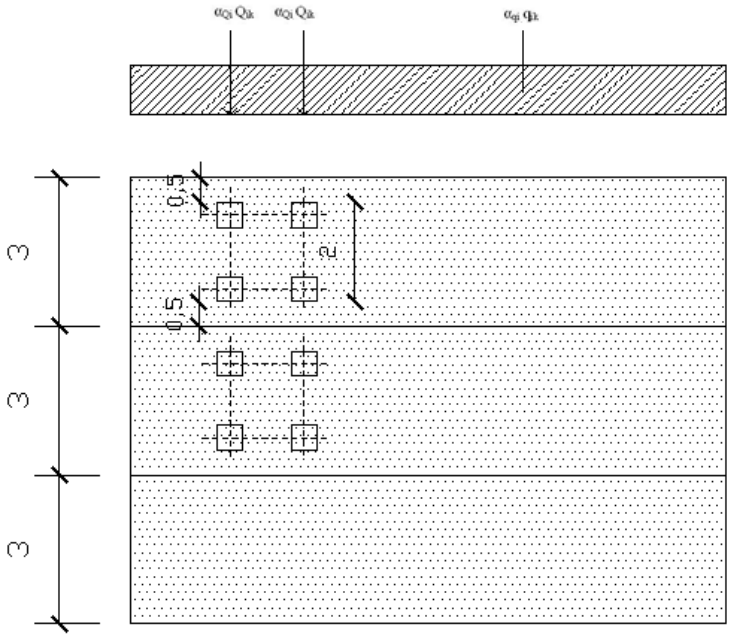


*Figure 4.2- Illustration of the load application for load model 1, adopted from Eurocode 1, CEN(2002).*

The α- factors in Figure 4.2 are so called adjustment factors and are obtained from the national appendices to Eurocode. The factors used for the calculation in the slab bridge and the slab frame bridge model can be found in appendix A.

### 4.3.2 Slab Bridge

The partition of the carriageway width was performed according to Figure 4.1and Table 4.1. The carriageway width of the slab bridge was 7.6 meters and the width of each lane was 3 m. The obtained number of lanes was two with one remaining area with the width 1.6 m. In order to cover all possible load positions, nine different traffic lanes were created and placed in three groups, see Figure 4.3.

In the first group, the notional lanes start from the left side of the bridge and the remaining area was then found on the right. Due to symmetry, group 2 was only mirrored from group 1. Group 3 consists of one notional lane positioned in the center while two larger remaining areas cover the outer parts of the bridge deck; see Figure 4.3. These three groups were estimated to cover all relevant load positions that can arise from traffic. The alternatives not included are considered not to have a major impact on the results.

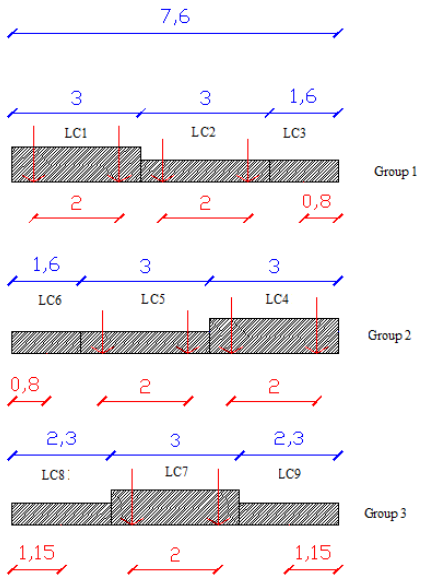


*Figure 4.3- Illustrates how the influence lines have been obtained for the slab bridge model*

### 4.3.3 Frame Slab Bridge

The partition of the carriageway width was performed according to Figure 4.1 and Table 4.1. The width of the carriageway of the slab frame bridge was 24.5 meters and the width of each notational lane was 3 m. The obtained number of notional lanes was eight with one remaining area of 0.5 m width; see Figure 4.4. To cover all relevant positions of the traffic load, two groups were created. In the first group, the notional lanes start from the left side of the bridge and the remaining area is then found on the right. Due to symmetry, group 2 positions the notional lanes are mirrored and the lanes start on the right side of the bridge leaving the remaining area on the left.

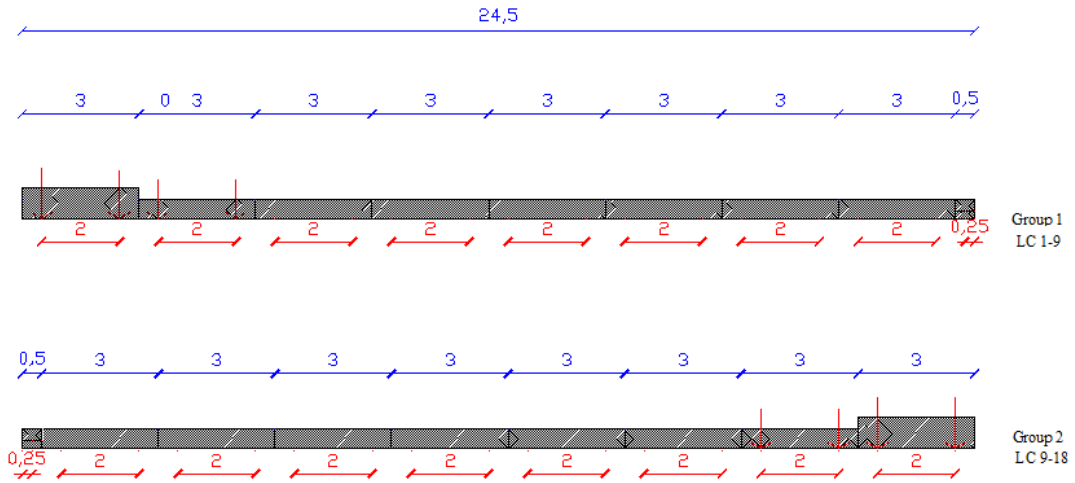


*Figure 4.4- Illustration of how the influence lines have been obtained for the frame slab bridge model*

## 4.4 Shrinkage

Since the boundary conditions for the slab bridge do not provide any are restraints for in-plane deformations, the shrinkage would only have caused a deformation but no secondary forces. Therefore, the shrinkage load was not included for the slab bridge.

Because the integral abutment walls provide restraints to movement when the structure tries to contract, the shrinkage load was included for the slab frame bridge as an equivalent temperature load of $\Delta T_{Shr} = -2.7 \quad ^{\circ}C$; see Appendix A.

Since the bottom slab and the integral abutment walls and deck slab were cast on different occasions, a part of the shrinkage had already developed in the bottom slab when the other parts were cast. This means that the different parts will shrink unevenly and secondary forces will occur. The shrinkage load was applied to the deck slab and the integral abutment walls. Since the bottom slab was also affected by shrinkage but not casted at the same time as the other parts, a reduced shrinkage load was applied. First the total shrinkage after 70 years was calculated for the bottom slab. By assuming that the casting of the integral abutment walls and top slab took place 6 months after the bottom slab, the shrinkage developed over 6 months for the bottom slab was calculated. The remaining shrinkage of the bottom slab is then the difference; see equation (4.1).

$$\Delta\varepsilon_{cs.slab} = \varepsilon_{cs.70.years.slab} - \varepsilon_{cs.6.months.slab} \qquad \text{Eq. (4.1)}$$

The total shrinkage for the integral abutment walls and top slab is then calculated for 70 years and reduced by $\Delta\varepsilon_{cs.slab}$. The remaining shrinkage, $\varepsilon_{cs.remaining}$ which is prevented to develop, will give rise to forces.

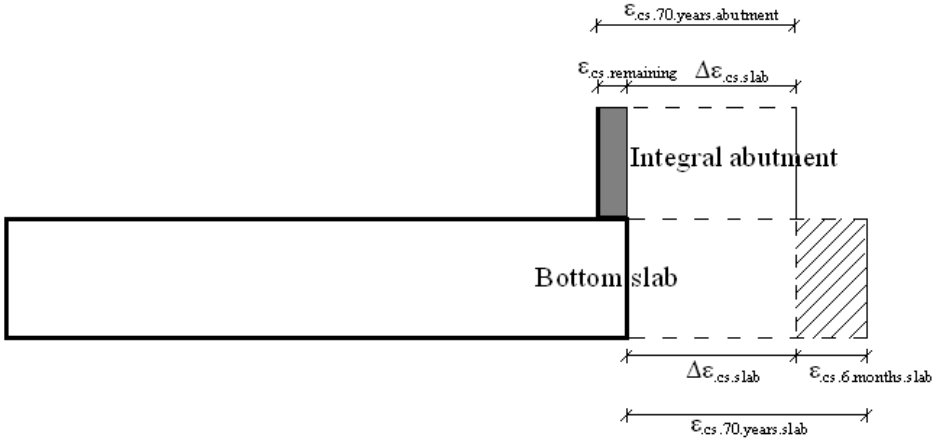


*Figure 4.5- Illustration of how the load coming from shrinkage is obtained.*

## 4.5 Earth pressure

The horizontal earth pressure against the integral abutment walls increases linearly from zero at the top of the wall (Z=0). Furthermore an increase of the earth pressure due to temperature expansion is taken into account. This load gives a resultant force which comes from both the temperature difference and the earth pressure; see Figure 4.6. The largest temperature difference is affecting the top slab. When elongation of the top slab occurs, it gives rise to a large earth pressure at the depth $Z = 0$. When inserting the behavior coming from both parameters into a figure, the resultant ends up at$0.5\ Z$.

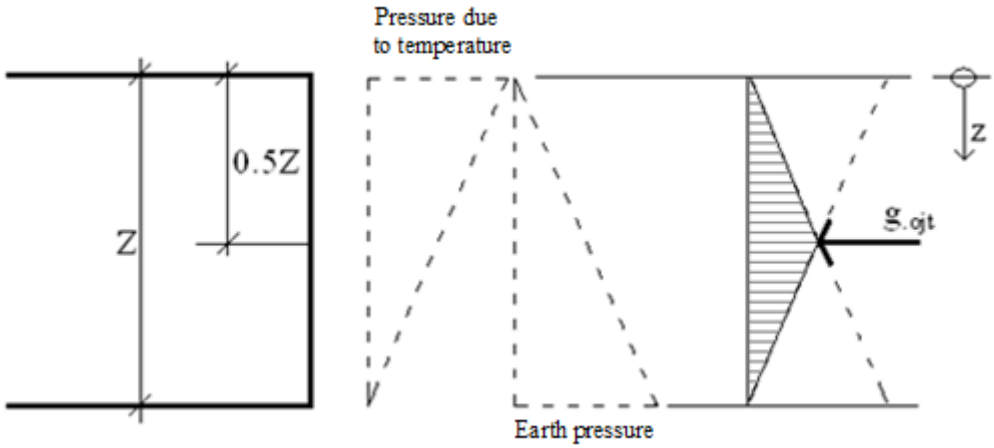


*Figure 4.6- Illustration of how the resultant coming from the earth pressure is obtained.*

The resultant force was then calculated to $g_{ojt} = 6.4\ kN/m^2$; see Appendix A.

## 4.6 Load combinations

The presented loads were combined in accordance with Eurocode to load combinations. Only load combinations for the ultimate limit state were studied. Safety class 3 was assumed for the slab bridge and safety class 2 for the slab frame bridge. Which safety class to select for a certain bridge depend on the span of the bridge. The analysis performed with 3D shell theory, as well as the 2D frame analysis, provided bending moment forces from each load individually. The moments due to selfweight, pavement, thermal action, traffic loads, shrinkage, earth pressure and support displacements were combined into maximum- and minimum bending moments. A table of partial coefficients is presented in Appendix C. Two different load combinations were performed to obtain ultimate limit state design values, ULS A, ULS B. To be able to calculate the reinforcement amount, a SLS (quasi permanent) load combination was performed; see Appendix C.

# 5 Investigations

The most important results and discussions of results are presented in this chapter. More detailed explanations with figures, illustrations and calculations are presented in the appendices. The chapter has been divided in subchapters for the three investigations made regarding the thermal actions, the point load evaluation and the comparison between 2D frame and 3D shell analysis.

## 5.1 Thermal action study

A thermal action study was made where three different load applications has been compared. The load was applied assuming either a linear variation, a constant temperature or an uneven temperature distribution; see Figure 5.1.The aim of the study was to evaluate how the load should be applied in order to obtain as realistic structural response as possible and to avoid obtaining too great secondary forces. The load application of thermal actions in 3D shell FE modeling is of importance in order to avoid obtaining large secondary forces, that the reinforcement needs to be designed for. The study was performed on the slab frame bridge with two different assumptions regarding the boundary conditions at the bottom slab in the two different bridge models, model 1 and model 2. The results provided a basis regarding how to apply the thermal action in the 3D shell FE model. The modeling and analysis results are reported more in detail in Appendix B.

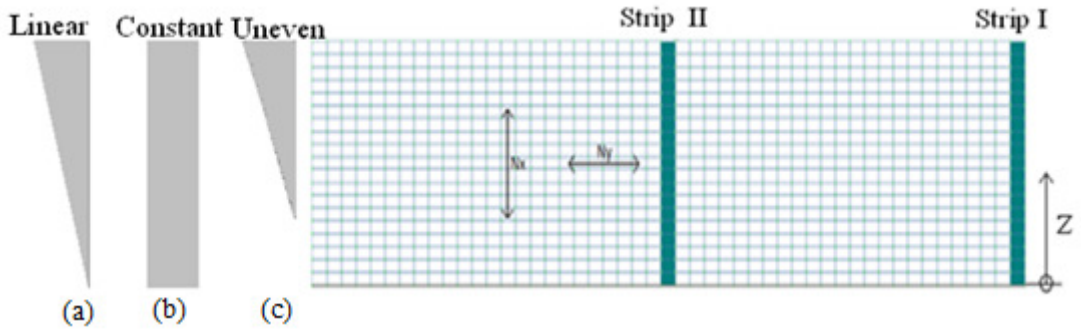


*Figure 5.1–Illustration of the application of the temperature loads*

### 5.1.1 Results from Slab Frame Bridge model 1

The boundary conditions for model 1 are modeled as springs under the bottom slab with a certain spring stiffness. Calculation of the thermal actions have been performed in accordance to Eurocode, see section 4.2. The value of the expanding temperature load was calculated to $\Delta T_{EXP} = 23.5 \ ^{\circ}C$ and contracting temperature load to $\Delta T_{CON} = -27.6 \ ^{\circ}C$ , see Appendix A. Figure 5.1 illustrates the behavior of an integral abutment wall loaded with uniform expanding thermal action over the entire wall height according to figure 5.1 (b).Due to symmetry, both integral abutment walls will behave in the same way.

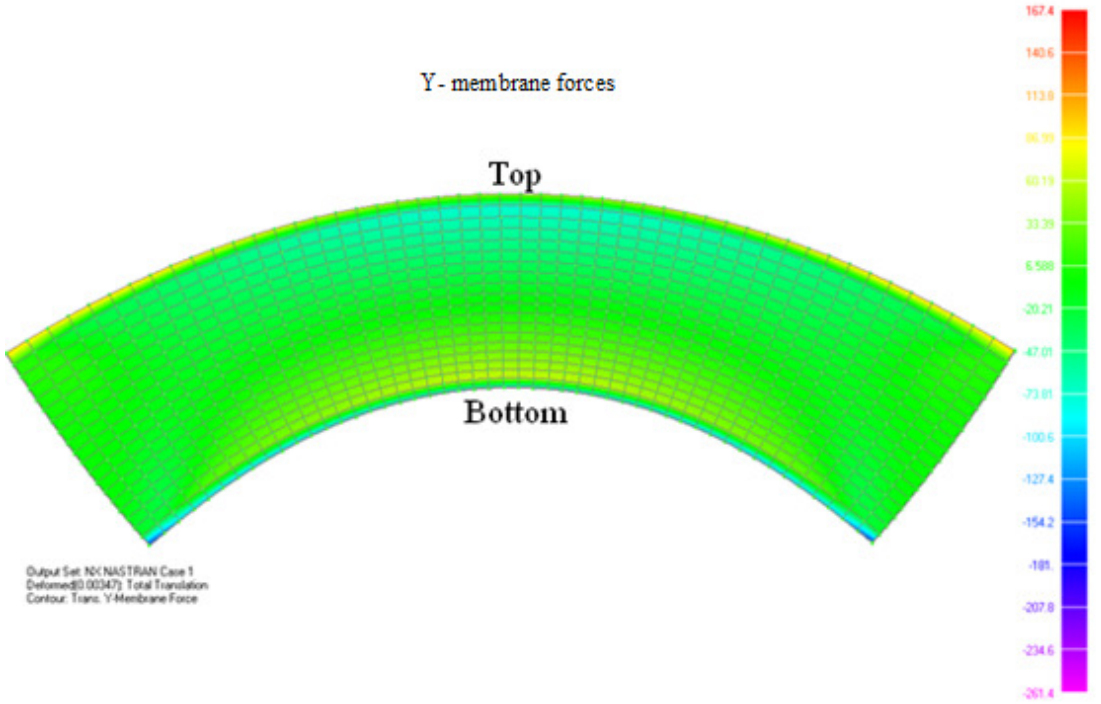


*Figure 5.2–Deformed shape and membrane force magnitude [kN] in horizontal direction in one of the integral abutment walls constant loaded with expanding thermal actions for 3D shell analysis*

The shape indicates that the integral abutment wall will bend upwards because the top expands together with the deck slab. Because no thermal actions was applied to the bottom slab, basically no elongating will take place here and the integral abutment walls will be restricted for horizontal movement along its lower boundary. This restriction will cause the lower slab to lift and the integral abutment wall to curve. The reason why the lower slab is able to lift is because it is modeled as resting on springs with a certain stiffness. Since the bridge structure with the abutment walls is stiffer that the foundation springs, the high secondary forces will cause the walls to bend and the bottom slab will lift.

Figure 5.2 illustrates the general behavior of an integral abutment wall loaded with contracting thermal actions. The explanation of the response is similar to the one with an expanding load. The top side will contract together with the deck slab, while the bottom side will be horizontally restricted by the bottom slab. The contraction of the top side will be larger than for the bottom side which will make the integral abutment wall curve upwards.

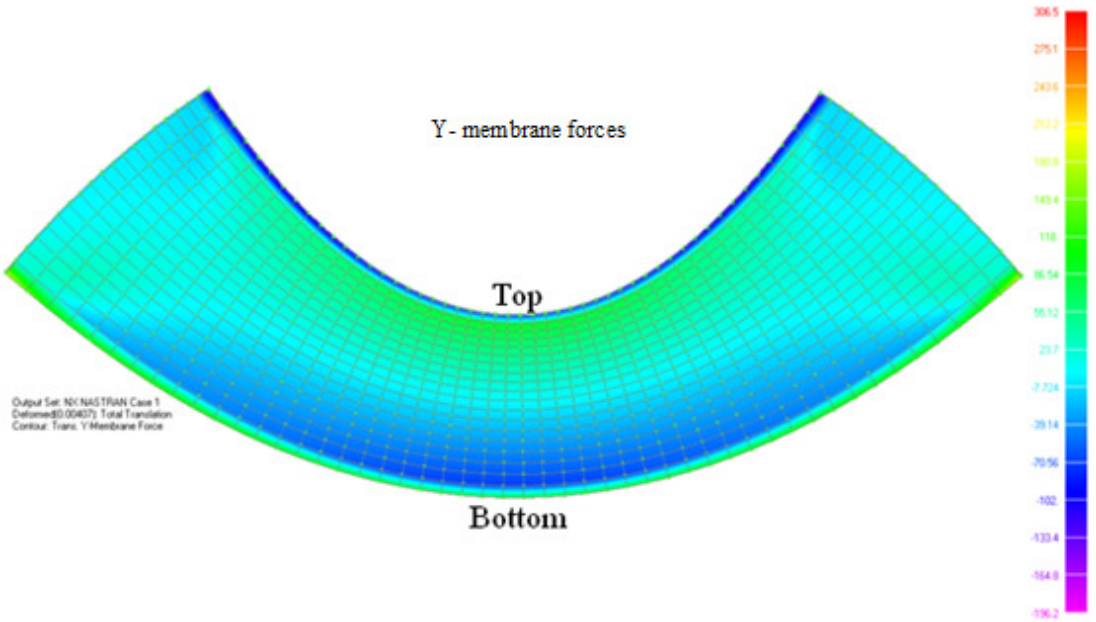


*Figure 5.3–Deformed shape and membrane force magnitude [kN] in horizontal direction in one of the integral abutment walls constant loaded with contracting thermal actions for 3D shell analysis*

As a result of the curvature, the maximum membrane forces are obtained at the end of the integral abutment wall shown in Figure 5.2 and 5.3 for the horizontal membrane force. Therefore, the values used to compare the three different load application possibilities are extracted from strip I, see Figure 5.4, and reported more in detail in Appendix B.

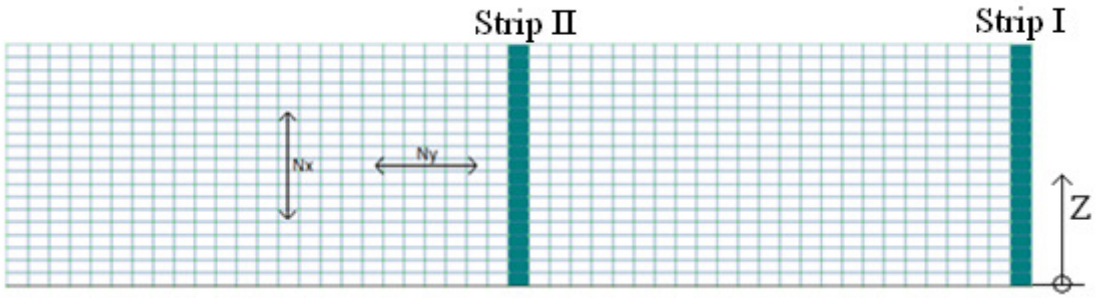


*Figure 5.4- Illustration of where results have been extracted from the integral abutment walls for the two different models*

For the vertical $N_x$ membrane force obtained from the expanding thermal actions, the values for the three different load application possibilities are illustrated in Figure 5.4. What can be discerned from the graphs is there is a largedifferenfe in results. All load applications gives compressive forces at the connection to the lower slab at about $z = 0.3$ m. The membrane force due to constant temperature for the entire wall changes into a tention force with a maximum of about 1680 kN/m at $z = 1.5$ m. The tension force then slowly descends in magnitude up to the top of the wall at$z =$ 5.45 m. The linear and uneven temperature load applications lead on the contrary to a compressive force with much lower values over the major parts of the wall height.

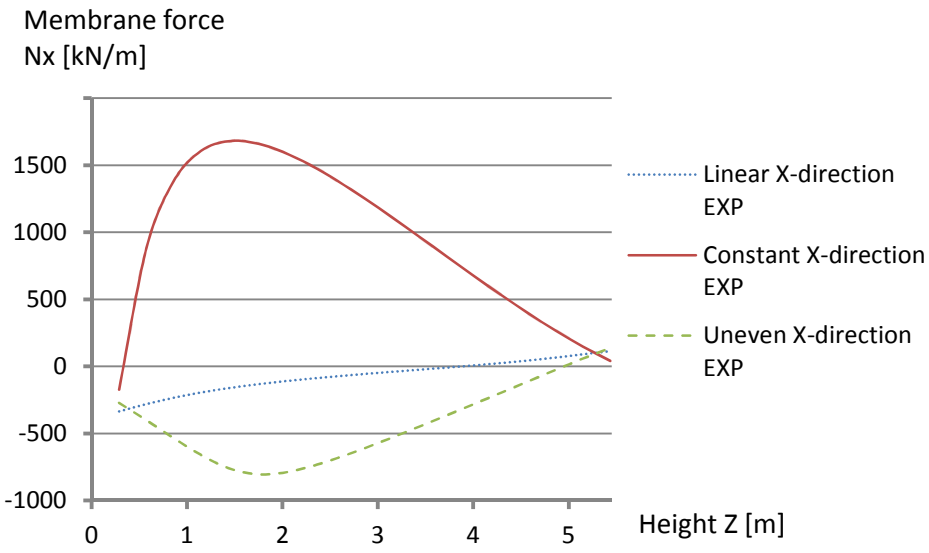


*Figure 5.5- $N_x$ membrane force over the height of the abutment wall for the three different load applications studied for increase temperature load for 3D shell analysis.*

For the horizontal $N_y$ membrane force obtained from the expanding thermal actions, the values difference between the results are mostly much smaller. One exception is the lower1.5 m of the wall for the constant temperature load, which exhibits a compressive force of about $2300\ \mathrm{kN/m}$ at the connection to the bottom slab, atz=0.3 m; see Figure 5.5.

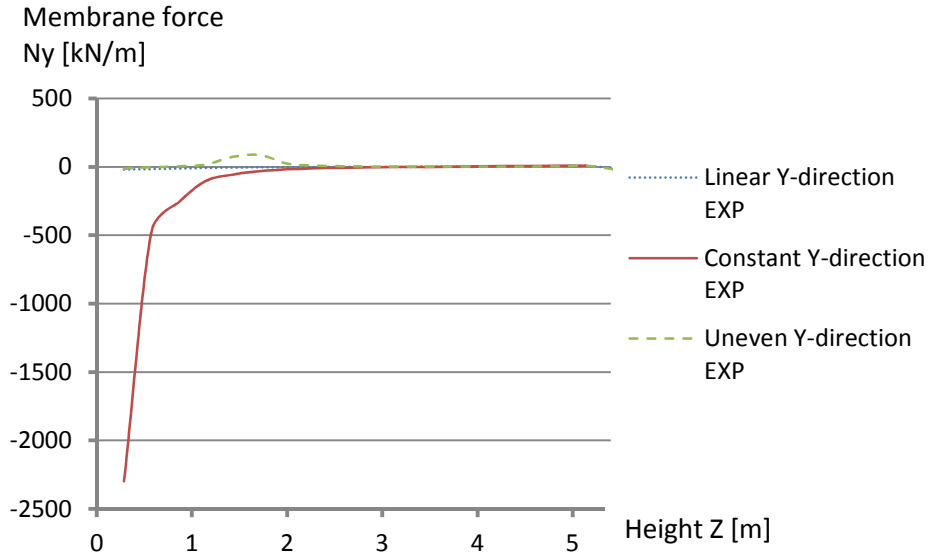


*Figure 5.6- $N_y$ membrane force over the height of the abutment wall for the different load applications studied for increased temperature load for 3D shell analysis*

The vertical $N_x$ membrane force obtained from the contraction thermal actions exhibits the similar scatter of results as for the expanding load; see Figure 5.7. The membrane force due to constant temperature changes from tension to compression force at about $z = 0.5\ \mathrm{m}$ and has the largest force amplitude of $-1970\ \mathrm{kN/m}$ at $z = 1.4\ \mathrm{m}$. The linear and uneven temperature loads exhibit a tensional force over most of the wall height, but changes to a compressive force close to the top of the wall.

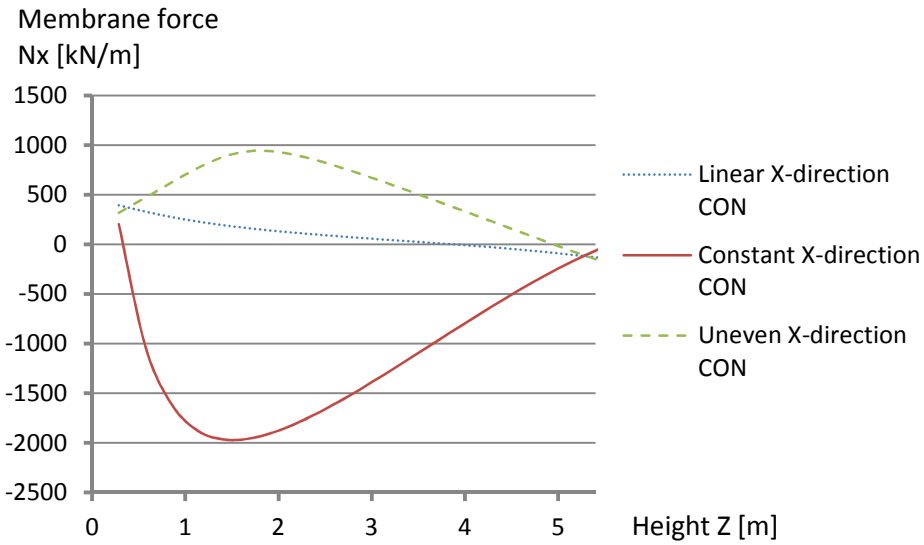


*Figure 5.7- $N_x$ membrane force over the height of the abutment wall for the different load applications studied for decreased temperature load for 3D shell analysis.*

For the horizontal $N_y$ membrane force obtained from the decreased temperature load, the values correspond in a similar manner to the expanding thermal actions; see Figure 5.8.

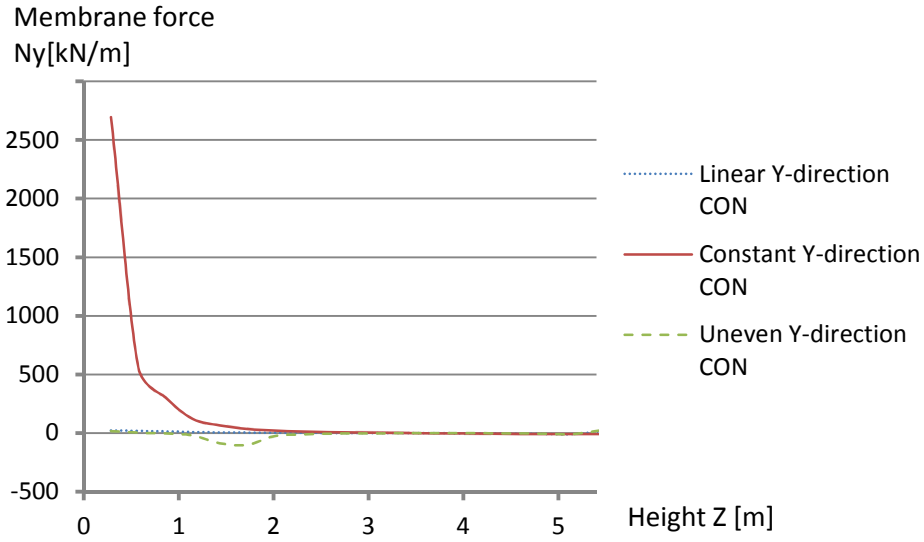


*Figure 5.8- $N_y$ membrane force over the height of the integral abutment wall for the different load applications studied for decreased temperature load for 3D shell analysis.*

Although the constant temperature load in most parts of the abutment wall gives lower membrane forces than the linear- and uneven temperature load variations, it still provides the largest tensional forces locally in this case about $N_y = 2200$ kN/m.

### 5.1.2 Results from Frame Slab Bridge model 2

The boundary conditions for model 2 are modeled as springs under the bottom slab with a certain spring stiffness in combination with vertical restraints under the abutment walls. The magnitude of the expanding- and contracting thermal actionsare the same as for model 1. Figure 5.9 illustrates the behavior of one of the integral abutment walls loaded with expanding thermal actions. Due to symmetry, both integral abutment walls will behave in the same way.

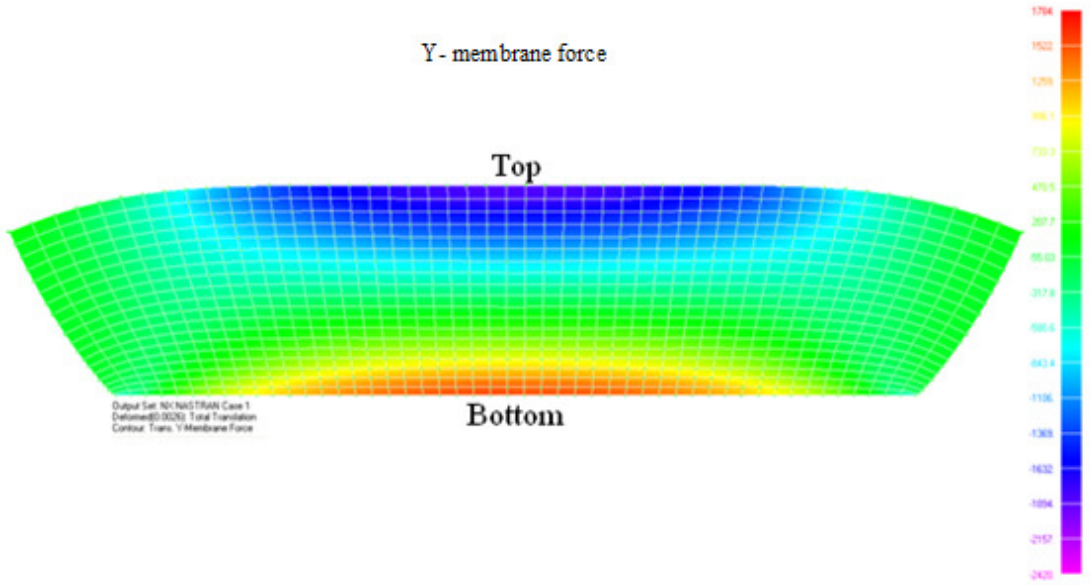


*Figure 5.9–Deformed shape and membrane force magnitude [kN] in horizontal direction in one of the integral abutment walls constant loaded with expanding thermal actions for 3D shell analysis.*

Unlike the previous model, no curvature will take place in the intersection between the bottom slab and the integral abutment wall. This is because the bottom slab is prevented from deflecting in vertical direction by boundary conditions that restrict translations in z-direction under the abutment walls. The upper part of the integral abutment wall will together with the top slab elongate, while the length of the lower part will remain unchanged. Due to lack of elongation of the bottom slab, secondary forces are created. Worth noticing is that the maximum forces for this model are not found in strip I as for model 1. Instead they are found in the mid- section, i.e. instrip II; see Figure 5.4.Figure 5.10 illustrates the behavior of the integral abutment wall loaded with contracting thermal actions. The response can be explained in a similar way as forthe expanding load. The top side will contract together with the deck slab, while the bottom side will be restricted by the bottom slab. This will in turn cause high constraint forces instrip II.

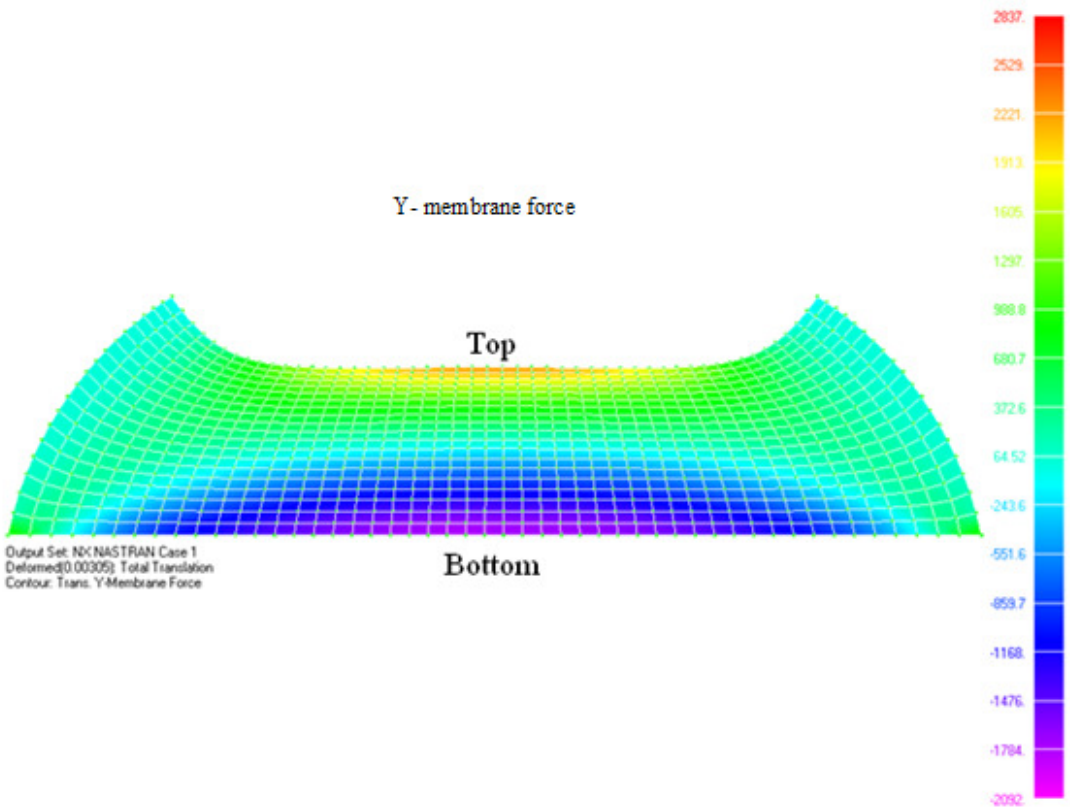


*Figure 5.10–Deformed shape and membrane force magnitude [kN] in horizontal direction in one of the integral abutment walls loaded with constant contracting thermal actions over the entire height for 3D shell analysis.*

For the vertical $N_x$ membrane force obtained from the expanding thermal actions, the values for the three different temperature load application possibilities are illustrated in Figure 5.11. What can be discerned from the graphs is that the constant temperature variation gives the smallest forces closly follwed by the linear- and the uneven temperature variations. The three graphs shows that the section is loaded in tension only. A maximal tensile force of 742 kN/m is obtained close to the bottom slab.

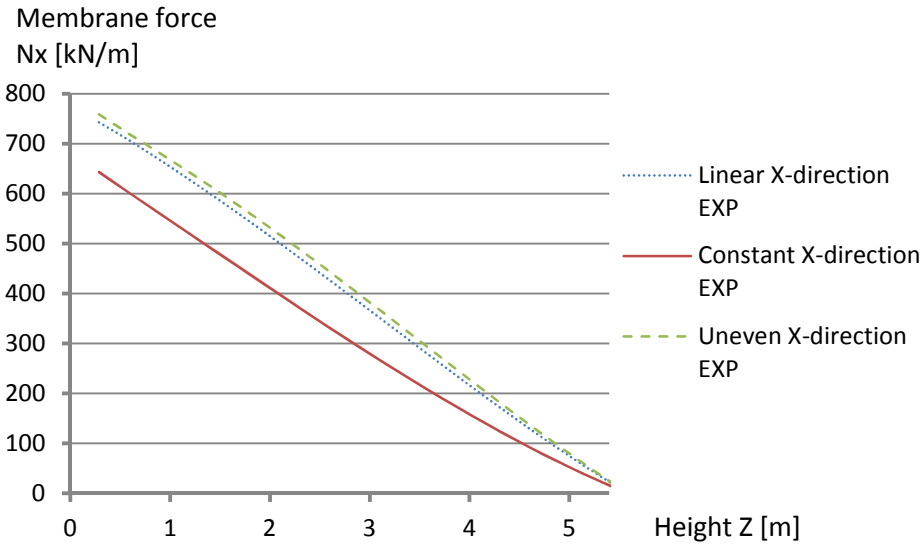


*Figure 5.11- $N_x$ membrane force over the height of the abutment wall for the three*

*different load applications studied for increased temperature load for 3D shell analysis.*

For the horizontal $N_y$ membrane force obtained from the expanding thermal actions, the behavior differs between the three temperature load applications. The constant temperature variation gives rise to compressive forces only, while the linear and uneven temperature variations consists of tensional forces in the main lower part of the wall, while the top part obtains compressive forces.

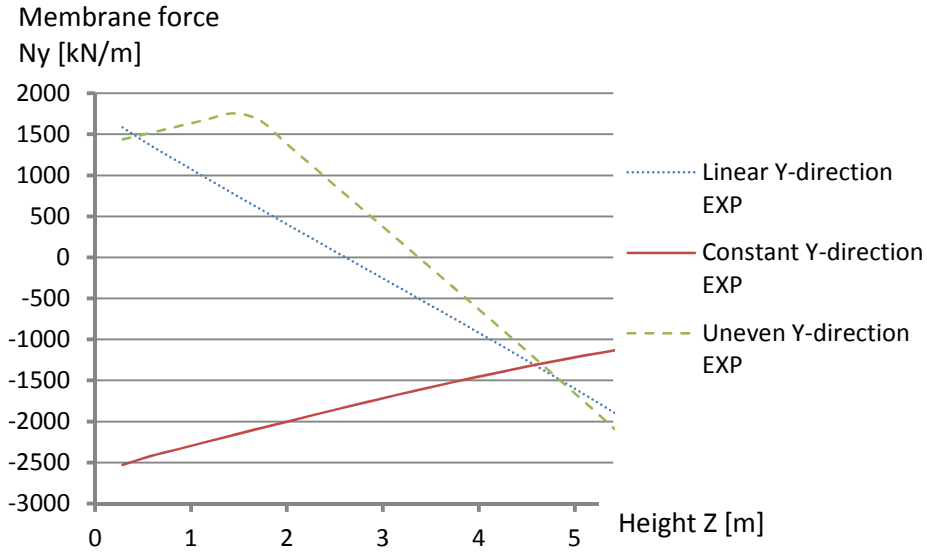


*Figure 5.12- $N_y$ membrane force over the height of the abutment wall for the three different load applications studied for increased temperature load for 3D shell analysis.*

The vertical $N_x$ membrane force obtained from the contraction thermal actions exhibits similar response as for the expanding load, but with opposite signs. Again, the constant temperature variation gives once again the smallest value while for the linear- and uneven application gives the highest compressive forces about 870 kN/m.

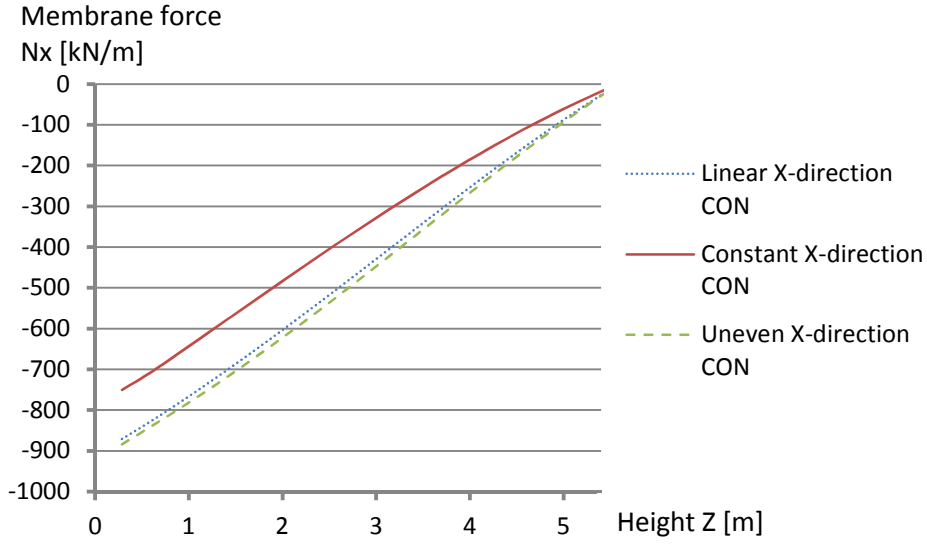


*Figure 5.13-$N_x$ membrane force over the height of the abutment wall for the three different load applications studied for decreased temperature load for 3D shell analysis.*

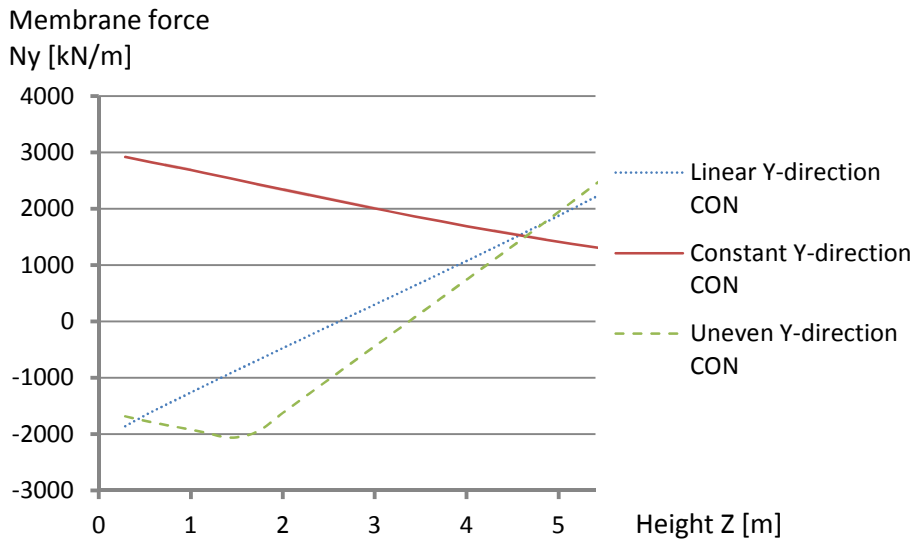


*Figure 5.14- $N_y$ membrane force over the height of the abutment wall for the three different load applications studied for decreased temperature load for 3D shell analysis.*

Similarly to model 1, the constant temperature load provides in many cases lower membrane forces than the linear- and uneven temperature variation. Still, it provides a tensional force of about $N_y = 2900$ kN/m which is much than for model 1. However, as discussed for model 1, the design value is normally obtained from the linear variation of temperature over the height of the abutment wall.

### 5.1.3 Discussion

By modeling the slab with only springs acting as vertical restraints, the correspondence with the real structural behavior can be questioned. One effect that this model does not take into account is the friction between the soil and the bridge. This friction force will to a large extent prevent the bridge structure from curving. Another effect that is not included is the impact coming from the wing wall. The wing wall is connected to the integral abutment wall and prevents it from curving. By examining the results obtained from the analysis performed in model1, we can see that the highest membrane forces are located at the edges. This means that most of the cracks on today´s integral abutment walls should be found at the edges, which is not the case. Apparently, the effects coming from friction and the wing walls would have an large influence, and model 1with springs representing the foundation, does not fully represent the real structural behavior.

Modeling the slab with springs in combination with additional translational restrictions in z- direction under the abutment walls will instead provide a model that responds more similar to the real structure. The bottom slab will in this way be prevented from lifting which will have influence on the location of the critical load values. Experience from existing structures show that cracks are mainly located somewhere in the middle of the integral abutment wall, which is also the case for this model. Due to this, there is a good reason to believe that modeling with restrictions in z- direction will provide a solution on the safe side. This means that the reinforcement will be provided at a location where cracking is known to occur. Consequently, the model with springs in combination with restraints in z- direction under the abutment walls is selected for the further studies.

When evaluating the analysis results, the linear temperature variation gives the lowest membrane forces. Despite the fact that the constant temperature load in large parts of the abutment walls gives lower values than the linear one, it still gives rise to the largest tension force of about $3000\ \mathrm{kN/m}$. The constant temperature variation can hardly occur in reality. In reality, there must be a gradual change of the temperature over the abutment walls height. Consequently, it seems reasonable to assume a linear temperature variation over the height of the abutment wall, unless a different temperature variation, such as the uneven temperature variation according to Figure 5.1 (c) is shown to be more realistic for the specific bridge.

An additional aspect to keep in mind is that the forces occurring in the linear analysis will be substantially reduced in reality as soon as the first cracks appear. Although it seems reasonable to apply the temperature load assuming a linear temperature variation, the forces obtained from the linear analysis will still overestimate the amount of reinforcement. In order to avoid too much reinforcement in the structure, knowledge of how concrete behaves must be used for a further refinement in design. In practice, engineers may use an effective modulus of elasticity corresponding to a cracked concrete section, giving reduced membrane forces to design for.

## 5.2 Evaluation of envelope of maximum load actions

The purpose of this section is toverify the method for maximum load action evaluation in 3D shell analysis made for traffic point loads.Maximum bending moments were compared with three different methods.More figures and illustrations are presented in appendix D.

### 5.2.1 Critical elements for loading with a point load

To investigate the design for one critical point load with the 3D shell model, two methods have been used. For both methods, an envelope for a unit point load has been used to identify the critical element of the slab, see figure 5.15 and 5.17.The most critical element for the slab frame bridge is at mid span along the edge of the slab see figure 5.16. An element from the center of the slab was also studied, with the aim to investigate which part of the slab that has the largest similarities with the 2D frame model. For the slab bridge, the most critical element is close to the edge in the longest span see figure 5.18. An element also from the center of the cross-section was investigated as for the slab frame bridge.

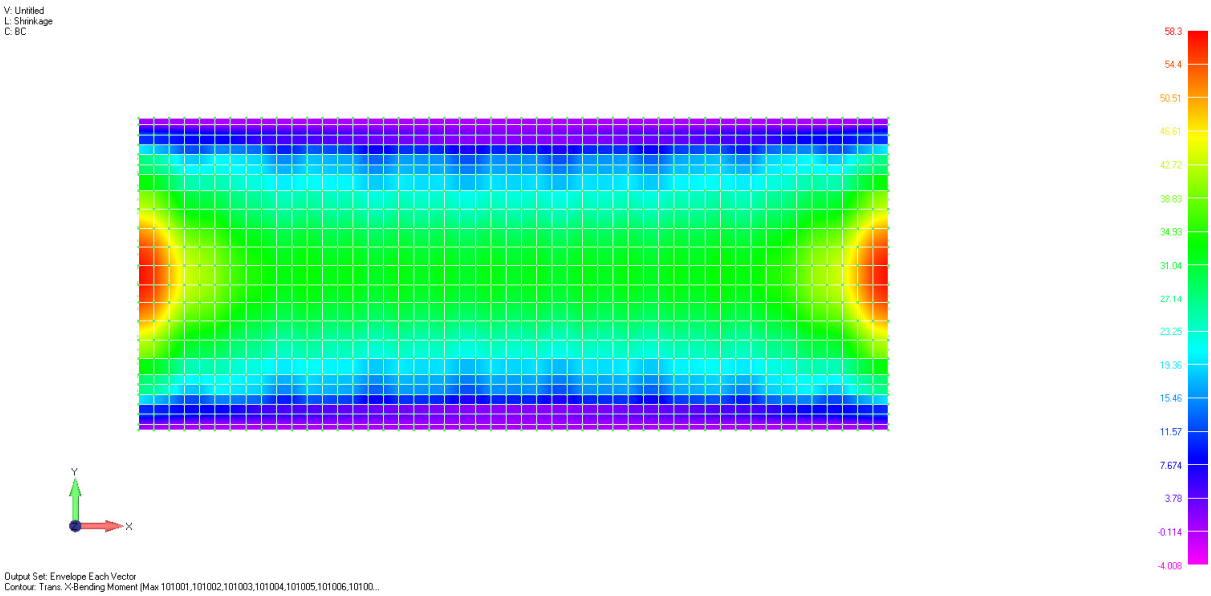


*Figure 5.15 - Envelop of the maximum positive bending moment $m_x$ for a unit point load on the slab deck, for the slab frame bridge .*

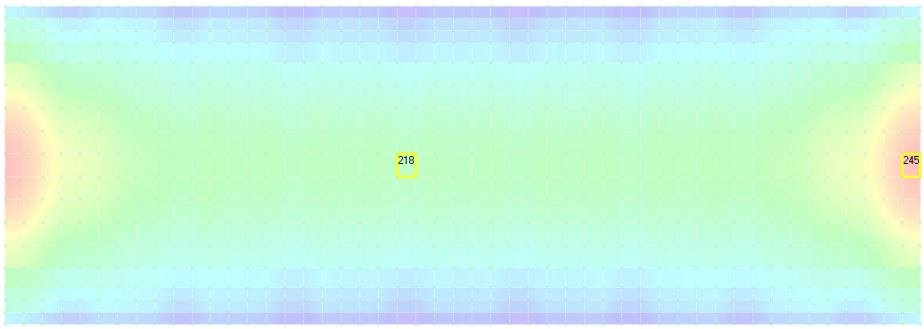


*Figure 5.16 - The critical element at the edge (no 245) and the central element (no 218) in the 3D shell analysis.*

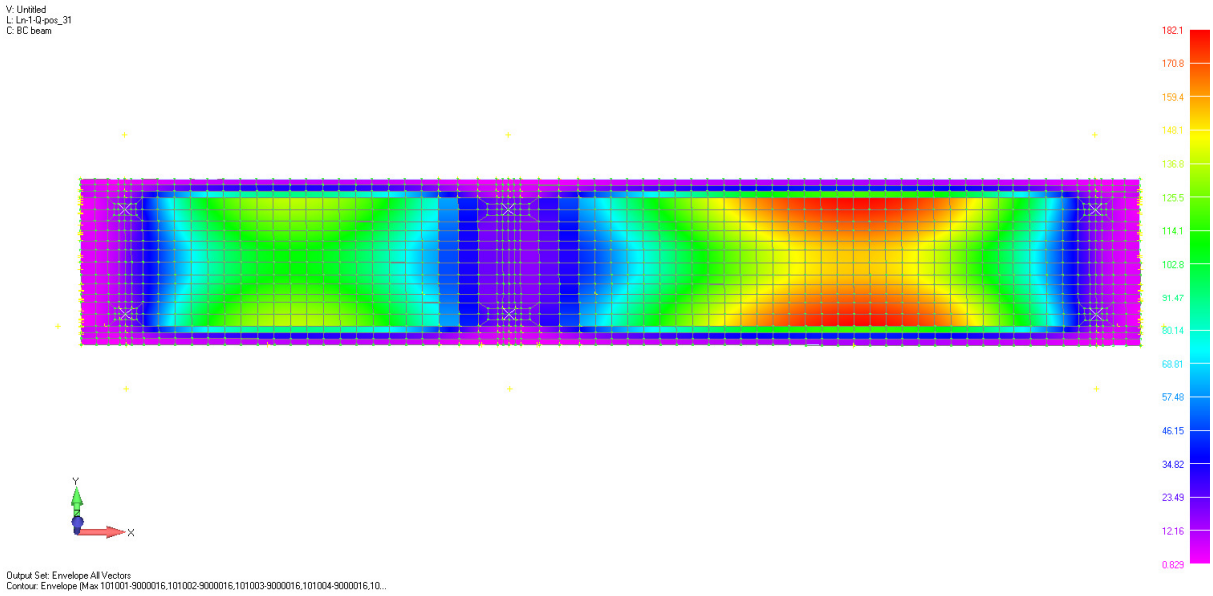


*Figure 5.17- Envelop of the maximum positive bending moment $m_x$ for a unit load on the slab deck, for the slab bridge .*

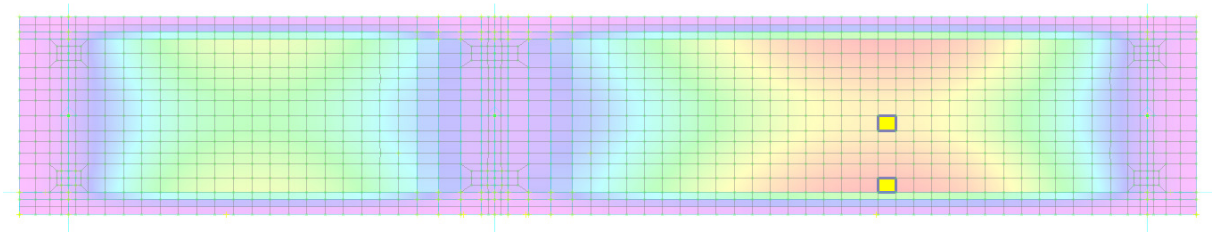

*Figure 5.18 - The critical element (no 260) by the edge and the central element (no 388) in the 3D shell analysis.*

### 5.2.2 Evaluation of maximum moment: Method 1

Influence lines for the unit point load were calculated and plotted for the critical elements determined in 5.2.1 . Figure 5.19 below shows the influence line for the critical element at the edge of the frame slab bridge.

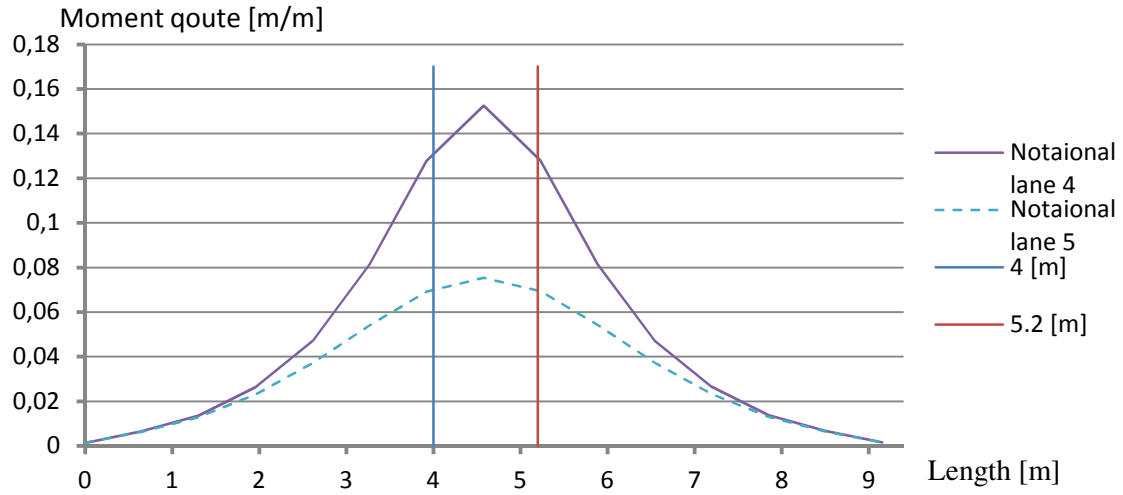


*Figure 5.19- Influence lines for the critical element (no 245) in the slab frame bridge, for 3D shell analysis. The vertical lines shows the positions of the critical axel loads.*

Axle loads were positioned according to figure 4.2 with magnitude according to table 4.2. The positions of the axle loads giving the maximum moments in the critical elements were evaluated graphically from the influence lines. Finally, the maximum moments were calculated for the summing up the moments at the fore critical points were the lines intersect.

### 5.2.3 Evaluation of critical load positions: Method 2

Method 2 works in a similar way as method 1. The critical load position were evaluated in the same way as in method 1.The 3D shell model was then loaded with the point loads in the critical positions. A separate analysis was then done for loading with the point loads, see figure 5.20. From these analysis the maximum bending moment is obtained .

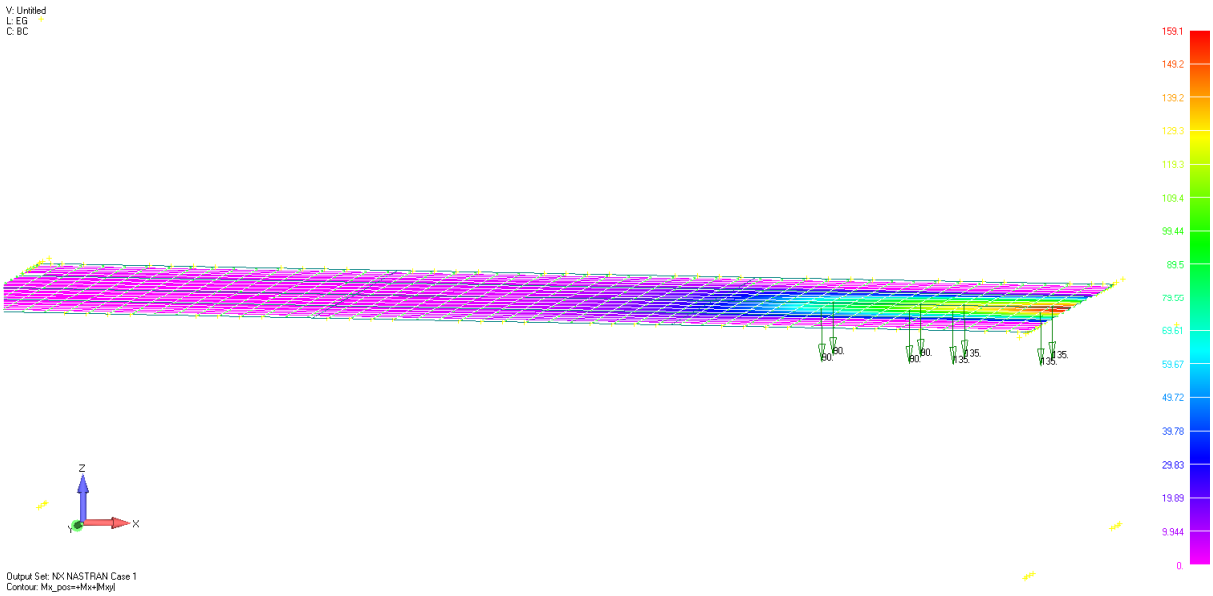


*Figure 5.20- Point load placed in positions that determine the maximum bending moment $m_x$ for the frame slab bridge, for 3D shell analysis.*

### 5.2.4 Envelope of all critical load positions

The two most critical influence lines in the critical load group for an element is summed up in. These have been done for all elements in an envelope. In a similar method an envelope is done in the 2D frame models. The iso plots for the envelops in the 3D shell models are showed below; see Figure 5.22 and 5.23.

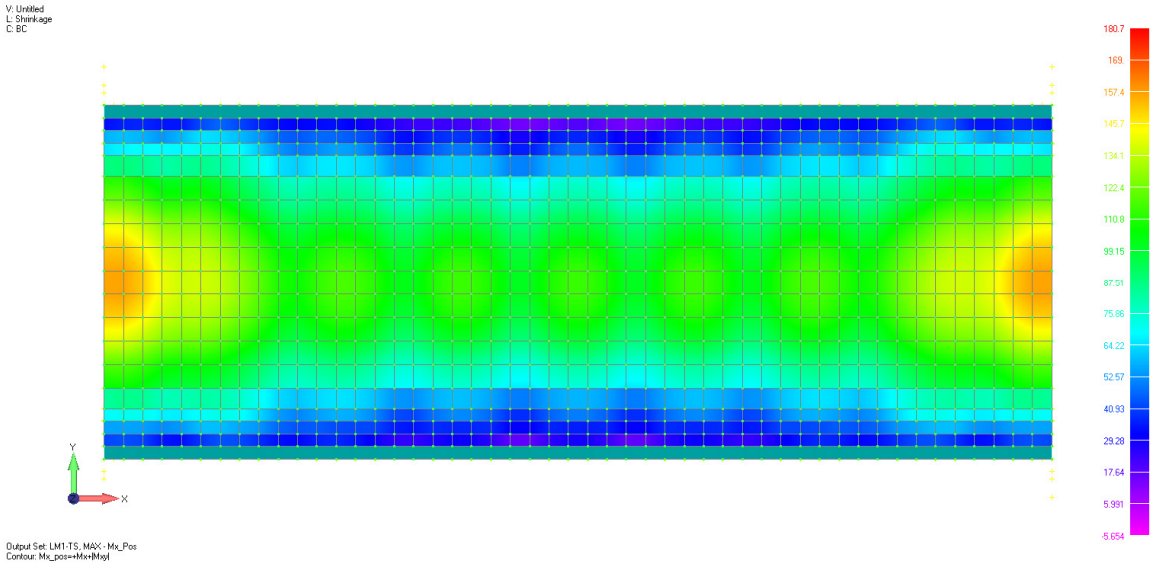


*Figure 5.22- Envelop for positive transvers bending moment for the slab frame bridge for 3D shell analysis..*

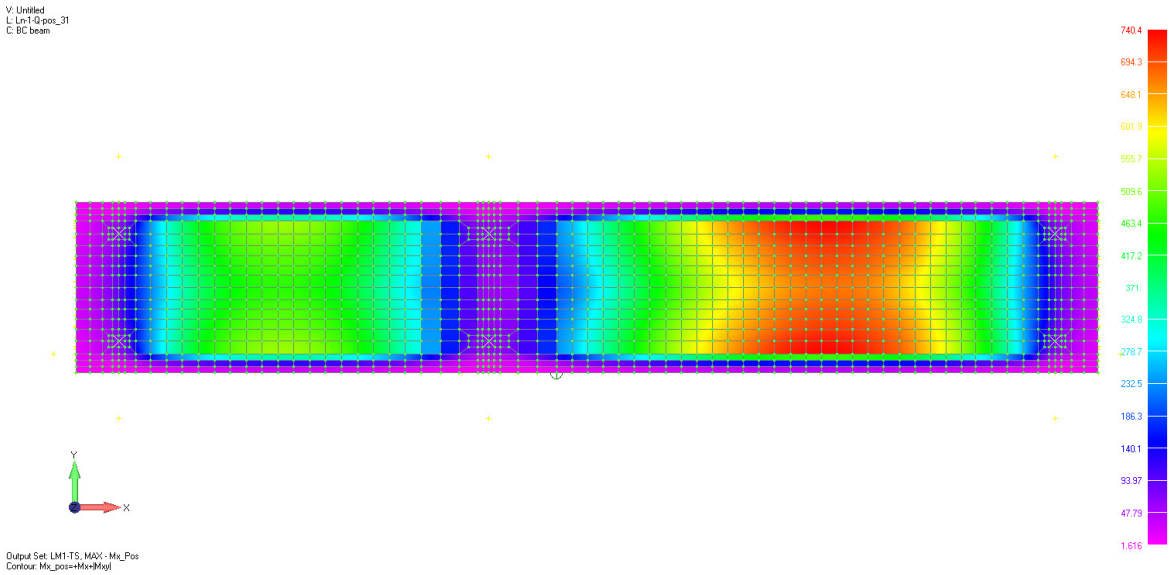


*Figure 5.23 - Envelop for positive bending moment for the slab frame bridge for 3D shell analysis.*

### 5.2.5 Result

The results from 2D and 3D shell for the envelop of all critical load position is presented in the figures below. Results from the slab frame bridge is shown in figure 5.24. The results from the 3D shell model are shown for two strips figure 3.4.

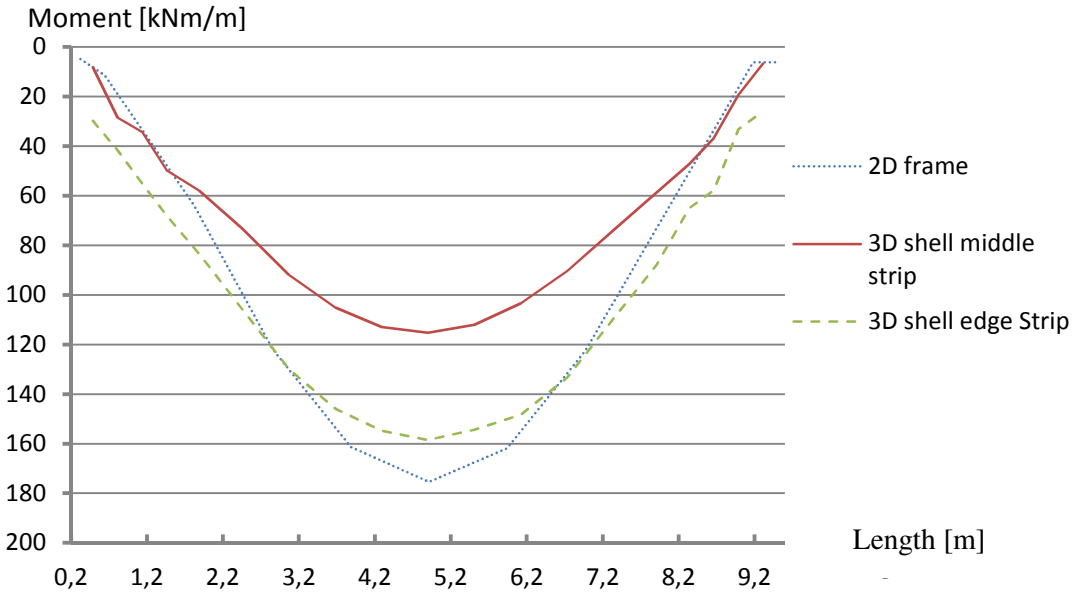


*Figure 5.24- Envelop of the maximum bending moment for 3D shell and 2D frame analysis*

For the slab bridge the corresponding results are plotted in figure 5.25. The result from the3D shell model is from the strips according to figure 3.6.

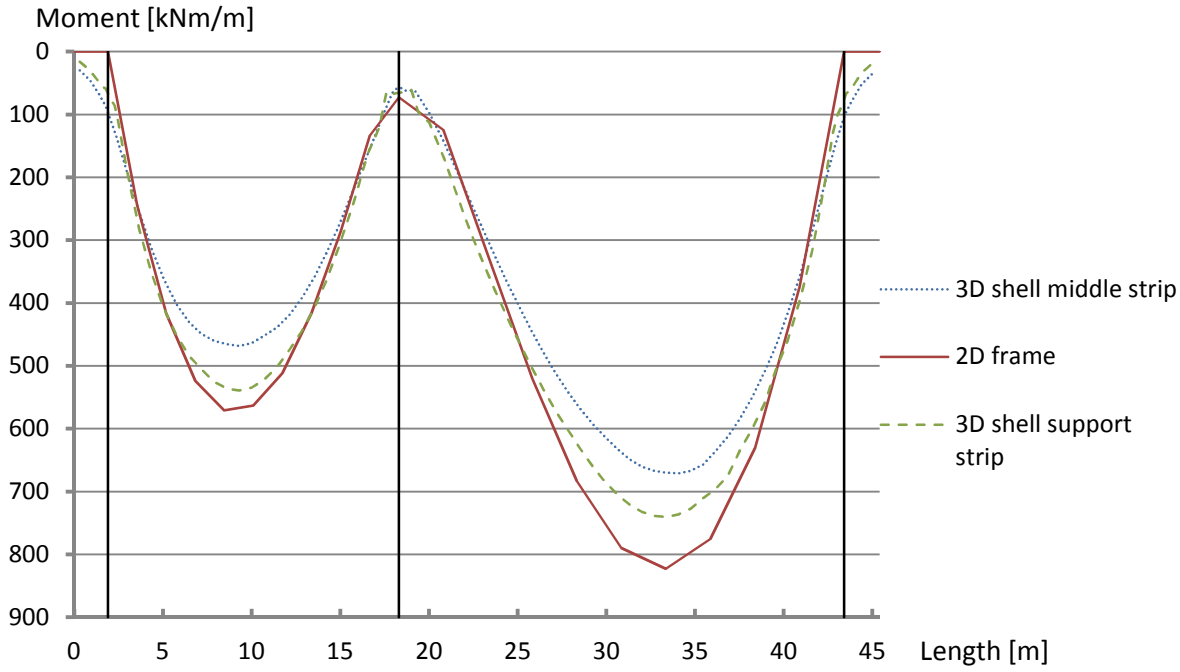


*Figure 5.25 - Envelop of the maximum bending moment for 3D shell and 2D frame analysis*

The results from the two methods for one critical load position are presented in table 5.1 and 5.2 below. The three 3D shell models differ up to 3 % for slab frame bridge

see table 5.1. For the slab bridge the results differ up to 4 % see table 5.2. For the slab Frame Bridge the 2D frame model varies up to 45 % from the 3D shell model depending on which strip or method that is compared see table 5.1. For the slab bridge the results differ up to 20 % see table 5.2 below.

*Table 5.1- Results from 3D shell and 2D frame in kNm/m for the frame slab bridge*

| Slab bridge | End strip | Middle strip |
|---|---|---|
| 3D shell method 1 | 155.9 | 97.1 |
| 3D shell method 2 | 159 | 96.2 |
| 3D shell envelop | 158.5 | 99.4 |
| 2D frame | 175 | 175 |

*Table 5.2- Results from 3D shell and 2D frame in kNm/m for the slab bridge*

| Slab frame bridge | Edge strip | Middle strip |
|---|---|---|
| 3D shell method 1 | 723.4 | 659.5 |
| 3D shell method 2 | 718.5 | 643 |
| 3D shell envelop | 740 | 670.3 |
| 2D frame | 823 | 823 |

### 5.2.6 Discussion

In table 5.1 and 5.2 one could argue that that the difference between 2D frame and the 3D shell are large. However, the difference depends on that the 3D shell models can to a further extend can redistributed load in the transversal direction. Hence, the fact that the 3D shell values are smaller makes the result reasonable. That the central strips are smaller than the critical edge values are also reasonable due to the fact that central strips can redistribute the load in two directions see figure 5.24 and 5.25.

According to table 5.2 the difference between the 3D shell results varies up to 4 % even do that in theory it should be the same result. Hence, it should be mentioned that method 1 is not exact due to that it is graphically slowed. The load positions in method 2 is also graphical slowed and difficulties were obtained when position the point loads at the exact location on the slabs.

## 5.3 2D and 3D analysis for the Slab Bridge

The purpose of this sub-chapter is to compare the results from designs with 3D shell and 2D frame analysis for the slab bridge. The maximum bending moments from the 3D shell analysis have been extracted for two strips, have called support and span strip; see Figure 3.6

### 5.3.1 Results

The maximum bending moment obtained from the 3D shell analysis for the load combination ULS B is 3846 kNm/m and the minimum bending moment is $-5214$ kNm/m. These values are to be compared with a maximum bending moment of 3741 kNm/mand minimum bending moment of $-4523$ kNm/m obtained from

the 2D frame analysis. The highest moments were obtained in the support strip the 3D shell finite element analysis; see Figure 5.26.

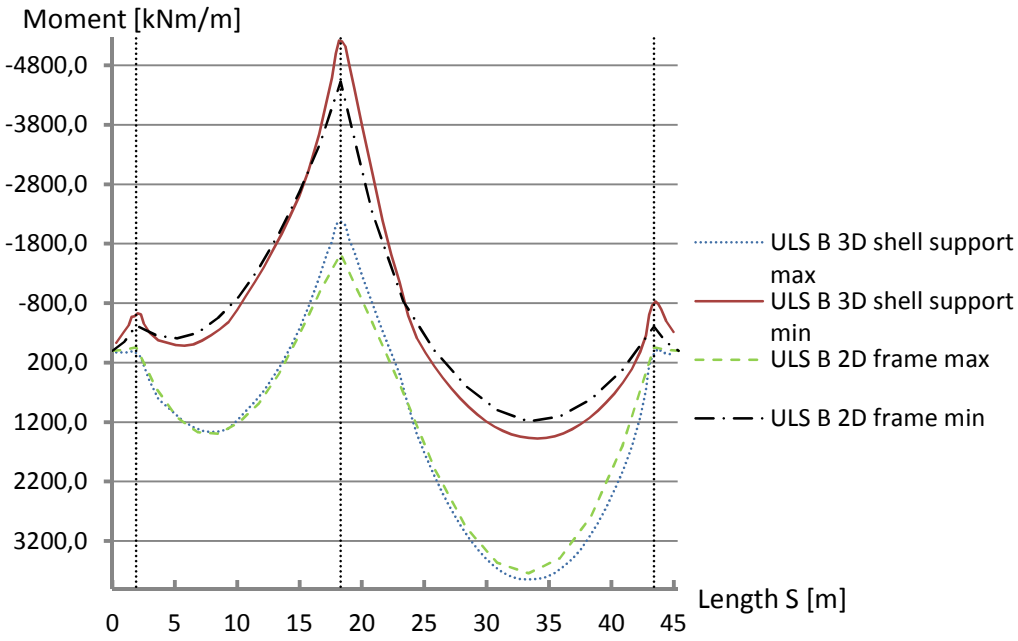


*Figure 5.26- Maximum bending moment distribution in the support strip for the 3D shell analysis, compared to the 2D frame analysis for ULS B. The vertical lines represent the location of the supports.*

The values for the support strip for ULS A are slightly smaller but the load combination shows a corresponding pattern; see Appendix C. For the bending moment in the span strip, the correspondence between the 3D shell- and 2D frame analyses is better. The maximum bending moment obtained from the 3D shell analysis is $3838\ \mathrm{kNm/m}$ and the minimum bending moment is $-4238\ \mathrm{kNm/m}$. The values from the 2D frame analysis are the same. Also for the span strip, the maximum bending moment in the longitudinal direction is larger for the 3D shell model.

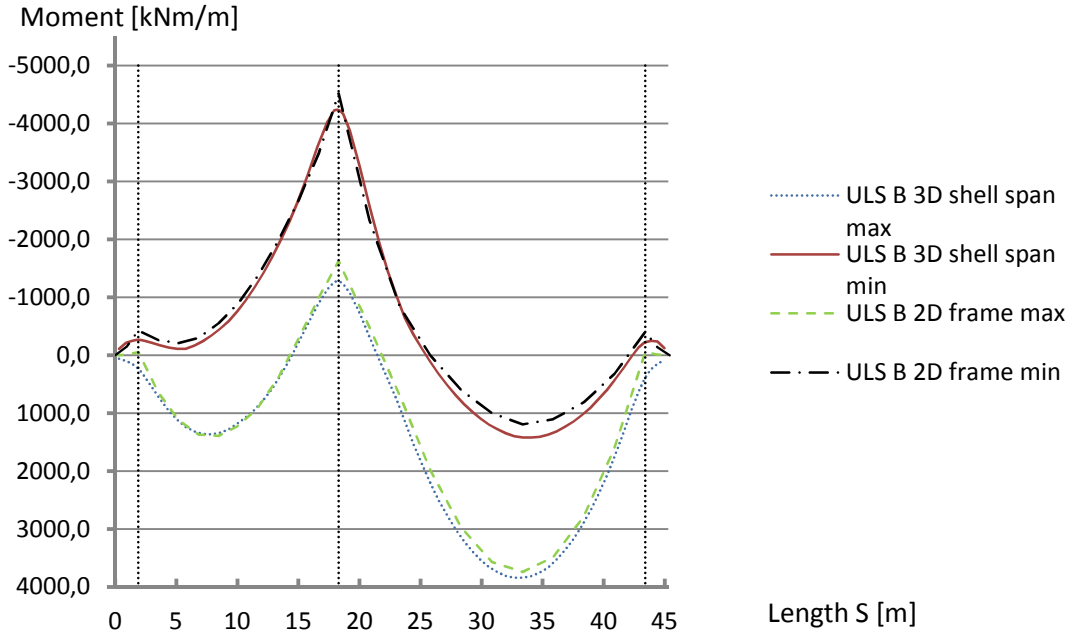


*Figure 5.27- Maximum bending moment distribution in the span strip for the 3D shell analysis, compared to the 2D frame analysis for ULS B. The vertical lines represent the location of the supports.*

### 5.3.2 Discussion

The reason why the 2D frame- and 3D shell models shows differences in results can be explained by redistribution of forces due to stiffness variations. More stiff regions tend to attract forces from adjacent regions with less stiffness and become thereby more stressed. What can be observed from Figures 5.26 and 5.27 is that both the span- and support strip in the 3D shell model exhibit larger moments then those produced by the 2D frame analysis. This can be explained by the geometry of the slab section and by the position of where the values have been extracted. By performing analysis with constant thickness over the slab cross section it becomes obvious that the inclined outer edges of the section have a substantially lower stiffness that the rectangular middle part; see Figure 3.2. This means that load will redistribute transversally from the edges towards the middle and cause the part with full thickness to carry more load. In the 2D frame analysis instead, a strip of 1 m width is used in which no transversal redistribution of force can take place.

An additional observation that can be discerned from Figures 5.26 and 5.27 is that the support strip exhibit larger values of bending moment than the span strip, also in the middle of the main spans. This might seem unexpected because the bending moments in the edge regions reduce due to redistribution. By plotting the bending moment in transverse direction, this can be explained. In order to read out the moments just above the support, the support strip was placed at a certain distance from the edge of the bridge. This caused the support strip to end up in a position which attracts most of the force coming from the redistribution; see Figure 5.28. By observing the graph it appears that the force coming from the outer edge, mainly is absorbed by the adjacent section, in this case at support strip. The further away the strip is the less impact from redistribution it has. The reason for wanting to read out values just above the support

is to be able to compare the influence of singularity problems coming from the 3D shell finite element analysis.

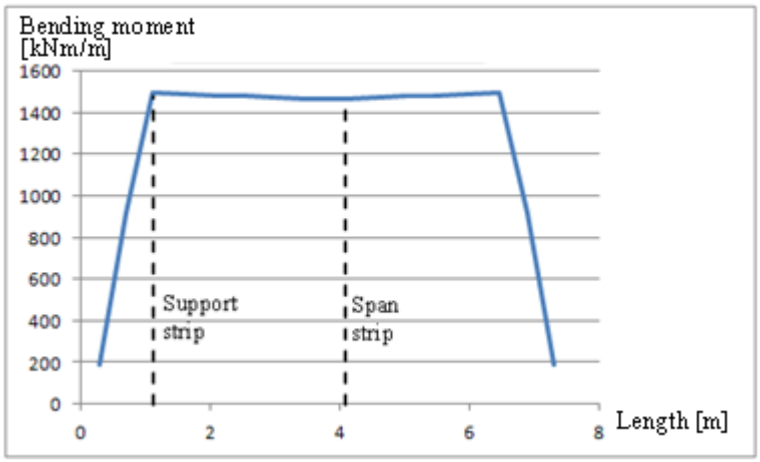


*Figure 5.28- Bending moment distribution for 3D shell analysis in transverse direction for slab bridge. Location of support- and span strip in transversal direction.*

The maximum bending moment over the mid support calculated with the 3D shell analysis is 5304 $kNm/m$ which can be compared with corresponding moment from the 2D frame analysis of 4523 kNm/m. A rather high difference can be observed which will require a higher amount of reinforcement over the columns.

## 5.4 2D and 3D analysis for the Slab Frame Bridge

The purpose of this sub chapter is to compare the results from design with 3D FE shell and 2D frame analysis for the slab frame bridge. The maximum bending moment for the 3D shell analysis has been extracted from two strips, middle-and edge strip; see Figure 3.11.

### 5.4.1 Results

For the middle strip the maximum bending moment for ULS B is312 kNm/m. The minimum bending moment is−347.4 kNm/m for ULS B. These values are to be compared with the values from the 2D frame analysis where the maximum bending moment is 341kNm/m and minimum bending moment value is −465.6 kNm/m; see Figure 5.29.

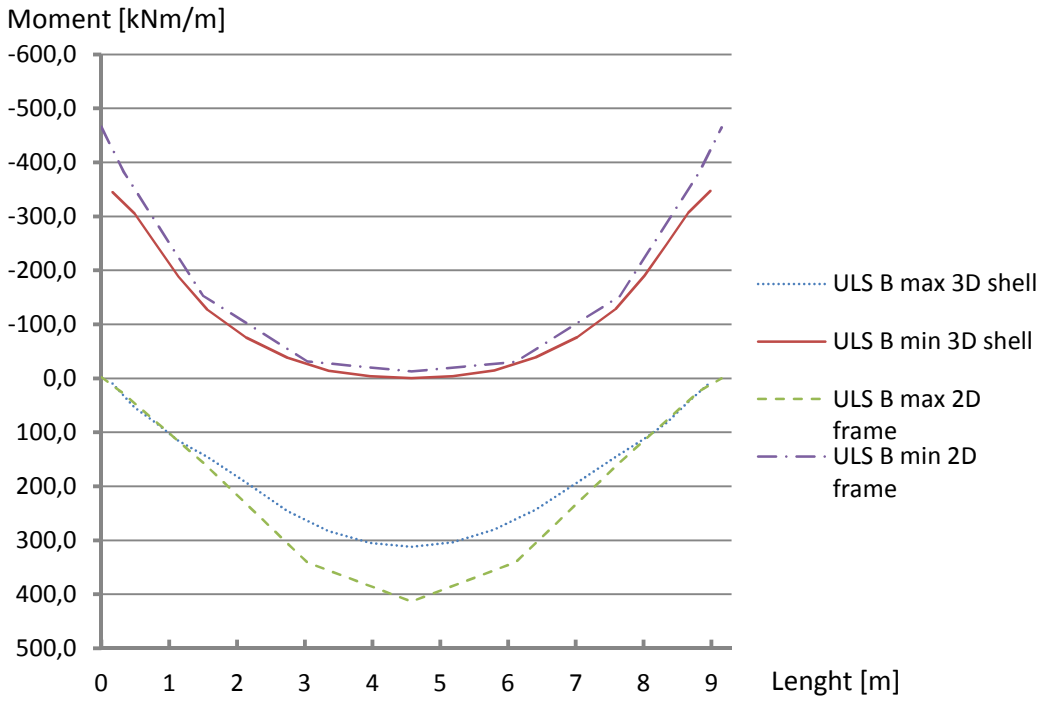


*Figure 5.29 Bending moment distribution in the middle strip for ULS B for 3D shell and 2D frame analysis*

For the end strip, the difference between the 3D shell and the 2D frame analysis is smaller, as can been seen in Figure 5.31. The maximum bending moment in the edge strip is $382\ \mathrm{kNm/m}$ for ULSB. The maximum of the minimum value is $-395.9\ \mathrm{kNm/m}$ for ULS B.

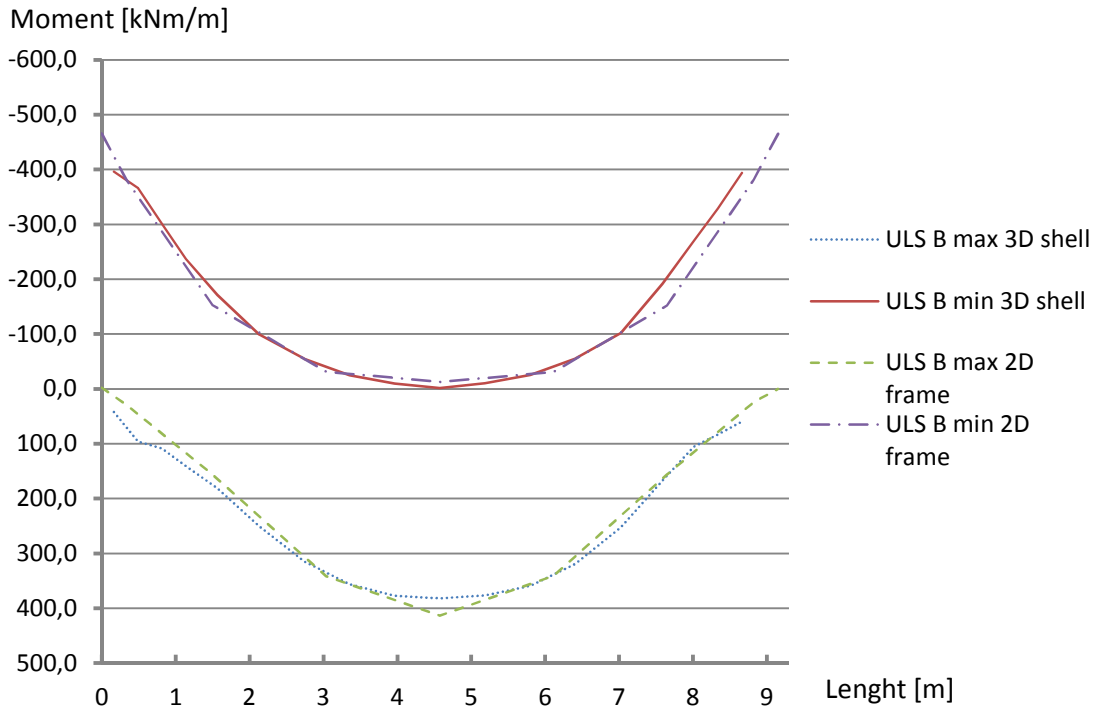


*Figure 5.30 Bending moment distribution in the edge strip for ULS B for 3D shell and 2D frame analysis*

To be able to compare the models in an more accurate way the reinforcement in the transversal direction have been calculated. As can be seen in table 5.3 below, more reinforcement is required for the 3D shell analysis. For the 2D frame analysis only the minimum required amount of reinforcement is provided in the transversal direction.

*Table 5.3 – The table contains the maximum and minimum bending moment for the models in [kNm/m]. It also contains the reinforcement amount in the transversal directional [mm^2/m]*

| | 3D shell | | | | 2D frame | | | |
|---|---|---|---|---|---|---|---|---|
| | Longitudinal | | Transversal | | Longitudinal | | Transversal | |
| | ULS | SLS | ULS | SLS | ULS | SLS | ULS | SLS |
| max moment | 382 | 109.5 | 237.4 | 79.17 | 413.4 | 108.41 | - | - |
| min moment | -395.9 | -114.5 | -265.3 | -77.98 | -465.62 | -122.16 | - | - |
| max reinforcement | | | 1309 | 1309 | | | 400 | 400 |
| min reinforcement | | | 1571 | 1571 | | | 400 | 400 |

## 5.4.2 Discussion

By comparing the 2D frame analysis with the 3D shell analysis, it can be seen that the values from the 2D analysis are generally larger. This is most clear for the middle strip where the largest difference is obtained. The values from the edge strip obtained from the 3D shell analysis has got a better correlation with the 2D frame analysis. The reason why the results differ is that the 3D shell analysis to a further extent can redistribute load in the transversal direction. The middle strip can redistribute the load

in two directions; due to this it got the largest difference compared to the 2D frame analysis. The edge strip can only redistribute the load in one direction which result in less redistribution.

Even if the 2D frame analysis has got a larger maximum bending moment, it is not clear if this will result in larger reinforcement amounts, the 3D shell analysis has up to five times larger need of reinforcement in the transversal direction. As can be seen in Table 5.3.

# 6 Conclusion

### 6.1.1 Temperature study

One of the aims of the thesis was to perform a thermal action study in order to evaluate the most suitable way to apply thermal actions in FE analysis. Three different ways to apply the temperature loads were evaluated and formed the basis for the selection of load application in the 3D shell FE models. By preventing the integral abutment walls from curving, the correct location of maximum membrane forces was obtained. This means that when creating a 3D shell model of a slab frame bridge in an FE software, the integral abutment walls can be given vertical restraints at the bottom slab in order to reflect the reality.

The second parameter that was evaluated was the effect of different ways to model the temperature variations. The aim was to apply the load in order to obtain as realistic membrane forces as possible. The conclusion that can be drawn from the results is that the most realistic way to model the temperature load, with a linear variation over the integral abutment wall, gives reasonable membrane forces and hence require reasonable amount of reinforcement. In design, cracked sections and an effective modulus of elasticity should be used, which reduces the initial stiffness with about 50-60 %.

### 6.1.2 Point load evaluation

One of the objectives of the thesis was to investigate the difference of design results for one critical load position with all load combinations using envelopes of maximum load actions. The comparison shows that different ways to determine the load effect show small differences and that the variations in results are rather depending on approximations in the graphical method. However, a notable difference in result between the 3D shell and 2D frame analysis is obtained, which depends on that the 3D shell model can redistribute the load in the transverse direction.

### 6.1.3 Slab Bridge and slab frame Bridge

The main interest of this report was to study the difference between 3D shell and 2D frame analysis for system analysis of slab bridges. It has already been established that the 3D shell models have benefits in contrast to the 2D frame by capturing the real structural behavior. However, possible increase of design forces coming from 3D shell models has not been enough investigated.

The maximum bending moment for the slab bridge was found to become slightly higher in the longitudinal direction for the 3D shell model compared to the 2D frame model, see figure 5.25 and 5.26. Nevertheless, The conclusion from the case study is that the 2D frame analysis is sufficient for design of the main reinforcement in the longitudinal direction but gives a solution on the unsafe side for the reinforcement in the transversal direction.

Existing bridges in Sweden today designed with the 2D frame method are often proved to remain either un-cracked or with small longitudinal cracks under service conditions. One could argue that the bridges becomes unnecessary strong with the 3D shell analysis, even if the 3D shell models in a better way describe the structural behavior. However, even if the bridge has not cracked in reality it does not mean that it is designed in a sufficient way. It rather tells us that the bridge designed with 2D frame analysis has not been designed for the forces it should have been designed for, due to that the 3D shell theory is a better way to model bridge structures.

The maximum bending moment in the longitudinal direction for the slab frame bridge is larger for the 2D frame analysis than for the 3D shell analysis. The conclusion that can be drawn from this is that the 2D frame analysis are sufficient in the longitudinal direction and provides a solution on the safe side.

However, what this leads to in an overall design situation is hard to draw any conclusion from. Based on reinforcement calculations for the 3D shell analysis it becomes clear that it has almost four times higher need of reinforcement in the transversal direction compared to the 2D frame analysis. The conclusion that can be drawn from this is that the 2D frame analysis do not describe the bending moment in the transversal direction in a proper theoretical way. However, major problems are not yet observed on most of the existing bridges.

Economics is an important aspect of engineering today. The work effort to perform a 3D shell analysis is much larger than for a 2D frame analysis. Only the verification of 3D shell analysis is a similar work effort as the whole 2D frame model.

### 6.1.4 Suggestions for further research

As one part, future studies can be performed as a continuation on this thesis. The results obtained and conclusions drawn were based on several assumptions regarding geometry and boundary conditions. As a future study, these boundary conditions can be varied in order to find an improved way of modeling. In this thesis a rather limited evaluation of boundary conditions in vertical direction was performed, which can be further refined. Also the geometry should be varied in order to verify that the conclusions are valid for geometrical variations for bridges of the same type. This could be made as a parameter study where the slab bridge and frame slab bridge are modeled with varying length, thickness and width.

As another part of further studies, a continuation on existing research fields can be resumed. Oscar Lars, (2012) has presented a new model for calculating the temperature at different positions for different structures based on climate data for the site. In order to be able to use this knowledge for FEM modeling, a suitable modeling methodology needs to be developed. This will be useful in order to be able to apply the thermal loads in a more correct way.

# 7 References


Blaauwendraad, J (2010): *Plates and FEM: Surprises and Pitfalls*. Springer Dordrecht Heidelberg, London (2010).

Davidson, M (2003): *Struktur analyser av bro konstruktiner med FEM-fördelning av krafter och moment*, Brosamverkan Väst. Göteborg .

Eurocode 1 CEN: (2002). Actions on structures – Part 2: Traffic loads on bridges, pr EN 1991-2, Brussels 2003

Eurocode 2 CEN: (2001). Design of concrete structures –Genaral Rules and Rules for Buildings, pr EN 1992-1, Brussels 2001

Engström, B (2007): *Design and analysis of continuous beams and columns.* Chalmers University of Technology, Göteborg, Sweden.

Engström, B (2003): Chapter 3.1 in Davidsson (2003): *Struktur analyser av bro konstruktiner med finita element metod -fördelning av krafter och moment*, Brosamverkan Väst. Göteborg.

Engström, B (2011): *Design and analysis of slabs and flat slabs.* Chalmers University of Technology, Göteborg, Sweden, pp. 9-14.

Rombach, G A. (2004): *Finite element design of concrete structures*. Thomas Telford Ltd, London, England, (2004)

Ottosen, N & Petersson, H. (1992): *Introduction to the Finite Element Method.* Prentice Hall, London, United Kingdom.

Samuelsson, A & Wiberg, N. (1998): Finite Element Method- Basics. Studentlitterature, Lund, Sweden.

Ingengöresfirma Åke Bengtsson AB: STRIP STEP 2 version PC-05, Stockholm 2004

Michigan Tech (2011), http://www.me.mtu.edu/~bettig/MEEM4405/Lecture12.pdf, MEEM4405 Introduction to Finite Element Analysis. 2011-11-21

Plos,M. (2007): Chapter 5 in Sustainable Bridges. Non-Linear Analysis and Remaining Fatigue Life of Reinforced Concrete Bridges.Background document D4.5. Chalmers, Göteborg, {Sweden},{2007}

Vägverket(2009): TK Bro, Banverket: BVS 1583.10 Publikation Vägverket: 2009:27, ISSN: 1401-9612

Vägverket(2009): TR Bro, Banverket: BVH 1583.10 Publikation Vägverket: 2009:28, ISSN: 1401-9612

Siemens PLM (2008): - Quick Reference Guide. http://www.kxcad.net/ugs/NX-Nastran/NX-Nastran-Users-Guid.pdf , 2012-06-07

# APPENDIX A – Calculation of loads

## A.1 Pavement

$$\gamma_{bel} := 24\frac{kN}{m^3}$$

10 mm isolation carpet, 2 layers
50 mm protection concrete
50 mm ABb
40 mmABs

$$t_{bel} := 150mm$$

$$g_{bel} := \gamma_{bel} \cdot t_{bel} = 3.6 \cdot \frac{kN}{m^2}$$

## A.2 Shrinkage

Calculation of shrinkageof slab bridgeaccording to EN 1992-1-1_2005 (3.1.4)

$$t := 70 \cdot 365 = 2.555 \times 10^4 \qquad \alpha := 1 \cdot 10^{-5}$$

$$t_s := 5$$

$$A_c := 8.023\,m^2$$

$$u := \left[\sqrt{(1.192m - 0.3m)^2 + (0.846m)^2} + 0.3m + 2.954m\right] \cdot 2 + 7.6m = 16.567 \cdot m$$

$$h_0 := 2 \cdot \frac{A_c}{u} = 0.969 \cdot m$$

$K_h$ is a coefficient that depends on the fictive thickness $h_0$

*Tabel A.1 –values of $K_h$*

| $h_0$ | $K_h$ |
|---|---|
| 100 | 1.0 |
| 200 | 0.85 |
| 300 | 0.75 |
| ≥ 500 | 0.70 |

$$k_h := 0.7$$

$$\beta_{ds}(t,t_s) = \frac{(t-t_s)}{(t-t_s)+0.04\sqrt{h_0^3}}$$

where:

t is the age of the concretein days

t.s is the age of the concrete (days) at the beginning of the drying shrinkage
This is normal at the end of the post treatment

h.0 is the fictive thickness (mm) of the cross-section =2A.0/u

where:

A.0 concrete section´s area

u is the circumferencefor the part of the cross-sectionthat is exposed of drying

$$\beta_{ds} := \frac{(t-t_s)}{(t-t_s)+0.04\cdot\sqrt{0.969^3}} = 1$$

Baseline for shrinkagefrom drying. ε .cd.0 can be calculated with following expression:

$$\varepsilon_{cd.0} := 0.85\cdot\left[(220+110\cdot\alpha_{ds.1})\cdot e^{\left(-\alpha_{ds.2}\cdot\frac{f_{cm}}{f_{cmo}}\right)}\right]\cdot 10^{-6}\cdot\beta_{RH}$$

där:

f.cm is the meanvalue of the compressive strength [MPa]

f.fm0 =10 [MPa)

α .ds1 coefficient depending on cementtype
= 3 for cementclass S
= 4 for cementclass N
= 6 for cementclass R

α .ds2 coefficient depending on cementtype
= 0.13 for cement class S
= 0,12 for cement class N
= 0.11 for cement class R

RH is the surroundings relative humidity [%]

RH.0 = 100%

$\alpha_{ds.1} := 4$

For cementclass N (for bridges)

$\alpha_{ds.2} := 0.12$

$RH_0 := 100$

$RH := 80$

$f_{cmo} := 10MPa$

$f_{cm} := 43MPa$

$$\beta_{RH} := 1.55 \cdot \left[ 1 - \left( \frac{RH}{RH_0} \right)^3 \right] = 0.756$$

$$\varepsilon_{cd.0} := 0.85 \cdot \left[ (220 + 110 \cdot \alpha_{ds.1}) \cdot e^{\left( -\alpha_{ds.2} \cdot \frac{f_{cm}}{f_{cmo}} \right)} \right] \cdot 10^{-6} \cdot \beta_{RH} = 0.025 \cdot \%$$

$$\varepsilon_{cd}(t) := \beta_{ds}(t, t_s) \cdot k_h \cdot (\varepsilon_{cd.0})$$

$$\varepsilon_{cd} := \beta_{ds} \cdot k_h \cdot \varepsilon_{cd.0} = 1.773 \times 10^{-4}$$

The autogenousshrinkageis obtained from:

$$\varepsilon_{ca}(t) := \beta_{ds}(t) \cdot \varepsilon_{cs}(\infty)$$

where:

$$\varepsilon_{ca}(\infty) := 2.5(f_{ck} - 10) \cdot 10^6$$

and:

$$\beta_{ds}(t) := 1 - \exp(-0.2 \cdot t^{0.5})$$

where: t is expressed in days

$f_{ck} := 35$

$$\varepsilon_{ca.inf} := 2.5 \cdot (f_{ck} - 10) \cdot 10^{-6} = 0.00625 \cdot \%$$

$$\beta_{as} := 1 - e^{(-0.2 \cdot t^{0.5})} = 1$$

$$\varepsilon_{ca} := \beta_{as} \cdot \varepsilon_{ca.inf} = 6.25 \times 10^{-5}$$

$$\varepsilon_{cs} := \varepsilon_{ca} + \varepsilon_{cd} = 0.024 \cdot \%$$

Calculation of the creep rate:

$$\alpha_1 := \left(35\frac{MPa}{f_{cm}}\right)^{0.7} = 0.866$$

$$\alpha_2 := \left(35\frac{MPa}{f_{cm}}\right)^{0.2} = 0.96$$

$$\alpha_3 := \left(\frac{35MPa}{f_{cm}}\right)^{0.5} = 0.902$$

$$h_{0.} := 0.968 \quad m$$

$$v := \begin{bmatrix} 1.5\cdot\left[1 + (0.012\cdot RH)^{18}\right]\cdot\frac{h_0}{mm} + \left(250\cdot\alpha_3\right) \\ 1500\cdot\alpha_3 \end{bmatrix}$$

Factor taking the relative humidity into consideration:

$$\varphi_{RH} := \left[\left[1 + \frac{\left(1 - \frac{RH}{100}\right)}{0.1\cdot\sqrt[3]{\frac{h_0}{mm}}}\right]\cdot\alpha_1\right]\cdot\alpha_2 = 0.999$$

for f.cm larger than 35 MPa

Factor taking the compressive strength of concrete into consideration:

$$\beta_{f.cm} := \frac{16.8}{\sqrt{\frac{f_{cm}}{MPa}}} = 2.562$$

Factor taking concrete age at loading into consideration:

$$\beta_t := \frac{1}{\left(0.1 + t_s^{0.20}\right)} = 0.676$$

Nominal creep rate:

$$\varphi_0 := \varphi_{RH}\cdot\beta_{f.cm}\cdot\beta_t = 1.676$$

$$\beta_H := \min(v) = 1.353\times 10^3$$

Koefficient describingshrinkage development over time after loading

$$\beta_c := \left[\frac{\left(t - t_s\right)}{\beta_H + t - t_s}\right]^{0.3} = 0.985$$

Creep rate$\varphi$is calculated according to:

$$\varphi := \varphi_{RH}\cdot\beta_{f.cm}\cdot\beta_t\cdot\beta_c = 1.65 \qquad \varphi_{ny} := 1.93$$

Even shrinkage is in system calculation consideredas an even temperature changeadjusted with respect to shrinkage

Because the creep rate is low compared to previous norm,
It is assumed to be equal to 1.95

Recalculate the shrinkage effect due to a temperature load.

$$\Delta T := \frac{\left(\varepsilon_{cs} - \varepsilon_{ca}\right)}{\left[\alpha\cdot\left(1 + \varphi_{ny}\right)\right]} = 6.051$$

Calculation of shrinkage for bottom slab of frame slab bridge 70 yearsaccording: EN 1992-1-1_2005 (3.1.4)

$t := 70 \cdot 365 = 2.555 \times 10^{4}$ $\alpha := 1 \cdot 10^{-5}$

$t_s := 5$

$A_c := 7.65\,m^2$

$u := 11.7\,m$

$h_0 := 2 \cdot \frac{A_c}{u} = 1.308 \times 10^{3} \cdot mm$

$k_h := 0.7$

$\alpha_{ds.1} := 4$ for cementclass N (for bridges)

$\alpha_{ds.2} := 0.12$

$RH_0 := 100$

$RH := 80$

$f_{cmo} := 10\,MPa$

$f_{cm} := 43\,MPa$

$f_{ck} := 35\,MPa$

$$\varepsilon_{cd.0} := 0.85 \cdot \left[ \left( 220 + 110 \cdot \alpha_{ds.1} \right) \cdot e^{\left( -\alpha_{ds.2} \cdot \frac{f_{cm}}{f_{cmo}} \right)} \right] \cdot 10^{-6} \cdot \beta_{RH} = 0.025 \cdot \%$$

$$\beta_{ds} := \frac{\left( t - t_s \right)}{\left( t - t_s \right) + 0.04 \cdot \sqrt{\left( \frac{h_0}{mm} \right)^3}} = 0.931$$

$\varepsilon_{cd} := \beta_{ds} \cdot k_h \cdot \varepsilon_{cd.0} = 1.651 \times 10^{-4}$

$\beta_{as} := 1 - e^{\left( -0.2 \cdot t^{0.5} \right)} = 1$

$$\varepsilon_{ca.inf} := \left[ 2.5 \cdot \left( \frac{f_{ck}}{MPa} - 10 \right) \cdot 10^{-6} \right] = 0.00625 \cdot \%$$

$\varepsilon_{ca} := \beta_{as} \cdot \varepsilon_{ca.inf} = 6.25 \times 10^{-3} \cdot \%$

$\varepsilon_{cs.70.years} := \varepsilon_{ca} + \varepsilon_{cd} = 0.023 \cdot \%$

Calculation of shrinkage for bottom slab of frame slab bridge 6 monthsaccording to EN 1992-1-1_2005 (3.1.4)

$t := 6 \cdot 30 = 180$ $\alpha := 1 \cdot 10^{-5}$

$t_s := 5$

$A_c := 7.65\,m^2$

$u := 11.7\,m$

$h_0 := 2 \cdot \frac{A_c}{u} = 1.308 \times 10^3 \cdot mm$

$k_h := 0.7$

$\alpha_{ds.1} := 4$ for cementclass N (for bridges)

$\alpha_{ds.2} := 0.12$

$RH_0 := 100$

$RH := 80$

$f_{cmo} := 10\,MPa$

$f_{cm} := 43\,MPa$

$f_{ck} := 35\,MPa$

$$\varepsilon_{cd.0} := 0.85 \cdot \left[ \left( 220 + 110 \cdot \alpha_{ds.1} \right) \cdot e^{\left( -\alpha_{ds.2} \cdot \frac{f_{cm}}{f_{cmo}} \right)} \right] \cdot 10^{-6} \cdot \beta_{RH} = 0.025 \cdot \%$$

$$\beta_{ds} := \frac{\left( t - t_s \right)}{\left( t - t_s \right) + 0.04 \cdot \sqrt{\left( \frac{h_0}{mm} \right)^3}} = 0.085$$

$\varepsilon_{cd} := \beta_{ds} \cdot k_h \cdot \varepsilon_{cd.0} = 1.501 \times 10^{-5}$

$\beta_{as} := 1 - e^{\left( -0.2 \cdot t^{0.5} \right)} = 0.932$

$$\varepsilon_{ca.inf} := \left[ 2.5 \cdot \left( \frac{f_{ck}}{MPa} - 10 \right) \cdot 10^{-6} \right] = 0.00625 \cdot \%$$

$\varepsilon_{ca} := \beta_{as} \cdot \varepsilon_{ca.inf} = 5.823 \times 10^{-3} \cdot \%$

$\varepsilon_{cs.6.months} := \varepsilon_{ca} + \varepsilon_{cd} = 7.324 \times 10^{-3} \cdot \%$

$\Delta\varepsilon := \varepsilon_{cs.70.years} - \varepsilon_{cs.6.months} = 0.015 \cdot \%$

Calculation of shrinkage for abutments for frame slab bridge 6 monthsaccording to EN 1992-1-1_2005 (3.1.4)

$t := 70 \cdot 365 = 2.555 \times 10^{4}$ $\alpha := 1 \cdot 10^{-5}$

$t_s := 5$

$A_c := 14.5\,m^2$

$u := 42.7m$

$h_0 := 2 \cdot \frac{A_c}{u} = 679.157\,mm$

$k_h := 0.7$

$\alpha_{ds.1} := 4$ for cementclass N (for bridges)

$\varepsilon_{cd.0} := 0.85 \cdot \left[ \left( 220 + 110 \cdot \alpha_{ds.1} \right) \cdot e^{\left( -\alpha_{ds.2} \cdot \frac{f_{cm}}{f_{cmo}} \right)} \right] \cdot 10^{-6} \cdot \beta_{RH} = 0.025 \cdot \%$

$\beta_{ds} := \frac{\left( t - t_s \right)}{\left( t - t_s \right) + 0.04 \cdot \sqrt{\left( \frac{h_0}{mm} \right)^3}} = 0.973$

$\varepsilon_{cd} := \beta_{ds} \cdot k_h \cdot \varepsilon_{cd.0} = 1.725 \times 10^{-4}$

$\beta_{as} := 1 - e^{\left( -0.2 \cdot t^{0.5} \right)} = 1$

$\varepsilon_{ca.inf} := \left[ 2.5 \cdot \left( \frac{f_{ck}}{MPa} - 10 \right) \cdot 10^{-6} \right] = 0.00625 \cdot \%$

$\varepsilon_{ca} := \beta_{as} \cdot \varepsilon_{ca.inf} = 6.25 \times 10^{-3} \cdot \%$

$\varepsilon_{cs.frame} := \varepsilon_{ca} + \varepsilon_{cd} = 0.024 \cdot \%$

$\Delta T_1 := \frac{\left( \varepsilon_{cs.frame} - \Delta\varepsilon \right)}{\left[ \alpha \cdot \left( 1 + \varphi_{ny} \right) \right]} = 2.754$ with reduction of integral abutment wall

$\Delta T_2 := \frac{\left( \varepsilon_{cs.frame} \right)}{\left[ \alpha \cdot \left( 1 + \varphi_{ny} \right) \right]} = 8.021$ without reduction of integral abutment wall

## A.3 Variable loads

### A.3.1 Traffic loads–loadmodel 1 (LM-1) according to EN1991-2 (4.3.2) + Appendix NA 4.3.2(3)

*Tabel A.2 –Number of notional lanes and their widths*

| Carriageway width $w$ | Number of notional lanes | Width of a notional lane $w_1$ | Width of the remaining area |
|---|---|---|---|
| $w$<5,4 m | $n_1 = 1$ | 3 m | $w$ - 3 m |
| 5,4 m ≤ $w$ < 6 m | $n_1 = 2$ | $\frac{w}{2}$ | 0 |
| 6 m ≤ $w$ | $n_1 = Int\left(\frac{w}{3}\right)$ | 3 m | $w - 3 \cdot n_1$ |

# For slab bridge

$w := 7.5 \cdot m$

$n_1 := \left(\frac{w}{3}\right) = 2.5m$

$w_1 := 3 \cdot m$

Width of remaining area:

$p := w - 2 \cdot w_1 = 1.5m$

# For frame slab bridge

$w := 24.5 \cdot m$

$n_1 := \left(\frac{w}{3}\right) = 8.167m$

$w_1 := 3 \cdot m$

Width of remaining area:

$p := w - 8 \cdot w_1 = 0.5m$

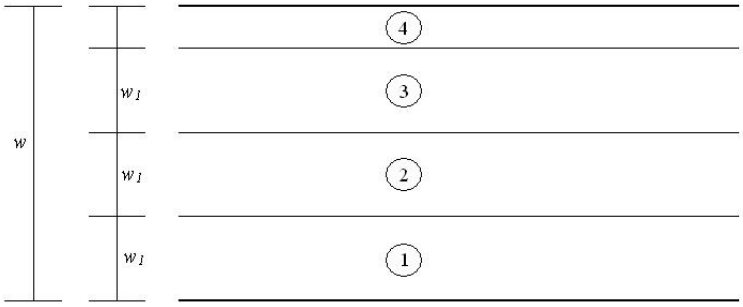


Explanation:
w Carriageway width
w1 Width of notional lane
1 Notional lane nr.1
2 Notional lane nr.2
3 Notional lane nr.3
4 Remaining area

*Figure A.1 –Example of the numbering of notional lanes in the general case*

Loadmodel 1 consists of two subsystems:
-One loadgroup with double axels (boggeisystem), whereeither axelloadhave the weightα q*Qk
-Evenly distributed loads with the weightper square meter laneα q*qk

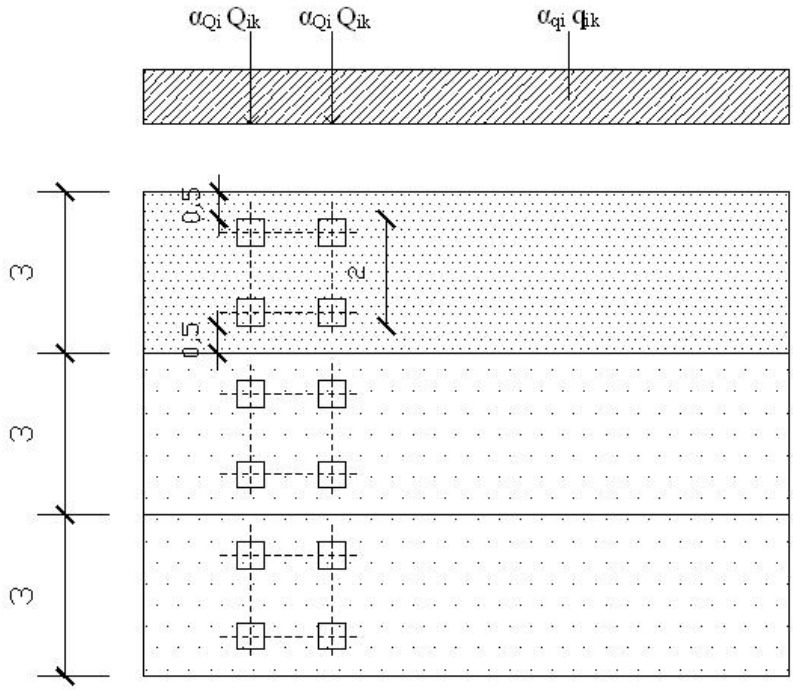


Explanation:
(1) Notional lane number 1: Q.1k=300kN; q.1k=9kN/m^2
(2) Notional lane number 2: Q.2k=200kN; q.2k=2.5kN/m^2
(3) Notional lane number 3: Q.3k=0 kN; q.3k=2.5kN/m^2

w=3.0 m

*Figure A.2 –Application of load model 1*

Notional lane number1:

$Q_{1k} := 300kN$

$\alpha_{Q1} := 0.9$

$q_{1k} := 9.0\frac{kN}{m^2}$

$\alpha_{q1} := 0.7$

For strip step correct the load to a 1.0m strip f=1/3

$f := \frac{1}{3}$

TS

$Q_1 := Q_{1k} \cdot \alpha_{Q1} = 270 \cdot kN$

$Q_{1.ss} := Q_1 \cdot f = 90 \cdot kN$

UDL

$q_1 := q_{1k} \cdot \alpha_{q1} = 6.3 \cdot \frac{kN}{m^2}$

Notional lane number2:

$Q_{2k} := 200kN$

$\alpha_{Q2} := 0.9$

$q_{2k} := 2.5\frac{kN}{m^2}$

$\alpha_{q2} := 1.0$

TS

$Q_2 := Q_{2k} \cdot \alpha_{Q2} = 180 \cdot kN$

$Q_{2.ss} := Q_2 \cdot f = 60 \cdot kN$

UDL

$q_2 := q_{2k} \cdot \alpha_{q2} = 2.5 \cdot \frac{kN}{m^2}$

For frame slab bridge, calculation of loads for notional lane number3:

$Q_{3k} := 0kN$

$\alpha_{Q3} := 0$

$q_{3k} := 2.5\frac{kN}{m^2}$

$\alpha_{q3} := 1.0$

TS

$$Q_3 := Q_{3k} \cdot \alpha_{Q3} = 0 \cdot kN$$

UDL

$$q_3 := q_{3k} \cdot \alpha_{q3} = 2.5 \cdot \frac{kN}{m^2}$$

Load model 2 and 3 are not considered!

### A.3.2 Temperature change according to EN 1991-1-5, Ch 6)

$$\alpha = 1 \times 10^{-5}$$

***Even Temperature change***

$$T_{max} := 36$$

Referes to Stockholm
[EN 1991-1-5, Appendix NB]

$$T_{min} := -29$$

$$T_0 := 10$$

[EN 1991-1-5, Appendix A, A1 (3)]
Bridge Type 3

[EN 1991-1-5, 6.1.1 (1)]

Secondary forces adjusted with respect to shrinkage

$$\varphi_{temp} := 1.23$$

$$\frac{\Delta T_{N.con}}{\varphi_{temp}} = -27.642$$

$$\frac{\Delta T_{N.exp}}{\varphi_{temp}} = 23.577$$

***Temperature difference***

Method 1 - vertical, linear temperature difference

$$T_{e.max} := 39$$

$$T_{e.min} := -24$$

The span forevenly distributed temperature component in bridges:

$$\Delta T_{M.heat} := 15$$

$$\Delta T_{M.cool} := -8$$

$$\Delta T_{N.con} := \left(T_0 - T_{e.min}\right) \cdot -1 = -34$$

$$\Delta T_{N.exp} := T_{e.max} - T_0 = 29$$

$$k_{sur.heat} := 0.5$$

$$k_{sur.cool} := 1.0$$

Secondary forces adjusted with respect to shrinkage

$$\frac{\Delta T_{M.heat} \cdot k_{sur.heat}}{\varphi_{temp}} = 6.098$$

$$\frac{\Delta T_{M.cool} \cdot k_{sur.cool}}{\varphi_{temp}} = -6.504$$

## A.4 Increased earthpressure

***Increased earthpressure caused by motion from soil caused by temperature difference.***

$L := 10200 \cdot mm$

$H_{max} := 5450 \cdot mm$

$\gamma_{jord} := 22 \cdot \frac{kN}{m^3}$

$\phi_d := 37.6 \cdot deg$

OCR isover consolidation quota which is not treated for friction soil. Therefore put =1

$OCR := 1$

$\sin(\phi_d) = 0.61$

$K_0 := 1 - \sin(\phi_d) \cdot \sqrt{OCR} = 0.39$

$K_{p.graph} := 4.12$

$K_{p.calculated} := \tan\left(45 \cdot deg + \frac{\phi_d}{2}\right)^2 = 4.13$

$\Delta := \frac{5}{100} = 5 \cdot \%$

$V_p := H_{max} \cdot \Delta = 272.5 \cdot mm$

$\Delta_{0.5} := \frac{1.1}{100} = 1.1 \cdot \%$

$V_{0.5} := H_{max} \cdot \Delta_{0.5} = 0.06m$

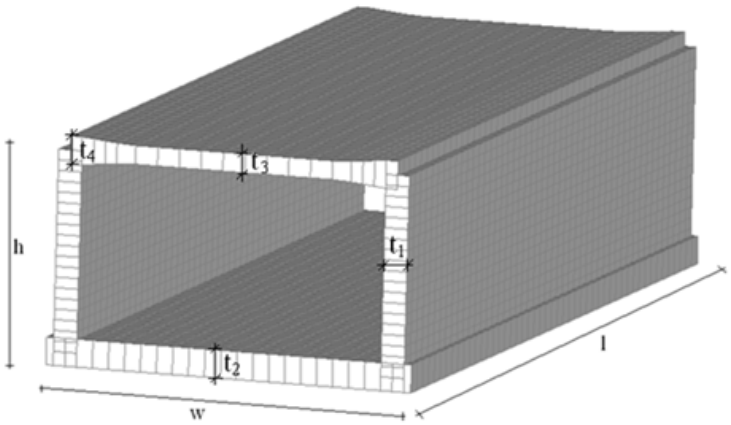


*Figure: A.3–Cross section of slab frame bridge*

$\Delta T_{EXP} := 23.577$

$\Delta T_{CON} := -27.642$

$\alpha := 1 \cdot 10^{-5}$

$h := H_{max} = 5.45m$

$w := L = 10.2m$

$V_{temp} := \alpha \cdot \frac{L}{2} \cdot (\Delta T_{EXP} - \Delta T_{CON}) = 2.612 \cdot mm$

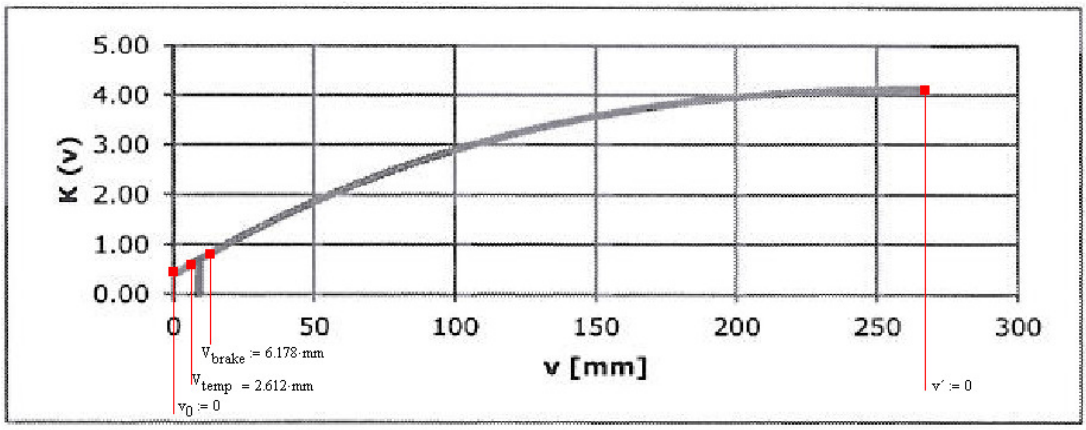


*Figure: A.4–Evaluation graph for K.v*

This graph is taken from Hristo Sokolov
It is built up from the third degree differential equation:

When the three points are known together with that the derivative is zero at the end, the equation can be solved and K.v obtained.

$$a \cdot x^3 + b \cdot x^2 \cdot c \cdot x + d = \blacksquare \cdot 0$$

K.v for this situation is only affected by the V.temp, otherwise a summation of contributions is made

$K_{v.tot} := 0.442$ Earth pressure coefficient

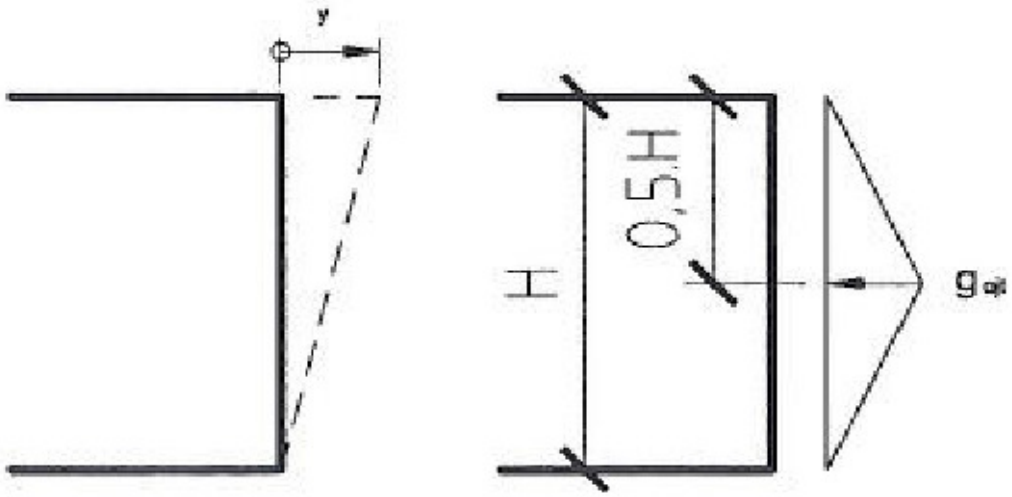


*F*
*difference*

$$g_{ojt} := \gamma_{jord} \cdot H_{max} \cdot \left(K_{v.tot} - K_0\right) = 6.336 \cdot \frac{kN}{m^2}$$

# APPENDIX B – Temperature study

Three different load application possibilities are evaluated.

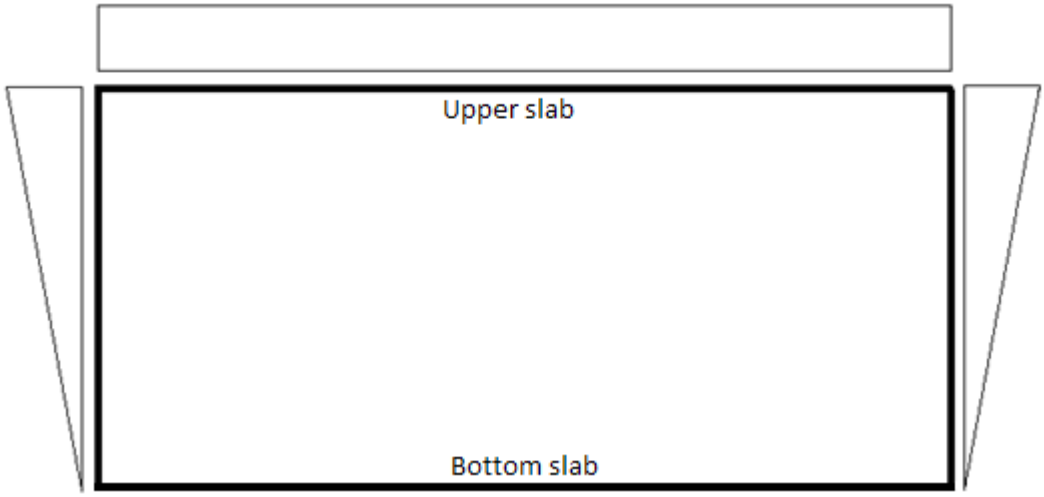


*FigureB.1 – Illustration of the linear application of thermal actions*

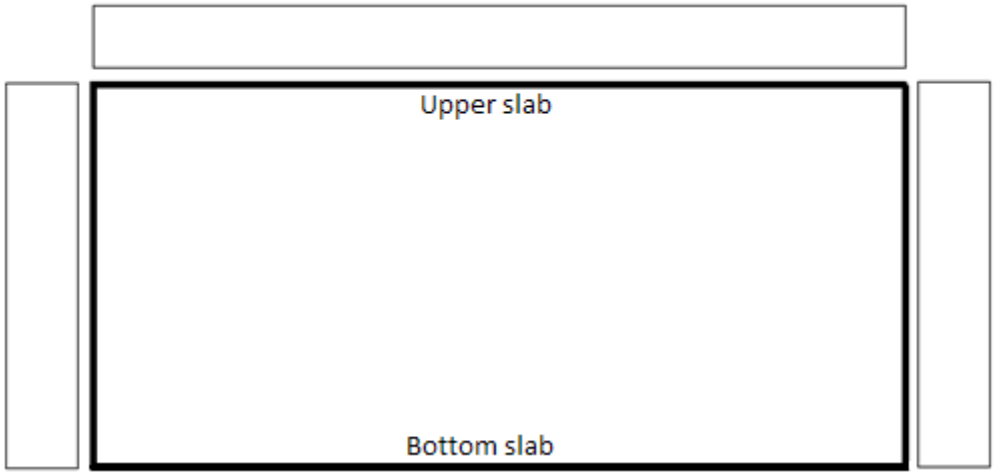


*Figure B.2 – Illustration of the constant application of thermal actions*

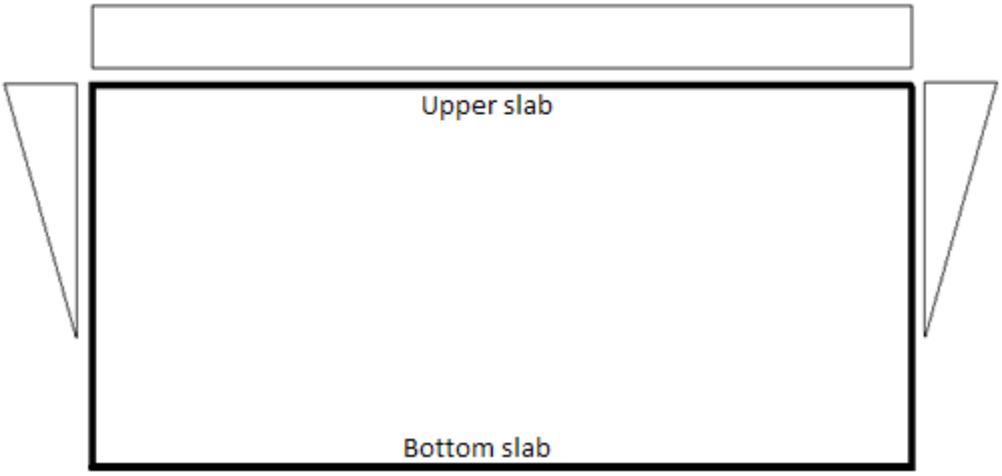


*Figure B.3 – Illustration of the uneven application of thermal actions*

Model 1.)

Consists of a frame slab bridge with no restrictions in z- direction except for the springs. Expansion, (EXP), and contraction, (CON) loads are applied according to Figure B1, B2 and B3. The expansion load is EXP=23.577 °C and contraction load CON=-27.642°C.

Model 2.)

Consists of the same frame slab bridge but with restrictions in z-direction together with the springs. The restriction in z- direction is placed on the bottom slab along the integral abutment walls. The loads are the same as for model 1.

Model 1 and 2 have different boundary conditions which gives rise to different locations of maximal forces. Since the maximal forces are of interest, the results have been extracted in the most critical sections. Figure B.4 illustrates that the values for model 1 are obtained in "Snitt I" and values for model 2 are obtained from "Snitt II".

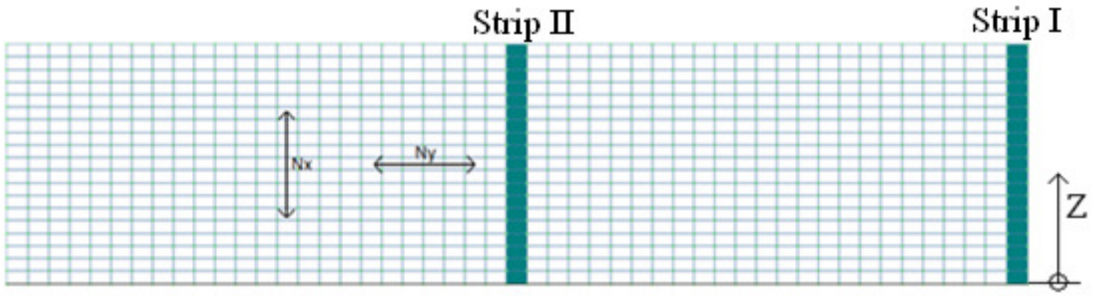


*Figure B.4 – Illustration of the integral abutment and the sections of where the values have been extracted for the two different models.*

The z- values in [m] and consistently the force values in [kN/m] are presented from the bottom and upward according to Figure B4.

## *Model 1 – Frame slab-bridge with no restrictions in z- direction except for springs.*

### *Linearly applied EXP load*

*Table B.1 – Values for linearly applied EXP load*

| Transformed X-Membrane force | | Transformed Y-Membrane force | |
|---|---|---|---|
| z [m] | Nx [kN/m] | z [m] | Ny [kN/m] |
| 0.2868 | -335.64 | 0.2868 | -19.8717 |
| 0.5736 | -281.171 | 0.5736 | -16.3203 |
| 0.8596 | -233.709 | 0.8596 | -12.7763 |
| 1.1456 | -194.46 | 1.1456 | -8.07304 |
| 1.4316 | -162.214 | 1.4316 | -5.41668 |
| 1.7176 | -135.234 | 1.7176 | -3.64146 |
| 2.0036 | -112.122 | 2.0036 | -2.50665 |
| 2.2896 | -91.8065 | 2.2896 | -1.72118 |
| 2.5756 | -73.4865 | 2.5756 | -1.14938 |
| 2.8616 | -56.5403 | 2.8616 | -0.69351 |
| 3.1476 | -40.4583 | 3.1476 | -0.28626 |
| 3.4336 | -24.7843 | 3.4336 | 0.1328 |
| 3.7196 | -9.06344 | 3.7196 | 0.63422 |
| 4.0056 | 7.20707 | 4.0056 | 1.30782 |
| 4.2916 | 24.623 | 4.2916 | 2.29968 |
| 4.5776 | 43.8902 | 4.5776 | 3.82346 |
| 4.8636 | 65.6939 | 4.8636 | 5.81043 |
| 5.1496 | 90.0417 | 5.1496 | 7.46304 |
| 5.4356 | 113.85 | 5.4356 | -11.6678 |

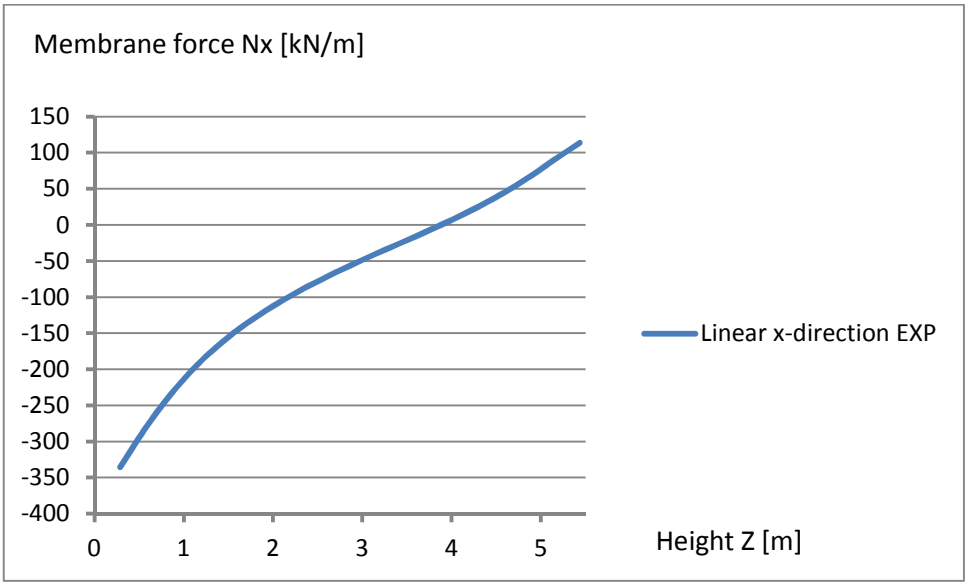


*Figure B.5 - Nx membrane force over height for linear EXP load*

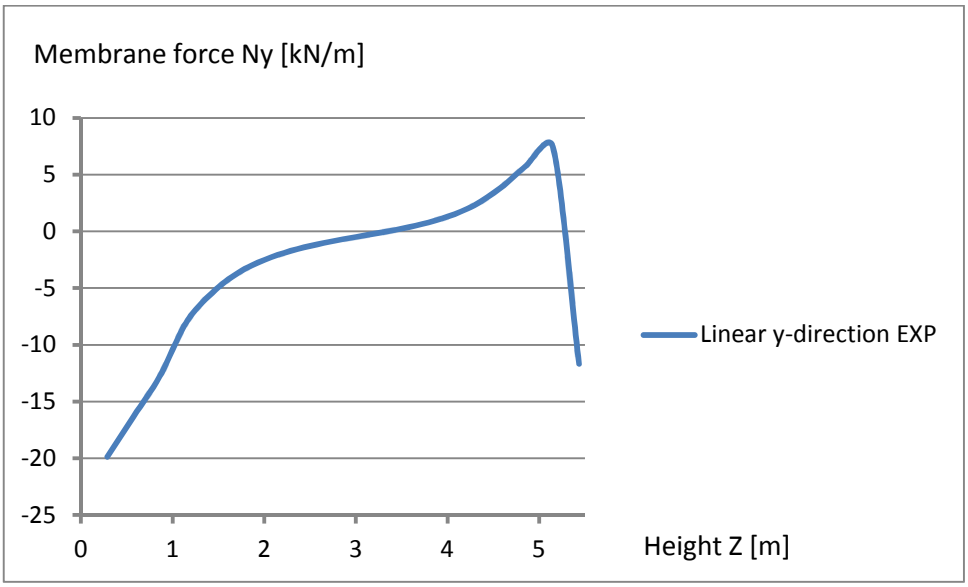


*Figure B.6 - Ny membrane force over height for linear EXP load*

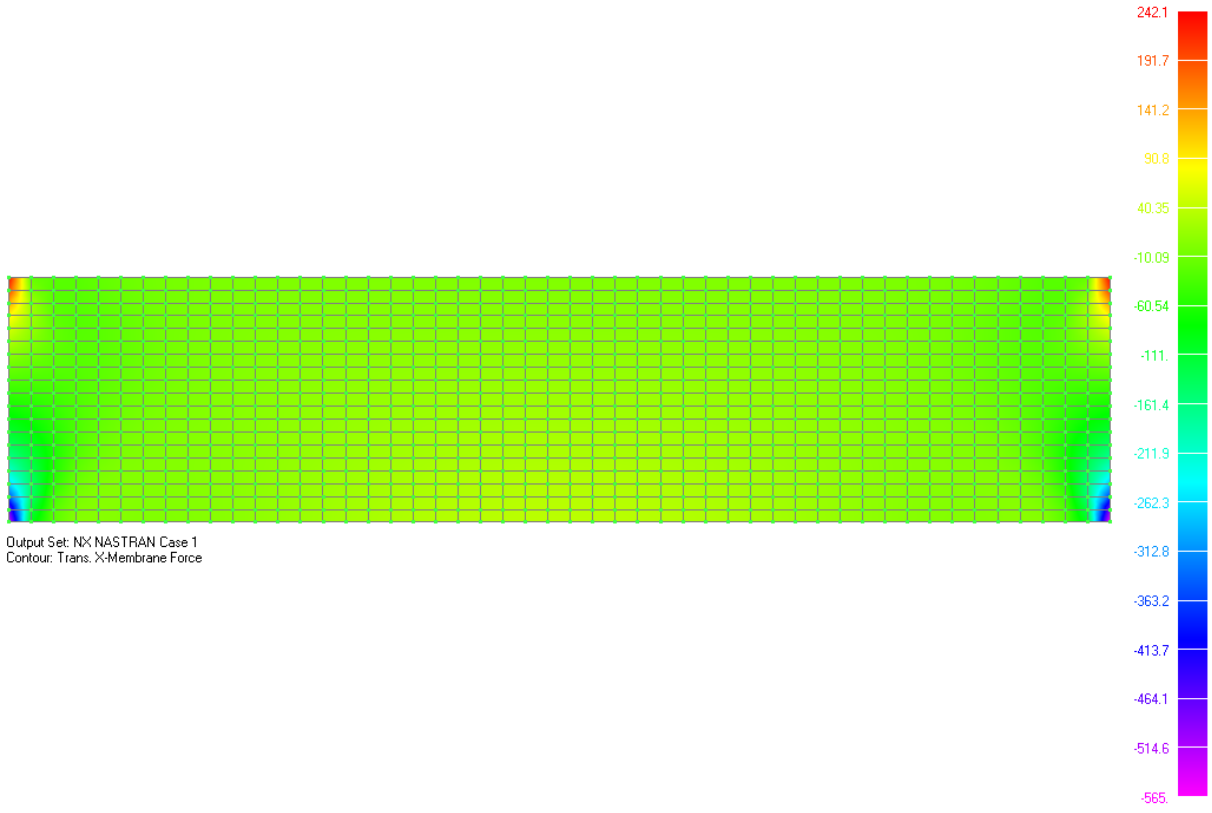


*Figure B.7 – Illustrating the contour plot for transformed Nx membrane force*

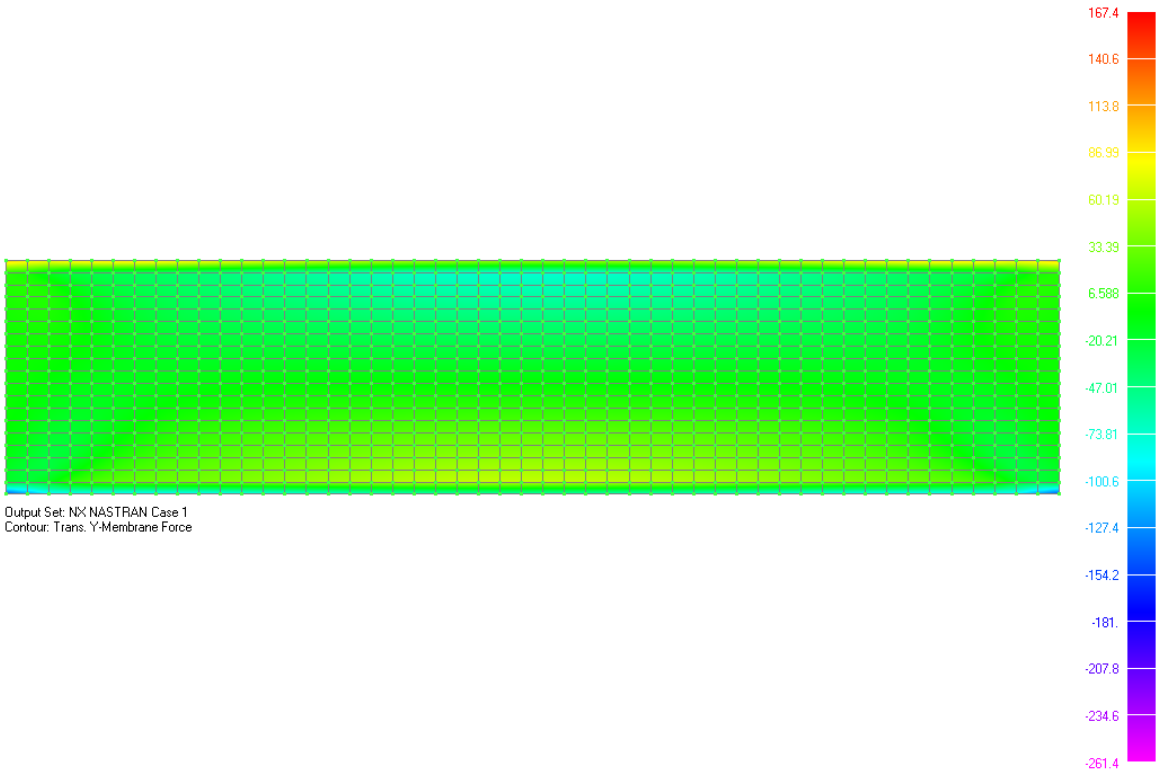


*Figure B.8 – Illustrating the contour plot for transformed Ny membrane force*

***Linearly applied CON load***

*Table B.2 – Values for linearly applied CON load*

| Transformed X-Membrane force | | Transformed Y-Membrane force | |
|---|---|---|---|
| z [m] | Nx [kN/m] | z [m] | Ny [kN/m] |
| 0.2868 | 393.509 | 0.2868 | 23.298 |
| 0.5736 | 329.649 | 0.5736 | 19.1335 |
| 0.8596 | 274.004 | 0.8596 | 14.9797 |
| 1.1456 | 227.988 | 1.1456 | 9.46494 |
| 1.4316 | 190.181 | 1.4316 | 6.35077 |
| 1.7176 | 158.55 | 1.7176 | 4.26918 |
| 2.0036 | 131.453 | 2.0036 | 2.9391 |
| 2.2896 | 107.635 | 2.2896 | 2.01433 |
| 2.5756 | 86.1563 | 2.5756 | 1.35303 |
| 2.8616 | 66.2889 | 2.8616 | 0.81321 |
| 3.1476 | 47.4347 | 3.1476 | 0.33021 |
| 3.4336 | 29.0581 | 3.4336 | -0.15117 |
| 3.7196 | 10.6262 | 3.7196 | -0.74846 |
| 4.0056 | -8.4503 | 4.0056 | -1.52848 |
| 4.2916 | -28.8695 | 4.2916 | -2.70063 |
| 4.5776 | -51.4589 | 4.5776 | -4.4771 |
| 4.8636 | -77.021 | 4.8636 | -6.81162 |
| 5.1496 | -105.566 | 5.1496 | -8.7565 |
| 5.4356 | -133.48 | 5.4356 | 13.6842 |

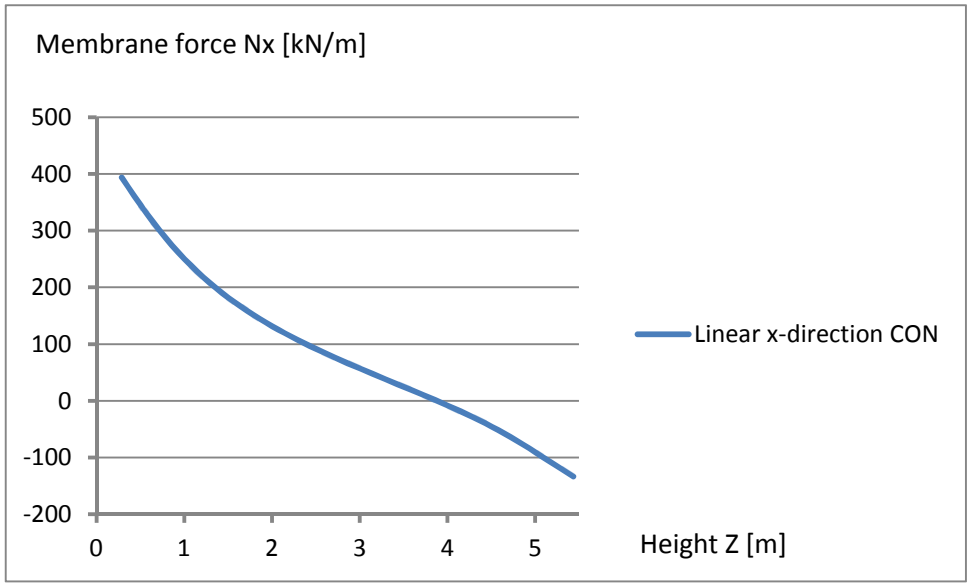


*Figure B.9 - Nx membrane force over height for linear CON load*

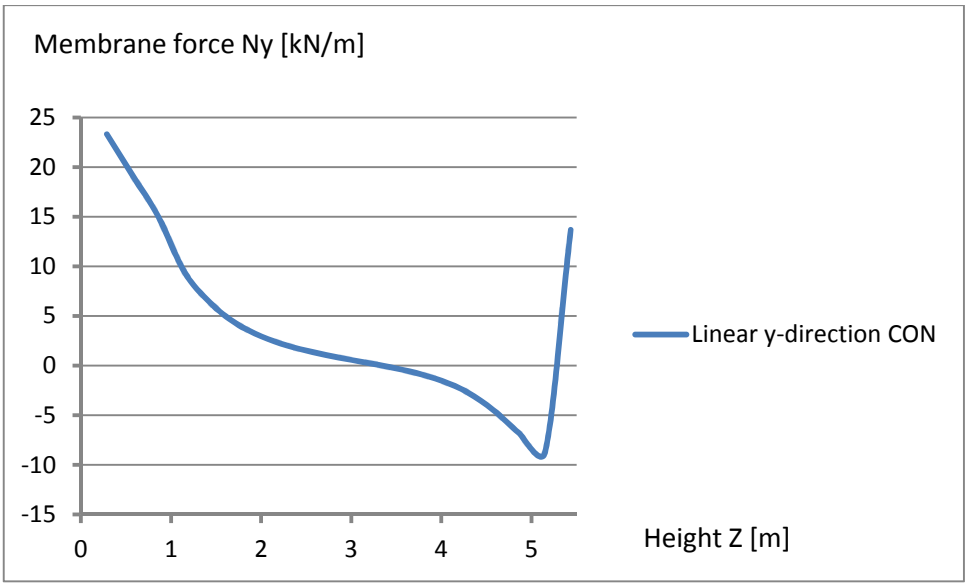


*Figure B.10 - Ny membrane force over height for linear CON load*

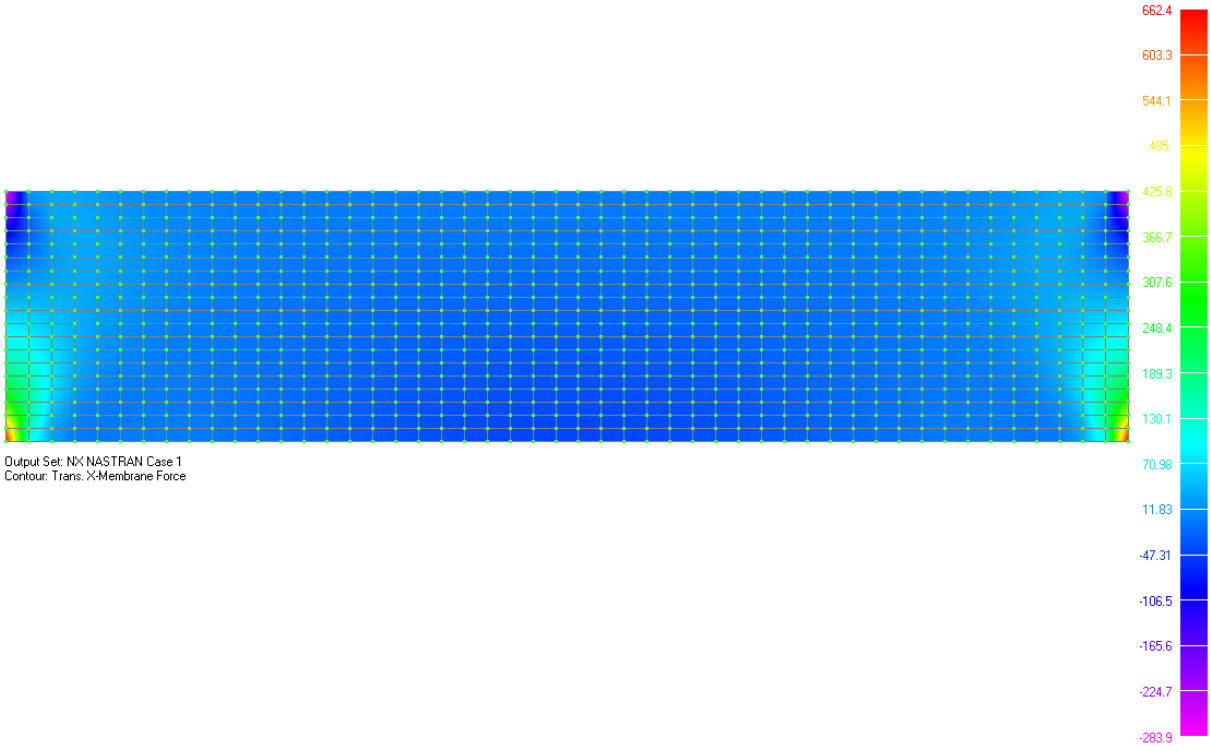


*Figure B.11 – Illustrating the contour plot for transformed Nx membrane force*

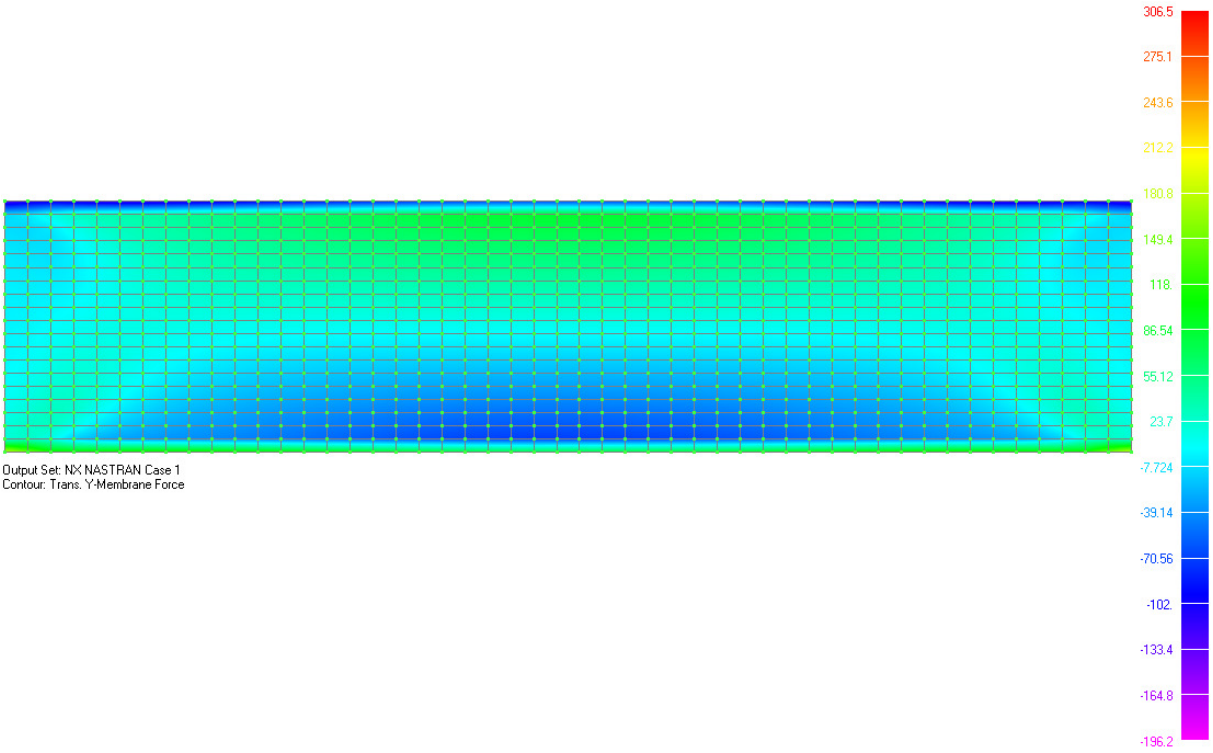


*Figure B.12 – Illustrating the contour plot for transformed Ny membrane force*

***Constant applied EXP load***

*Table B.3 – Values for constant applied EXP load*

| Transformed X-Membrane force | | Transformed Y-Membrane force | |
|---|---|---|---|
| z [m] | Nx [kN/m] | z [m] | Ny [kN/m] |
| 0.2868 | -173.171 | 0.2868 | -2298.58 |
| 0.5736 | 880.813 | 0.5736 | -478.802 |
| 0.8596 | 1381.43 | 0.8596 | -259.979 |
| 1.1456 | 1606.91 | 1.1456 | -103.428 |
| 1.4316 | 1678.7 | 1.4316 | -56.6479 |
| 1.7176 | 1664.7 | 1.7176 | -30.6071 |
| 2.0036 | 1599.16 | 2.0036 | -18.5516 |
| 2.2896 | 1501.56 | 2.2896 | -11.4591 |
| 2.5756 | 1383.33 | 2.5756 | -7.15824 |
| 2.8616 | 1251.74 | 2.8616 | -4.20066 |
| 3.1476 | 1111.75 | 3.1476 | -1.97396 |
| 3.4336 | 967.015 | 3.4336 | -0.10845 |
| 3.7196 | 820.51 | 3.7196 | 1.60517 |
| 4.0056 | 674.824 | 4.0056 | 3.2929 |
| 4.2916 | 532.384 | 4.2916 | 4.98744 |
| 4.5776 | 395.563 | 4.5776 | 6.60668 |
| 4.8636 | 266.67 | 4.8636 | 7.67096 |
| 5.1496 | 147.871 | 5.1496 | 7.5915 |
| 5.4356 | 40.9434 | 5.4356 | 6.01731 |

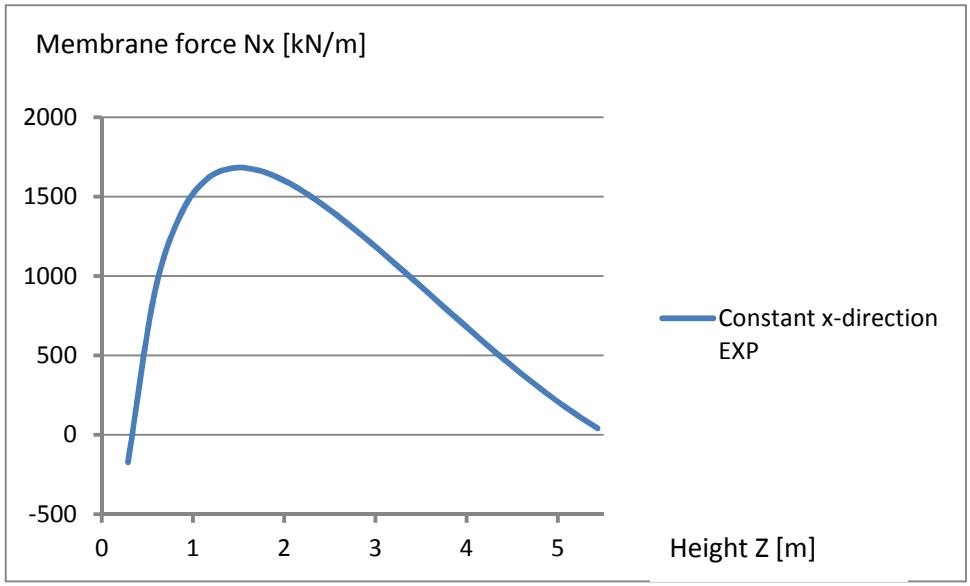


*Figure B.13 - Nx membrane force over height for constant EXP load*

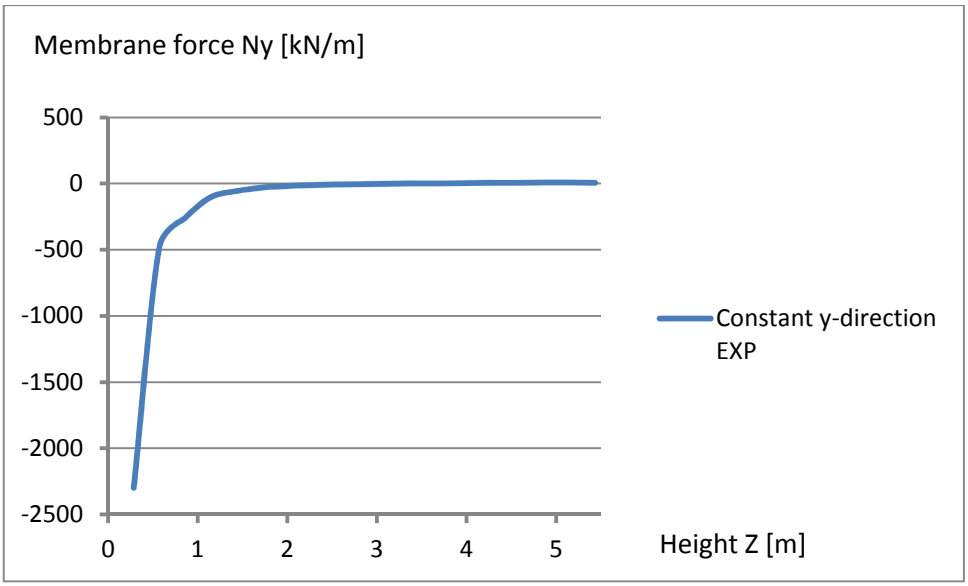


*Figure B.14 - Ny membrane force over height for constant EXP load*

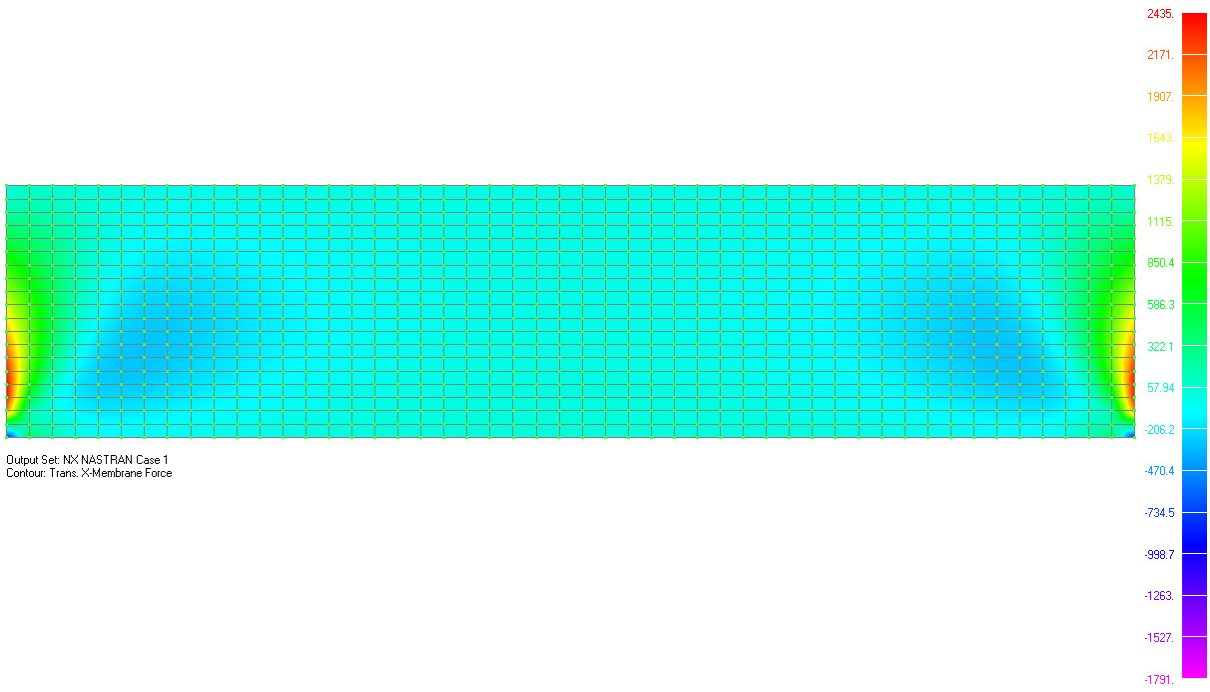


*Figure B.15 – Illustrating the contour plot for transformed Nx membrane force*

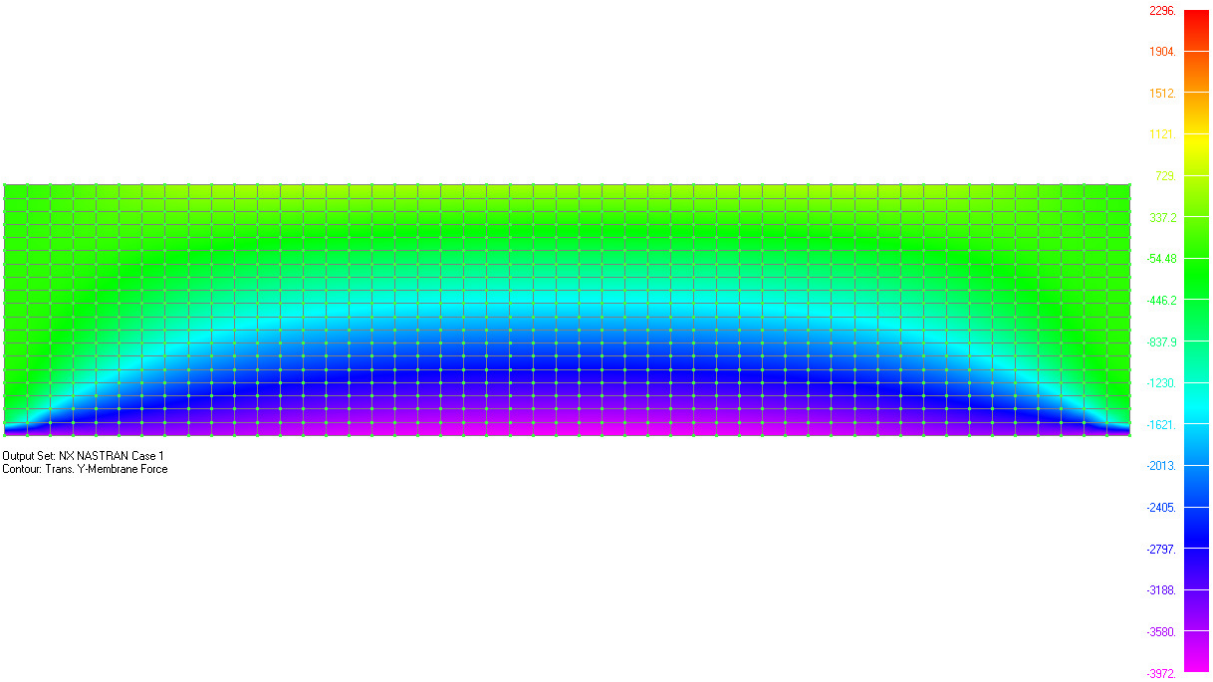


*Figure B.16 – Illustrating the contour plot for transformed Ny membrane force*

***Constant applied CON load***

*Table B.4 – Values for constant applied CON load*

| Transformed X-Membrane force | | Transformed Y-Membrane force | |
|---|---|---|---|
| z [m] | Nx [kN/m] | z [m] | Ny [kN/m] |
| 0.2868 | 203.028 | 0.2868 | 2694.89 |
| 0.5736 | -1032.68 | 0.5736 | 561.354 |
| 0.8596 | -1619.6 | 0.8596 | 304.803 |
| 1.1456 | -1883.97 | 1.1456 | 121.261 |
| 1.4316 | -1968.13 | 1.4316 | 66.4148 |
| 1.7176 | -1951.72 | 1.7176 | 35.8841 |
| 2.0036 | -1874.88 | 2.0036 | 21.7502 |
| 2.2896 | -1760.45 | 2.2896 | 13.4348 |
| 2.5756 | -1621.83 | 2.5756 | 8.39241 |
| 2.8616 | -1467.56 | 2.8616 | 4.92492 |
| 3.1476 | -1303.43 | 3.1476 | 2.31429 |
| 3.4336 | -1133.74 | 3.4336 | 0.12714 |
| 3.7196 | -961.978 | 3.7196 | -1.88193 |
| 4.0056 | -791.173 | 4.0056 | -3.86065 |
| 4.2916 | -624.174 | 4.2916 | -5.84734 |
| 4.5776 | -463.763 | 4.5776 | -7.74576 |
| 4.8636 | -312.648 | 4.8636 | -8.99354 |
| 5.1496 | -173.366 | 5.1496 | -8.90037 |
| 5.4356 | -48.0027 | 5.4356 | -7.05478 |

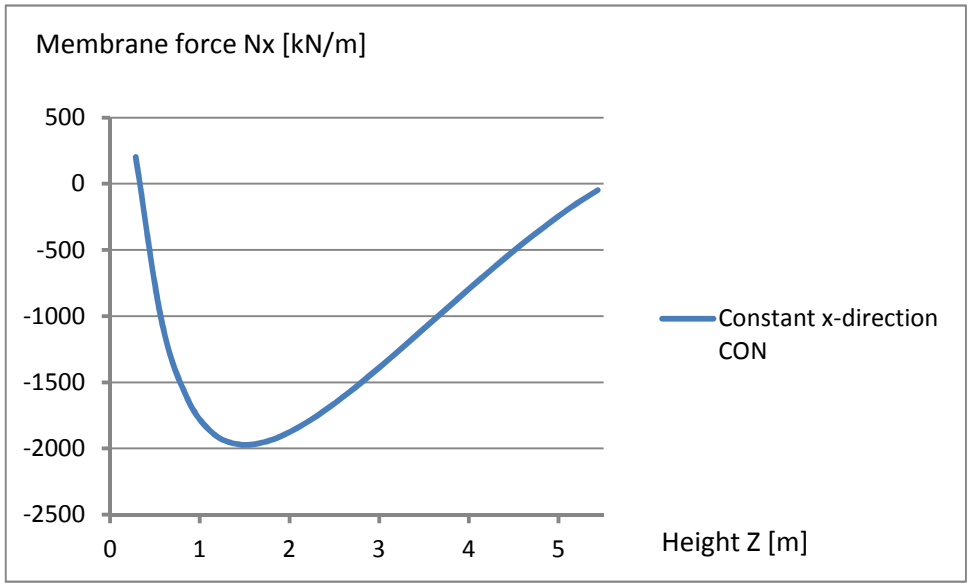


*Figure B.17 - Nx membrane force over height for constant CON load*

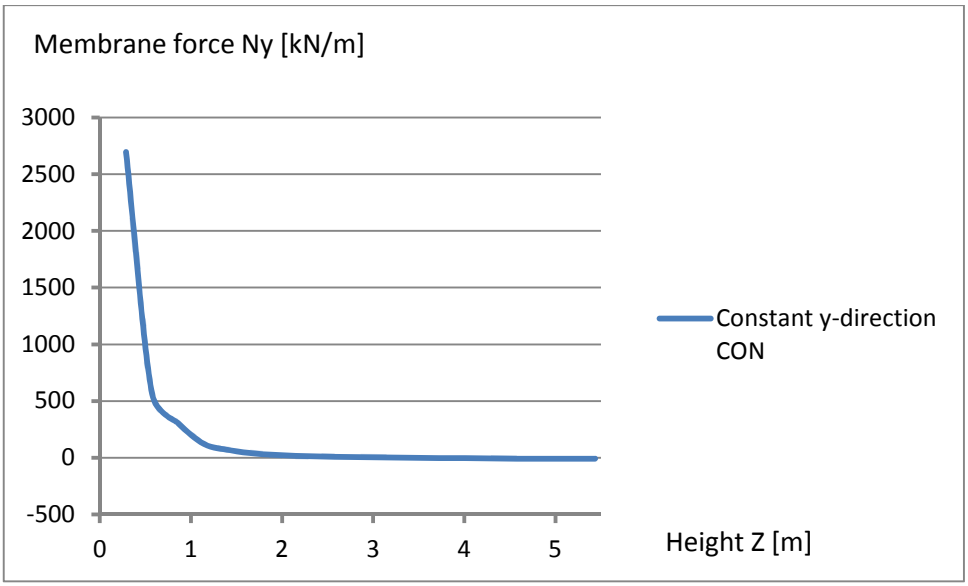


*Figure B.18 - Ny membrane force over height for constant CON load*

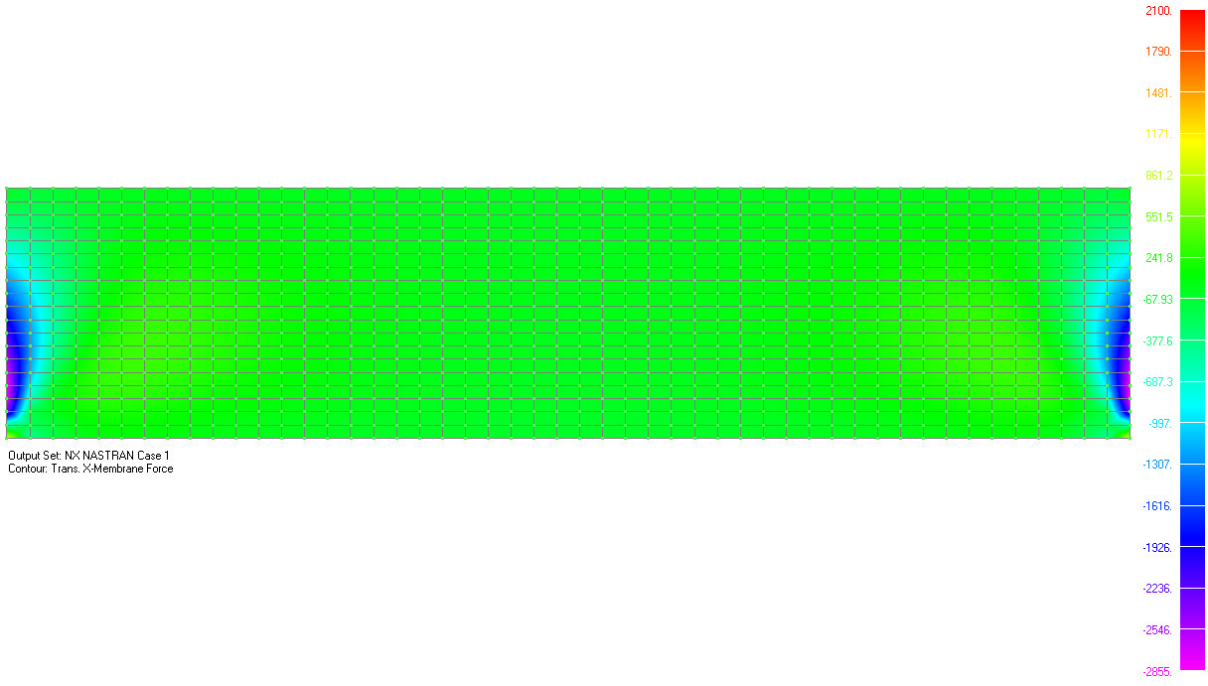


*Figure B.19 – Illustrating the contour plot for transformed Nx membrane force*

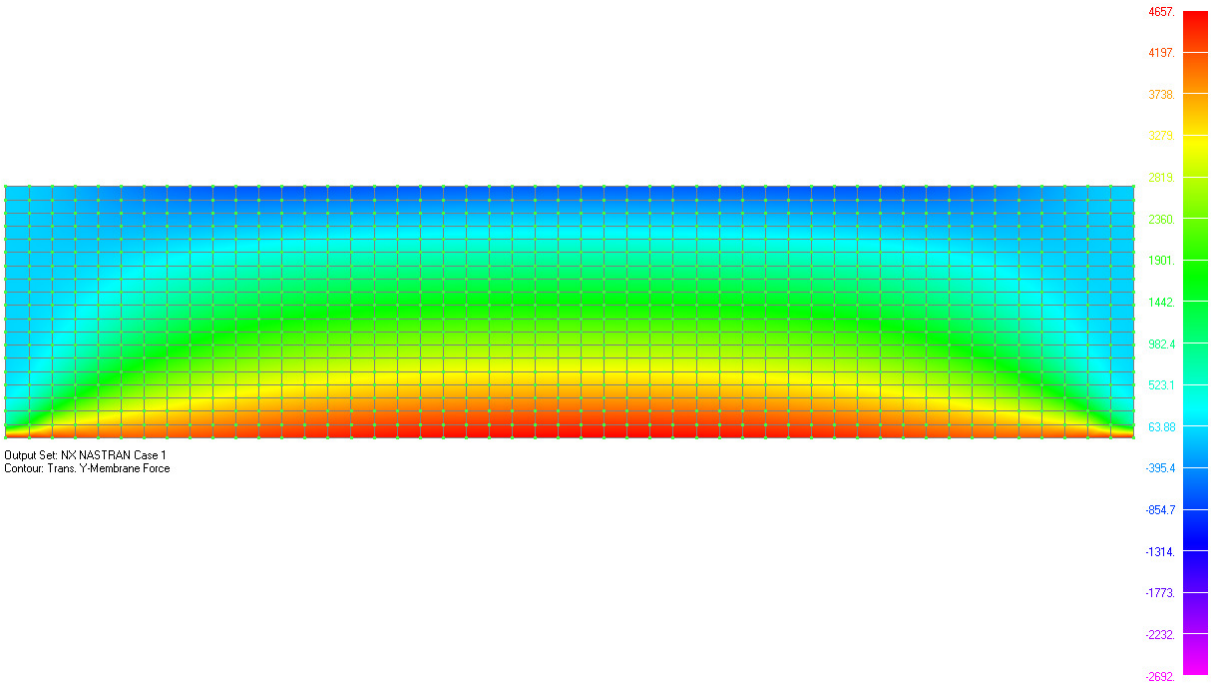


*Figure B.20 – Illustrating the contour plot for transformed Ny membrane force*

***Uneven applied EXP load***

*Table B.5 – Values for uneven applied EXP load*

| Transformed X-Membrane force | | Transformed Y-Membrane force | |
|---|---|---|---|
| z [m] | Nx [kN/m] | z [m] | Ny [kN/m] |
| 0.2868 | -272.042 | 0.2868 | -15.2267 |
| 0.5736 | -401.212 | 0.5736 | -2.9839 |
| 0.8596 | -534.766 | 0.8596 | 3.11097 |
| 1.1456 | -660.368 | 1.1456 | 16.9112 |
| 1.4316 | -757.847 | 1.4316 | 73.5027 |
| 1.7176 | -803.36 | 1.7176 | 86.0952 |
| 2.0036 | -793.307 | 2.0036 | 22.3102 |
| 2.2896 | -747.304 | 2.2896 | 9.87767 |
| 2.5756 | -683.375 | 2.5756 | 4.15677 |
| 2.8616 | -609.85 | 2.8616 | 2.05225 |
| 3.1476 | -531.024 | 3.1476 | 0.98701 |
| 3.4336 | -449.195 | 3.4336 | 0.4863 |
| 3.7196 | -365.695 | 3.7196 | 0.30726 |
| 4.0056 | -281.301 | 4.0056 | 0.44724 |
| 4.2916 | -196.434 | 4.2916 | 1.04374 |
| 4.5776 | -111.264 | 4.5776 | 2.40156 |
| 4.8636 | -25.9347 | 4.8636 | 4.62282 |
| 5.1496 | 58.5414 | 5.1496 | 6.84222 |
| 5.4356 | 137.073 | 5.4356 | -18.4908 |

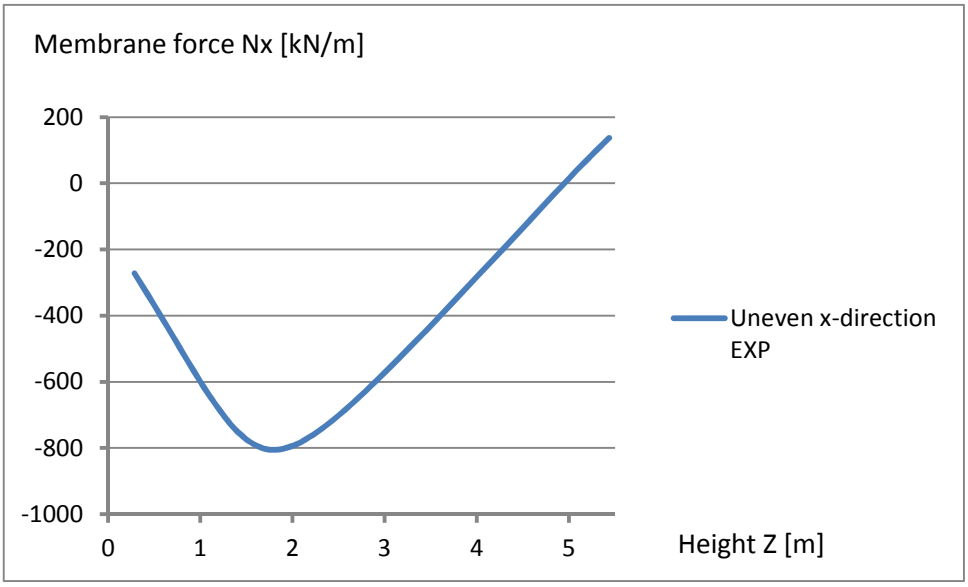


*Figure B.21 - Nx membrane force over height for uneven EXP load*

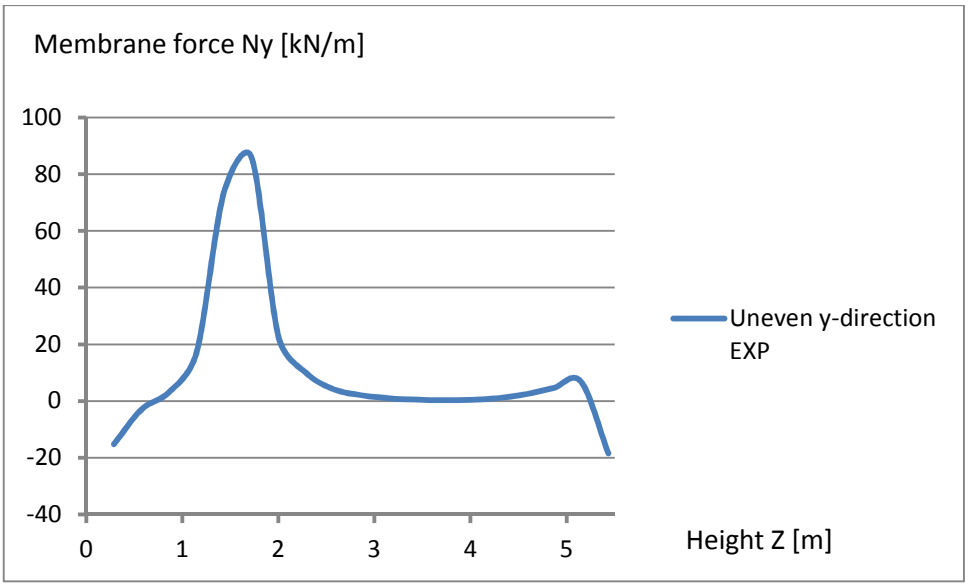


*Figure B.22 - Ny membrane force over height for uneven EXP load*

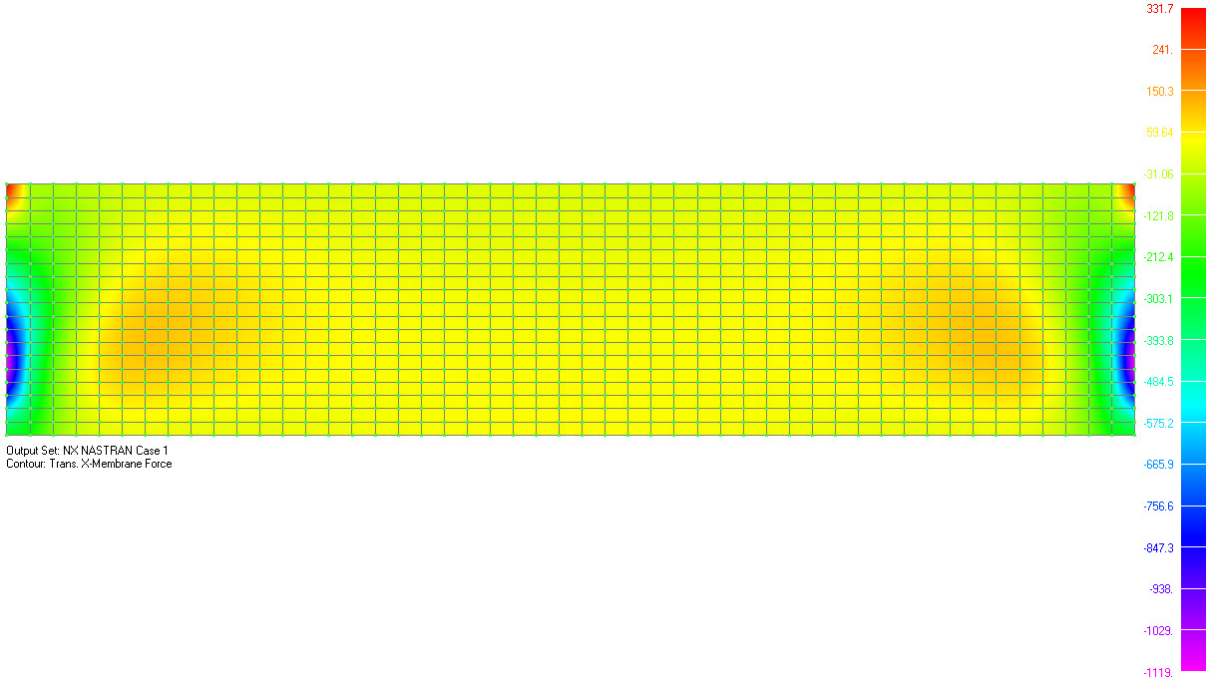


*Figure B.23 – Illustrating the contour plot for transformed Nx membrane force*

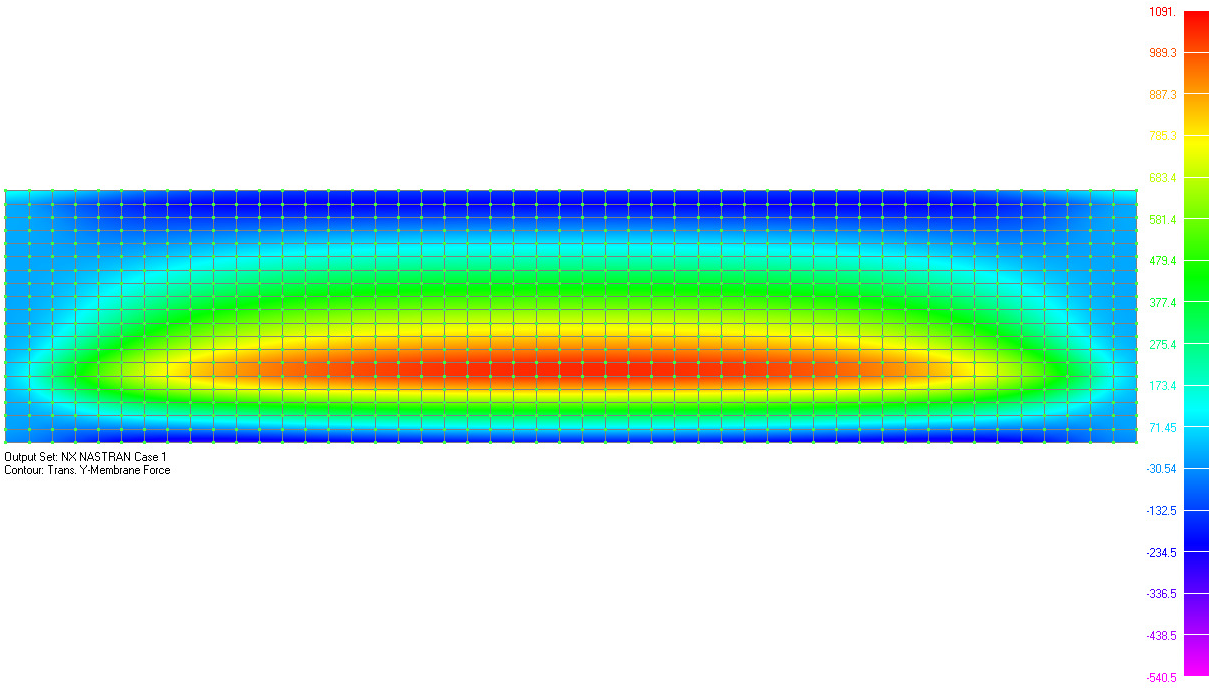


*Figure B.24 – Illustrating the contour plot for transformed Ny membrane force*

***Uneven applied CON load***

*Table B.6 – Values for uneven applied CON load*

| Transformed X-Membrane force | | Transformed Y-Membrane force | |
|---|---|---|---|
| z [m] | Nx [kN/m] | z [m] | Ny [kN/m] |
| 0.2868 | 318.946 | 0.2868 | 17.852 |
| 0.5736 | 470.386 | 0.5736 | 3.49837 |
| 0.8596 | 626.967 | 0.8596 | -3.64735 |
| 1.1456 | 774.224 | 1.1456 | -19.8269 |
| 1.4316 | 888.51 | 1.4316 | -86.1756 |
| 1.7176 | 941.87 | 1.7176 | -100.939 |
| 2.0036 | 930.084 | 2.0036 | -26.1568 |
| 2.2896 | 876.15 | 2.2896 | -11.5813 |
| 2.5756 | 801.199 | 2.5756 | -4.87272 |
| 2.8616 | 714.997 | 2.8616 | -2.40552 |
| 3.1476 | 622.58 | 3.1476 | -1.15685 |
| 3.4336 | 526.643 | 3.4336 | -0.57625 |
| 3.7196 | 428.745 | 3.7196 | -0.35417 |
| 4.0056 | 329.801 | 4.0056 | -0.52437 |
| 4.2916 | 230.302 | 4.2916 | -1.22292 |
| 4.5776 | 130.449 | 4.5776 | -2.8161 |
| 4.8636 | 30.4073 | 4.8636 | -5.42612 |
| 5.1496 | -68.6347 | 5.1496 | -8.01612 |
| 5.4356 | -160.707 | 5.4356 | 21.6788 |

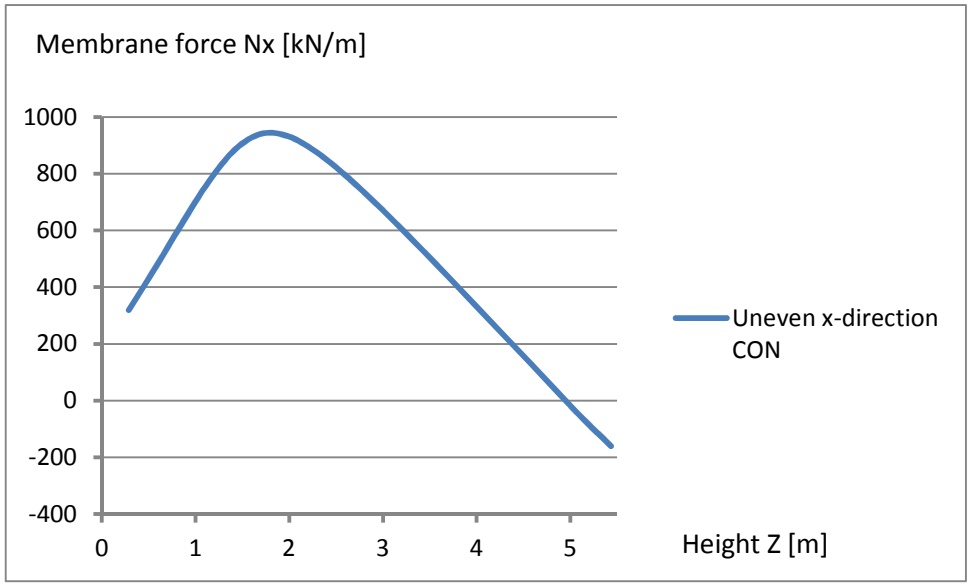


*Figure B.25 –Nx membrane force over height for uneven CON load*

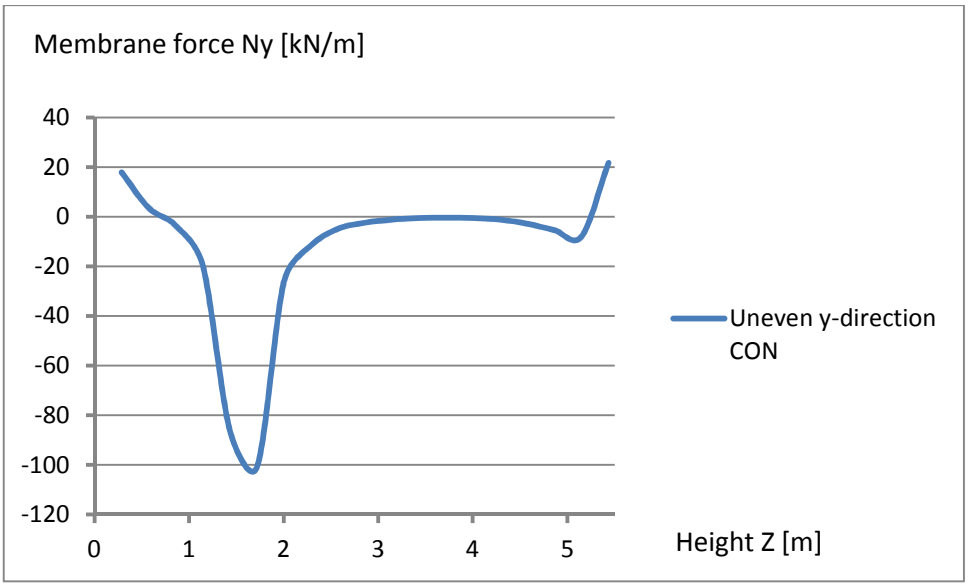


*Figure B.26 - Ny membrane force over height for uneven CON load*

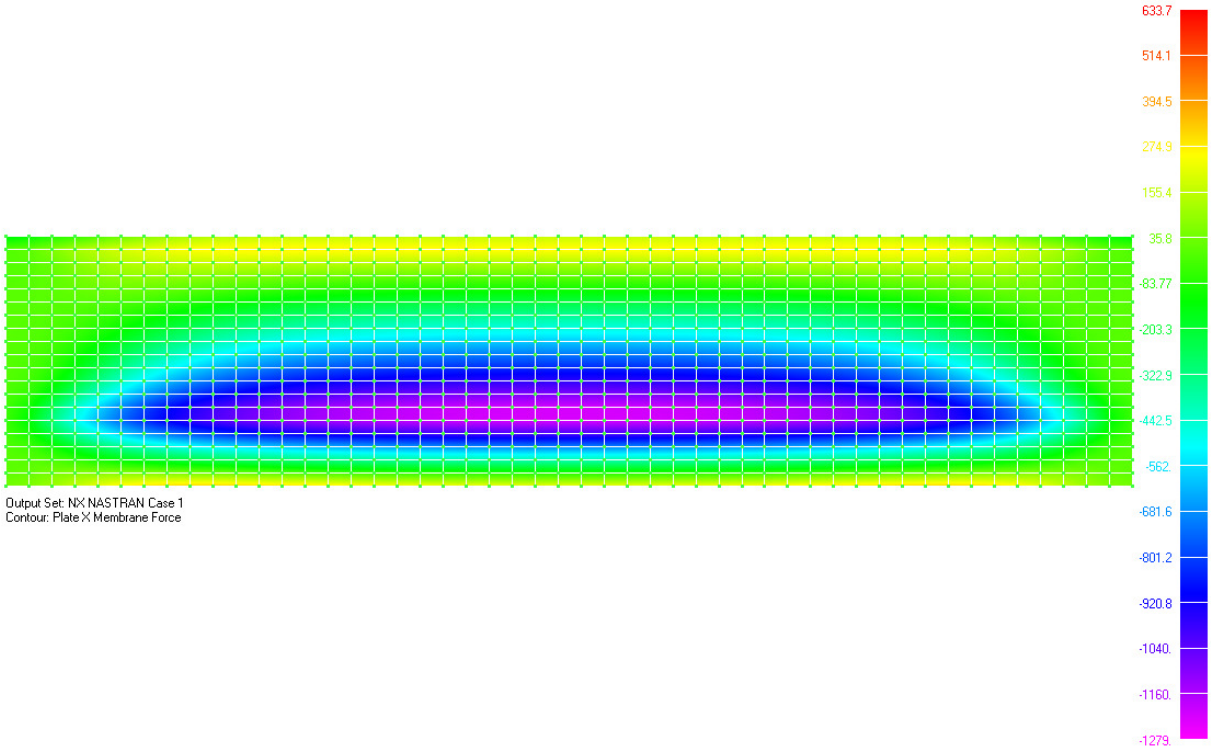


*Figure B.27 – Illustrating the contour plot for transformed Nx membrane force*

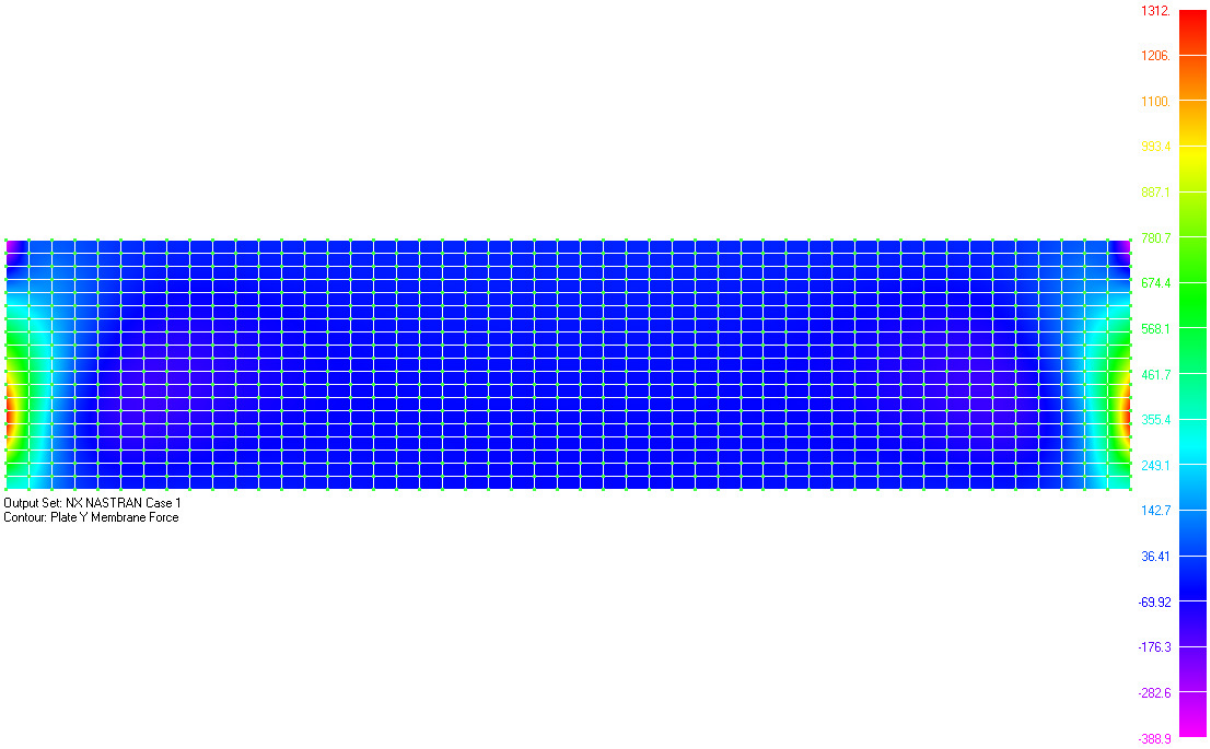


*Figure B.28 – Illustrating the contour plot for transformed Ny membrane force*

**A comparison between the different load application possibilities for each load has been made.**

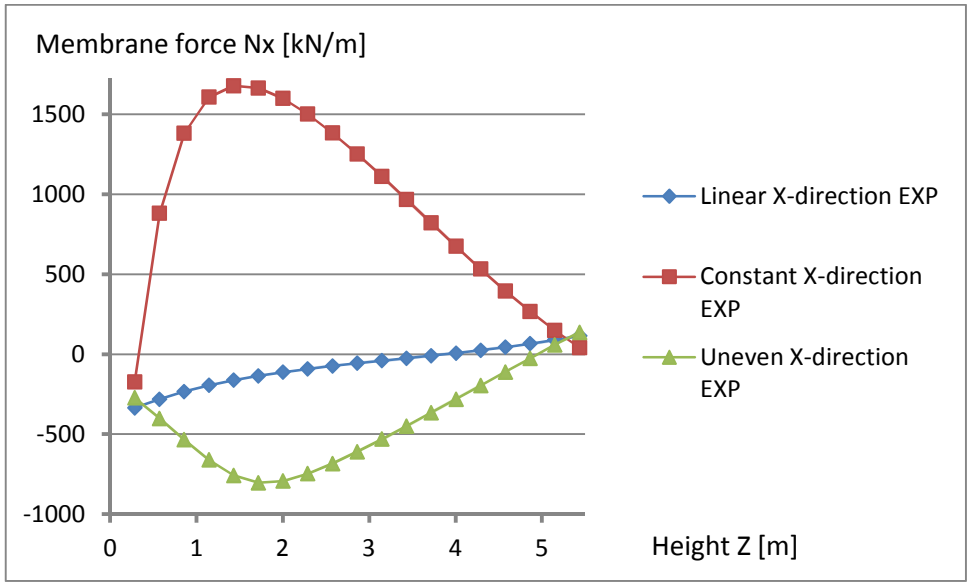


*Figure B.29 - Illustration of the Nx membrane force over height for the different load application possibilities for EXP load.*

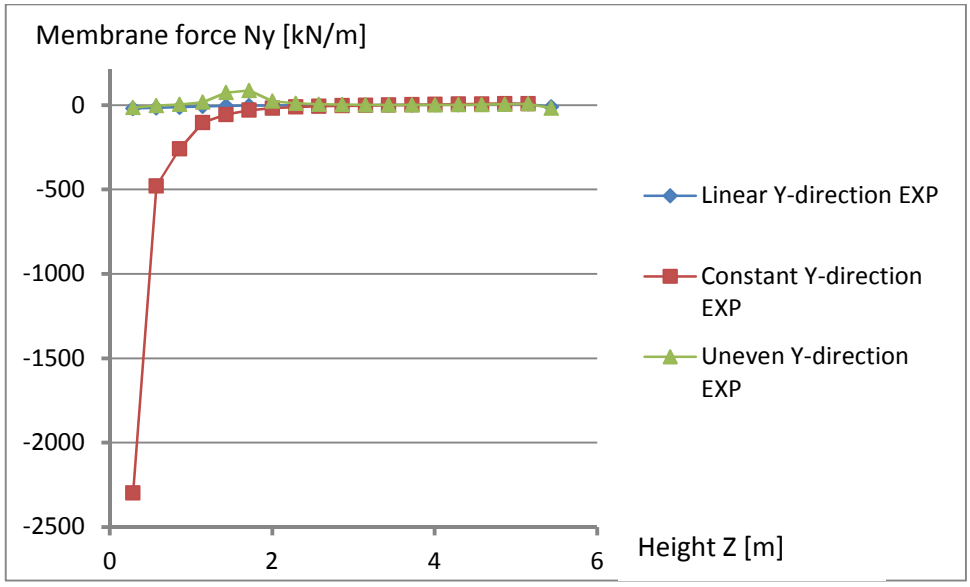


*Figure B.30 - Illustration of the Ny membrane force over height for the different load application possibilities for EXP load.*

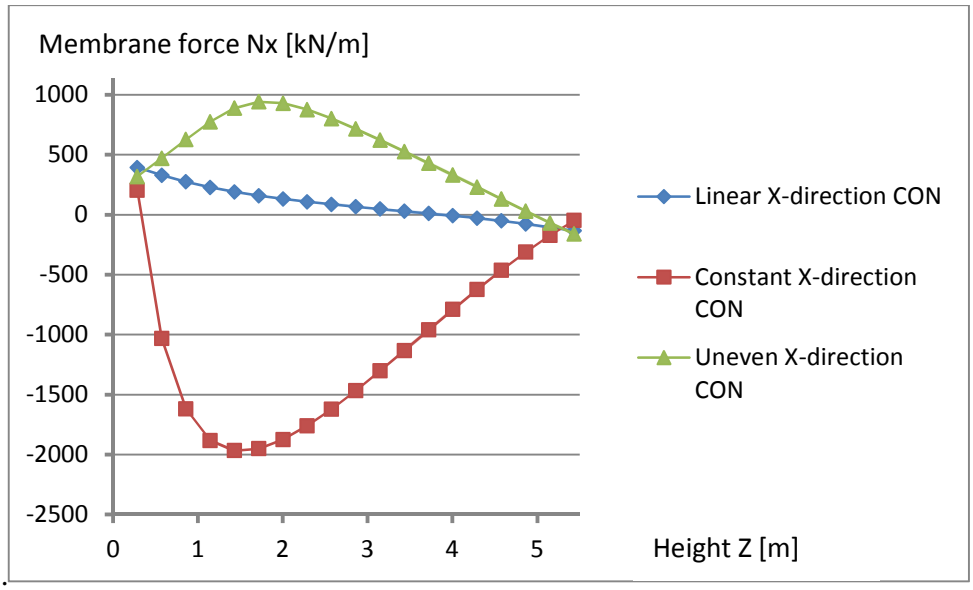


*Figure B.31 - Illustration of the Nx membrane force over height for the different load application possibilities for CON load.*

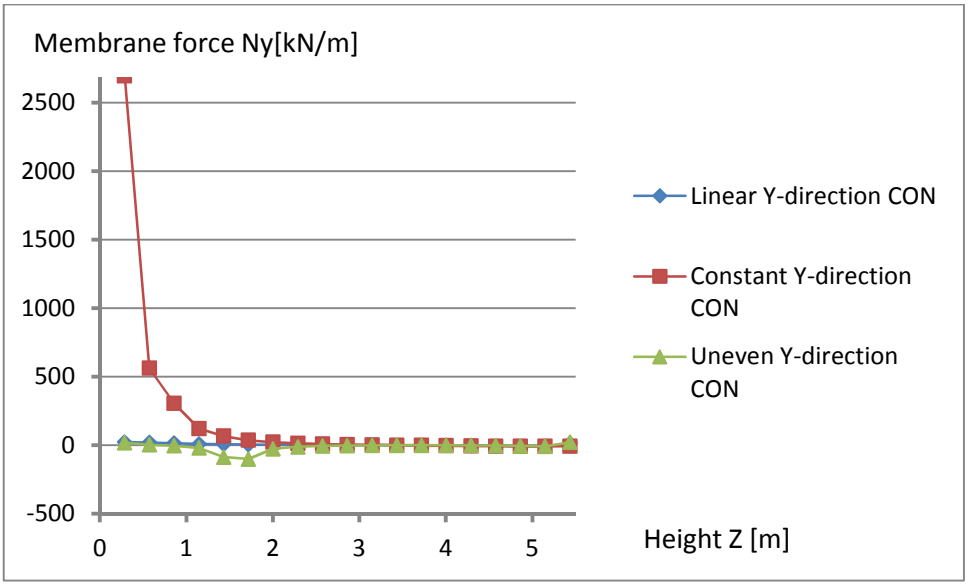


*Figure B.32- Illustrating the Ny membrane force over height for the different load application possibilities for CON load.*

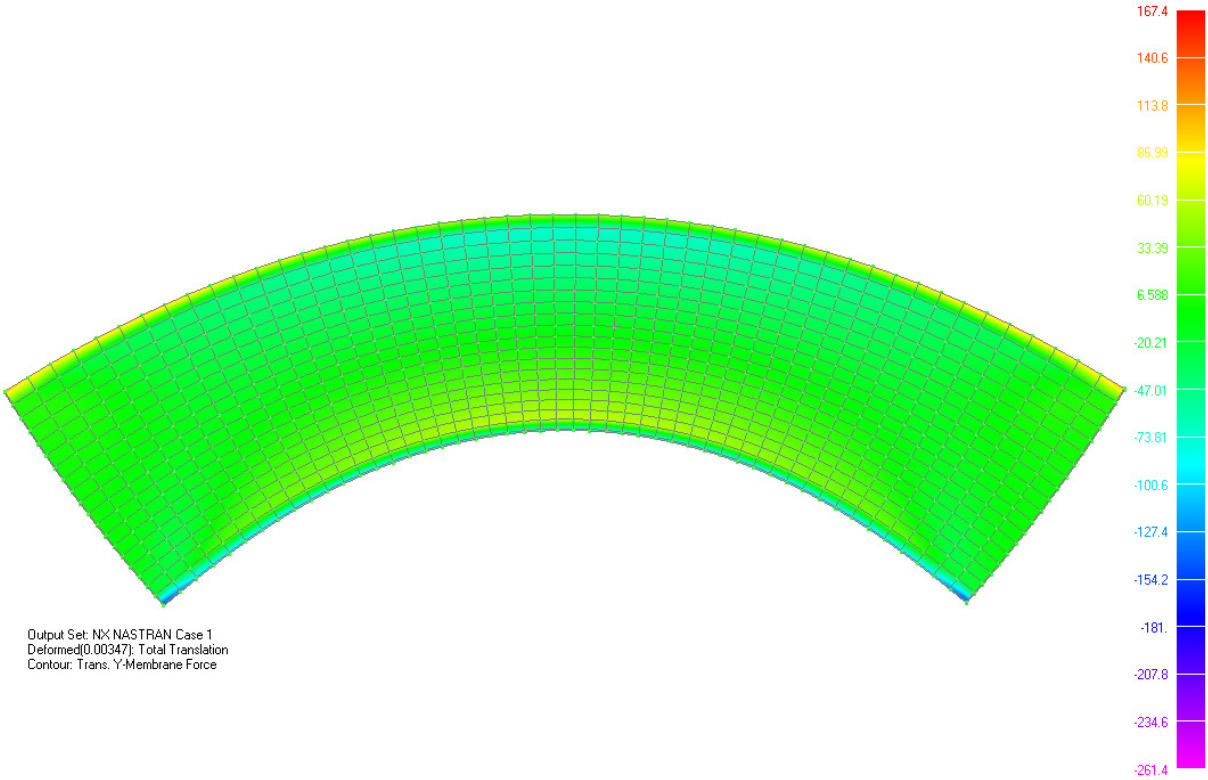


*Figure B.33 – Illustrating the principle behavior and contour plot for EXP loading*

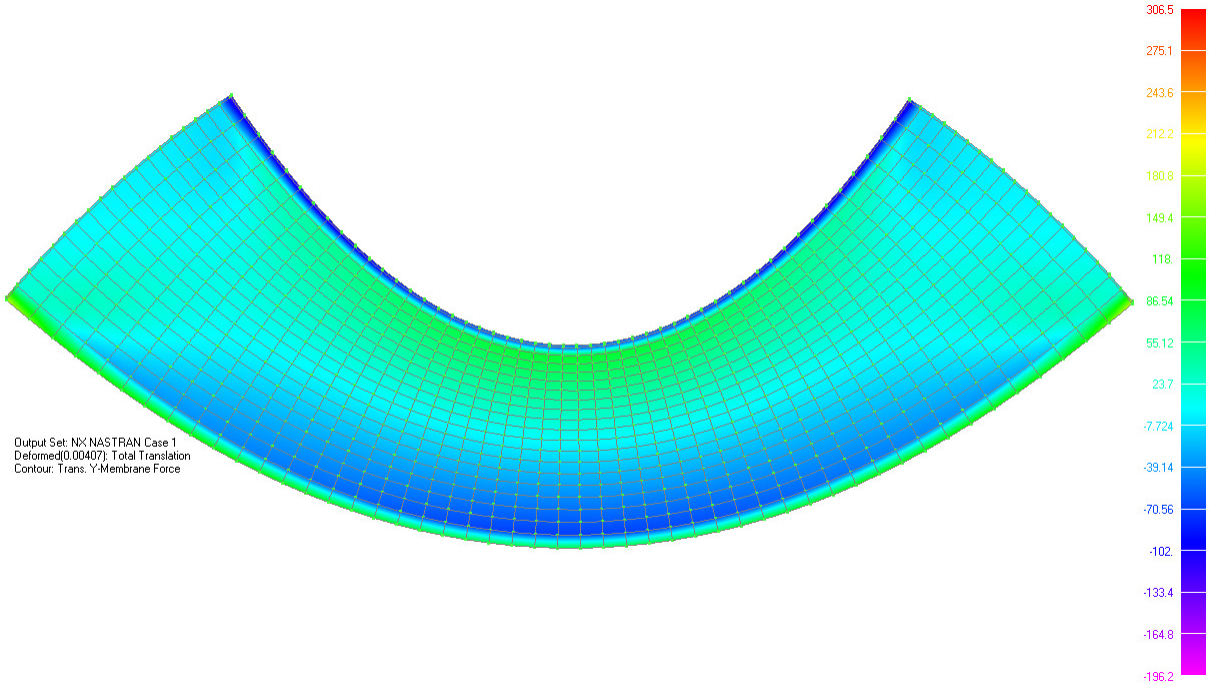


*Figure B.34 – Illustrating the principle behavior and contour plot for CON loading*

## *Model 2 – Frame slab-bridge with restrictions in z- direction in combination with springs.*

### *Linear applied EXP load*

*Table B.7 – Values for linear applied EXP load*

| Transformed X-Membrane force | | Transformed Y-Membrane force | |
|---|---|---|---|
| z [m] | Nx [kN/m] | z [m] | Ny [kN/m] |
| 0.2868 | 742.598 | 0.2868 | 1584.3 |
| 0.5736 | 708.348 | 0.5736 | 1368.24 |
| 0.8596 | 672.069 | 0.8596 | 1171.88 |
| 1.1456 | 634.193 | 1.1456 | 976.288 |
| 1.4316 | 595.225 | 1.4316 | 783.183 |
| 1.7176 | 555.185 | 1.7176 | 591.571 |
| 2.0036 | 514.206 | 2.0036 | 401.3 |
| 2.2896 | 472.419 | 2.2896 | 212.045 |
| 2.5756 | 429.989 | 2.5756 | 23.5021 |
| 2.8616 | 387.101 | 2.8616 | -164.672 |
| 3.1476 | 343.961 | 3.1476 | -352.846 |
| 3.4336 | 300.79 | 3.4336 | -541.419 |
| 3.7196 | 257.828 | 3.7196 | -730.807 |
| 4.0056 | 215.323 | 4.0056 | -921.453 |
| 4.2916 | 173.529 | 4.2916 | -1113.8 |
| 4.5776 | 132.702 | 4.5776 | -1308.31 |
| 4.8636 | 93.0973 | 4.8636 | -1505.43 |
| 5.1496 | 54.964 | 5.1496 | -1705.6 |
| 5.4356 | 18.5394 | 5.4356 | -1909.26 |

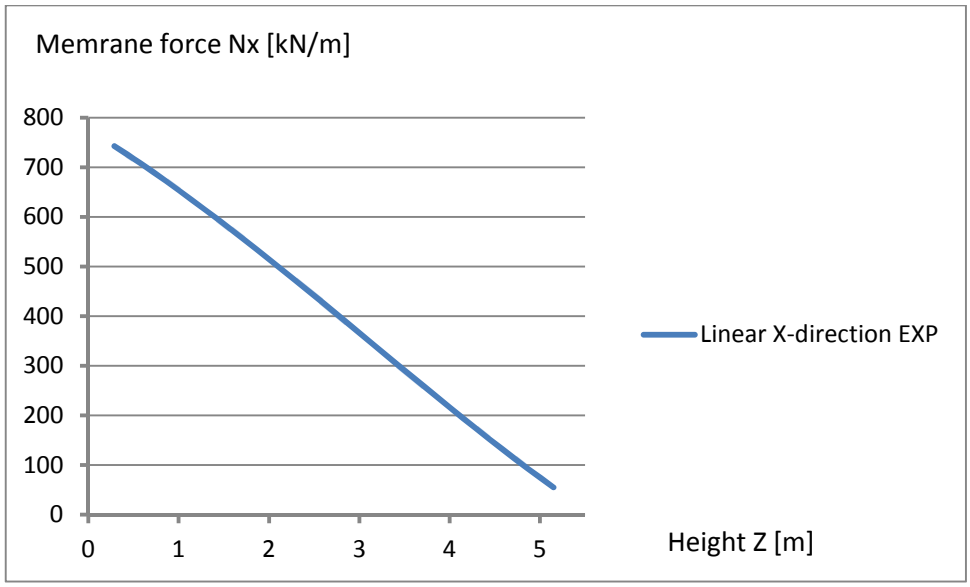


*Figure B.35 – Illustrating the Nx membrane force over height for linear EXP load*

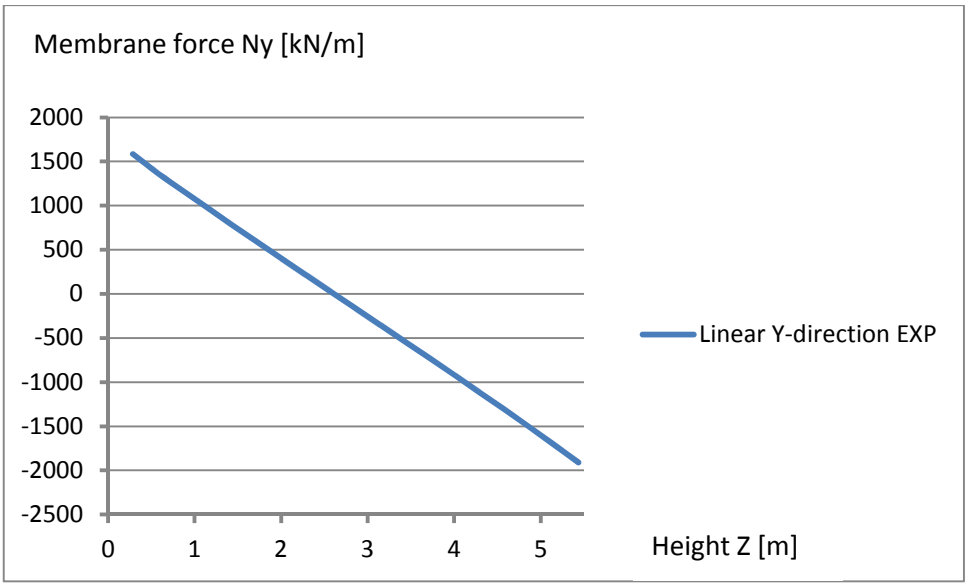


*Figure B.36 – Illustrating the Ny membrane force over height for linear EXP load*

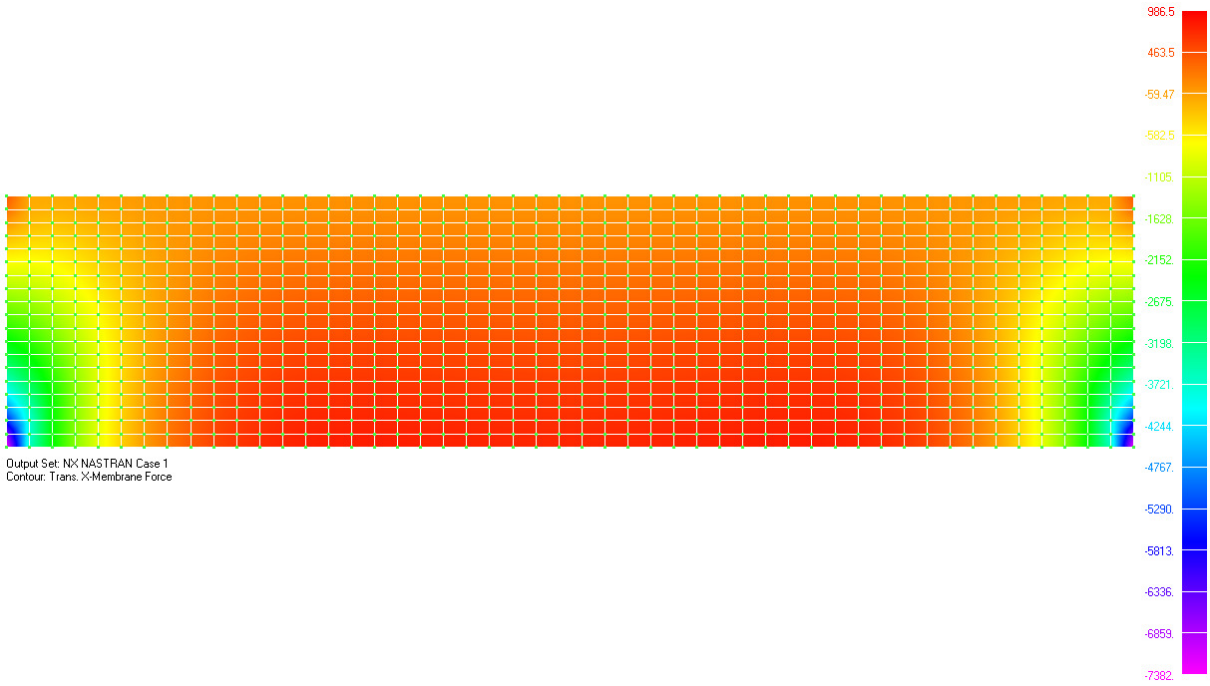


*Figure B.37 – Illustrating the contour plot for transformed Nx membrane force*

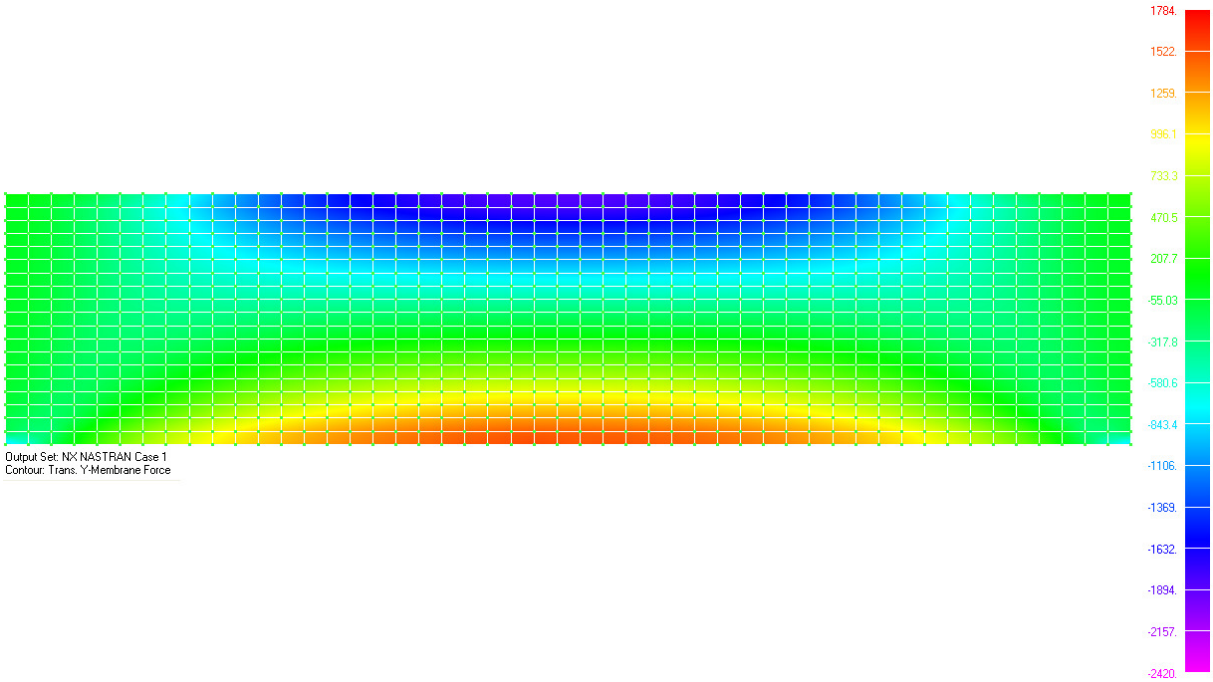


*Figure B.38 – Illustrating the contour plot for transformed Ny membrane force*

***Linear applied CON load***

*Table B.8 – Values for linear applied CON load*

| Transformed X-Membrane force | | Transformed Y-Membrane force | |
|---|---|---|---|
| z [m] | Nx [kN/m] | z [m] | Ny [kN/m] |
| 0.2868 | -870.632 | 0.2868 | -1857.45 |
| 0.5736 | -830.476 | 0.5736 | -1604.15 |
| 0.8596 | -787.943 | 0.8596 | -1373.93 |
| 1.1456 | -743.537 | 1.1456 | -1144.61 |
| 1.4316 | -697.85 | 1.4316 | -918.214 |
| 1.7176 | -650.906 | 1.7176 | -693.566 |
| 2.0036 | -602.862 | 2.0036 | -470.491 |
| 2.2896 | -553.871 | 2.2896 | -248.609 |
| 2.5756 | -504.125 | 2.5756 | -27.5463 |
| 2.8616 | -453.842 | 2.8616 | 193.063 |
| 3.1476 | -403.264 | 3.1476 | 413.674 |
| 3.4336 | -352.651 | 3.4336 | 634.77 |
| 3.7196 | -302.281 | 3.7196 | 856.803 |
| 4.0056 | -252.448 | 4.0056 | 1080.33 |
| 4.2916 | -203.447 | 4.2916 | 1305.83 |
| 4.5776 | -155.581 | 4.5776 | 1533.89 |
| 4.8636 | -109.149 | 4.8636 | 1764.98 |
| 5.1496 | -64.4406 | 5.1496 | 1999.66 |
| 5.4356 | -21.7359 | 5.4356 | 2238.45 |

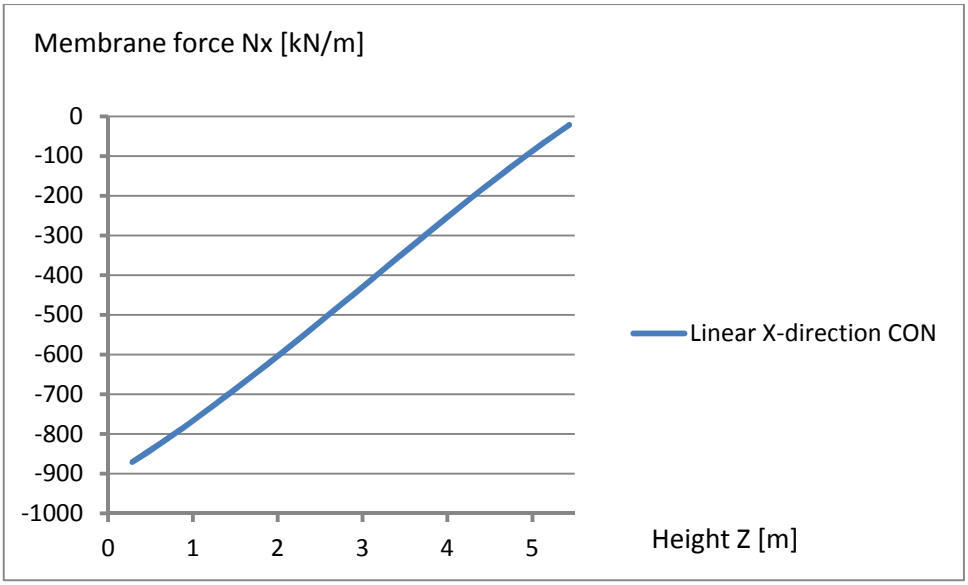


*Figure B.39 – Illustrating the Nx membrane force over height for linear CON load*

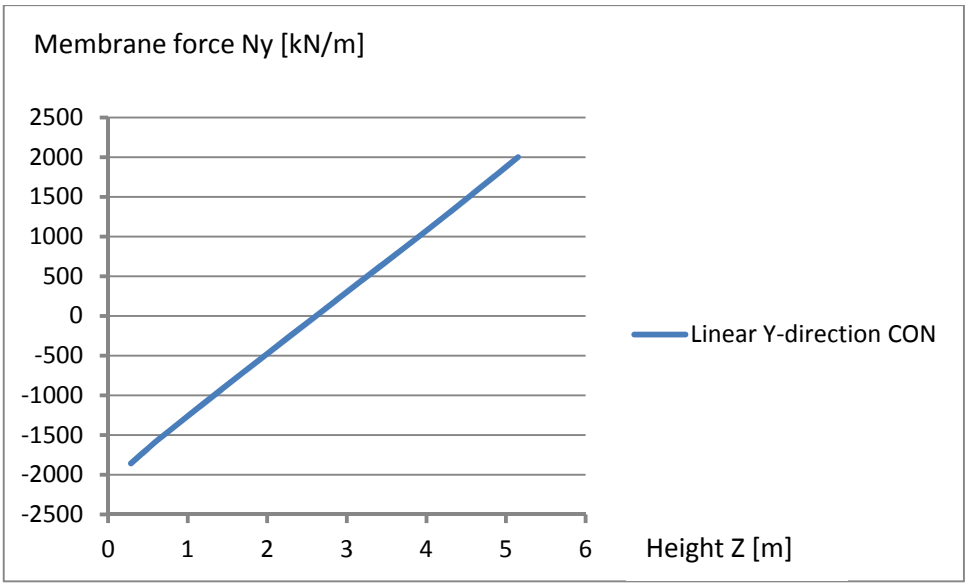


*Figure B.40 – Illustrating the Ny membrane force over height for linear CON load*

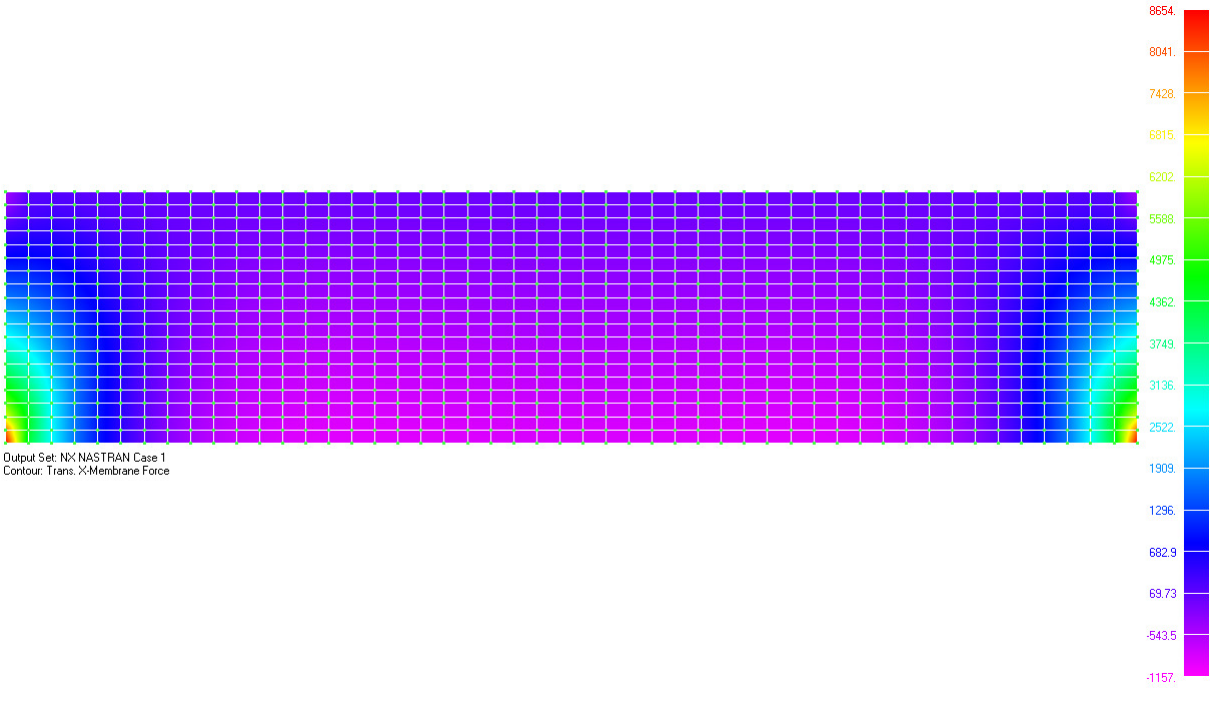


*Figure B.41 – Illustrating the contour plot for transformed Nx membrane force*

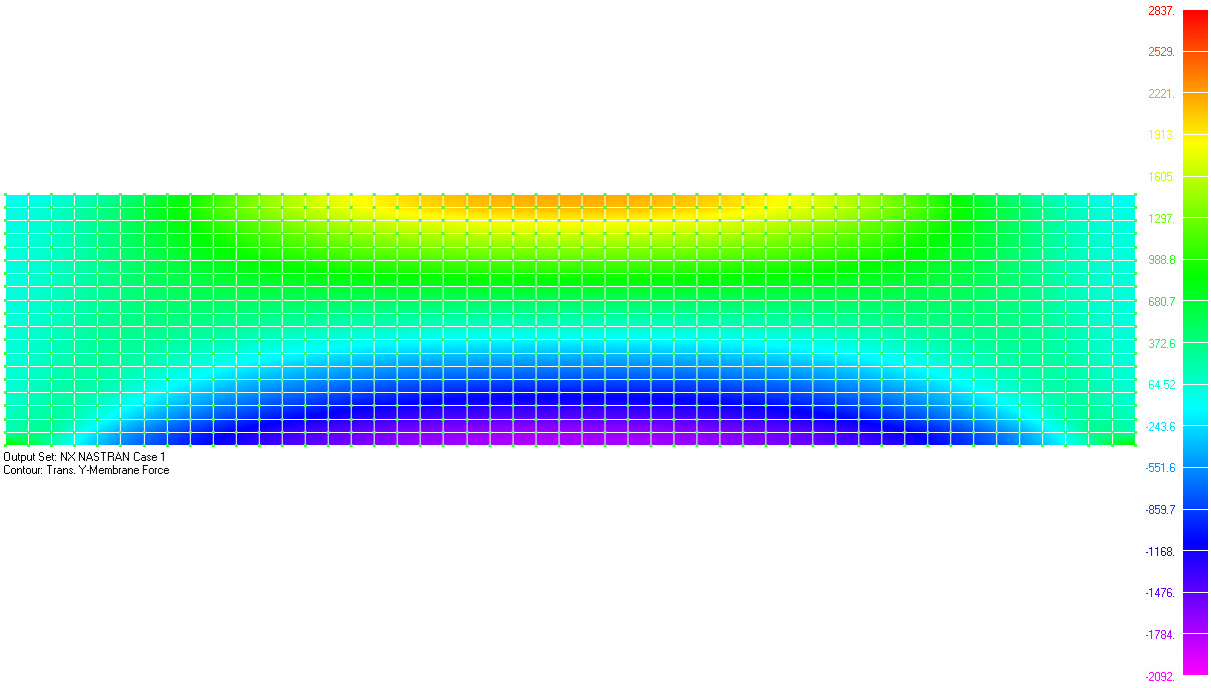


*Figure B.42 – Illustrating the contour plot for transformed Ny membrane force*

***Constant applied EXP load***

*Table B.9 – Values for constant applied EXP load*

| Transformed X-Membrane force | | Transformed Y-Membrane force | |
|---|---|---|---|
| z [m] | Nx [kN/m] | z [m] | Ny [kN/m] |
| 0.2868 | 643.094 | 0.2868 | -2529.17 |
| 0.5736 | 603.687 | 0.5736 | -2424.14 |
| 0.8596 | 564.846 | 0.8596 | -2339.55 |
| 1.1456 | 526.243 | 1.1456 | -2253.71 |
| 1.4316 | 487.494 | 1.4316 | -2168.98 |
| 1.7176 | 448.807 | 1.7176 | -2084.59 |
| 2.0036 | 410.293 | 2.0036 | -2000.85 |
| 2.2896 | 372.097 | 2.2896 | -1917.9 |
| 2.5756 | 334.357 | 2.5756 | -1835.98 |
| 2.8616 | 297.214 | 2.8616 | -1755.32 |
| 3.1476 | 260.809 | 3.1476 | -1676.17 |
| 3.4336 | 225.282 | 3.4336 | -1598.79 |
| 3.7196 | 190.776 | 3.7196 | -1523.45 |
| 4.0056 | 157.432 | 4.0056 | -1450.42 |
| 4.2916 | 125.389 | 4.2916 | -1379.96 |
| 4.5776 | 94.7821 | 4.5776 | -1312.34 |
| 4.8636 | 65.7416 | 4.8636 | -1247.83 |
| 5.1496 | 38.392 | 5.1496 | -1186.66 |
| 5.4356 | 12.8488 | 5.4356 | -1129.09 |

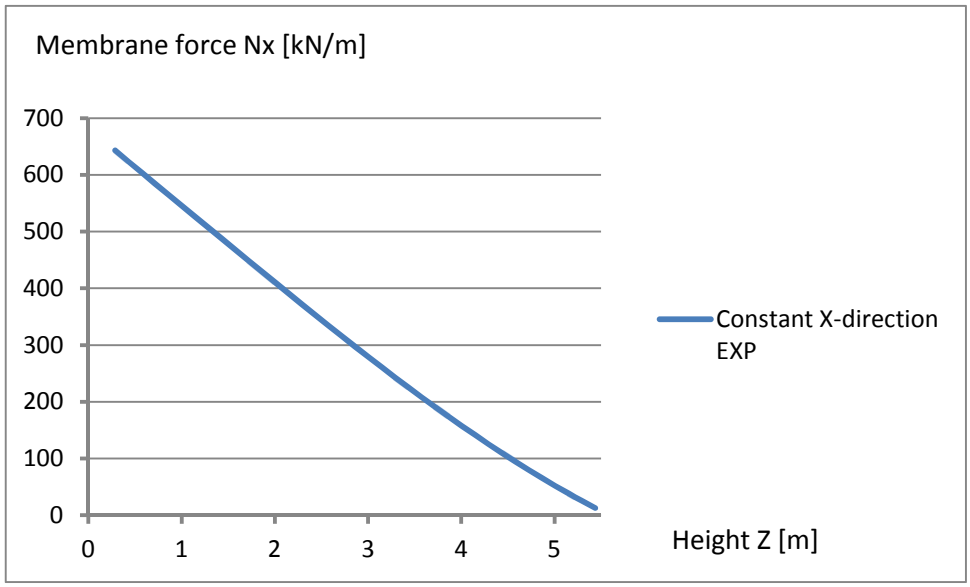


*Figure B.43 – Illustrating the Nx membrane force over height for constant EXP load*

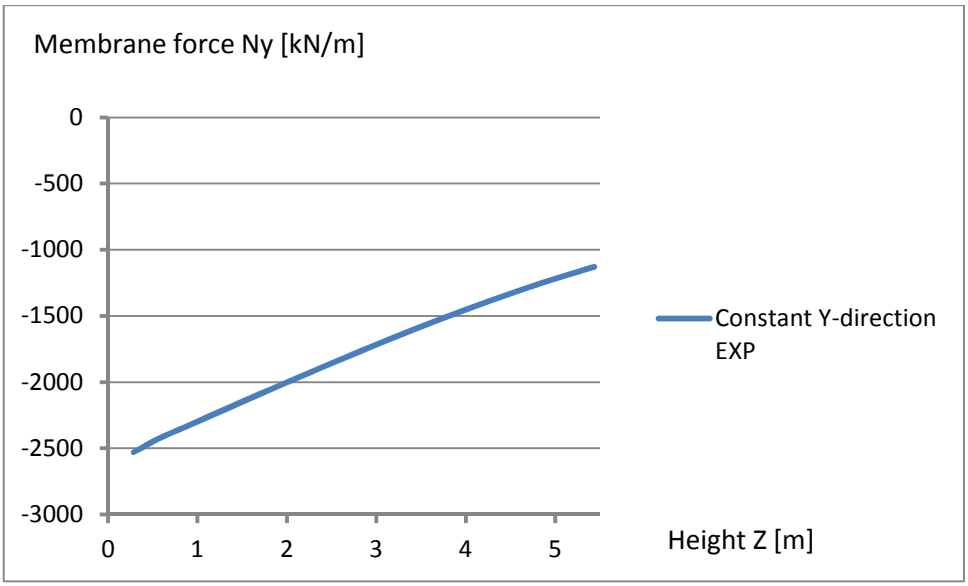


*Figure B.44 – Illustrating the Ny membrane force over height for constant EXP load*

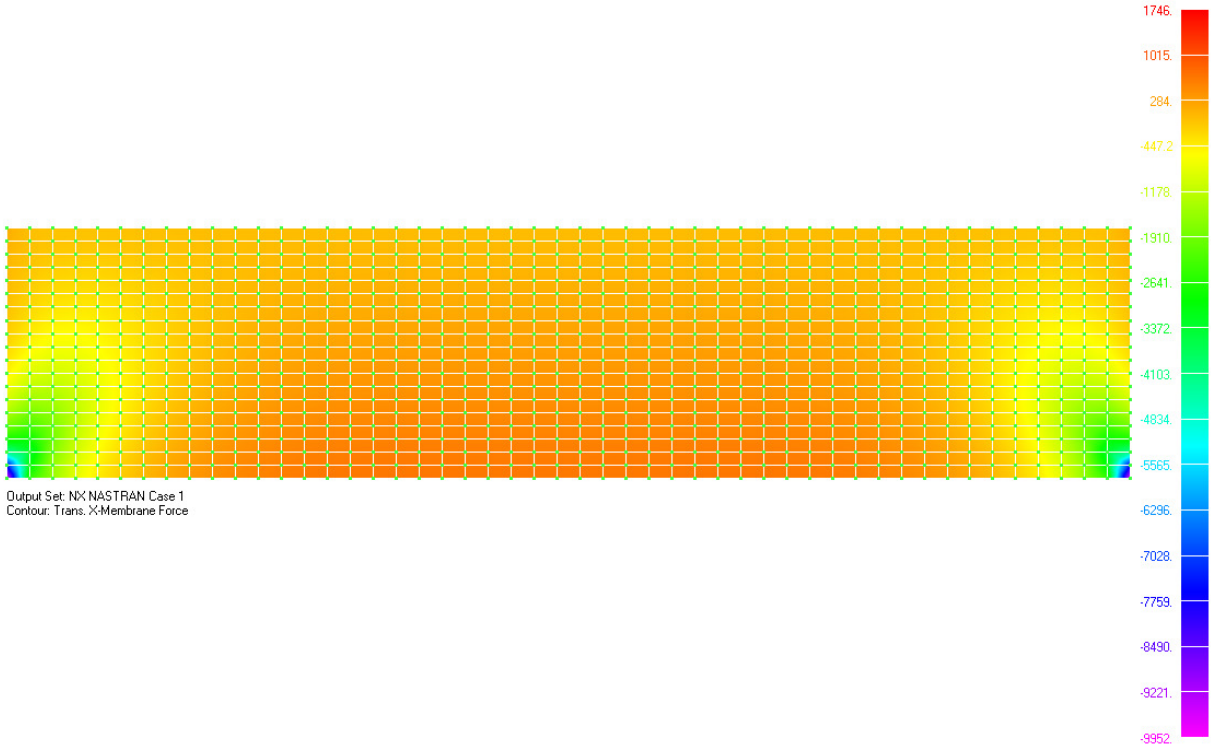


*Figure B.45 – Illustrating the contour plot for transformed Nx membrane force*

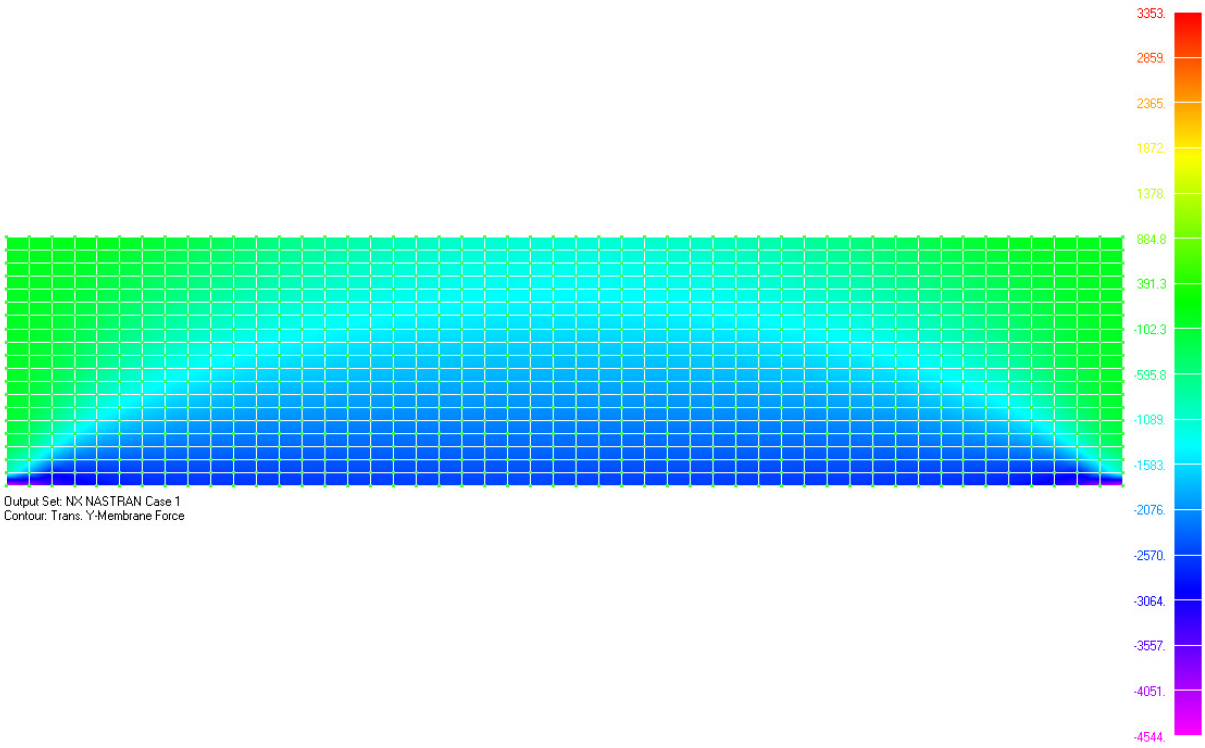


*Figure B.46 – Illustrating the contour plot for transformed Ny membrane force*

***Constant applied CON load***

*Table B.10 – Values for constant applied CON load*

| Transformed X-Membrane force | | Transformed Y-Membrane force | |
|---|---|---|---|
| z [m] | Nx [kN/m] | z [m] | Ny [kN/m] |
| 0.2868 | -750.364 | 0.2868 | 2920.09 |
| 0.5736 | -710.546 | 0.5736 | 2827.06 |
| 0.8596 | -665.767 | 0.8596 | 2734.91 |
| 1.1456 | -620.209 | 1.1456 | 2637.2 |
| 1.4316 | -574.277 | 1.4316 | 2538.88 |
| 1.7176 | -528.419 | 1.7176 | 2440.15 |
| 2.0036 | -482.816 | 2.0036 | 2341.73 |
| 2.2896 | -437.644 | 2.2896 | 2243.98 |
| 2.5756 | -393.064 | 2.5756 | 2147.27 |
| 2.8616 | -349.233 | 2.8616 | 2051.94 |
| 3.1476 | -306.313 | 3.1476 | 1958.31 |
| 3.4336 | -264.463 | 3.4336 | 1866.71 |
| 3.7196 | -223.849 | 3.7196 | 1777.48 |
| 4.0056 | -184.635 | 4.0056 | 1690.95 |
| 4.2916 | -146.982 | 4.2916 | 1607.45 |
| 4.5776 | -111.051 | 4.5776 | 1527.31 |
| 4.8636 | -76.9976 | 4.8636 | 1450.85 |
| 5.1496 | -44.9705 | 5.1496 | 1378.39 |
| 5.4356 | -15.1116 | 5.4356 | 1310.23 |

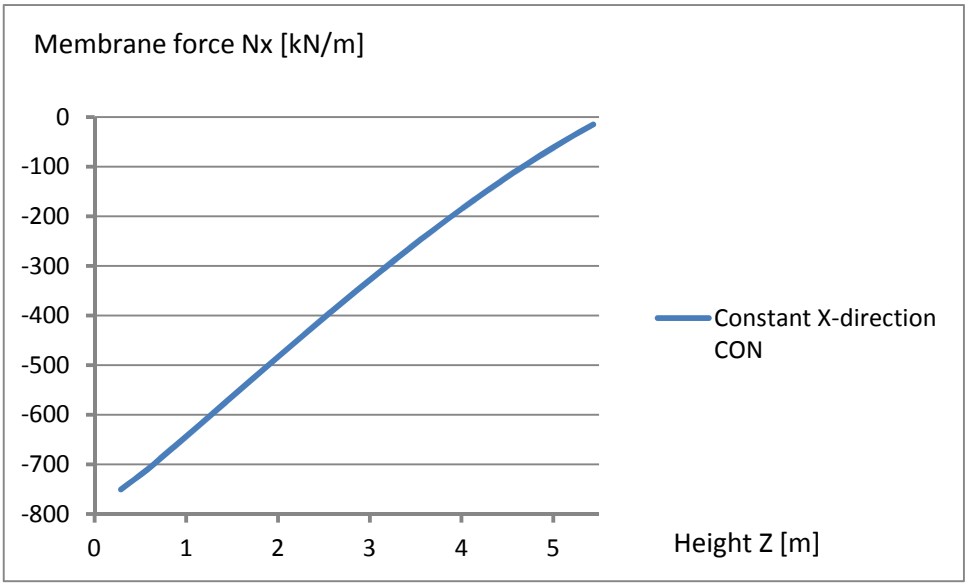


*Figure B.46 – Illustrating the Nx membrane force over height for constant CON load*

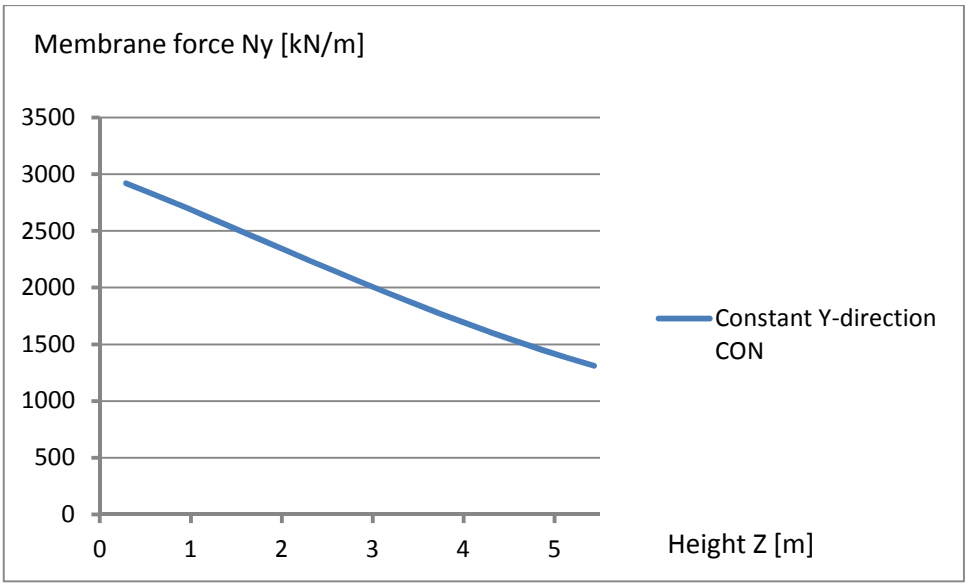


*Figure B.47 – Illustrating the Ny membrane force over height for constant CON load*

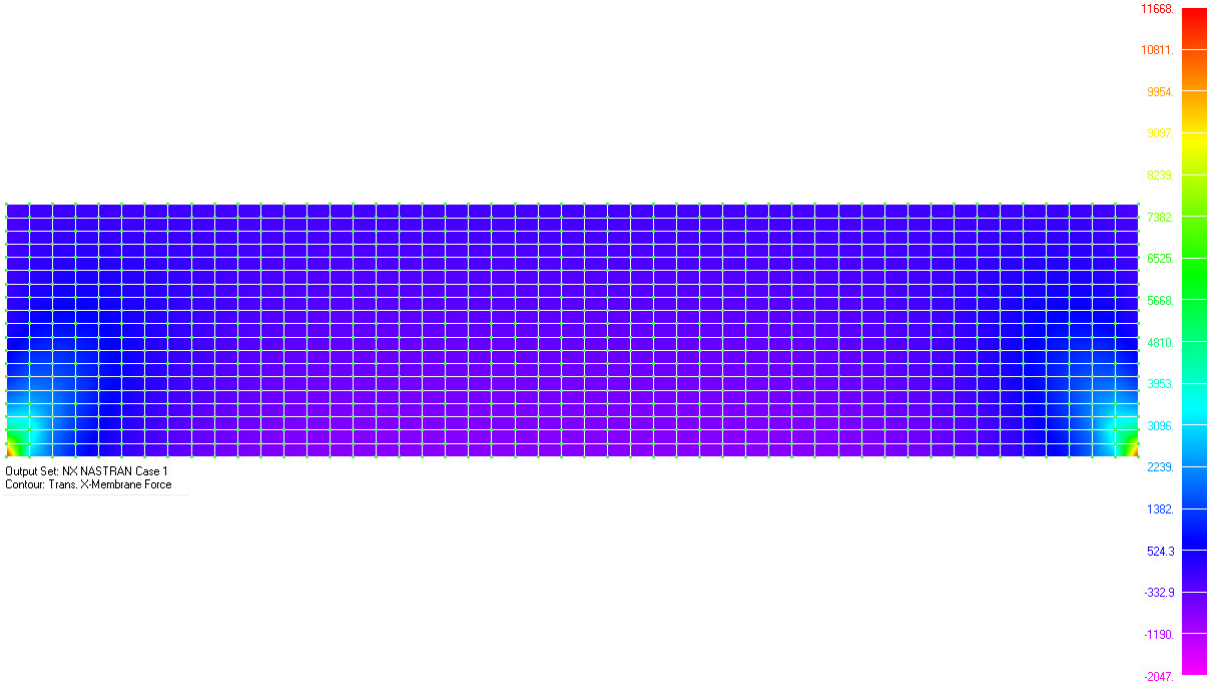


*Figure B.48 – Illustrating the contour plot for transformed Nx membrane force*

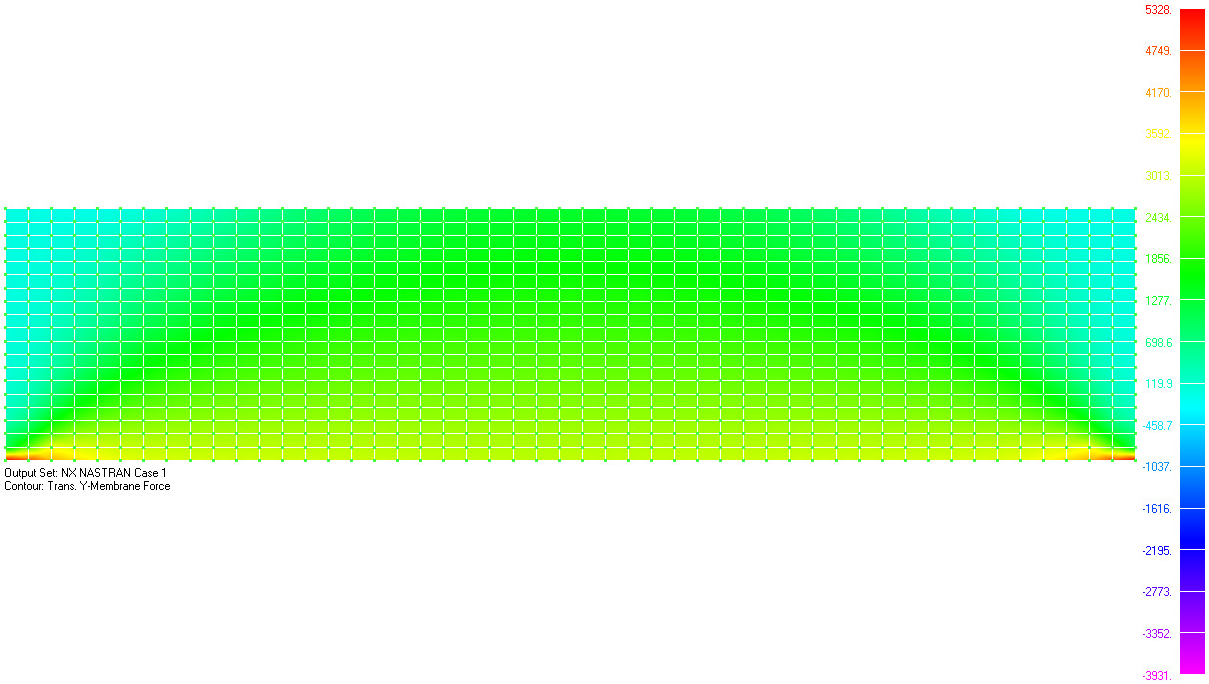


*Figure B.49 – Illustrating the contour plot for transformed Ny membrane force*

***Uneven applied EXP load***

*Table B.11 – Values for uneven applied EXP load*

| Transformed X-Membrane force | | Transformed Y-Membrane force | |
|---|---|---|---|
| z [m] | Nx [kN/m] | z [m] | Ny [kN/m] |
| 0.2868 | 758.71 | 0.2868 | 1438.15 |
| 0.5736 | 721.231 | 0.5736 | 1515.4 |
| 0.8596 | 685.524 | 0.8596 | 1595.64 |
| 1.1456 | 648.777 | 1.1456 | 1674.18 |
| 1.4316 | 610.846 | 1.4316 | 1754.22 |
| 1.7176 | 571.592 | 1.7176 | 1669.34 |
| 2.0036 | 531.097 | 2.0036 | 1378.53 |
| 2.2896 | 489.478 | 2.2896 | 1089.01 |
| 2.5756 | 446.899 | 2.5756 | 800.544 |
| 2.8616 | 403.552 | 2.8616 | 512.823 |
| 3.1476 | 359.654 | 3.1476 | 225.492 |
| 3.4336 | 315.442 | 3.4336 | -61.8476 |
| 3.7196 | 271.173 | 3.7196 | -349.628 |
| 4.0056 | 227.117 | 4.0056 | -638.309 |
| 4.2916 | 183.552 | 4.2916 | -928.362 |
| 4.5776 | 140.76 | 4.5776 | -1220.28 |
| 4.8636 | 99.0228 | 4.8636 | -1514.54 |
| 5.1496 | 58.6154 | 5.1496 | -1811.62 |
| 5.4356 | 19.8024 | 5.4356 | -2111.99 |

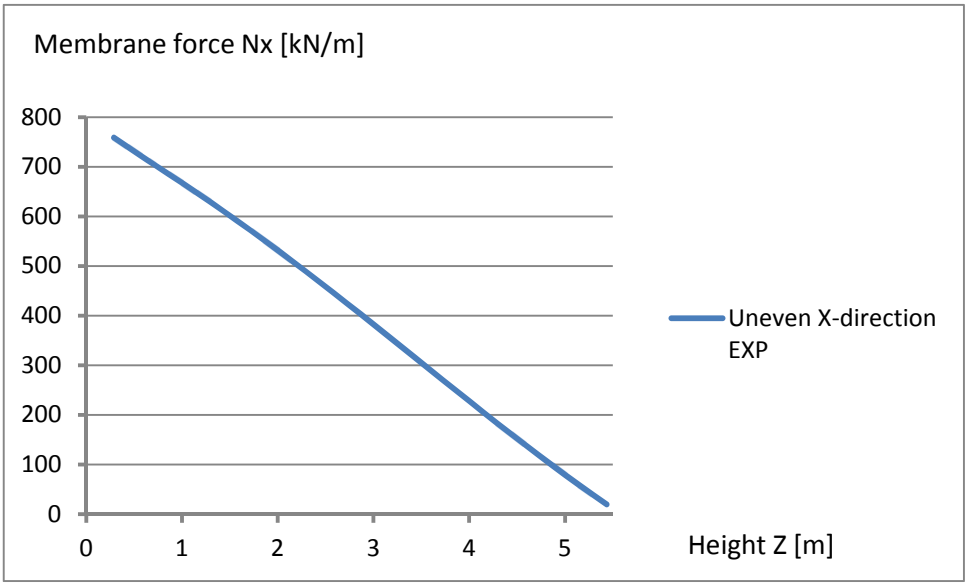


*Figure B.50 – Illustrating the Nx membrane force over height for uneven EXP load*

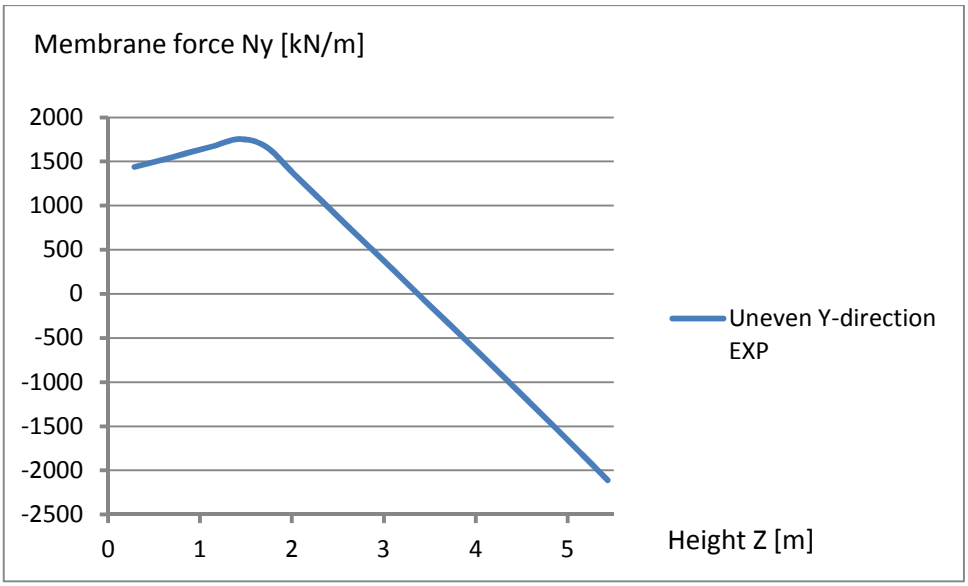


*Figure B.51 – Illustrating the Ny membrane force over height for uneven EXP load*

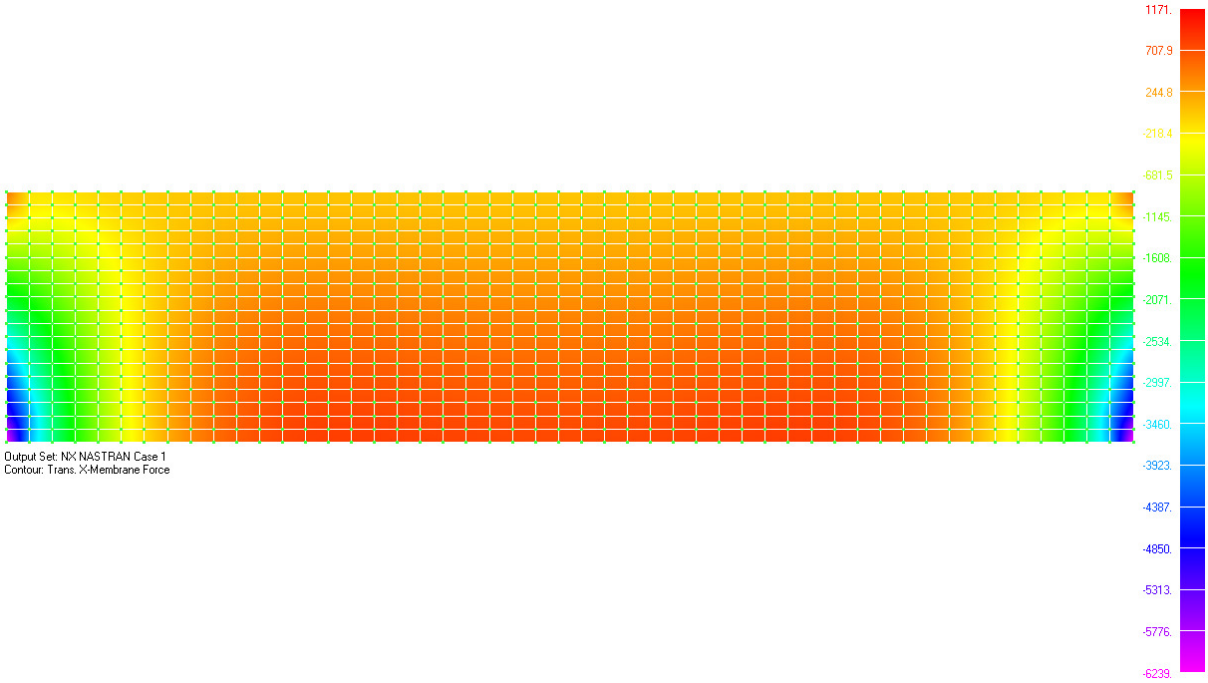


*Figure B.52 – Illustrating the contour plot for transformed Nx membrane force*

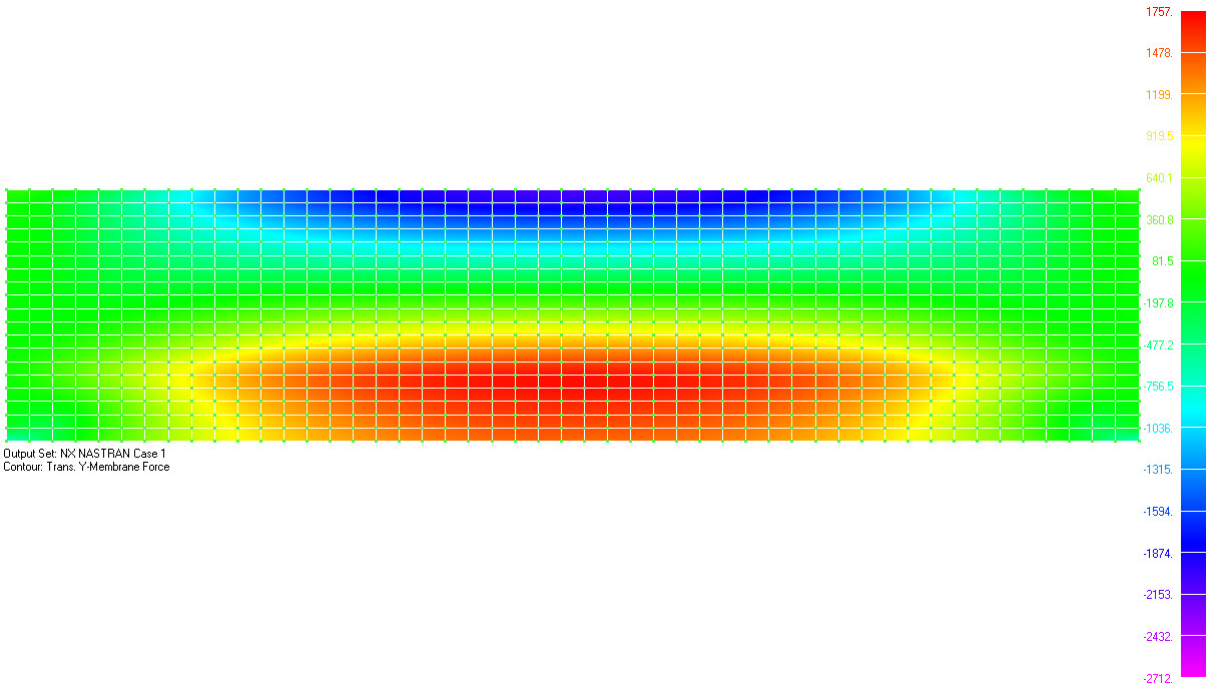


*Figure B.53 – Illustrating the contour plot for transformed Ny membrane force*

***Uneven applied CON load***

*Table B.12 – Values for uneven applied CON load*

| Transformed X-Membrane force | | Transformed Y-Membrane force | |
|---|---|---|---|
| z [m] | Nx [kN/m] | z [m] | Ny [kN/m] |
| 0.2868 | -883.908 | 0.2868 | -1682.73 |
| 0.5736 | -843.507 | 0.5736 | -1788.22 |
| 0.8596 | -802.185 | 0.8596 | -1876.23 |
| 1.1456 | -759.536 | 1.1456 | -1967.69 |
| 1.4316 | -715.129 | 1.4316 | -2060.45 |
| 1.7176 | -669.136 | 1.7176 | -1960.35 |
| 2.0036 | -621.664 | 2.0036 | -1618.87 |
| 2.2896 | -572.886 | 2.2896 | -1278.95 |
| 2.5756 | -522.999 | 2.5756 | -940.28 |
| 2.8616 | -472.231 | 2.8616 | -602.478 |
| 3.1476 | -420.833 | 3.1476 | -265.123 |
| 3.4336 | -369.082 | 3.4336 | 72.255 |
| 3.7196 | -317.276 | 3.7196 | 410.185 |
| 4.0056 | -265.727 | 4.0056 | 749.159 |
| 4.2916 | -214.756 | 4.2916 | 1089.75 |
| 4.5776 | -164.691 | 4.5776 | 1432.51 |
| 4.8636 | -115.857 | 4.8636 | 1778.02 |
| 5.1496 | -68.5743 | 5.1496 | 2126.84 |
| 5.4356 | -23.1478 | 5.4356 | 2479.46 |

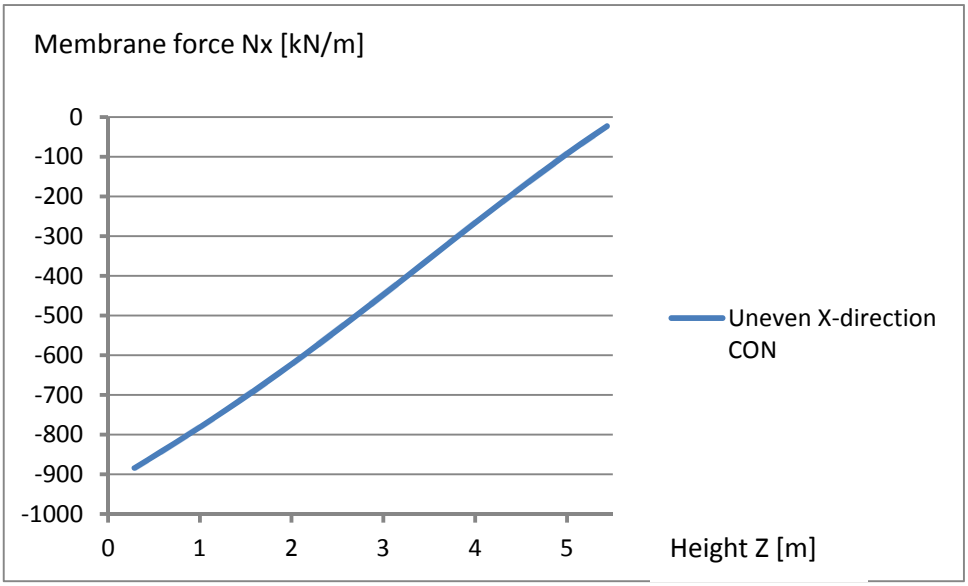


*Figure B.54 – Illustrating the Nx membrane force over height for uneven CON load*

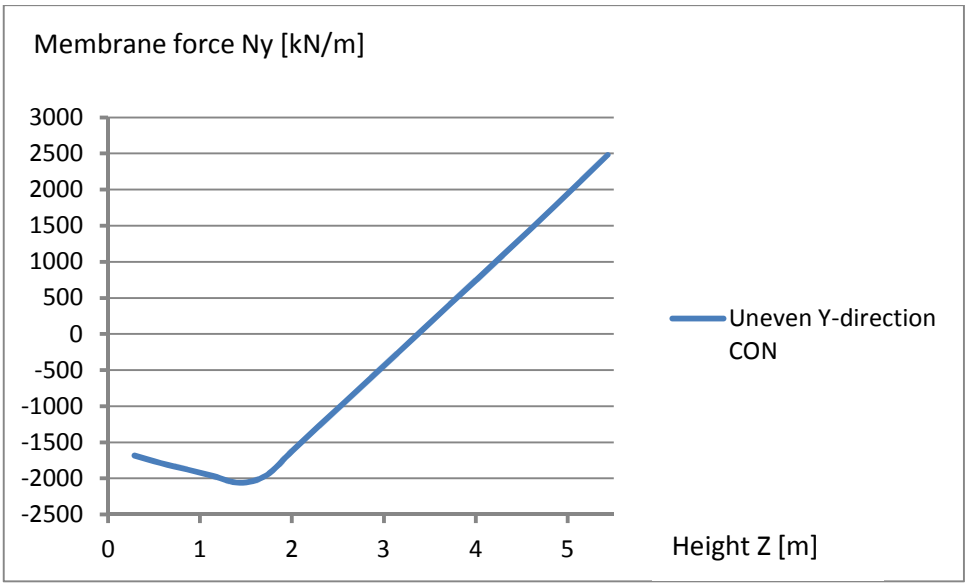


*Figure B.55 – Illustrating the Ny membrane force over height for uneven CON load*

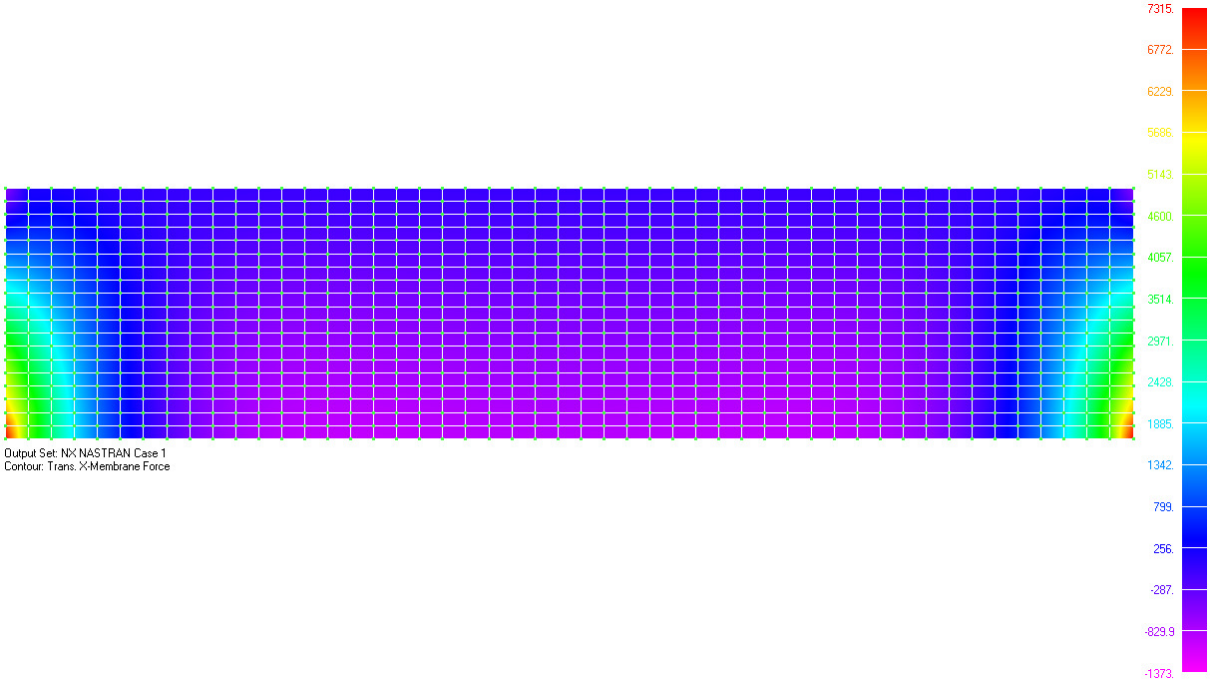


*Figure B.56 – Illustrating the contour plot for transformed Nx membrane force*

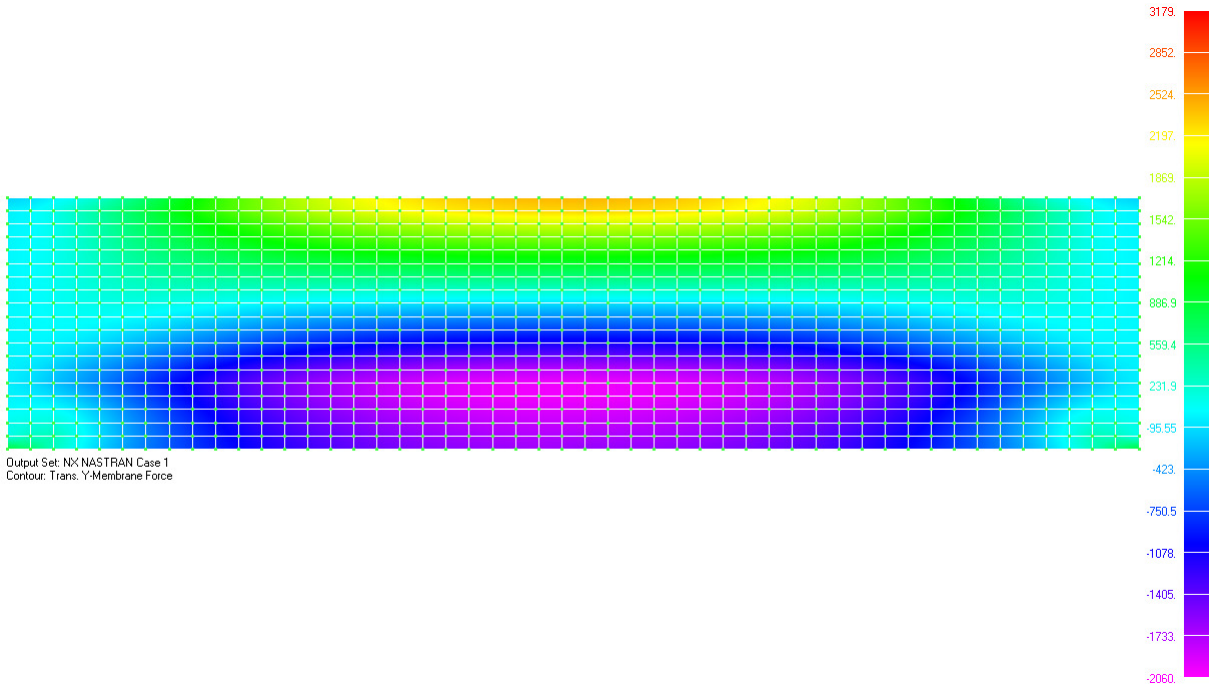


*Figure B.57 – Illustrating the contour plot for transformed Ny membrane force*

**A comparison between the different load application possibilities for each load has been made.**

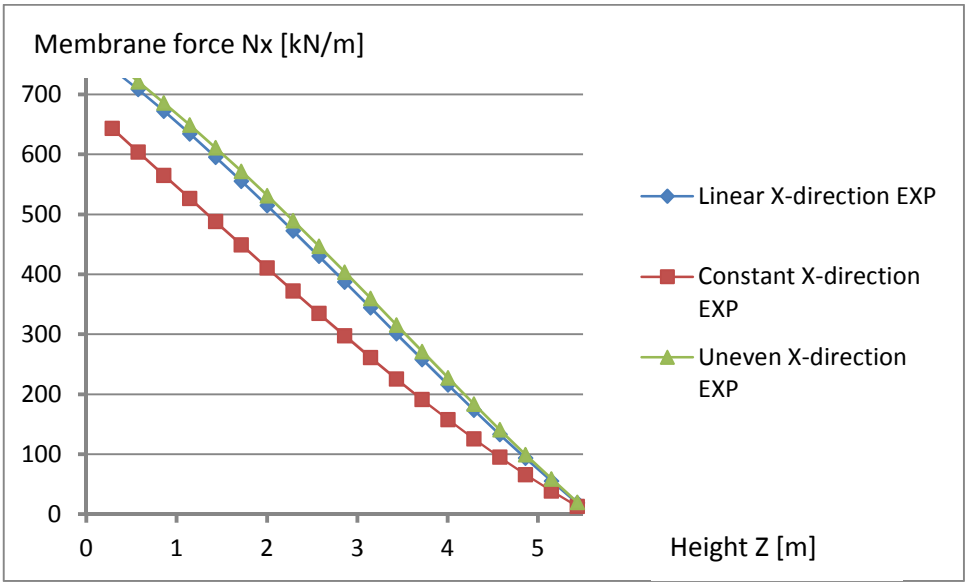


*Figure B.58 – Illustrating the Nx membrane force over height for the different load application possibilities for EXP load.*

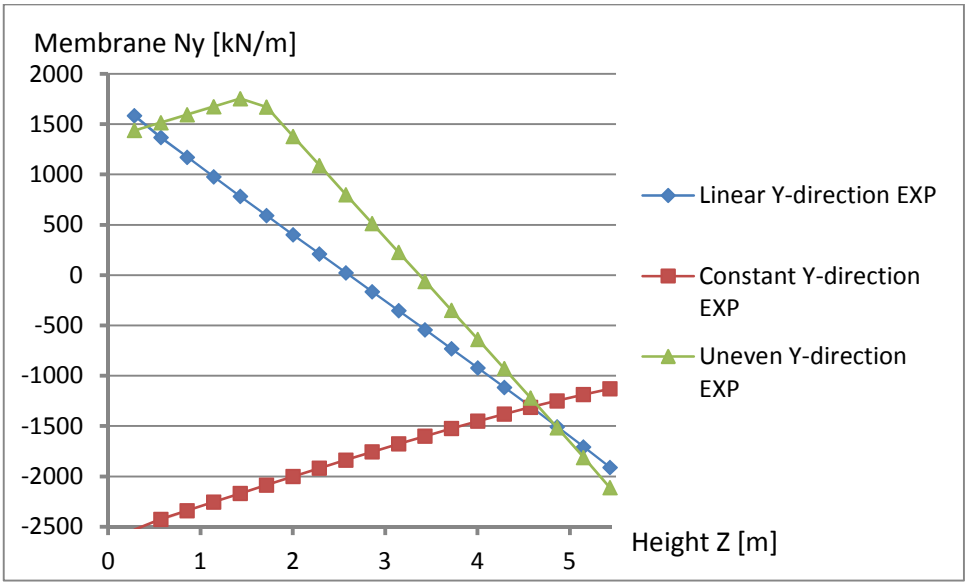


*Figure B.59 – Illustrating the Ny membrane force over height for the different load application possibilities for EXP load.*

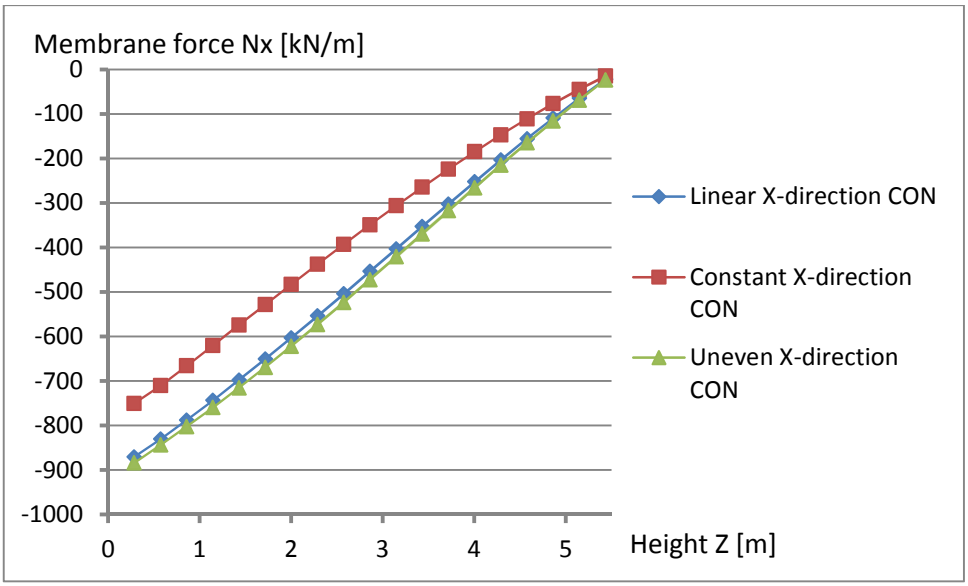


*Figure B.60 – Illustrating the Nx membrane force over height for the different load application possibilities for CON load.*

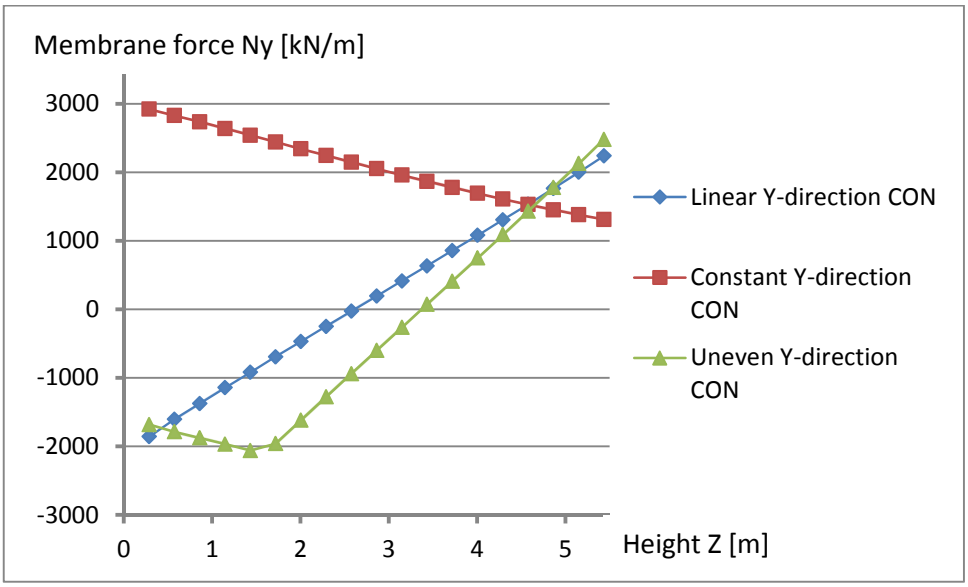


*Figure B.61 – Illustrating the Ny membrane force over height for the different load application possibilities for CON load.*

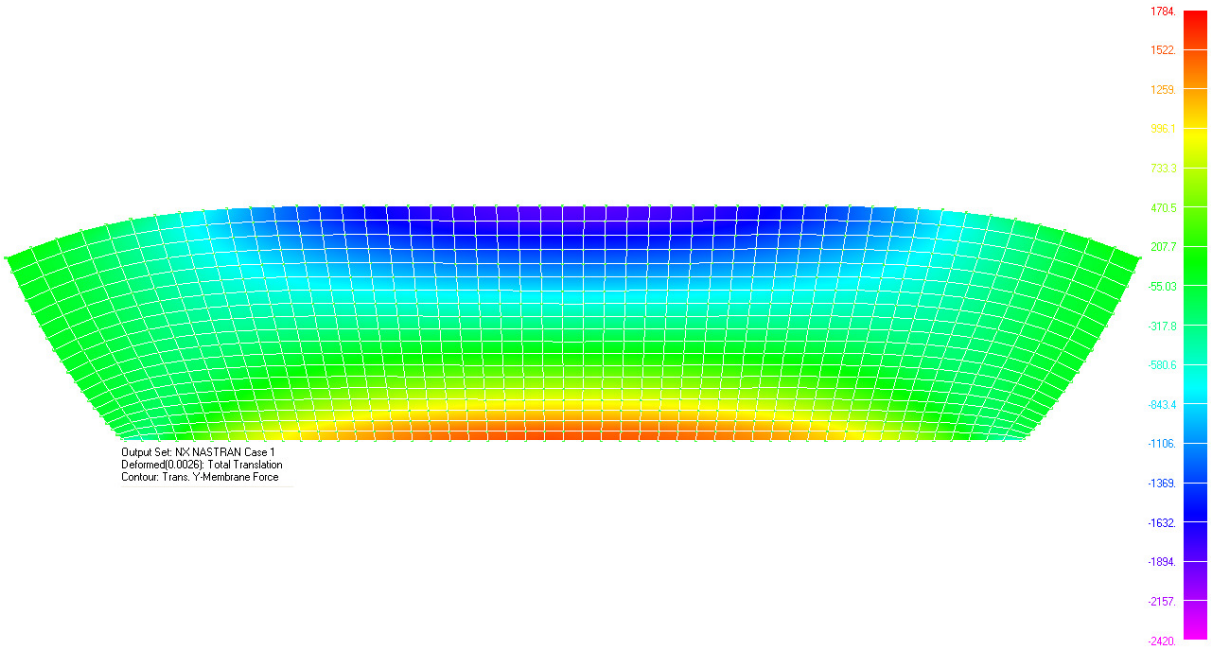


*Figure B.62 – Illustrating the principle behavior and contour plot for EXP loading*

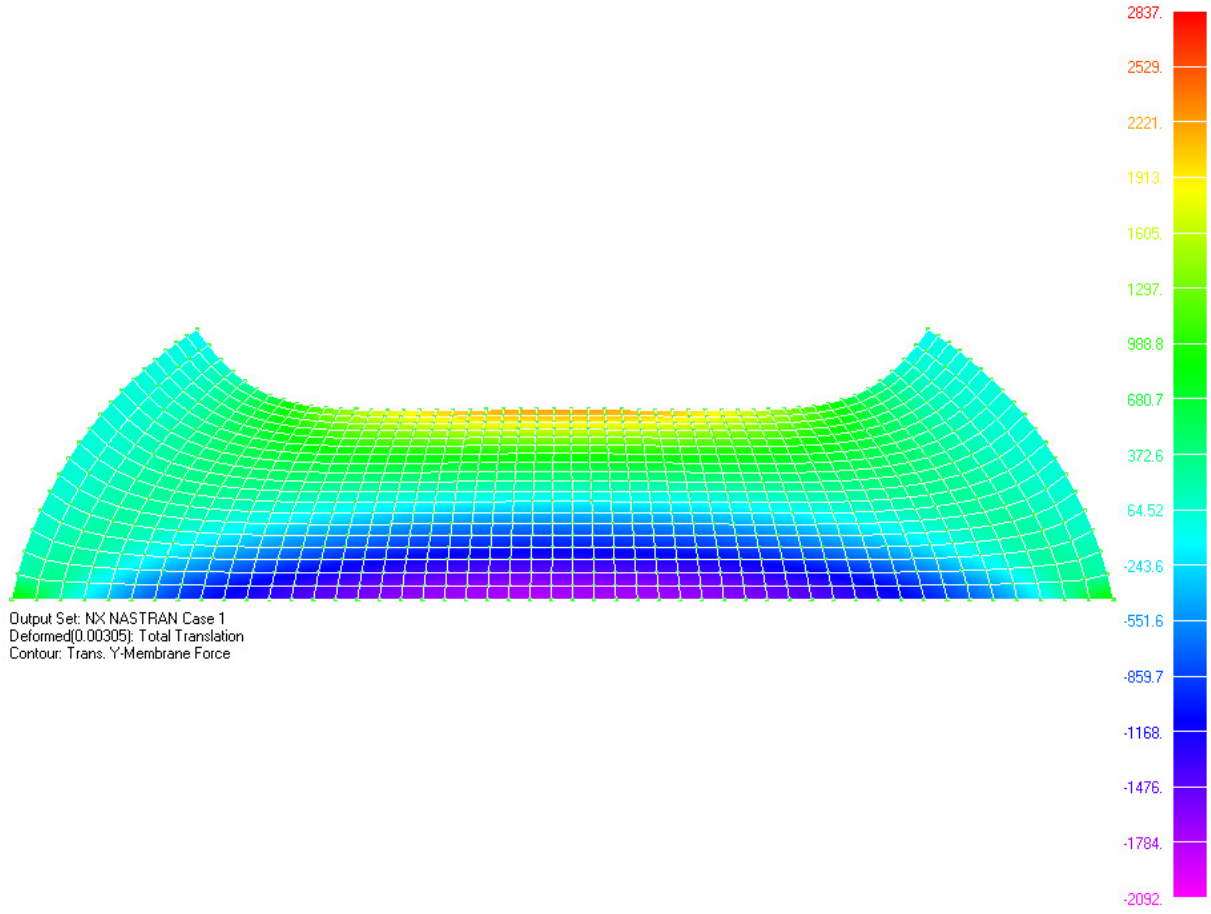


*Figure B.63 – Illustrating the principle behavior and contour plot for CON loading*

# APPENDIX C – Comparison 2D and 3D

## *Slab-bridge*

The values are extracted from two strips, span strip and over support strip; see Figure C1

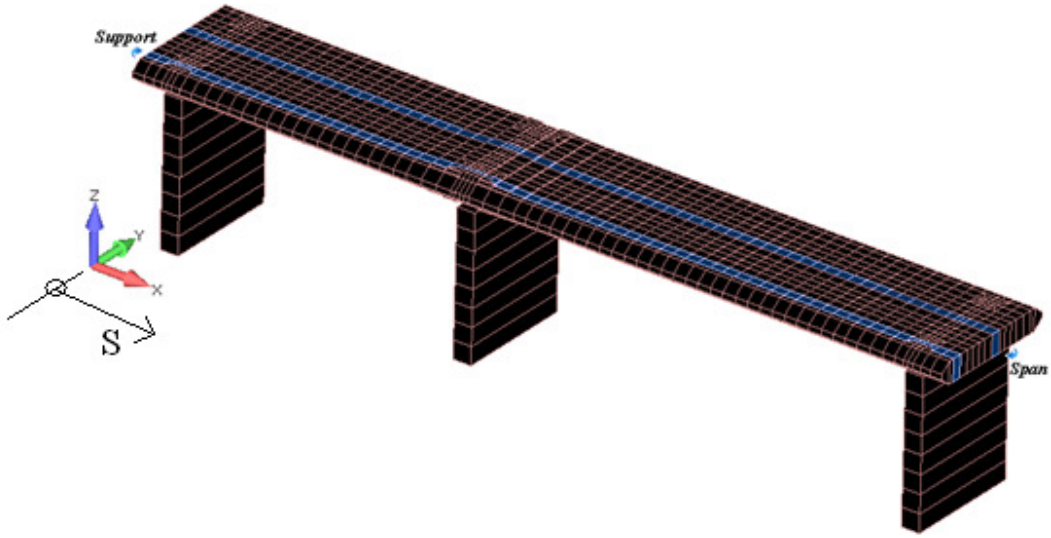


*Figure C.1 – Illustration of the location of the span- and support strip.*

*Table C.1 –Partial factors*

Partial factors

Safety class: 3

| | | | | | | | | ULS | | | | SLS |
|---|---|---|---|---|---|---|---|---|---|---|---|---|
| | Load case | | Load coefficient | | | | | ULS-A | | ULS-B | | SLS-QP |
| | Permanente loads | | sup | inf | Y.G.jsup | Y.G.jinf | ξ | max | min | max | min | |
| 1 | EG | Self-weight | 1 | 1 | 1.35 | 1 | 0.89 | 1.35 | 1 | 1 | 1 | 1 |
| 2 | BEL | Pavement | 1.1 | 0.9 | 1.35 | 1 | 0.89 | 1.49 | 0.9 | 1.1 | 0.9 | 1.3 |
| 4 | GL | Support settlement | 1 | 1 | 1.1 | 1 | 1 | 0.66 | 0 | 1 | 1 | 1 |
| 5 | KRYMP | Shrinkage | 1 | 1 | 1.35 | 1 | 0.89 | 0.81 | 0 | 1 | 1 | 1 |
| | Variabla loads | | k | Ψ.0 | Ψ.1 | Ψ.2 | Y.Q | | | | | |
| 6 | TS | Traffic loads | k | 0.75 | 0.75 | 0 | 1.5 | 1.13 | 1.13 | 1.5 | 1.5 | 0 |
| 7 | UDL | Traffic loads | k | 0.4 | 0.4 | 0 | 1.5 | 0.6 | 0.6 | 1.5 | 0.6 | 0 |
| 8 | TEMP | Thermal actions | k | 0.6 | 0.6 | 0.5 | 1.5 | 0.54 | 0.54 | 0.9 | 0.5 | 0.5 |

# Support

| s [m] | Selfweight [kNm/m] | | Selfweight edge-beam [kNm/m] | | Selfweight total [kNm/m] | |
|---|---|---|---|---|---|---|
| | pos | neg | pos | neg | max | min |
| 0.31667 | 0 | -6.21045 | 0.57093 | -1.51334 | 0.57 | -7.72 |
| 0.9 | 0 | -30.9308 | 0 | -3.27184 | 0.00 | -34.20 |
| 1.30813 | 0 | -62.4261 | 0 | -4.81721 | 0.00 | -67.24 |
| 1.54104 | 0 | -93.5285 | 0 | -8.10401 | 0.00 | -101.63 |
| 1.76625 | 0 | -95.0613 | 0 | -8.64115 | 0.00 | -103.70 |
| 2.03375 | 0 | -85.0583 | 0 | -8.26766 | 0.00 | -93.33 |
| 2.27694 | 0 | -69.9574 | 0 | -6.85837 | 0.00 | -76.82 |
| 2.52082 | 19.2983 | -17.767 | 0 | -3.41246 | 19.30 | -21.18 |
| 2.98289 | 84.6485 | 0 | 1.62388 | 0 | 86.27 | 0.00 |
| 3.66316 | 159.136 | 0 | 5.45436 | 0 | 164.59 | 0.00 |
| 5.07368 | 230.23 | 0 | 10.2332 | 0 | 240.46 | 0.00 |
| 5.77895 | 237.815 | 0 | 11.1178 | 0 | 248.93 | 0.00 |
| 6.48421 | 230.442 | 0 | 11.4549 | 0 | 241.90 | 0.00 |
| 7.18947 | 223.007 | 0 | 10.8959 | 0 | 233.90 | 0.00 |
| 7.89474 | 199.797 | 0 | 9.42896 | 0 | 209.23 | 0.00 |
| 8.6 | 160.787 | 0 | 7.04703 | 0 | 167.83 | 0.00 |
| 9.30526 | 105.933 | 0 | 3.74578 | -0.56035 | 109.68 | -0.56 |
| 10.0105 | 35.1975 | -42.6055 | 0 | -5.63695 | 35.20 | -48.24 |
| 10.7158 | 0 | -143.061 | 0 | -11.6372 | 0.00 | -154.70 |
| 11.4211 | 0 | -258.753 | 0 | -18.5577 | 0.00 | -277.31 |
| 12.1263 | 0 | -389.57 | 0 | -26.3933 | 0.00 | -415.96 |
| 12.8316 | 0 | -535.177 | 0 | -35.1344 | 0.00 | -570.31 |
| 13.5368 | 0 | -694.926 | 0 | -44.7589 | 0.00 | -739.68 |
| 14.2421 | 0 | -867.544 | 0 | -55.2316 | 0.00 | -922.78 |
| 14.9474 | 0 | -1057.31 | 0 | -66.8303 | 0.00 | -1124.14 |
| 15.725 | 0 | -1311.62 | 0 | -82.1125 | 0.00 | -1393.73 |
| 16.575 | 0 | -1651.79 | 0 | -101.489 | 0.00 | -1753.28 |
| 17.2 | 0 | -1923.32 | 0 | -116.319 | 0.00 | -2039.64 |
| 17.6 | 0 | -2056.66 | 0 | -124.34 | 0.00 | -2181.00 |
| 17.9163 | 0 | -2255.32 | 0 | -135.92 | 0.00 | -2391.24 |
| 18.1663 | 0 | -2309.87 | 0 | -138.156 | 0.00 | -2448.03 |
| 18.4338 | 0 | -2298.83 | 0 | -136.988 | 0.00 | -2435.82 |
| 18.6838 | 0 | -2255.22 | 0 | -135.811 | 0.00 | -2391.03 |
| 19 | 0 | -2035.18 | 0 | -123.319 | 0.00 | -2158.50 |
| 19.4 | 0 | -1858.94 | 0 | -112.909 | 0.00 | -1971.85 |
| 20.025 | 0 | -1531.1 | 0 | -94.5197 | 0.00 | -1625.62 |
| 20.875 | 0 | -1109.75 | 0 | -69.5757 | 0.00 | -1179.33 |
| 21.6453 | 0 | -785.313 | 0 | -49.5738 | 0.00 | -834.89 |
| 22.3359 | 0 | -533.222 | 0 | -33.9267 | 0.00 | -567.15 |
| 23.0266 | 0 | -297.752 | 0 | -19.4331 | 0.00 | -317.19 |
| 23.7172 | 122.862 | -75.109 | 7.00412 | -5.78817 | 129.87 | -80.90 |
| 24.4078 | 320.546 | 0 | 18.8788 | 0 | 339.42 | 0.00 |

| | | | | | | |
|---|---|---|---|---|---|---|
| 25.0984 | 502.755 | 0 | 29.8457 | 0 | 532.60 | 0.00 |
| 25.7891 | 669.52 | 0 | 39.8983 | 0 | 709.42 | 0.00 |
| 26.4797 | 821.013 | 0 | 49.0477 | 0 | 870.06 | 0.00 |
| 27.1703 | 957.283 | 0 | 57.2911 | 0 | 1014.57 | 0.00 |
| 27.8609 | 1078.4 | 0 | 64.6307 | 0 | 1143.03 | 0.00 |
| 28.5516 | 1184.41 | 0 | 71.0659 | 0 | 1255.48 | 0.00 |
| 29.2422 | 1275.35 | 0 | 76.5974 | 0 | 1351.95 | 0.00 |
| 29.9328 | 1351.25 | 0 | 81.225 | 0 | 1432.48 | 0.00 |
| 30.6234 | 1412.11 | 0 | 84.9492 | 0 | 1497.06 | 0.00 |
| 31.3141 | 1457.97 | 0 | 87.7698 | 0 | 1545.74 | 0.00 |
| 32.0047 | 1488.83 | 0 | 89.6872 | 0 | 1578.52 | 0.00 |
| 32.6953 | 1504.69 | 0 | 90.7014 | 0 | 1595.39 | 0.00 |
| 33.3859 | 1505.84 | 0 | 90.8126 | 0 | 1596.65 | 0.00 |
| 34.0766 | 1507.22 | 0 | 90.8813 | 0 | 1598.10 | 0.00 |
| 34.7672 | 1493.73 | 0 | 90.0976 | 0 | 1583.83 | 0.00 |
| 35.4578 | 1465.4 | 0 | 88.4094 | 0 | 1553.81 | 0.00 |
| 36.1484 | 1422.27 | 0 | 85.8158 | 0 | 1508.09 | 0.00 |
| 36.8391 | 1364.37 | 0 | 82.3178 | 0 | 1446.69 | 0.00 |
| 37.5297 | 1291.81 | 0 | 77.9171 | 0 | 1369.73 | 0.00 |
| 38.2203 | 1204.64 | 0 | 72.6304 | 0 | 1277.27 | 0.00 |
| 38.9109 | 1102.58 | 0 | 66.4573 | 0 | 1169.04 | 0.00 |
| 39.565 | 992.797 | 0 | 59.7887 | 0 | 1052.59 | 0.00 |
| 40.2263 | 867.076 | 0 | 51.9924 | 0 | 919.07 | 0.00 |
| 40.9316 | 715.444 | 0 | 42.521 | 0 | 757.97 | 0.00 |
| 41.6368 | 535.926 | 0 | 31.4105 | 0 | 567.34 | 0.00 |
| 42.3171 | 318.868 | 0 | 18.3721 | 0 | 337.24 | 0.00 |
| 42.7792 | 151.744 | 0 | 8.2839 | 0 | 160.03 | 0.00 |
| 43.0231 | 27.1189 | -84.8997 | 0.39857 | -4.17155 | 27.52 | -89.07 |
| 43.2663 | 0 | -111.462 | 0 | -5.501 | 0.00 | -116.96 |
| 43.5337 | 0 | -163.464 | 0 | -10.2971 | 0.00 | -173.76 |
| 43.759 | 0 | -164.575 | 0 | -9.8308 | 0.00 | -174.41 |
| 43.9919 | 0 | -114.114 | 0 | -6.29978 | 0.00 | -120.41 |
| 44.4 | 0 | -60.1567 | 0 | -2.86924 | 0.00 | -63.03 |
| 44.9833 | 0 | -14.627 | 0 | -0.45904 | 0.00 | -15.09 |

| s | Support disp 1 | | Support disp 2 | | Support disp 3 | | Support disp tot | |
|---|---|---|---|---|---|---|---|---|
| [m] | [kNm/m] | | [kNm/m] | | [kNm/m] | | [kNm/m] | |
| | pos | neg | pos | neg | pos | neg | max | min |
| 0.31667 | 0.22882 | -0.05831 | 0.096408 | -0.37833 | 0.14951 | -0.0381 | 0.47 | -0.47 |
| 0.9 | 0.79592 | -0.03203 | 0.052952 | -1.31596 | 0.52004 | -0.02093 | 1.37 | -1.37 |
| 1.30813 | 1.41093 | 0 | 0 | -2.33282 | 0.92189 | 0 | 2.33 | -2.33 |
| 1.54104 | 1.93368 | 0 | 0 | -3.19711 | 1.26344 | 0 | 3.20 | -3.20 |
| 1.76625 | 1.87139 | 0 | 0 | -3.09414 | 1.22274 | 0 | 3.09 | -3.09 |
| 2.03375 | 0.70327 | -0.72124 | 1.19249 | -1.16278 | 0.45951 | -0.47125 | 2.36 | -2.36 |
| 2.27694 | 0.39613 | -1.67591 | 2.77092 | -0.65496 | 0.25883 | -1.09502 | 3.43 | -3.43 |
| 2.52082 | 0 | -3.61918 | 5.98391 | 0 | 0 | -2.36472 | 5.98 | -5.98 |
| 2.98289 | 0 | -6.40653 | 10.5925 | 0 | 0 | -4.18594 | 10.59 | -10.59 |
| 3.66316 | 0 | -10.3053 | 17.0386 | 0 | 0 | -6.73334 | 17.04 | -17.04 |
| 5.07368 | 0 | -17.411 | 28.7871 | 0 | 0 | -11.3761 | 28.79 | -28.79 |
| 5.77895 | 0 | -20.8485 | 34.4706 | 0 | 0 | -13.6221 | 34.47 | -34.47 |
| 6.48421 | 0 | -24.2761 | 40.1378 | 0 | 0 | -15.8617 | 40.14 | -40.14 |
| 7.18947 | 0 | -27.7047 | 45.8066 | 0 | 0 | -18.1019 | 45.81 | -45.81 |
| 7.89474 | 0 | -31.134 | 51.4765 | 0 | 0 | -20.3425 | 51.48 | -51.48 |
| 8.6 | 0 | -34.5625 | 57.1453 | 0 | 0 | -22.5827 | 57.15 | -57.15 |
| 9.30526 | 0 | -37.9876 | 62.8082 | 0 | 0 | -24.8206 | 62.81 | -62.81 |
| 10.0105 | 0 | -41.4058 | 68.4598 | 0 | 0 | -27.054 | 68.46 | -68.46 |
| 10.7158 | 0 | -44.8132 | 74.0936 | 0 | 0 | -29.2803 | 74.09 | -74.09 |
| 11.4211 | 0 | -48.2033 | 79.6987 | 0 | 0 | -31.4954 | 79.70 | -79.70 |
| 12.1263 | 0 | -51.5679 | 85.2616 | 0 | 0 | -33.6937 | 85.26 | -85.26 |
| 12.8316 | 0 | -54.8866 | 90.7487 | 0 | 0 | -35.8621 | 90.75 | -90.75 |
| 13.5368 | 0 | -58.1144 | 96.0855 | 0 | 0 | -37.9711 | 96.09 | -96.09 |
| 14.2421 | 0 | -61.1931 | 101.176 | 0 | 0 | -39.9827 | 101.18 | -101.18 |
| 14.9474 | 0 | -64.3357 | 106.372 | 0 | 0 | -42.0361 | 106.37 | -106.37 |
| 15.725 | 0 | -68.9698 | 114.034 | 0 | 0 | -45.0639 | 114.03 | -114.03 |
| 16.575 | 0 | -75.1844 | 124.309 | 0 | 0 | -49.1245 | 124.31 | -124.31 |
| 17.2 | 0 | -80.2119 | 132.621 | 0 | 0 | -52.4093 | 132.62 | -132.62 |
| 17.6 | 0 | -80.9319 | 133.812 | 0 | 0 | -52.8798 | 133.81 | -133.81 |
| 17.9163 | 0 | -83.8665 | 138.664 | 0 | 0 | -54.7972 | 138.66 | -138.66 |
| 18.1663 | 0 | -82.7155 | 136.761 | 0 | 0 | -54.0452 | 136.76 | -136.76 |
| 18.4338 | 0 | -82.9374 | 137.128 | 0 | 0 | -54.1902 | 137.13 | -137.13 |
| 18.6838 | 0 | -85.3234 | 141.073 | 0 | 0 | -55.7492 | 141.07 | -141.07 |
| 19 | 0 | -82.8691 | 137.015 | 0 | 0 | -54.1455 | 137.02 | -137.01 |
| 19.4 | 0 | -82.5913 | 136.555 | 0 | 0 | -53.964 | 136.56 | -136.56 |
| 20.025 | 0 | -77.3794 | 127.938 | 0 | 0 | -50.5587 | 127.94 | -127.94 |
| 20.875 | 0 | -72.6455 | 120.111 | 0 | 0 | -47.4656 | 120.11 | -120.11 |
| 21.6453 | 0 | -69.3576 | 114.675 | 0 | 0 | -45.3173 | 114.68 | -114.67 |
| 22.3359 | 0 | -67.4805 | 111.571 | 0 | 0 | -44.0909 | 111.57 | -111.57 |
| 23.0266 | 0 | -65.6691 | 108.576 | 0 | 0 | -42.9073 | 108.58 | -108.58 |
| 23.7172 | 0 | -63.706 | 105.331 | 0 | 0 | -41.6247 | 105.33 | -105.33 |
| 24.4078 | 0 | -61.6432 | 101.92 | 0 | 0 | -40.2769 | 101.92 | -101.92 |

| | | | | | | | | |
|---|---|---|---|---|---|---|---|---|
| 25.0984 | 0 | -59.5303 | 98.4265 | 0 | 0 | -38.8963 | 98.43 | -98.43 |
| 25.7891 | 0 | -57.3884 | 94.8852 | 0 | 0 | -37.4968 | 94.89 | -94.89 |
| 26.4797 | 0 | -55.2266 | 91.311 | 0 | 0 | -36.0843 | 91.31 | -91.31 |
| 27.1703 | 0 | -53.0513 | 87.7143 | 0 | 0 | -34.663 | 87.71 | -87.71 |
| 27.8609 | 0 | -50.866 | 84.1012 | 0 | 0 | -33.2352 | 84.10 | -84.10 |
| 28.5516 | 0 | -48.6735 | 80.4761 | 0 | 0 | -31.8026 | 80.48 | -80.48 |
| 29.2422 | 0 | -46.4755 | 76.842 | 0 | 0 | -30.3665 | 76.84 | -76.84 |
| 29.9328 | 0 | -44.2736 | 73.2014 | 0 | 0 | -28.9278 | 73.20 | -73.20 |
| 30.6234 | 0 | -42.0688 | 69.5559 | 0 | 0 | -27.4872 | 69.56 | -69.56 |
| 31.3141 | 0 | -39.8618 | 65.9069 | 0 | 0 | -26.0452 | 65.91 | -65.91 |
| 32.0047 | 0 | -37.6533 | 62.2555 | 0 | 0 | -24.6022 | 62.26 | -62.26 |
| 32.6953 | 0 | -35.4439 | 58.6024 | 0 | 0 | -23.1585 | 58.60 | -58.60 |
| 33.3859 | 0 | -33.2338 | 54.9484 | 0 | 0 | -21.7145 | 54.95 | -54.95 |
| 34.0766 | 0 | -31.0236 | 51.294 | 0 | 0 | -20.2704 | 51.29 | -51.29 |
| 34.7672 | 0 | -28.8135 | 47.6398 | 0 | 0 | -18.8263 | 47.64 | -47.64 |
| 35.4578 | 0 | -26.6039 | 43.9866 | 0 | 0 | -17.3826 | 43.99 | -43.99 |
| 36.1484 | 0 | -24.3953 | 40.3349 | 0 | 0 | -15.9396 | 40.33 | -40.33 |
| 36.8391 | 0 | -22.1881 | 36.6855 | 0 | 0 | -14.4974 | 36.69 | -36.69 |
| 37.5297 | 0 | -19.9835 | 33.0405 | 0 | 0 | -13.057 | 33.04 | -33.04 |
| 38.2203 | 0 | -17.782 | 29.4005 | 0 | 0 | -11.6185 | 29.40 | -29.40 |
| 38.9109 | 0 | -15.579 | 25.758 | 0 | 0 | -10.1791 | 25.76 | -25.76 |
| 39.565 | 0 | -13.4958 | 22.3138 | 0 | 0 | -8.81797 | 22.31 | -22.31 |
| 40.2263 | 0 | -11.3899 | 18.8319 | 0 | 0 | -7.442 | 18.83 | -18.83 |
| 40.9316 | 0 | -9.1175 | 15.0748 | 0 | 0 | -5.95725 | 15.07 | -15.07 |
| 41.6368 | 0 | -6.73893 | 11.1421 | 0 | 0 | -4.40313 | 11.14 | -11.14 |
| 42.3171 | 0 | -4.18961 | 6.92704 | 0 | 0 | -2.73743 | 6.93 | -6.93 |
| 42.7792 | 0 | -2.36884 | 3.91661 | 0 | 0 | -1.54777 | 3.92 | -3.92 |
| 43.0231 | 0.2673 | -1.09634 | 1.81268 | -0.44195 | 0.17465 | -0.71634 | 2.25 | -2.25 |
| 43.2663 | 0.46855 | -0.47595 | 0.78693 | -0.7747 | 0.30615 | -0.31098 | 1.56 | -1.56 |
| 43.5337 | 1.22598 | 0 | 0 | -2.02702 | 0.80104 | 0 | 2.03 | -2.03 |
| 43.759 | 1.26944 | 0 | 0 | -2.09887 | 0.82943 | 0 | 2.10 | -2.10 |
| 43.9919 | 0.92547 | 0 | 0 | -1.53016 | 0.60469 | 0 | 1.53 | -1.53 |
| 44.4 | 0.52289 | -0.02242 | 0.03706 | -0.86453 | 0.34165 | -0.01465 | 0.90 | -0.90 |
| 44.9833 | 0.15062 | -0.03878 | 0.064119 | -0.24903 | 0.09841 | -0.02534 | 0.31 | -0.31 |

| s | Coating | | Heat | | cool | | TEMP total | |
|---|---|---|---|---|---|---|---|---|
| [m] | [kNm/m] | | [kNm/m] | | [kNm/m] | | [kNm/m] | |
| | pos | neg | pos | neg | pos | neg | max | min |
| 0.31667 | 0 | -0.78686 | 0.31754 | -1.53163 | 1.6336 | -0.33868 | 1.95 | -2.66 |
| 0.9 | 0 | -4.10125 | 0 | -4.99865 | 5.33146 | 0 | 5.33 | -9.10 |
| 1.30813 | 0 | -8.40763 | 0 | -7.96333 | 8.49352 | 0 | 8.49 | -16.37 |
| 1.54104 | 0 | -12.6984 | 0 | -10.498 | 11.1969 | 0 | 11.20 | -23.20 |
| 1.76625 | 0 | -12.9997 | 2.68011 | 0 | 0 | -2.85855 | 2.68 | -15.86 |
| 2.03375 | 0 | -11.4172 | 18.5839 | 0 | 0 | -19.8212 | 18.58 | -31.24 |
| 2.27694 | 0 | -9.47083 | 11.9873 | -7.27679 | 7.76127 | -12.7854 | 19.75 | -29.53 |
| 2.52082 | 2.75255 | -2.29509 | 23.3384 | 0 | 0 | -24.8923 | 23.34 | -27.19 |
| 2.98289 | 11.7021 | 0 | 39.8679 | 0 | 0 | -42.5223 | 39.87 | -42.52 |
| 3.66316 | 21.8534 | 0 | 64.1061 | 0 | 0 | -68.3743 | 64.11 | -68.37 |
| 5.07368 | 31.5334 | 0 | 108.513 | 0 | 0 | -115.738 | 108.51 | -115.74 |
| 5.77895 | 32.552 | 0 | 129.937 | 0 | 0 | -138.588 | 129.94 | -138.59 |
| 6.48421 | 31.5516 | 0 | 151.29 | 0 | 0 | -161.363 | 151.29 | -161.36 |
| 7.18947 | 30.5191 | 0 | 172.648 | 0 | 0 | -184.143 | 172.65 | -184.14 |
| 7.89474 | 27.3299 | 0 | 194.009 | 0 | 0 | -206.926 | 194.01 | -206.93 |
| 8.6 | 21.9806 | 0 | 215.367 | 0 | 0 | -229.706 | 215.37 | -229.71 |
| 9.30526 | 14.466 | 0 | 236.704 | 0 | 0 | -252.464 | 236.70 | -252.46 |
| 10.0105 | 4.78103 | -5.92018 | 257.999 | 0 | 0 | -275.177 | 258.00 | -281.10 |
| 10.7158 | 0 | -19.6821 | 279.227 | 0 | 0 | -297.818 | 279.23 | -317.50 |
| 11.4211 | 0 | -35.5297 | 300.347 | 0 | 0 | -320.344 | 300.35 | -355.87 |
| 12.1263 | 0 | -53.4485 | 321.308 | 0 | 0 | -342.701 | 321.31 | -396.15 |
| 12.8316 | 0 | -73.3938 | 341.982 | 0 | 0 | -364.751 | 341.98 | -438.14 |
| 13.5368 | 0 | -95.2797 | 362.089 | 0 | 0 | -386.197 | 362.09 | -481.48 |
| 14.2421 | 0 | -118.935 | 381.263 | 0 | 0 | -406.648 | 381.26 | -525.58 |
| 14.9474 | 0 | -144.956 | 400.827 | 0 | 0 | -427.514 | 400.83 | -572.47 |
| 15.725 | 0 | -179.835 | 429.648 | 0 | 0 | -458.253 | 429.65 | -638.09 |
| 16.575 | 0 | -226.445 | 468.184 | 0 | 0 | -499.355 | 468.18 | -725.80 |
| 17.2 | 0 | -263.592 | 499.07 | 0 | 0 | -532.298 | 499.07 | -795.89 |
| 17.6 | 0 | -281.903 | 504.345 | 0 | 0 | -537.924 | 504.35 | -819.83 |
| 17.9163 | 0 | -308.959 | 524.838 | 0 | 0 | -559.781 | 524.84 | -868.74 |
| 18.1663 | 0 | -316.124 | 529.328 | 0 | 0 | -564.571 | 529.33 | -880.70 |
| 18.4338 | 0 | -314.616 | 530.699 | 0 | 0 | -566.032 | 530.70 | -880.65 |
| 18.6838 | 0 | -308.945 | 533.884 | 0 | 0 | -569.429 | 533.88 | -878.37 |
| 19 | 0 | -278.966 | 516.375 | 0 | 0 | -550.755 | 516.38 | -829.72 |
| 19.4 | 0 | -254.794 | 514.276 | 0 | 0 | -548.516 | 514.28 | -803.31 |
| 20.025 | 0 | -209.95 | 481.864 | 0 | 0 | -513.946 | 481.86 | -723.90 |
| 20.875 | 0 | -152.246 | 452.55 | 0 | 0 | -482.681 | 452.55 | -634.93 |
| 21.6453 | 0 | -107.783 | 432.117 | 0 | 0 | -460.887 | 432.12 | -568.67 |
| 22.3359 | 0 | -73.2453 | 420.438 | 0 | 0 | -448.431 | 420.44 | -521.68 |
| 23.0266 | 0 | -41.0007 | 409.159 | 0 | 0 | -436.401 | 409.16 | -477.40 |
| 23.7172 | 16.7071 | -10.5197 | 396.933 | 0 | 0 | -423.36 | 396.93 | -433.88 |
| 24.4078 | 43.7344 | 0 | 384.083 | 0 | 0 | -409.655 | 384.08 | -409.66 |

| | | | | | | | | |
|---|---|---|---|---|---|---|---|---|
| 25.0984 | 68.6493 | 0 | 370.919 | 0 | 0 | -395.615 | 370.92 | -395.62 |
| 25.7891 | 91.4557 | 0 | 357.575 | 0 | 0 | -381.382 | 357.58 | -381.38 |
| 26.4797 | 112.177 | 0 | 344.107 | 0 | 0 | -367.017 | 344.11 | -367.02 |
| 27.1703 | 130.818 | 0 | 330.553 | 0 | 0 | -352.561 | 330.55 | -352.56 |
| 27.8609 | 147.389 | 0 | 316.938 | 0 | 0 | -338.039 | 316.94 | -338.04 |
| 28.5516 | 161.894 | 0 | 303.277 | 0 | 0 | -323.469 | 303.28 | -323.47 |
| 29.2422 | 174.34 | 0 | 289.582 | 0 | 0 | -308.863 | 289.58 | -308.86 |
| 29.9328 | 184.729 | 0 | 275.863 | 0 | 0 | -294.23 | 275.86 | -294.23 |
| 30.6234 | 193.063 | 0 | 262.125 | 0 | 0 | -279.578 | 262.13 | -279.58 |
| 31.3141 | 199.345 | 0 | 248.375 | 0 | 0 | -264.911 | 248.38 | -264.91 |
| 32.0047 | 203.576 | 0 | 234.615 | 0 | 0 | -250.235 | 234.62 | -250.24 |
| 32.6953 | 205.756 | 0 | 220.848 | 0 | 0 | -235.552 | 220.85 | -235.55 |
| 33.3859 | 205.91 | 0 | 207.079 | 0 | 0 | -220.866 | 207.08 | -220.87 |
| 34.0766 | 206.11 | 0 | 193.308 | 0 | 0 | -206.179 | 193.31 | -206.18 |
| 34.7672 | 204.277 | 0 | 179.539 | 0 | 0 | -191.493 | 179.54 | -191.49 |
| 35.4578 | 200.415 | 0 | 165.774 | 0 | 0 | -176.811 | 165.77 | -176.81 |
| 36.1484 | 194.527 | 0 | 152.015 | 0 | 0 | -162.136 | 152.02 | -162.14 |
| 36.8391 | 186.62 | 0 | 138.266 | 0 | 0 | -147.472 | 138.27 | -147.47 |
| 37.5297 | 176.708 | 0 | 124.534 | 0 | 0 | -132.825 | 124.53 | -132.83 |
| 38.2203 | 164.798 | 0 | 110.822 | 0 | 0 | -118.2 | 110.82 | -118.20 |
| 38.9109 | 150.851 | 0 | 97.0997 | 0 | 0 | -103.565 | 97.10 | -103.57 |
| 39.565 | 135.848 | 0 | 84.1221 | 0 | 0 | -89.7229 | 84.12 | -89.72 |
| 40.2263 | 118.665 | 0 | 70.995 | 0 | 0 | -75.7218 | 71.00 | -75.72 |
| 40.9316 | 97.9404 | 0 | 56.8012 | 0 | 0 | -60.583 | 56.80 | -60.58 |
| 41.6368 | 73.4046 | 0 | 41.8742 | 0 | 0 | -44.6621 | 41.87 | -44.66 |
| 42.3171 | 43.7471 | 0 | 26.0298 | 0 | 0 | -27.7629 | 26.03 | -27.76 |
| 42.7792 | 20.8735 | 0 | 15.5141 | 0 | 0 | -16.547 | 15.51 | -16.55 |
| 43.0231 | 3.78454 | -11.5167 | 8.32754 | -6.50241 | 6.93534 | -8.88198 | 15.26 | -26.90 |
| 43.2663 | 0 | -15.0313 | 17.2 | 0 | 0 | -18.3452 | 17.20 | -33.38 |
| 43.5337 | 0 | -22.3585 | 6.60264 | 0 | 0 | -7.04223 | 6.60 | -29.40 |
| 43.759 | 0 | -22.4195 | 0 | -7.486 | 7.98441 | 0 | 7.98 | -29.91 |
| 43.9919 | 0 | -15.4798 | 0 | -4.9716 | 5.30261 | 0 | 5.30 | -20.45 |
| 44.4 | 0 | -8.10031 | 0 | -3.32074 | 3.54183 | 0 | 3.54 | -11.42 |
| 44.9833 | 0 | -1.93857 | 0.20159 | -1.05236 | 1.12242 | -0.21501 | 1.32 | -3.21 |

| s | TS | | UDL | |
|---|---|---|---|---|
| [m] | [kNm/m] | | [kNm/m] | |
| | max | min | max | min |
| 0.31667 | 15.9427 | -71.9625 | 6.02197 | -10.1192 |
| 0.9 | 29.735 | -147.883 | 14.1129 | -25.6219 |
| 1.30813 | 45.3151 | -183.828 | 21.107 | -39.9536 |
| 1.54104 | 55.3956 | -234.002 | 25.4081 | -50.981 |
| 1.76625 | 58.7088 | -238.556 | 26.4074 | -52.5455 |
| 2.03375 | 74.7241 | -275.592 | 29.9145 | -52.324 |
| 2.27694 | 86.132 | -276.205 | 32.9881 | -54.9342 |
| 2.52082 | 116.645 | -244.171 | 40.1979 | -46.7831 |
| 2.98289 | 190.302 | -208.894 | 53.8887 | -42.8825 |
| 3.66316 | 283.492 | -171.031 | 80.6896 | -43.5278 |
| 5.07368 | 353.95 | -146.617 | 100.724 | -53.0743 |
| 5.77895 | 409.635 | -130.101 | 115.875 | -62.934 |
| 6.48421 | 452.219 | -120.513 | 127.819 | -72.9301 |
| 7.18947 | 484.091 | -139.219 | 137.067 | -83.0877 |
| 7.89474 | 506.103 | -158.885 | 143.853 | -93.3642 |
| 8.6 | 525.431 | -178.558 | 148.587 | -103.686 |
| 9.30526 | 536.312 | -198.234 | 151.281 | -114.015 |
| 10.0105 | 539.254 | -217.9 | 151.746 | -124.339 |
| 10.7158 | 534.583 | -237.543 | 150.311 | -134.647 |
| 11.4211 | 522.01 | -257.148 | 146.665 | -144.965 |
| 12.1263 | 501.94 | -276.692 | 141.09 | -155.257 |
| 12.8316 | 474.728 | -296.149 | 133.04 | -165.511 |
| 13.5368 | 444.406 | -315.439 | 122.776 | -175.688 |
| 14.2421 | 408.026 | -334.358 | 109.949 | -185.727 |
| 14.9474 | 362.758 | -352.661 | 93.8324 | -196.434 |
| 15.725 | 308.521 | -371.795 | 74.2093 | -213.507 |
| 16.575 | 242.872 | -400.748 | 51.1907 | -246.029 |
| 17.2 | 160.848 | -451.501 | 28.8548 | -302.729 |
| 17.6 | 120.485 | -512.518 | 19.3088 | -363.265 |
| 17.9163 | 64.1754 | -544.051 | 13.3708 | -403.541 |
| 18.1663 | 67.6346 | -589.59 | 10.5525 | -446.794 |
| 18.4338 | 66.1116 | -590.589 | 8.99046 | -445.226 |
| 18.6838 | 64.9511 | -577.709 | 6.65918 | -443.334 |
| 19 | 65.2782 | -585.657 | 8.08069 | -446.325 |
| 19.4 | 60.711 | -536.115 | 9.59744 | -402.267 |
| 20.025 | 96.5359 | -490.832 | 13.6648 | -359.817 |
| 20.875 | 112.862 | -413.964 | 17.6299 | -295.317 |
| 21.6453 | 171.162 | -309.699 | 27.9859 | -222.241 |
| 22.3359 | 233.382 | -230.038 | 41.7795 | -170.914 |
| 23.0266 | 285.95 | -188.247 | 58.9378 | -135.922 |
| 23.7172 | 334.611 | -158.548 | 79.9322 | -106.85 |
| 24.4078 | 379.803 | -152.776 | 104.891 | -83.2487 |

| | | | | |
|---|---|---|---|---|
| 25.0984 | 422.652 | -147.58 | 131.124 | -65.5987 |
| 25.7891 | 463.734 | -142.361 | 155.844 | -54.6322 |
| 26.4797 | 502.567 | -137.135 | 179.414 | -50.0771 |
| 27.1703 | 538.991 | -131.901 | 200.277 | -48.4309 |
| 27.8609 | 572.746 | -126.66 | 219.185 | -46.8903 |
| 28.5516 | 603.543 | -121.414 | 235.846 | -45.348 |
| 29.2422 | 633.156 | -116.18 | 250.304 | -43.7997 |
| 29.9328 | 660.752 | -110.932 | 262.601 | -42.2466 |
| 30.6234 | 684.644 | -105.675 | 272.753 | -40.6904 |
| 31.3141 | 704.868 | -100.411 | 280.77 | -39.1323 |
| 32.0047 | 720.894 | -95.1427 | 286.636 | -37.5726 |
| 32.6953 | 732.353 | -89.8712 | 290.331 | -36.0119 |
| 33.3859 | 738.958 | -84.5978 | 292.106 | -34.4507 |
| 34.0766 | 740.436 | -89.1181 | 291.664 | -32.8897 |
| 34.7672 | 736.527 | -95.9483 | 289.128 | -31.3296 |
| 35.4578 | 727.053 | -102.841 | 284.615 | -29.7716 |
| 36.1484 | 710.304 | -109.796 | 277.879 | -28.2174 |
| 36.8391 | 696.382 | -116.843 | 268.88 | -26.6685 |
| 37.5297 | 675.958 | -124.021 | 257.565 | -25.1259 |
| 38.2203 | 634.897 | -131.388 | 243.822 | -23.5943 |
| 38.9109 | 599.968 | -139.052 | 228.076 | -22.1189 |
| 39.565 | 560.483 | -147.468 | 211.384 | -20.7574 |
| 40.2263 | 506.021 | -156.149 | 194.393 | -19.5273 |
| 40.9316 | 459.249 | -167.436 | 174.248 | -18.3846 |
| 41.6368 | 393.523 | -184.181 | 148.704 | -17.4243 |
| 42.3171 | 312.89 | -209.303 | 116.954 | -20.2455 |
| 42.7792 | 208.097 | -248.948 | 84.0486 | -37.2675 |
| 43.0231 | 129.4 | -286.445 | 63.2885 | -52.6781 |
| 43.2663 | 101.271 | -320.968 | 52.4293 | -71.8699 |
| 43.5337 | 87.2586 | -320.093 | 46.5685 | -71.1097 |
| 43.759 | 66.161 | -285.594 | 36.4975 | -73.9464 |
| 43.9919 | 62.0525 | -283.305 | 34.4806 | -71.7163 |
| 44.4 | 50.9419 | -217.071 | 28.9035 | -56.219 |
| 44.9833 | 33.5848 | -161.832 | 19.5173 | -35.7264 |
| | 18.7803 | -74.2684 | 8.32322 | -13.5264 |

| s [m] | Var1 [kNm/m] | | Var2 [kNm/m] | | ULS A [kNm/m] | | ULS-B [kNm/m] | |
|---|---|---|---|---|---|---|---|---|
| | max | min | max | min | max | min | max | min |
| 0.31667 | 34.00 | -124.13 | 23.38 | -89.07 | 15.33417 | -99.741 | 26.3 | -133.9 |
| 0.9 | 68.65 | -262.96 | 46.87 | -186.98 | 7.956995 | -238.368 | 30.8 | -309.4 |
| 1.30813 | 104.22 | -339.97 | 71.51 | -238.86 | -4.81375 | -340.843 | 29.4 | -431.8 |
| 1.54104 | 127.25 | -433.14 | 87.92 | -304.46 | -27.0628 | -458.914 | 14.2 | -571.9 |
| 1.76625 | 129.12 | -438.20 | 84.60 | -303.67 | -29.7274 | -464.049 | 13.7 | -579.8 |
| 2.03375 | 166.99 | -502.58 | 119.11 | -360.65 | 10.37528 | -498.073 | 63.4 | -629.6 |
| 2.27694 | 189.34 | -507.54 | 134.90 | -363.13 | 44.70781 | -475.98 | 104.0 | -612.2 |
| 2.52082 | 247.87 | -449.87 | 176.93 | -326.39 | 179.3887 | -331.611 | 251.4 | -456.5 |
| 2.98289 | 387.81 | -400.63 | 283.26 | -300.05 | 409.798 | -194.929 | 506.8 | -303.8 |
| 3.66316 | 580.89 | -358.76 | 426.46 | -280.92 | 669.381 | -83.2909 | 807.2 | -174.5 |
| 5.07368 | 740.61 | -362.04 | 558.06 | -301.69 | 909.6045 | -10.1765 | 1070.8 | -93.2 |
| 5.77895 | 858.43 | -364.39 | 649.36 | -309.50 | 1009.891 | -4.13305 | 1200.1 | -86.2 |
| 6.48421 | 951.75 | -377.30 | 723.86 | -325.16 | 1069.459 | -23.2714 | 1283.7 | -107.0 |
| 7.18947 | 1024.97 | -432.90 | 784.65 | -372.90 | 1113.968 | -75.4696 | 1345.9 | -171.5 |
| 7.89474 | 1079.70 | -490.11 | 832.82 | -421.79 | 1120.124 | -147.45 | 1366.8 | -256.3 |
| 8.6 | 1127.33 | -547.41 | 876.72 | -470.72 | 1096.23 | -238.123 | 1357.7 | -359.8 |
| 9.30526 | 1159.21 | -604.70 | 909.83 | -519.63 | 1035.135 | -348.256 | 1309.4 | -482.7 |
| 10.0105 | 1175.82 | -661.95 | 932.60 | -568.49 | 885.9773 | -549.057 | 1170.8 | -688.2 |
| 10.7158 | 1178.12 | -719.11 | 945.57 | -617.25 | 721.5377 | -797.104 | 1005.7 | -930.7 |
| 11.4211 | 1165.20 | -776.16 | 948.18 | -665.87 | 583.3714 | -1030.45 | 855.9 | -1155.8 |
| 12.1263 | 1138.05 | -832.98 | 941.02 | -714.25 | 417.5582 | -1288.34 | 674.0 | -1402.7 |
| 12.8316 | 1096.32 | -889.46 | 924.05 | -762.23 | 224.4652 | -1570.09 | 460.0 | -1670.7 |
| 13.5368 | 1046.30 | -945.24 | 901.72 | -809.44 | 9.35224 | -1874.36 | 220.9 | -1958.6 |
| 14.2421 | 982.84 | -999.72 | 870.18 | -855.24 | -230.12 | -2198.59 | -47.0 | -2264.0 |
| 14.9474 | 901.33 | -1054.50 | 826.96 | -901.13 | -501.733 | -2551 | -353.3 | -2594.8 |
| 15.725 | 806.11 | -1125.41 | 779.84 | -960.66 | -855.157 | -3020.44 | -749.5 | -3035.3 |
| 16.575 | 693.91 | -1239.82 | 726.53 | -1049.88 | -1317.06 | -3656.49 | -1230.6 | -3642.7 |
| 17.2 | 554.05 | -1418.79 | 648.23 | -1170.90 | -1720.77 | -4213.07 | -1628.6 | -4214.3 |
| 17.6 | 482.04 | -1604.15 | 601.64 | -1281.24 | -1926.32 | -4540.28 | -1833.1 | -4593.5 |
| 17.9163 | 399.73 | -1723.67 | 552.89 | -1360.71 | -2213.83 | -4939.22 | -2116.4 | -5001.0 |
| 18.1663 | 403.12 | -1859.44 | 559.15 | -1442.43 | -2273.68 | -5105.3 | -2173.4 | -5214.4 |
| 18.4338 | 399.23 | -1859.38 | 557.73 | -1443.93 | -2261.79 | -5087.79 | -2161.2 | -5197.7 |
| 18.6838 | 395.71 | -1839.06 | 557.89 | -1431.30 | -2210.29 | -5007.63 | -2111.2 | -5116.1 |
| 19 | 388.88 | -1845.38 | 543.35 | -1425.27 | -1961.68 | -4647.06 | -1866.2 | -4803.8 |
| 19.4 | 383.17 | -1703.77 | 537.21 | -1340.83 | -1758.97 | -4275.13 | -1664.0 | -4406.3 |
| 20.025 | 425.51 | -1553.50 | 550.96 | -1233.08 | -1352.64 | -3639.91 | -1263.6 | -3781.4 |
| 20.875 | 440.11 | -1324.57 | 545.41 | -1079.38 | -854.585 | -2803.83 | -770.9 | -2940.7 |
| 21.6453 | 532.07 | -1046.79 | 599.11 | -898.10 | -412.658 | -2095.56 | -332.8 | -2190.9 |
| 22.3359 | 639.78 | -843.58 | 667.18 | -766.08 | -43.6067 | -1553.07 | 34.1 | -1620.8 |
| 23.0266 | 738.28 | -721.91 | 726.73 | -687.03 | 297.0065 | -1090.88 | 384.2 | -1156.7 |
| 23.7172 | 836.16 | -626.71 | 783.31 | -624.29 | 819.78 | -521.385 | 923.7 | -592.8 |
| 24.4078 | 934.45 | -575.25 | 837.79 | -591.28 | 1290.172 | -132.281 | 1399.5 | -212.5 |

| | | | | | | | | |
|---|---|---|---|---|---|---|---|---|
| 25.0984 | 1030.96 | -533.40 | 890.10 | -562.18 | 1642.827 | 109.6668 | 1760.7 | 32.2 |
| 25.7891 | 1122.46 | -501.44 | 939.34 | -536.89 | 1967.224 | 329.5107 | 2094.5 | 254.8 |
| 26.4797 | 1208.79 | -479.01 | 985.25 | -515.32 | 2263.358 | 527.5568 | 2400.9 | 455.7 |
| 27.1703 | 1287.40 | -460.88 | 1026.72 | -495.41 | 2530.21 | 705.9293 | 2677.6 | 636.9 |
| 27.8609 | 1359.04 | -442.87 | 1063.96 | -475.50 | 2768.068 | 866.373 | 2925.2 | 800.2 |
| 28.5516 | 1422.85 | -424.82 | 1096.46 | -455.53 | 2976.51 | 1008.986 | 3143.1 | 945.7 |
| 29.2422 | 1481.56 | -406.76 | 1126.27 | -435.54 | 3157.634 | 1133.788 | 3334.0 | 1073.3 |
| 29.9328 | 1534.00 | -388.65 | 1152.49 | -415.51 | 3310.577 | 1240.833 | 3496.8 | 1183.2 |
| 30.6234 | 1577.64 | -370.52 | 1173.21 | -395.45 | 3433.448 | 1330.11 | 3629.0 | 1275.4 |
| 31.3141 | 1612.58 | -352.37 | 1188.50 | -375.36 | 3526.357 | 1401.656 | 3730.6 | 1349.8 |
| 32.0047 | 1637.99 | -334.20 | 1197.75 | -355.27 | 3588.699 | 1455.465 | 3800.9 | 1406.5 |
| 32.6953 | 1653.28 | -316.02 | 1200.52 | -335.16 | 3620.048 | 1491.535 | 3839.4 | 1445.4 |
| 33.3859 | 1658.42 | -297.84 | 1196.66 | -315.05 | 3620.662 | 1510.172 | 3846.2 | 1466.9 |
| 34.0766 | 1652.54 | -294.35 | 1185.67 | -306.00 | 3614.472 | 1517.972 | 3842.3 | 1477.6 |
| 34.7672 | 1635.43 | -294.32 | 1167.34 | -299.56 | 3576.686 | 1505.609 | 3805.7 | 1468.1 |
| 35.4578 | 1607.02 | -294.40 | 1141.54 | -293.20 | 3507.149 | 1475.601 | 3736.1 | 1439.8 |
| 36.1484 | 1564.36 | -294.57 | 1106.18 | -286.92 | 3403.841 | 1427.986 | 3630.8 | 1388.6 |
| 36.8391 | 1522.56 | -294.90 | 1072.68 | -280.76 | 3278.208 | 1362.765 | 3504.9 | 1319.7 |
| 37.5297 | 1467.53 | -295.45 | 1030.45 | -274.76 | 3119.853 | 1280.013 | 3344.5 | 1233.3 |
| 38.2203 | 1377.92 | -296.30 | 963.47 | -269.01 | 2912.839 | 1179.731 | 3128.2 | 1129.3 |
| 38.9109 | 1294.50 | -297.68 | 902.20 | -263.61 | 2687.212 | 1061.478 | 2896.5 | 1007.1 |
| 39.565 | 1203.23 | -300.79 | 835.89 | -259.84 | 2443.733 | 932.5782 | 2645.6 | 874.1 |
| 40.2263 | 1088.96 | -304.40 | 752.34 | -256.31 | 2156.759 | 784.3833 | 2348.5 | 721.5 |
| 40.9316 | 980.92 | -311.45 | 674.62 | -254.76 | 1833.306 | 603.2138 | 2019.8 | 534.7 |
| 41.6368 | 835.95 | -326.53 | 571.59 | -258.78 | 1439.146 | 383.3502 | 1613.7 | 306.9 |
| 42.3171 | 658.82 | -359.31 | 447.16 | -273.65 | 962.8234 | 108.389 | 1121.3 | 17.3 |
| 42.7792 | 446.60 | -438.26 | 299.54 | -318.56 | 543.6805 | -136.378 | 666.2 | -259.4 |
| 43.0231 | 297.27 | -516.99 | 197.93 | -369.14 | 137.2764 | -471.568 | 235.9 | -608.2 |
| 43.2663 | 239.84 | -599.16 | 161.37 | -422.33 | 25.72132 | -597.05 | 109.3 | -759.4 |
| 43.5337 | 204.31 | -590.61 | 132.49 | -410.71 | -62.4372 | -677.403 | 10.4 | -828.6 |
| 43.759 | 158.30 | -543.35 | 103.85 | -373.83 | -92.2261 | -641.37 | -36.3 | -782.2 |
| 43.9919 | 147.66 | -535.22 | 95.58 | -367.64 | -39.6646 | -552.483 | 13.3 | -700.1 |
| 44.4 | 121.68 | -411.73 | 78.09 | -282.01 | 7.097872 | -378.564 | 51.4 | -498.1 |
| 44.9833 | 80.37 | -297.02 | 50.85 | -205.45 | 33.75209 | -228.452 | 63.5 | -317.7 |

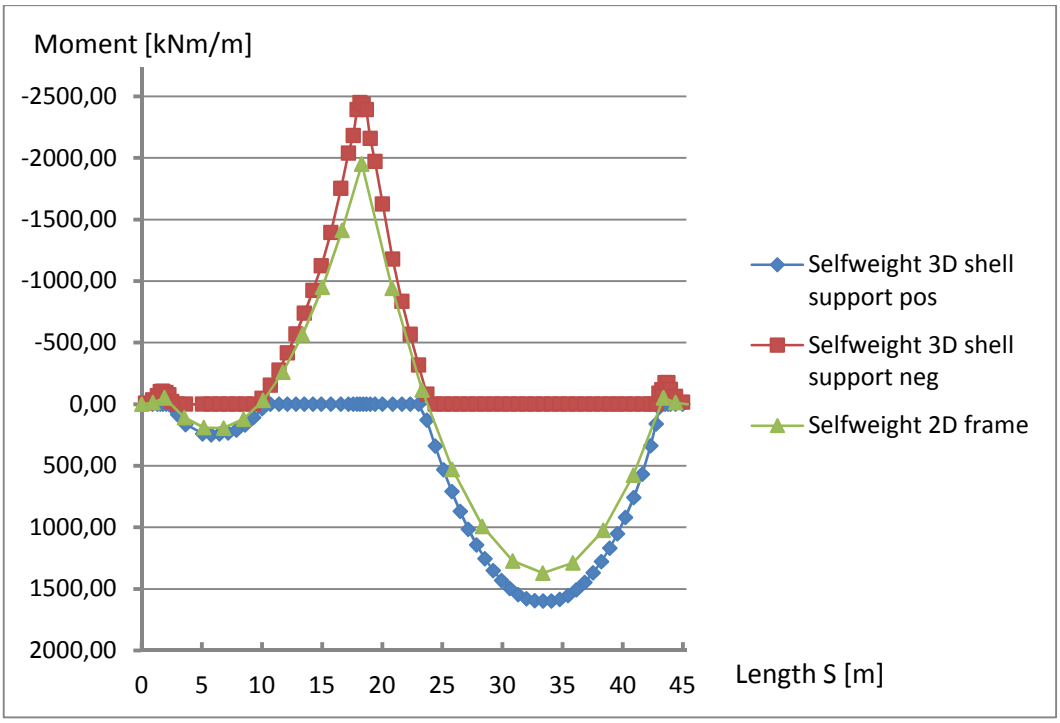


*Figure C.2 – Illustration of the bending moment distribution over the support due to selfweight.*

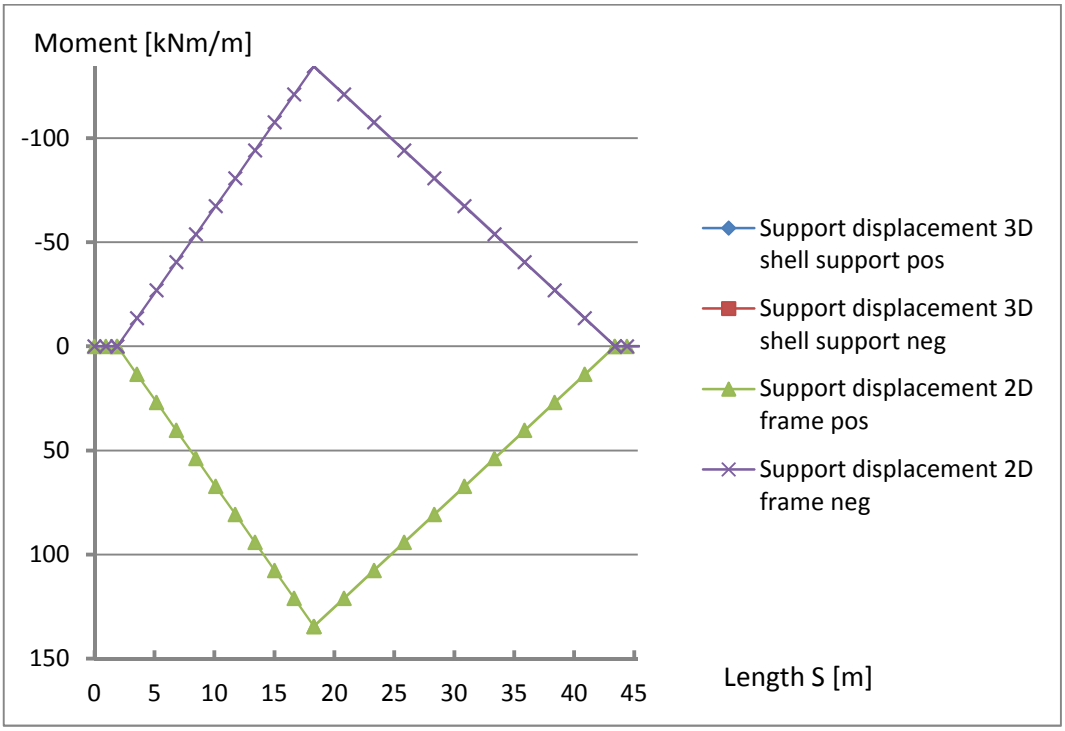


*Figure C.3 – Illustration of the bending moment distribution over the support due to support displacement*

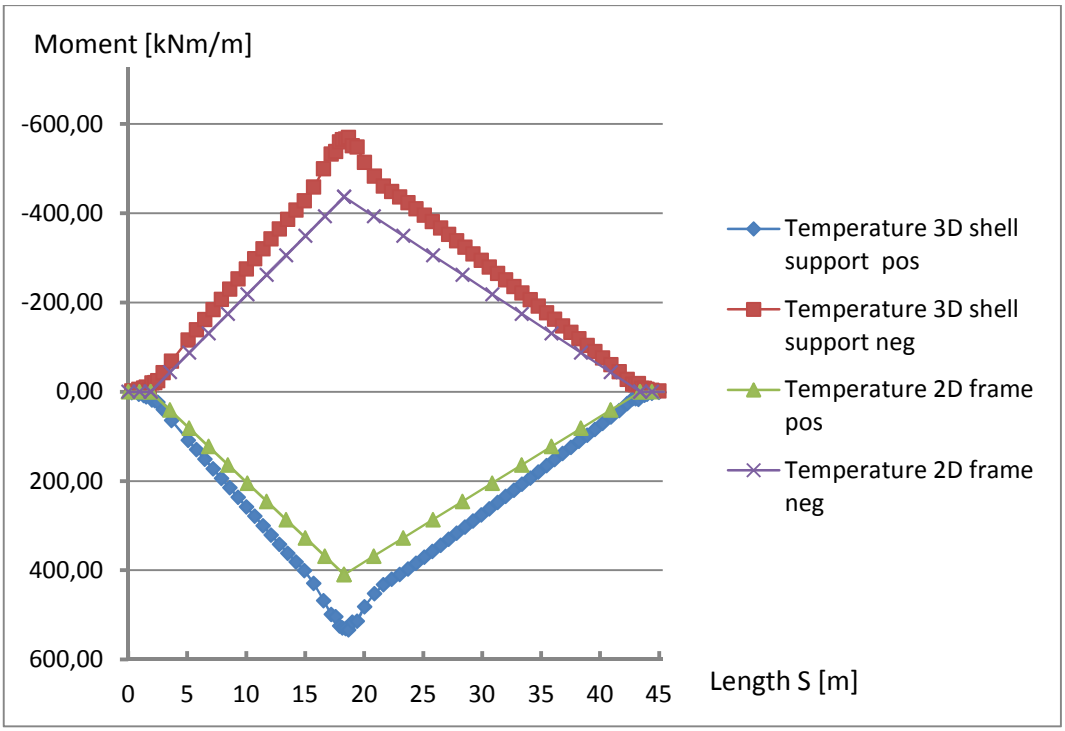


*Figure C.4 – Illustration of the bending moment distribution over the support due to temperature load*

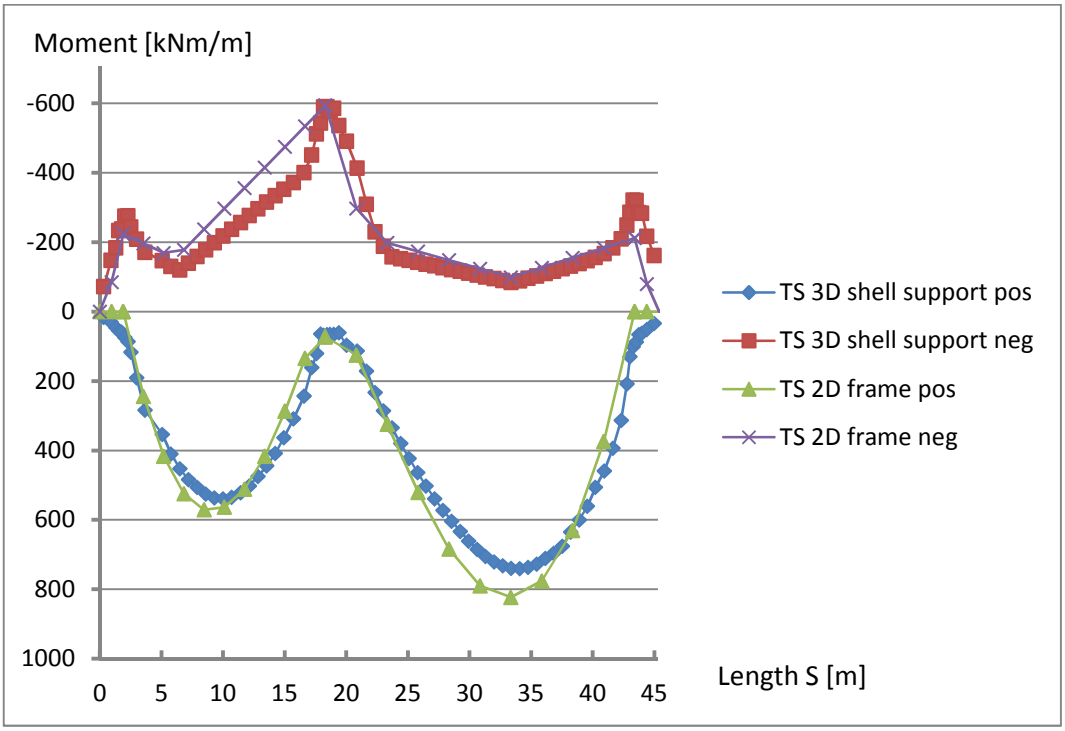


*Figure C.5 – Illustration of the bending moment distribution over the support due to traffic load TS*

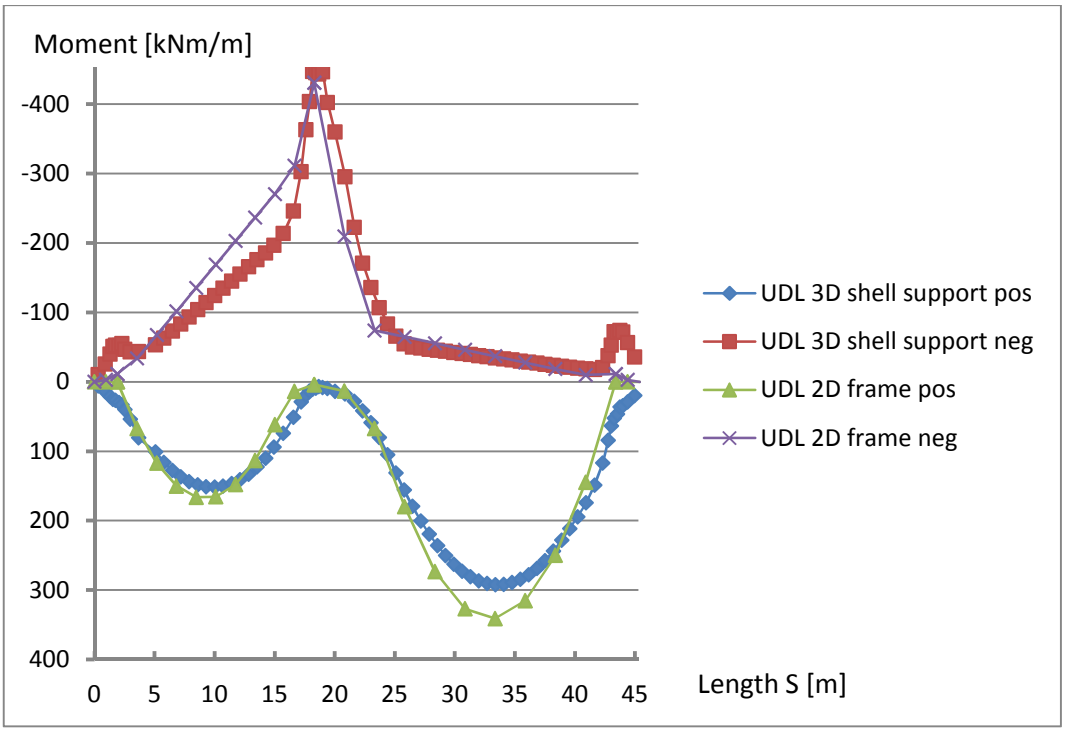


*Figure C.6 – Illustration of the bending moment distribution over the support due to traffic load UDL*

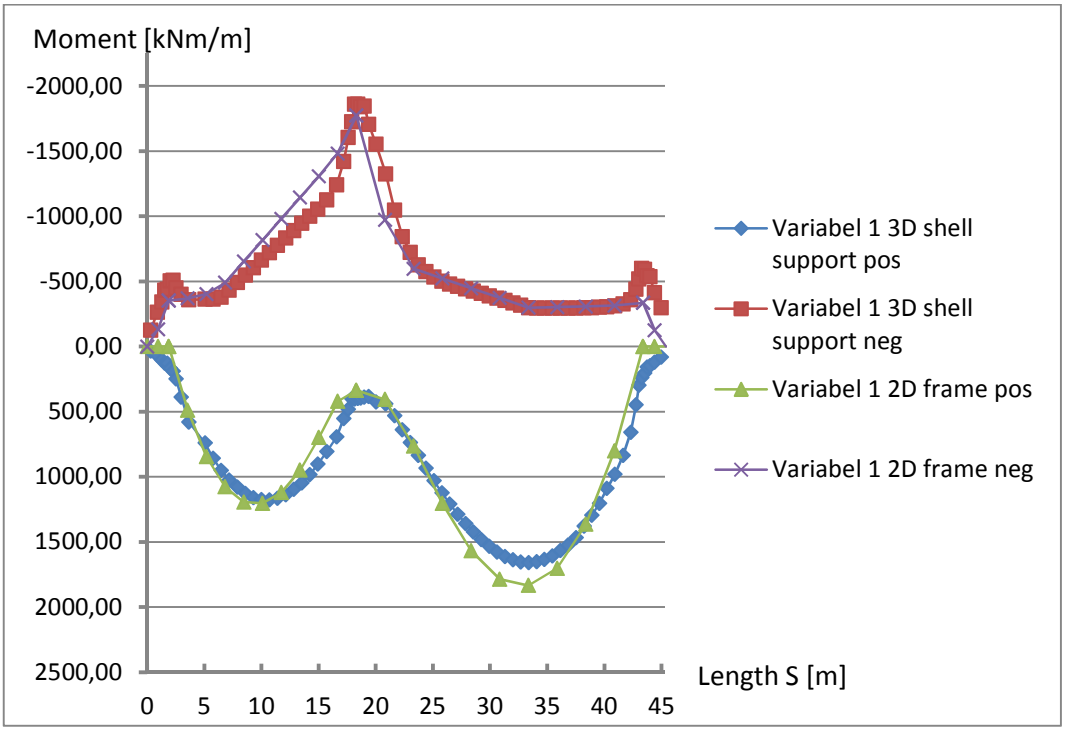


*Figure C.7 – Illustration of the bending moment distribution over the support due to variable load 1*

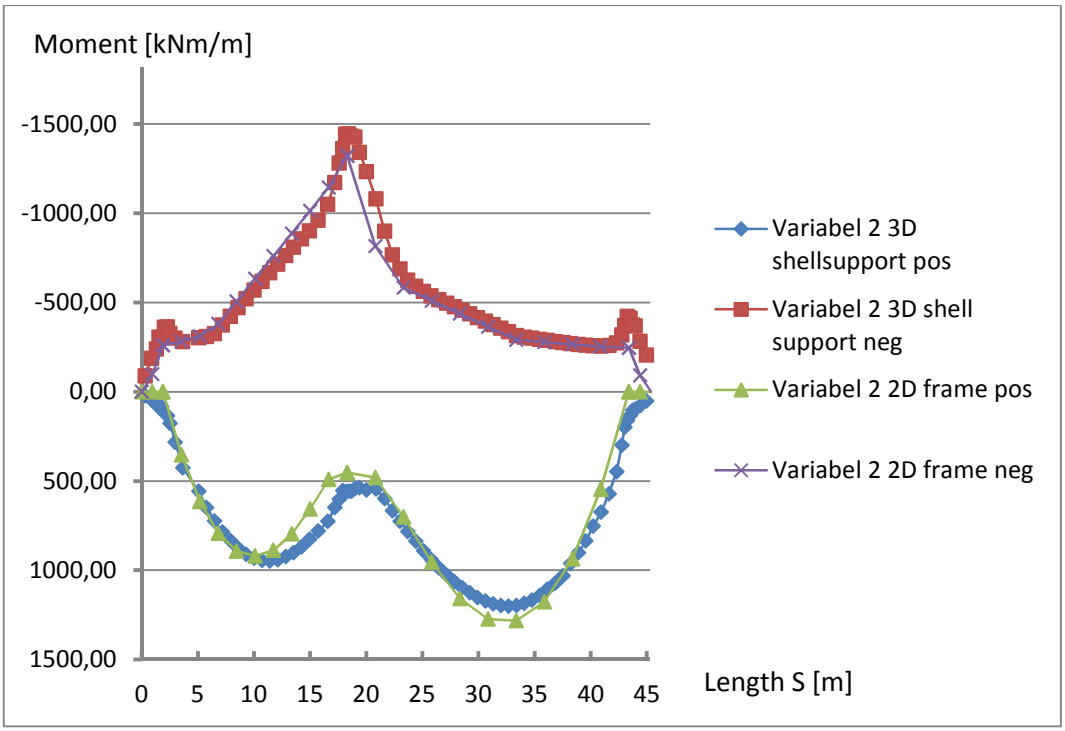


*Figure C.8 – Illustration of the bending moment distribution over the support due to variable load 2*

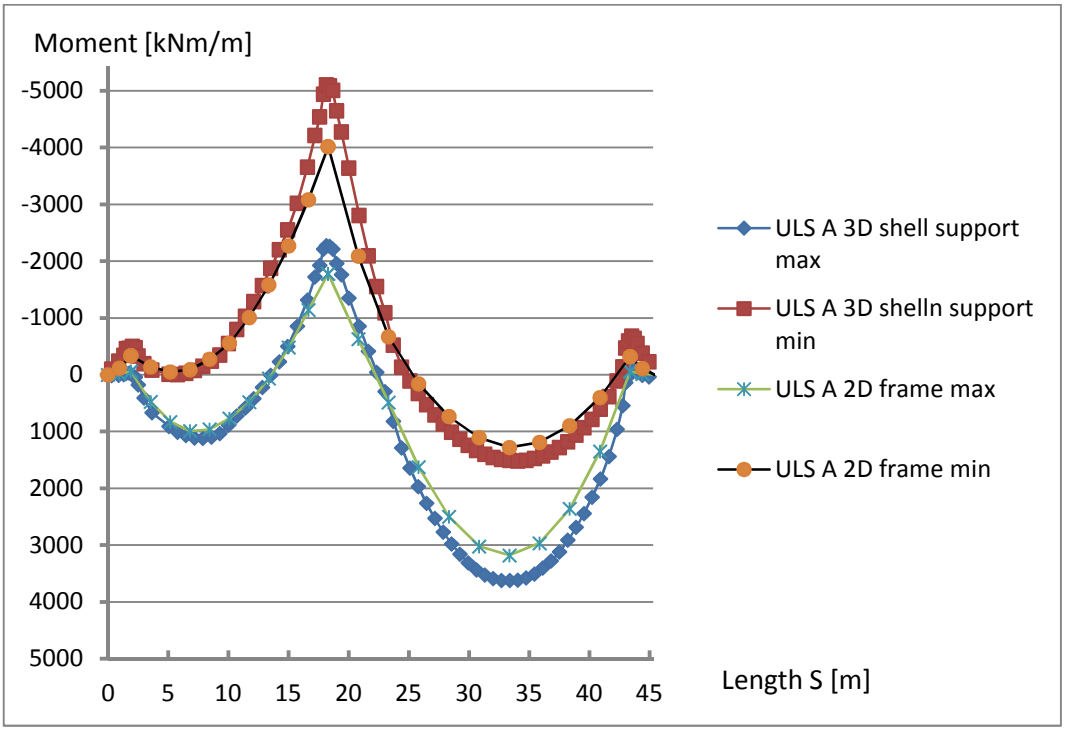


*Figure C.9 – Illustration of the bending moment distribution over the support due to load combination ULS A*

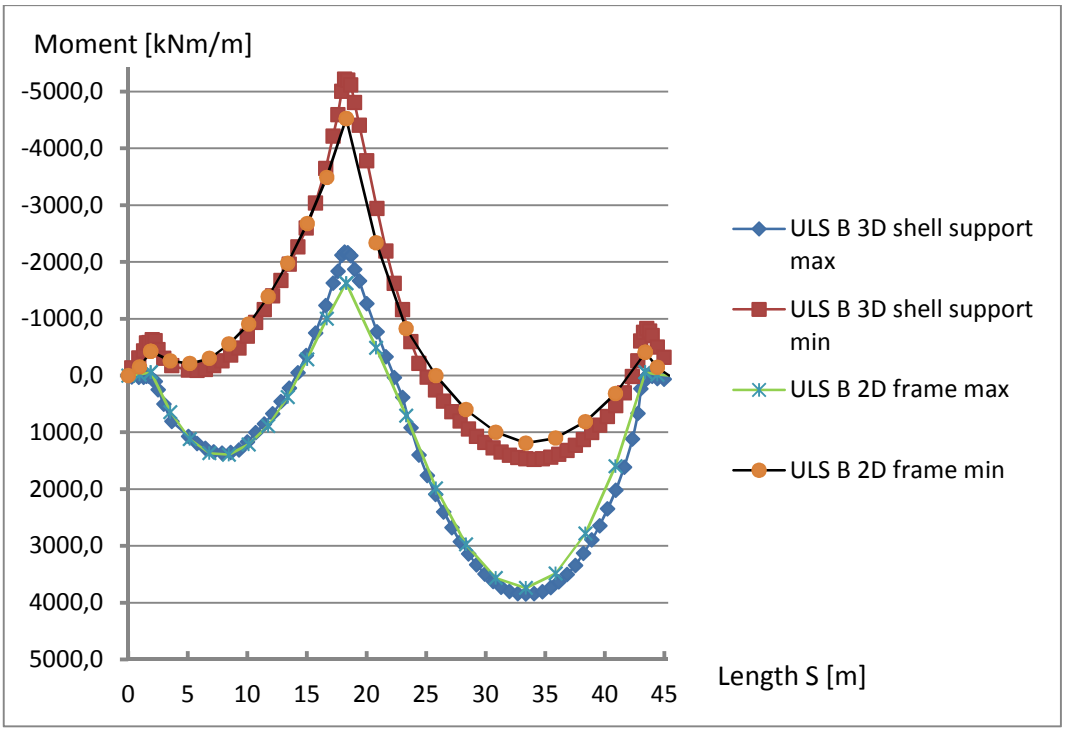


*Figure C.10 – Illustration of the bending moment distribution over the support due to load combination ULS B*

# Span

| s [m] | Selfweight [kNm/m] | | Selfweight edge-beam [kNm/m] | | Selfweight total [kNm/m] | |
|---|---|---|---|---|---|---|
| | pos | neg | pos | neg | max | min |
| 0.31667 | 0.28802 | -1.67732 | 0 | -0.65741 | 0.29 | -2.33 |
| 0.9 | 0.10755 | -2.65791 | 0 | -1.66343 | 0.11 | -4.32 |
| 1.39958 | 2.61358 | 0 | 0 | -2.15932 | 2.61 | -2.16 |
| 1.76625 | 11.7089 | 0 | 0 | -2.08519 | 11.71 | -2.09 |
| 2.03375 | 22.9592 | 0 | 0 | -1.67513 | 22.96 | -1.68 |
| 2.41138 | 44.5211 | 0 | 0 | -0.84458 | 44.52 | -0.84 |
| 2.98289 | 83.0258 | 0 | 1.45049 | 0 | 84.48 | 0.00 |
| 3.66316 | 129.889 | 0 | 4.12988 | 0 | 134.02 | 0.00 |
| 4.36842 | 171.544 | 0 | 6.55092 | 0 | 178.09 | 0.00 |
| 5.07368 | 200.832 | 0 | 8.23952 | 0 | 209.07 | 0.00 |
| 5.77895 | 215.51 | 0 | 9.07042 | 0 | 224.58 | 0.00 |
| 6.48421 | 214.893 | 0 | 9.08836 | 0 | 223.98 | 0.00 |
| 7.18947 | 200.646 | 0 | 8.17799 | 0 | 208.82 | 0.00 |
| 7.89474 | 171.178 | 0 | 6.34395 | 0 | 177.52 | 0.00 |
| 8.6 | 126.033 | 0 | 3.58892 | 0 | 129.62 | 0.00 |
| 9.30526 | 65.241 | 0 | 0 | -0.66637 | 65.24 | -0.67 |
| 10.0105 | 0 | -21.3599 | 0 | -5.37462 | 0.00 | -26.73 |
| 10.7158 | 0 | -115.177 | 0 | -11.0035 | 0.00 | -126.18 |
| 11.4211 | 0 | -224.497 | 0 | -17.554 | 0.00 | -242.05 |
| 12.1263 | 0 | -349.384 | 0 | -25.0292 | 0.00 | -374.41 |
| 12.8316 | 0 | -490.066 | 0 | -33.4364 | 0.00 | -523.50 |
| 13.5368 | 0 | -647.014 | 0 | -42.7883 | 0.00 | -689.80 |
| 14.2421 | 0 | -820.791 | 0 | -53.0882 | 0.00 | -873.88 |
| 14.9474 | 0 | -1012.06 | 0 | -64.3427 | 0.00 | -1076.40 |
| 15.725 | 0 | -1243.64 | 0 | -77.8802 | 0.00 | -1321.52 |
| 16.575 | 0 | -1503.81 | 0 | -93.0461 | 0.00 | -1596.86 |
| 17.4 | 0 | -1710.27 | 0 | -105.058 | 0.00 | -1815.33 |
| 17.925 | 0 | -1792.32 | 0 | -109.795 | 0.00 | -1902.12 |
| 18.175 | 0 | -1793.8 | 0 | -109.822 | 0.00 | -1903.62 |
| 18.425 | 0 | -1788.2 | 0 | -109.458 | 0.00 | -1897.66 |
| 18.675 | 0 | -1760.91 | 0 | -107.848 | 0.00 | -1868.76 |
| 19.2 | 0 | -1626.07 | 0 | -99.8494 | 0.00 | -1725.92 |
| 20.025 | 0 | -1339.64 | 0 | -82.8323 | 0.00 | -1422.47 |
| 20.875 | 0 | -1001.29 | 0 | -62.686 | 0.00 | -1063.98 |
| 21.6453 | 0 | -702.595 | 0 | -44.8292 | 0.00 | -747.42 |
| 22.3359 | 0 | -452.765 | 0 | -29.8003 | 0.00 | -482.57 |
| 23.0266 | 0 | -218.655 | 0 | -15.6363 | 0.00 | -234.29 |
| 23.7172 | 26.7442 | 0 | 0 | -2.35219 | 26.74 | -2.35 |
| 24.4078 | 228.622 | 0 | 11.676 | 0 | 240.30 | 0.00 |
| 25.0984 | 415.488 | 0 | 23.0226 | 0 | 438.51 | 0.00 |
| 25.7891 | 587.377 | 0 | 33.4661 | 0 | 620.84 | 0.00 |
| 26.4797 | 744.311 | 0 | 43.0062 | 0 | 787.32 | 0.00 |

| | | | | | | |
|---|---|---|---|---|---|---|
| 27.1703 | 886.298 | 0 | 51.6429 | 0 | 937.94 | 0.00 |
| 27.8609 | 1013.34 | 0 | 59.376 | 0 | 1072.72 | 0.00 |
| 28.5516 | 1125.44 | 0 | 66.2059 | 0 | 1191.65 | 0.00 |
| 29.2422 | 1222.59 | 0 | 72.1324 | 0 | 1294.72 | 0.00 |
| 29.9328 | 1304.78 | 0 | 77.1556 | 0 | 1381.94 | 0.00 |
| 30.6234 | 1372.03 | 0 | 81.2756 | 0 | 1453.31 | 0.00 |
| 31.3141 | 1424.32 | 0 | 84.4924 | 0 | 1508.81 | 0.00 |
| 32.0047 | 1461.65 | 0 | 86.806 | 0 | 1548.46 | 0.00 |
| 32.6953 | 1484.01 | 0 | 88.2165 | 0 | 1572.23 | 0.00 |
| 33.3859 | 1491.54 | 0 | 88.7239 | 0 | 1580.26 | 0.00 |
| 34.0766 | 1486.1 | 0 | 88.4324 | 0 | 1574.53 | 0.00 |
| 34.7672 | 1465.71 | 0 | 87.2577 | 0 | 1552.97 | 0.00 |
| 35.4578 | 1430.36 | 0 | 85.1794 | 0 | 1515.54 | 0.00 |
| 36.1484 | 1380.04 | 0 | 82.1969 | 0 | 1462.24 | 0.00 |
| 36.8391 | 1314.75 | 0 | 78.309 | 0 | 1393.06 | 0.00 |
| 37.5297 | 1234.48 | 0 | 73.5135 | 0 | 1307.99 | 0.00 |
| 38.2203 | 1139.22 | 0 | 67.8067 | 0 | 1207.03 | 0.00 |
| 38.9109 | 1029 | 0 | 61.1848 | 0 | 1090.18 | 0.00 |
| 39.565 | 911.288 | 0 | 54.093 | 0 | 965.38 | 0.00 |
| 40.2263 | 778.31 | 0 | 46.0551 | 0 | 824.37 | 0.00 |
| 40.9316 | 623.666 | 0 | 36.6728 | 0 | 660.34 | 0.00 |
| 41.6368 | 459.58 | 0 | 26.6754 | 0 | 486.26 | 0.00 |
| 42.3171 | 301.765 | 0 | 17.0394 | 0 | 318.80 | 0.00 |
| 42.8886 | 180.656 | 0 | 9.66689 | 0 | 190.32 | 0.00 |
| 43.2663 | 113.115 | 0 | 5.59969 | 0 | 118.71 | 0.00 |
| 43.5337 | 75.9064 | 0 | 3.4108 | 0 | 79.32 | 0.00 |
| 43.9004 | 40.504 | 0 | 1.45288 | 0 | 41.96 | 0.00 |
| 44.4 | 14.2197 | 0 | 0.44015 | 0 | 14.66 | 0.00 |
| 44.9833 | 3.55583 | 0 | 0.12358 | -0.18426 | 3.68 | -0.18 |

| s | Support disp 1 | | Support disp 2 | | Support disp 3 | | Support disp tot | |
|---|---|---|---|---|---|---|---|---|
| [m] | [kNm/m] | | [kNm/m] | | [kNm/m] | | [kNm/m] | |
| | pos | neg | pos | neg | pos | neg | max | min |
| 0.31667 | 0 | -0.08938 | 0.14778 | 0 | 0 | -0.0584 | 0.15 | -0.15 |
| 0.9 | 0 | -0.40626 | 0.6717 | 0 | 0 | -0.26544 | 0.67 | -0.67 |
| 1.39958 | 0 | -1.0398 | 1.71918 | 0 | 0 | -0.67939 | 1.72 | -1.72 |
| 1.76625 | 0 | -1.75447 | 2.90081 | 0 | 0 | -1.14635 | 2.90 | -2.90 |
| 2.03375 | 0 | -2.46452 | 4.07481 | 0 | 0 | -1.61028 | 4.07 | -4.07 |
| 2.41138 | 0 | -3.72231 | 6.15441 | 0 | 0 | -2.43211 | 6.15 | -6.15 |
| 2.98289 | 0 | -5.98183 | 9.89028 | 0 | 0 | -3.90845 | 9.89 | -9.89 |
| 3.66316 | 0 | -9.01672 | 14.9081 | 0 | 0 | -5.8914 | 14.91 | -14.91 |
| 4.36842 | 0 | -12.3654 | 20.4447 | 0 | 0 | -8.07936 | 20.44 | -20.44 |
| 5.07368 | 0 | -15.7936 | 26.113 | 0 | 0 | -10.3193 | 26.11 | -26.11 |
| 5.77895 | 0 | -19.2448 | 31.8191 | 0 | 0 | -12.5743 | 31.82 | -31.82 |
| 6.48421 | 0 | -22.7013 | 37.5341 | 0 | 0 | -14.8328 | 37.53 | -37.53 |
| 7.18947 | 0 | -26.1566 | 43.247 | 0 | 0 | -17.0904 | 43.25 | -43.25 |
| 7.89474 | 0 | -29.6089 | 48.955 | 0 | 0 | -19.3461 | 48.96 | -48.96 |
| 8.6 | 0 | -33.0572 | 54.6564 | 0 | 0 | -21.5992 | 54.66 | -54.66 |
| 9.30526 | 0 | -36.5005 | 60.3495 | 0 | 0 | -23.849 | 60.35 | -60.35 |
| 10.0105 | 0 | -39.9377 | 66.0324 | 0 | 0 | -26.0947 | 66.03 | -66.03 |
| 10.7158 | 0 | -43.3675 | 71.7032 | 0 | 0 | -28.3357 | 71.70 | -71.70 |
| 11.4211 | 0 | -46.7902 | 77.3623 | 0 | 0 | -30.5721 | 77.36 | -77.36 |
| 12.1263 | 0 | -50.2104 | 83.0172 | 0 | 0 | -32.8068 | 83.02 | -83.02 |
| 12.8316 | 0 | -53.6442 | 88.6946 | 0 | 0 | -35.0504 | 88.69 | -88.69 |
| 13.5368 | 0 | -57.1278 | 94.4544 | 0 | 0 | -37.3265 | 94.45 | -94.45 |
| 14.2421 | 0 | -60.7171 | 100.389 | 0 | 0 | -39.6717 | 100.39 | -100.39 |
| 14.9474 | 0 | -64.4703 | 106.594 | 0 | 0 | -42.124 | 106.59 | -106.59 |
| 15.725 | 0 | -68.807 | 113.765 | 0 | 0 | -44.9576 | 113.77 | -113.76 |
| 16.575 | 0 | -73.5105 | 121.541 | 0 | 0 | -48.0307 | 121.54 | -121.54 |
| 17.4 | 0 | -77.3674 | 127.918 | 0 | 0 | -50.5508 | 127.92 | -127.92 |
| 17.925 | 0 | -79.2057 | 130.958 | 0 | 0 | -51.7519 | 130.96 | -130.96 |
| 18.175 | 0 | -79.6468 | 131.687 | 0 | 0 | -52.0401 | 131.69 | -131.69 |
| 18.425 | 0 | -79.8408 | 132.008 | 0 | 0 | -52.1669 | 132.01 | -132.01 |
| 18.675 | 0 | -79.7997 | 131.94 | 0 | 0 | -52.14 | 131.94 | -131.94 |
| 19.2 | 0 | -78.9008 | 130.453 | 0 | 0 | -51.5527 | 130.45 | -130.45 |
| 20.025 | 0 | -76.4989 | 126.482 | 0 | 0 | -49.9834 | 126.48 | -126.48 |
| 20.875 | 0 | -73.2184 | 121.058 | 0 | 0 | -47.8399 | 121.06 | -121.06 |
| 21.6453 | 0 | -70.18 | 116.035 | 0 | 0 | -45.8546 | 116.04 | -116.03 |
| 22.3359 | 0 | -67.6348 | 111.826 | 0 | 0 | -44.1917 | 111.83 | -111.83 |
| 23.0266 | 0 | -65.2667 | 107.911 | 0 | 0 | -42.6444 | 107.91 | -107.91 |
| 23.7172 | 0 | -63.0175 | 104.192 | 0 | 0 | -41.1748 | 104.19 | -104.19 |
| 24.4078 | 0 | -60.8263 | 100.569 | 0 | 0 | -39.7431 | 100.57 | -100.57 |
| 25.0984 | 0 | -58.6532 | 96.9764 | 0 | 0 | -38.3232 | 96.98 | -96.98 |

| | | | | | | | | |
|---|---|---|---|---|---|---|---|---|
| 25.7891 | 0 | -56.4793 | 93.382 | 0 | 0 | -36.9028 | 93.38 | -93.38 |
| 26.4797 | 0 | -54.2986 | 89.7766 | 0 | 0 | -35.478 | 89.78 | -89.78 |
| 27.1703 | 0 | -52.1107 | 86.1592 | 0 | 0 | -34.0484 | 86.16 | -86.16 |
| 27.8609 | 0 | -49.9166 | 82.5314 | 0 | 0 | -32.6148 | 82.53 | -82.53 |
| 28.5516 | 0 | -47.7175 | 78.8955 | 0 | 0 | -31.178 | 78.90 | -78.90 |
| 29.2422 | 0 | -45.5146 | 75.2532 | 0 | 0 | -29.7386 | 75.25 | -75.25 |
| 29.9328 | 0 | -43.3088 | 71.6062 | 0 | 0 | -28.2974 | 71.61 | -71.61 |
| 30.6234 | 0 | -41.1008 | 67.9556 | 0 | 0 | -26.8547 | 67.96 | -67.96 |
| 31.3141 | 0 | -38.8912 | 64.3023 | 0 | 0 | -25.411 | 64.30 | -64.30 |
| 32.0047 | 0 | -36.6804 | 60.6469 | 0 | 0 | -23.9665 | 60.65 | -60.65 |
| 32.6953 | 0 | -34.4686 | 56.99 | 0 | 0 | -22.5213 | 56.99 | -56.99 |
| 33.3859 | 0 | -32.2562 | 53.3319 | 0 | 0 | -21.0757 | 53.33 | -53.33 |
| 34.0766 | 0 | -30.0431 | 49.6729 | 0 | 0 | -19.6298 | 49.67 | -49.67 |
| 34.7672 | 0 | -27.8296 | 46.0132 | 0 | 0 | -18.1835 | 46.01 | -46.01 |
| 35.4578 | 0 | -25.6158 | 42.3528 | 0 | 0 | -16.737 | 42.35 | -42.35 |
| 36.1484 | 0 | -23.4016 | 38.6919 | 0 | 0 | -15.2903 | 38.69 | -38.69 |
| 36.8391 | 0 | -21.1871 | 35.0304 | 0 | 0 | -13.8434 | 35.03 | -35.03 |
| 37.5297 | 0 | -18.9722 | 31.3683 | 0 | 0 | -12.3961 | 31.37 | -31.37 |
| 38.2203 | 0 | -16.7568 | 27.7055 | 0 | 0 | -10.9487 | 27.71 | -27.71 |
| 38.9109 | 0 | -14.5414 | 24.0425 | 0 | 0 | -9.50113 | 24.04 | -24.04 |
| 39.565 | 0 | -12.4439 | 20.5746 | 0 | 0 | -8.13068 | 20.57 | -20.57 |
| 40.2263 | 0 | -10.3275 | 17.0753 | 0 | 0 | -6.74782 | 17.08 | -17.08 |
| 40.9316 | 0 | -8.08552 | 13.3685 | 0 | 0 | -5.28297 | 13.37 | -13.37 |
| 41.6368 | 0 | -5.89604 | 9.74844 | 0 | 0 | -3.85239 | 9.75 | -9.75 |
| 42.3171 | 0 | -3.91197 | 6.46799 | 0 | 0 | -2.55603 | 6.47 | -6.47 |
| 42.8886 | 0 | -2.43484 | 4.02573 | 0 | 0 | -1.59089 | 4.03 | -4.03 |
| 43.2663 | 0 | -1.61262 | 2.66629 | 0 | 0 | -1.05366 | 2.67 | -2.67 |
| 43.5337 | 0 | -1.14841 | 1.89876 | 0 | 0 | -0.75035 | 1.90 | -1.90 |
| 43.9004 | 0 | -0.68103 | 1.12601 | 0 | 0 | -0.44498 | 1.13 | -1.13 |
| 44.4 | 0 | -0.2665 | 0.44063 | 0 | 0 | -0.17413 | 0.44 | -0.44 |
| 44.9833 | 0 | -0.05842 | 0.09659 | 0 | 0 | -0.03817 | 0.10 | -0.10 |

| s | Coating | | Heat | | cool | | TEMP tot | |
|---|---|---|---|---|---|---|---|---|
| [m] | [kNm/m] | | [kNm/m] | | [kNm/m] | | [kNm/m] | |
| | pos | neg | pos | neg | pos | neg | max | min |
| 0.31667 | 0.028143 | -0.25425 | 0.66446 | 0 | 0 | -0.7087 | 0.66 | -0.71 |
| 0.9 | 0 | -0.42361 | 2.87756 | 0 | 0 | -3.06914 | 2.88 | -3.07 |
| 1.39958 | 0.28176 | 0 | 6.97382 | 0 | 0 | -7.43813 | 6.97 | -7.44 |
| 1.76625 | 1.50087 | 0 | 11.4724 | 0 | 0 | -12.2362 | 11.47 | -12.24 |
| 2.03375 | 3.03007 | 0 | 15.8784 | 0 | 0 | -16.9355 | 15.88 | -16.94 |
| 2.41138 | 5.96681 | 0 | 23.6182 | 0 | 0 | -25.1907 | 23.62 | -25.19 |
| 2.98289 | 11.2158 | 0 | 37.5466 | 0 | 0 | -40.0464 | 37.55 | -40.05 |
| 3.66316 | 17.6064 | 0 | 56.3148 | 0 | 0 | -60.0642 | 56.31 | -60.06 |
| 4.36842 | 23.2852 | 0 | 77.1035 | 0 | 0 | -82.237 | 77.10 | -82.24 |
| 5.07368 | 27.2728 | 0 | 98.4296 | 0 | 0 | -104.983 | 98.43 | -104.98 |
| 5.77895 | 29.2622 | 0 | 119.919 | 0 | 0 | -127.903 | 119.92 | -127.90 |
| 6.48421 | 29.1593 | 0 | 141.45 | 0 | 0 | -150.868 | 141.45 | -150.87 |
| 7.18947 | 27.197 | 0 | 162.977 | 0 | 0 | -173.828 | 162.98 | -173.83 |
| 7.89474 | 23.1489 | 0 | 184.488 | 0 | 0 | -196.771 | 184.49 | -196.77 |
| 8.6 | 16.9563 | 0 | 205.973 | 0 | 0 | -219.687 | 205.97 | -219.69 |
| 9.30526 | 8.62386 | 0 | 227.428 | 0 | 0 | -242.57 | 227.43 | -242.57 |
| 10.0105 | 0 | -3.24956 | 248.843 | 0 | 0 | -265.411 | 248.84 | -265.41 |
| 10.7158 | 0 | -16.102 | 270.214 | 0 | 0 | -288.204 | 270.21 | -288.20 |
| 11.4211 | 0 | -31.0757 | 291.539 | 0 | 0 | -310.95 | 291.54 | -310.95 |
| 12.1263 | 0 | -48.1798 | 312.849 | 0 | 0 | -333.679 | 312.85 | -333.68 |
| 12.8316 | 0 | -67.4447 | 334.244 | 0 | 0 | -356.498 | 334.24 | -356.50 |
| 13.5368 | 0 | -88.9332 | 355.951 | 0 | 0 | -379.65 | 355.95 | -379.65 |
| 14.2421 | 0 | -112.719 | 378.32 | 0 | 0 | -403.508 | 378.32 | -403.51 |
| 14.9474 | 0 | -138.886 | 401.723 | 0 | 0 | -428.47 | 401.72 | -428.47 |
| 15.725 | 0 | -170.554 | 428.803 | 0 | 0 | -457.352 | 428.80 | -457.35 |
| 16.575 | 0 | -206.122 | 458.26 | 0 | 0 | -488.771 | 458.26 | -488.77 |
| 17.4 | 0 | -234.339 | 482.526 | 0 | 0 | -514.653 | 482.53 | -514.65 |
| 17.925 | 0 | -245.547 | 494.102 | 0 | 0 | -526.999 | 494.10 | -527.00 |
| 18.175 | 0 | -245.736 | 496.847 | 0 | 0 | -529.927 | 496.85 | -529.93 |
| 18.425 | 0 | -244.975 | 498.056 | 0 | 0 | -531.216 | 498.06 | -531.22 |
| 18.675 | 0 | -241.254 | 497.713 | 0 | 0 | -530.85 | 497.71 | -530.85 |
| 19.2 | 0 | -222.832 | 492.078 | 0 | 0 | -524.84 | 492.08 | -524.84 |
| 20.025 | 0 | -183.685 | 476.877 | 0 | 0 | -508.627 | 476.88 | -508.63 |
| 20.875 | 0 | -137.433 | 456.288 | 0 | 0 | -486.667 | 456.29 | -486.67 |
| 21.6453 | 0 | -96.5917 | 437.299 | 0 | 0 | -466.414 | 437.30 | -466.41 |
| 22.3359 | 0 | -62.4212 | 421.423 | 0 | 0 | -449.481 | 421.42 | -449.48 |
| 23.0266 | 0 | -30.391 | 406.663 | 0 | 0 | -433.738 | 406.66 | -433.74 |
| 23.7172 | 3.2173 | -0.45703 | 392.648 | 0 | 0 | -418.79 | 392.65 | -418.79 |
| 24.4078 | 30.8386 | 0 | 378.996 | 0 | 0 | -404.229 | 379.00 | -404.23 |
| 25.0984 | 56.4074 | 0 | 365.456 | 0 | 0 | -389.788 | 365.46 | -389.79 |

| | | | | | | | | |
|---|---|---|---|---|---|---|---|---|
| 25.7891 | 79.928 | 0 | 351.912 | 0 | 0 | -375.342 | 351.91 | -375.34 |
| 26.4797 | 101.403 | 0 | 338.325 | 0 | 0 | -360.851 | 338.33 | -360.85 |
| 27.1703 | 120.834 | 0 | 324.693 | 0 | 0 | -346.311 | 324.69 | -346.31 |
| 27.8609 | 138.221 | 0 | 311.022 | 0 | 0 | -331.73 | 311.02 | -331.73 |
| 28.5516 | 153.564 | 0 | 297.32 | 0 | 0 | -317.116 | 297.32 | -317.12 |
| 29.2422 | 166.862 | 0 | 283.595 | 0 | 0 | -302.476 | 283.60 | -302.48 |
| 29.9328 | 178.115 | 0 | 269.851 | 0 | 0 | -287.817 | 269.85 | -287.82 |
| 30.6234 | 187.323 | 0 | 256.093 | 0 | 0 | -273.144 | 256.09 | -273.14 |
| 31.3141 | 194.486 | 0 | 242.326 | 0 | 0 | -258.46 | 242.33 | -258.46 |
| 32.0047 | 199.603 | 0 | 228.55 | 0 | 0 | -243.767 | 228.55 | -243.77 |
| 32.6953 | 202.674 | 0 | 214.769 | 0 | 0 | -229.068 | 214.77 | -229.07 |
| 33.3859 | 203.712 | 0 | 200.983 | 0 | 0 | -214.365 | 200.98 | -214.37 |
| 34.0766 | 202.98 | 0 | 187.194 | 0 | 0 | -199.657 | 187.19 | -199.66 |
| 34.7672 | 200.203 | 0 | 173.402 | 0 | 0 | -184.947 | 173.40 | -184.95 |
| 35.4578 | 195.379 | 0 | 159.608 | 0 | 0 | -170.235 | 159.61 | -170.24 |
| 36.1484 | 188.509 | 0 | 145.812 | 0 | 0 | -155.52 | 145.81 | -155.52 |
| 36.8391 | 179.592 | 0 | 132.013 | 0 | 0 | -140.802 | 132.01 | -140.80 |
| 37.5297 | 168.625 | 0 | 118.212 | 0 | 0 | -126.083 | 118.21 | -126.08 |
| 38.2203 | 155.608 | 0 | 104.409 | 0 | 0 | -111.361 | 104.41 | -111.36 |
| 38.9109 | 140.546 | 0 | 90.6074 | 0 | 0 | -96.64 | 90.61 | -96.64 |
| 39.565 | 124.457 | 0 | 77.5442 | 0 | 0 | -82.707 | 77.54 | -82.71 |
| 40.2263 | 106.281 | 0 | 64.371 | 0 | 0 | -68.6568 | 64.37 | -68.66 |
| 40.9316 | 85.1428 | 0 | 50.4371 | 0 | 0 | -53.7952 | 50.44 | -53.80 |
| 41.6368 | 62.7135 | 0 | 36.8714 | 0 | 0 | -39.3262 | 36.87 | -39.33 |
| 42.3171 | 41.143 | 0 | 24.6505 | 0 | 0 | -26.2917 | 24.65 | -26.29 |
| 42.8886 | 24.5924 | 0 | 15.5966 | 0 | 0 | -16.635 | 15.60 | -16.64 |
| 43.2663 | 15.365 | 0 | 10.57 | 0 | 0 | -11.2738 | 10.57 | -11.27 |
| 43.5337 | 10.2843 | 0 | 7.6953 | 0 | 0 | -8.20765 | 7.70 | -8.21 |
| 43.9004 | 5.45593 | 0 | 4.73701 | 0 | 0 | -5.0524 | 4.74 | -5.05 |
| 44.4 | 1.9014 | 0 | 2.00506 | 0 | 0 | -2.13856 | 2.01 | -2.14 |
| 44.9833 | 0.47523 | 0 | 0.48032 | 0 | 0 | -0.5123 | 0.48 | -0.51 |

| s | TS | | UDL | |
|---|---|---|---|---|
| [m] | [kNm/m] | | [kNm/m] | |
| | max | min | max | min |
| 0.31667 | 30.0949 | -60.0463 | 10.9351 | -11.5381 |
| 0.9 | 45.6865 | -117.793 | 20.0561 | -20.8461 |
| 1.39958 | 67.7126 | -139.134 | 25.8137 | -24.0685 |
| 1.76625 | 86.542 | -151.639 | 32.2948 | -26.258 |
| 2.03375 | 106.827 | -157.155 | 38.0458 | -27.2909 |
| 2.41138 | 137.739 | -160.233 | 47.4419 | -28.2644 |
| 2.98289 | 192.485 | -159.806 | 62.7831 | -30.0756 |
| 3.66316 | 255.389 | -150.064 | 80.6662 | -37.6028 |
| 4.36842 | 314.591 | -137.196 | 96.7487 | -47.3565 |
| 5.07368 | 363.79 | -124.993 | 109.875 | -57.4417 |
| 5.77895 | 402.672 | -114.1 | 120.335 | -67.6898 |
| 6.48421 | 431.016 | -130.189 | 128.575 | -78.0222 |
| 7.18947 | 449.515 | -150.001 | 134.83 | -88.4238 |
| 7.89474 | 460.316 | -169.796 | 139.145 | -98.8367 |
| 8.6 | 465.224 | -189.569 | 141.538 | -109.251 |
| 9.30526 | 468.299 | -209.313 | 141.969 | -119.657 |
| 10.0105 | 463.773 | -229.022 | 140.492 | -130.049 |
| 10.7158 | 452.345 | -248.703 | 137.131 | -140.426 |
| 11.4211 | 439.092 | -268.385 | 131.811 | -150.794 |
| 12.1263 | 419.055 | -288.086 | 124.49 | -161.176 |
| 12.8316 | 392.276 | -307.919 | 115.06 | -171.661 |
| 13.5368 | 358.868 | -328.122 | 103.418 | -182.442 |
| 14.2421 | 319.399 | -349.337 | 89.3971 | -194.087 |
| 14.9474 | 275.401 | -372.263 | 73.17 | -210.062 |
| 15.725 | 221.652 | -400.268 | 55.1432 | -238.261 |
| 16.575 | 161.14 | -434.048 | 35.5016 | -281.597 |
| 17.4 | 102.334 | -465.476 | 20.7692 | -327.77 |
| 17.925 | 66.2297 | -481.111 | 13.8726 | -352.105 |
| 18.175 | 58.824 | -481.975 | 11.3072 | -356.13 |
| 18.425 | 58.0906 | -478.313 | 9.82091 | -355.802 |
| 18.675 | 62.0657 | -469.809 | 9.54701 | -350.726 |
| 19.2 | 62.1645 | -434.407 | 11.6986 | -324.45 |
| 20.025 | 97.6207 | -361.961 | 17.8171 | -270.08 |
| 20.875 | 145.096 | -281.958 | 26.8754 | -212.397 |
| 21.6453 | 194.652 | -214.969 | 39.4261 | -167.659 |
| 22.3359 | 238.287 | -175.253 | 55.5054 | -134.919 |
| 23.0266 | 281.969 | -156.967 | 75.7977 | -106.871 |
| 23.7172 | 325.18 | -151.071 | 100.43 | -83.4748 |
| 24.4078 | 367.08 | -145.491 | 125.866 | -65.422 |
| 25.0984 | 407.019 | -140.177 | 149.654 | -53.9057 |

| | | | | |
|---|---|---|---|---|
| 25.7891 | 444.814 | -134.926 | 172.274 | -49.3792 |
| 26.4797 | 480.222 | -129.68 | 192.759 | -47.6646 |
| 27.1703 | 512.952 | -124.431 | 211.093 | -46.0974 |
| 27.8609 | 542.686 | -119.177 | 227.355 | -44.5401 |
| 28.5516 | 569.356 | -113.917 | 241.572 | -42.9814 |
| 29.2422 | 592.979 | -108.651 | 253.744 | -41.4211 |
| 29.9328 | 613.348 | -103.382 | 263.868 | -39.8599 |
| 30.6234 | 632.458 | -98.1092 | 271.943 | -38.2975 |
| 31.3141 | 648.637 | -92.8339 | 277.972 | -36.7343 |
| 32.0047 | 660.281 | -87.5566 | 281.963 | -35.1704 |
| 32.6953 | 667.099 | -82.2777 | 283.892 | -33.6065 |
| 33.3859 | 670.354 | -86.703 | 283.704 | -32.0424 |
| 34.0766 | 671.251 | -93.5016 | 281.445 | -30.4779 |
| 34.7672 | 667.066 | -100.324 | 277.165 | -28.9133 |
| 35.4578 | 657.133 | -107.18 | 270.901 | -27.3487 |
| 36.1484 | 636.245 | -114.082 | 262.674 | -25.7845 |
| 36.8391 | 612.98 | -121.047 | 252.376 | -24.2238 |
| 37.5297 | 584.675 | -128.102 | 239.769 | -22.671 |
| 38.2203 | 550.167 | -135.284 | 225.188 | -21.1279 |
| 38.9109 | 510.052 | -143.389 | 209.329 | -19.61 |
| 39.565 | 468.536 | -151.876 | 192.852 | -18.2724 |
| 40.2263 | 415.911 | -161.52 | 173.769 | -16.9949 |
| 40.9316 | 354.981 | -173.328 | 150.44 | -15.7282 |
| 41.6368 | 283.256 | -186.222 | 123.783 | -15.1541 |
| 42.3171 | 209.679 | -196.679 | 95.8976 | -19.872 |
| 42.8886 | 150.954 | -198.603 | 72.9837 | -26.5855 |
| 43.2663 | 116.739 | -192.316 | 58.7886 | -29.8987 |
| 43.5337 | 95.2953 | -180.298 | 50.0707 | -30.9315 |
| 43.9004 | 75.141 | -165.83 | 40.2581 | -30.5 |
| 44.4 | 51.8216 | -139.378 | 31.0059 | -28.4758 |
| 44.9833 | 35.3518 | -69.3178 | 16.5775 | -16.6749 |

| s | Var1 | | Var2 | | ULS A | | ULS-B | |
|---|---|---|---|---|---|---|---|---|
| [m] | [kNm/m] | | [kNm/m] | | [kNm/m] | | [kNm/m] | |
| | max | min | max | min | max | min | max | min |
| 0.31667 | 61.90 | -107.76 | 41.17 | -75.41 | 38.89185 | -78.4728 | 60.2 | -110.6 |
| 0.9 | 100.17 | -209.62 | 66.25 | -148.38 | 61.09921 | -154.072 | 97.5 | -215.3 |
| 1.39958 | 144.06 | -248.82 | 98.28 | -178.36 | 98.69282 | -176.862 | 150.0 | -248.4 |
| 1.76625 | 184.45 | -273.45 | 127.49 | -198.12 | 141.2371 | -185.384 | 206.0 | -261.9 |
| 2.03375 | 225.88 | -285.81 | 157.83 | -209.20 | 188.6403 | -182.369 | 266.2 | -260.1 |
| 2.41138 | 290.53 | -296.35 | 205.37 | -220.69 | 269.0754 | -166.936 | 366.6 | -243.5 |
| 2.98289 | 403.18 | -306.45 | 288.97 | -234.67 | 412.7352 | -132.208 | 544.1 | -204.5 |
| 3.66316 | 534.49 | -313.93 | 387.67 | -246.19 | 584.3977 | -84.5434 | 755.7 | -152.5 |
| 4.36842 | 658.65 | -321.24 | 482.93 | -257.46 | 743.7895 | -42.2953 | 954.0 | -106.8 |
| 5.07368 | 763.65 | -330.34 | 565.59 | -270.19 | 870.2773 | -16.0154 | 1115.5 | -78.7 |
| 5.77895 | 849.27 | -341.75 | 635.15 | -284.66 | 959.7615 | -8.69871 | 1236.5 | -71.5 |
| 6.48421 | 915.77 | -393.79 | 691.50 | -329.71 | 1011.171 | -49.9434 | 1316.4 | -124.3 |
| 7.18947 | 964.53 | -451.50 | 735.53 | -379.00 | 1027.836 | -111.664 | 1358.6 | -200.3 |
| 7.89474 | 998.82 | -509.21 | 769.68 | -428.27 | 1009.724 | -191.382 | 1364.2 | -295.6 |
| 8.6 | 1021.37 | -566.86 | 796.00 | -477.48 | 958.179 | -289.585 | 1335.2 | -410.8 |
| 9.30526 | 1038.21 | -624.44 | 819.04 | -526.63 | 877.2596 | -407.033 | 1277.3 | -546.5 |
| 10.0105 | 1040.77 | -681.93 | 832.32 | -575.69 | 756.6562 | -564.661 | 1175.3 | -718.3 |
| 10.7158 | 1030.13 | -739.32 | 836.62 | -624.67 | 645.9958 | -762.58 | 1067.8 | -912.0 |
| 11.4211 | 1013.79 | -796.68 | 837.65 | -673.61 | 513.7316 | -985.795 | 936.2 | -1128.2 |
| 12.1263 | 984.26 | -854.08 | 829.79 | -722.55 | 354.1809 | -1234.47 | 773.0 | -1367.0 |
| 12.8316 | 941.50 | -911.88 | 813.13 | -771.79 | 167.1354 | -1509.21 | 577.9 | -1629.1 |
| 13.5368 | 885.64 | -970.86 | 787.93 | -821.93 | -47.7171 | -1811.34 | 350.7 | -1916.0 |
| 14.2421 | 817.49 | -1033.03 | 755.05 | -874.36 | -290.218 | -2143.04 | 91.9 | -2230.5 |
| 14.9474 | 739.79 | -1104.86 | 716.66 | -932.32 | -559.013 | -2508.5 | -196.5 | -2579.9 |
| 15.725 | 646.75 | -1204.76 | 669.48 | -1006.88 | -884.828 | -2955.49 | -522.5 | -3015.7 |
| 16.575 | 542.42 | -1337.40 | 615.82 | -1099.33 | -1251.3 | -3466.46 | -864.1 | -3525.7 |
| 17.4 | 445.22 | -1467.78 | 562.37 | -1185.84 | -1553.14 | -3884.85 | -1145.4 | -3955.5 |
| 17.925 | 386.97 | -1534.40 | 527.85 | -1229.22 | -1686.7 | -4059.65 | -1269.1 | -4141.1 |
| 18.175 | 373.49 | -1543.32 | 520.42 | -1235.24 | -1696.32 | -4067.42 | -1276.4 | -4152.0 |
| 18.425 | 370.82 | -1538.03 | 519.79 | -1232.07 | -1690.53 | -4054.81 | -1269.6 | -4138.6 |
| 18.675 | 376.18 | -1517.46 | 523.80 | -1219.08 | -1654.18 | -3997.35 | -1233.6 | -4078.4 |
| 19.2 | 376.52 | -1421.70 | 520.14 | -1157.91 | -1497.38 | -3717.07 | -1081.6 | -3786.9 |
| 20.025 | 430.67 | -1222.72 | 550.19 | -1028.83 | -1125.8 | -3123.23 | -722.9 | -3172.2 |
| 20.875 | 504.35 | -1004.33 | 590.74 | -884.05 | -681.288 | -2429.89 | -295.8 | -2462.5 |
| 21.6453 | 587.26 | -825.81 | 637.18 | -763.28 | -278.02 | -1824.9 | 91.4 | -1850.2 |
| 22.3359 | 668.26 | -707.98 | 681.85 | -683.52 | 65.19675 | -1339.98 | 421.2 | -1369.5 |
| 23.0266 | 756.25 | -629.98 | 730.10 | -631.86 | 393.2797 | -908.511 | 763.0 | -953.1 |
| 23.7172 | 850.44 | -577.97 | 781.09 | -597.71 | 746.643 | -489.925 | 1143.2 | -569.4 |
| 24.4078 | 944.08 | -534.65 | 831.42 | -567.46 | 1131.705 | -220.265 | 1523.3 | -279.1 |
| 25.0984 | 1032.36 | -501.61 | 878.63 | -541.55 | 1487.111 | 24.04389 | 1874.2 | -15.0 |

| | | | | | | | | |
|---|---|---|---|---|---|---|---|---|
| 25.7891 | 1115.66 | -479.14 | 922.73 | -519.90 | 1814.9 | 246.3675 | 2198.4 | 225.6 |
| 26.4797 | 1192.17 | -460.88 | 962.80 | -499.90 | 2114.223 | 449.3306 | 2494.1 | 445.6 |
| 27.1703 | 1261.40 | -442.80 | 998.52 | -479.95 | 2384.754 | 634.5531 | 2760.7 | 646.5 |
| 27.8609 | 1323.01 | -424.71 | 1029.57 | -459.95 | 2626.187 | 802.1159 | 2998.0 | 828.4 |
| 28.5516 | 1376.94 | -406.59 | 1055.90 | -439.92 | 2838.472 | 952.0248 | 3205.9 | 991.3 |
| 29.2422 | 1423.23 | -388.45 | 1077.55 | -419.86 | 3021.621 | 1084.266 | 3384.3 | 1135.2 |
| 29.9328 | 1461.54 | -370.28 | 1094.27 | -399.77 | 3175.388 | 1198.82 | 3533.1 | 1260.0 |
| 30.6234 | 1494.89 | -352.11 | 1108.33 | -379.67 | 3302.058 | 1295.706 | 3655.1 | 1365.9 |
| 31.3141 | 1520.77 | -333.92 | 1117.84 | -359.56 | 3399.719 | 1374.899 | 3748.0 | 1452.7 |
| 32.0047 | 1536.78 | -315.72 | 1120.99 | -339.43 | 3466.563 | 1436.396 | 3809.2 | 1520.4 |
| 32.6953 | 1542.46 | -297.52 | 1117.45 | -319.30 | 3502.236 | 1480.185 | 3838.4 | 1569.1 |
| 33.3859 | 1539.62 | -293.88 | 1108.61 | -310.13 | 3508.339 | 1495.449 | 3837.5 | 1587.9 |
| 34.0766 | 1530.13 | -293.78 | 1095.86 | -303.63 | 3489.308 | 1492.672 | 3811.0 | 1587.5 |
| 34.7672 | 1509.98 | -293.73 | 1076.15 | -297.17 | 3438.898 | 1472.196 | 3752.3 | 1568.1 |
| 35.4578 | 1478.24 | -293.72 | 1048.75 | -290.73 | 3356.335 | 1433.978 | 3660.1 | 1526.6 |
| 36.1484 | 1427.12 | -293.78 | 1007.79 | -284.35 | 3235.735 | 1377.994 | 3526.9 | 1462.5 |
| 36.8391 | 1369.32 | -293.94 | 962.90 | -278.04 | 3086.722 | 1304.221 | 3365.2 | 1379.3 |
| 37.5297 | 1300.50 | -294.24 | 910.93 | -271.83 | 2906.124 | 1212.61 | 3170.7 | 1276.8 |
| 38.2203 | 1219.41 | -294.75 | 850.77 | -265.77 | 2692.81 | 1103.106 | 2942.2 | 1155.0 |
| 38.9109 | 1128.00 | -296.68 | 783.50 | -260.77 | 2447.915 | 974.827 | 2681.5 | 1012.8 |
| 39.565 | 1033.96 | -299.88 | 714.95 | -257.02 | 2189.315 | 836.568 | 2407.9 | 859.6 |
| 40.2263 | 919.28 | -304.85 | 632.17 | -254.51 | 1891.522 | 678.9591 | 2091.3 | 685.3 |
| 40.9316 | 785.37 | -312.63 | 536.79 | -253.71 | 1545.772 | 493.7971 | 1723.5 | 480.5 |
| 41.6368 | 630.47 | -323.30 | 427.53 | -254.92 | 1170.582 | 295.5041 | 1321.1 | 260.8 |
| 42.3171 | 471.68 | -339.02 | 316.66 | -257.83 | 803.745 | 103.1962 | 924.8 | 44.0 |
| 42.8886 | 344.33 | -346.77 | 228.41 | -255.34 | 519.026 | -39.5565 | 615.5 | -118.1 |
| 43.2663 | 269.00 | -339.41 | 176.70 | -245.40 | 357.8145 | -110.561 | 438.7 | -196.7 |
| 43.5337 | 222.20 | -321.28 | 144.65 | -229.68 | 265.5366 | -139.408 | 336.0 | -225.9 |
| 43.9004 | 175.66 | -297.22 | 113.33 | -210.24 | 177.1365 | -162.292 | 236.3 | -246.8 |
| 44.4 | 125.32 | -252.94 | 78.97 | -176.51 | 101.1594 | -159.657 | 146.7 | -235.3 |
| 44.9833 | 78.15 | -129.27 | 50.33 | -88.80 | 55.70819 | -84.8161 | 83.3 | -125.1 |

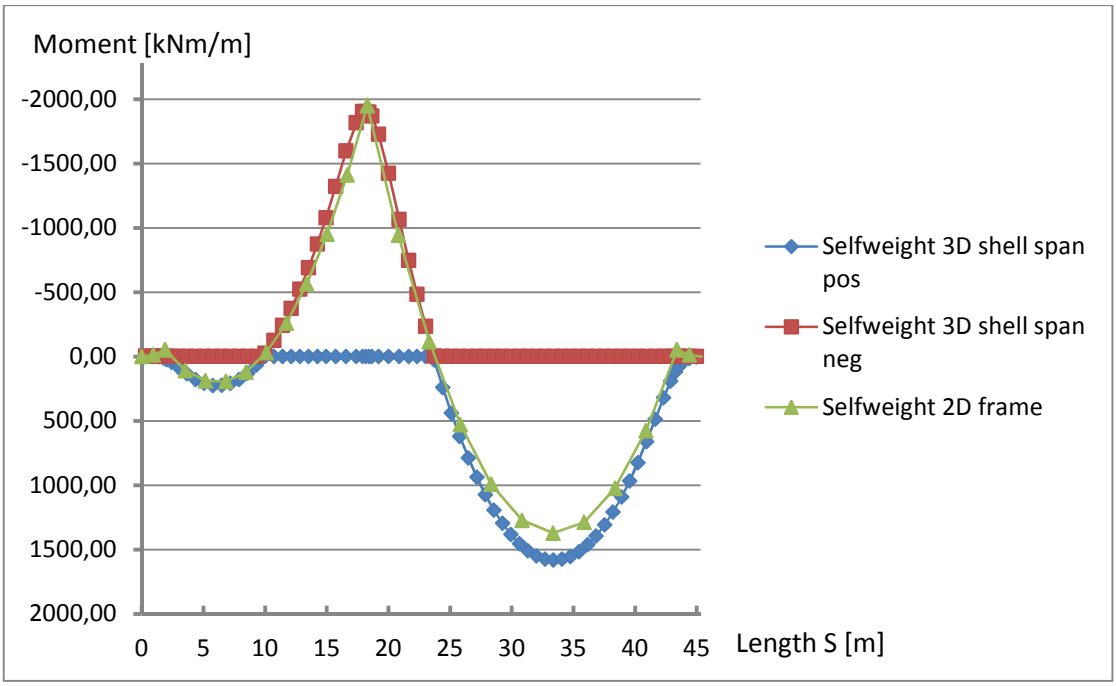


*Figure C.11 – Illustration of the bending moment distribution in span due to selfweight*

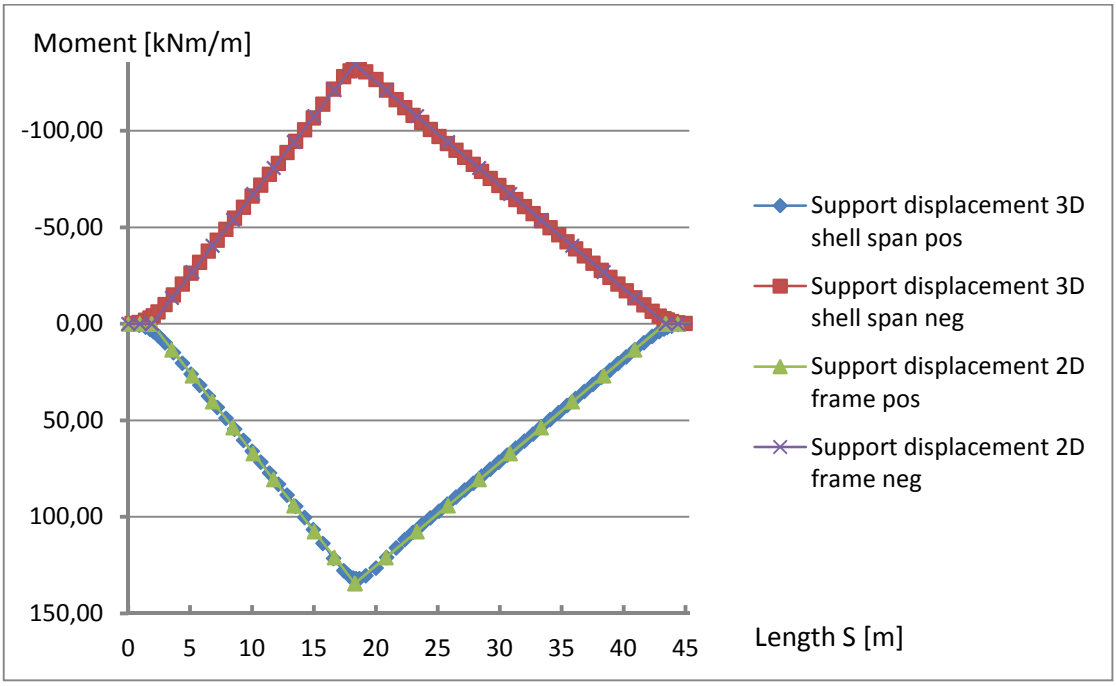


*Figure C.12 – Illustration of the bending moment distribution in span due to support displacement*

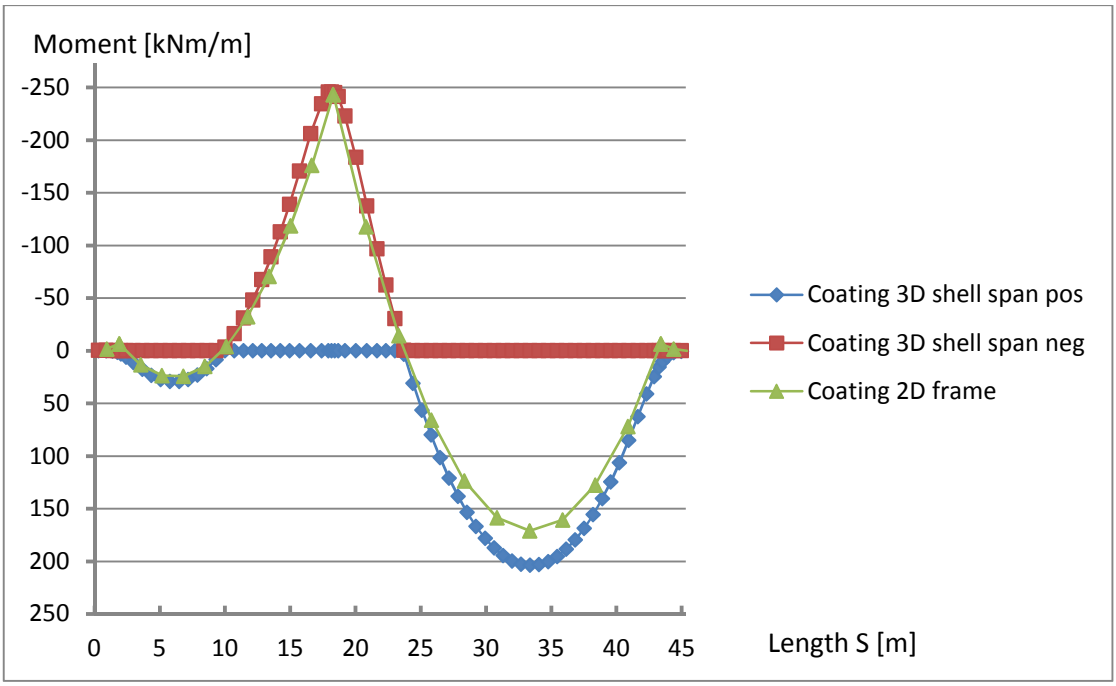


*Figure C.13 – Illustration of the bending moment distribution in span due to coating*

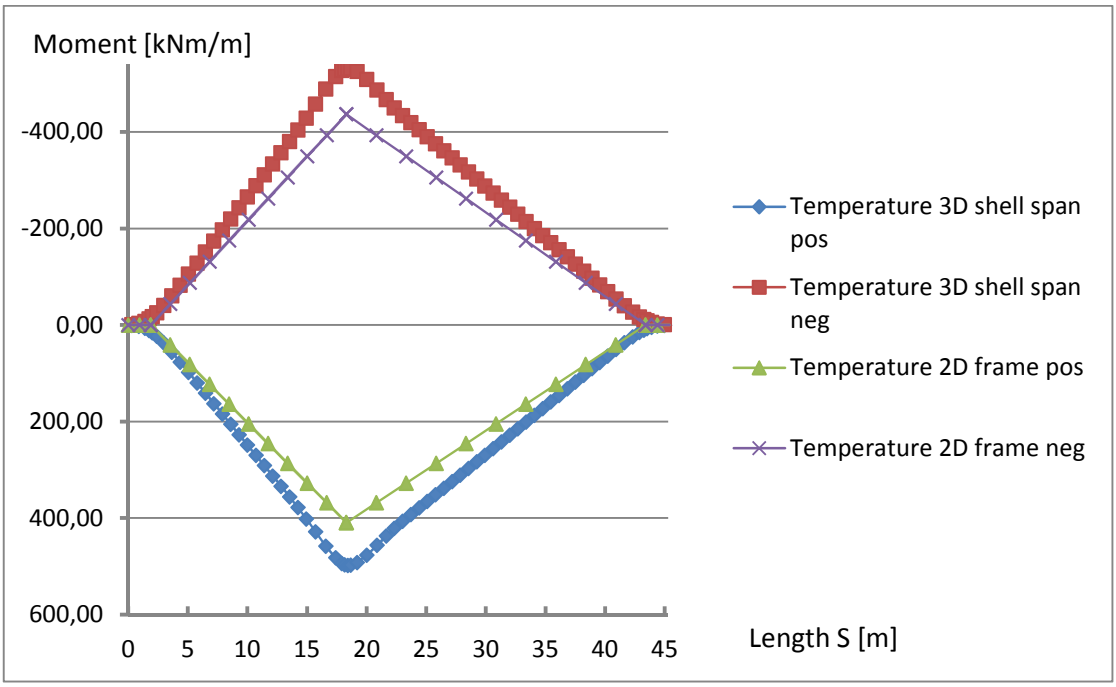


*Figure C.14 – Illustration of the bending moment distribution in span due to temperature load*

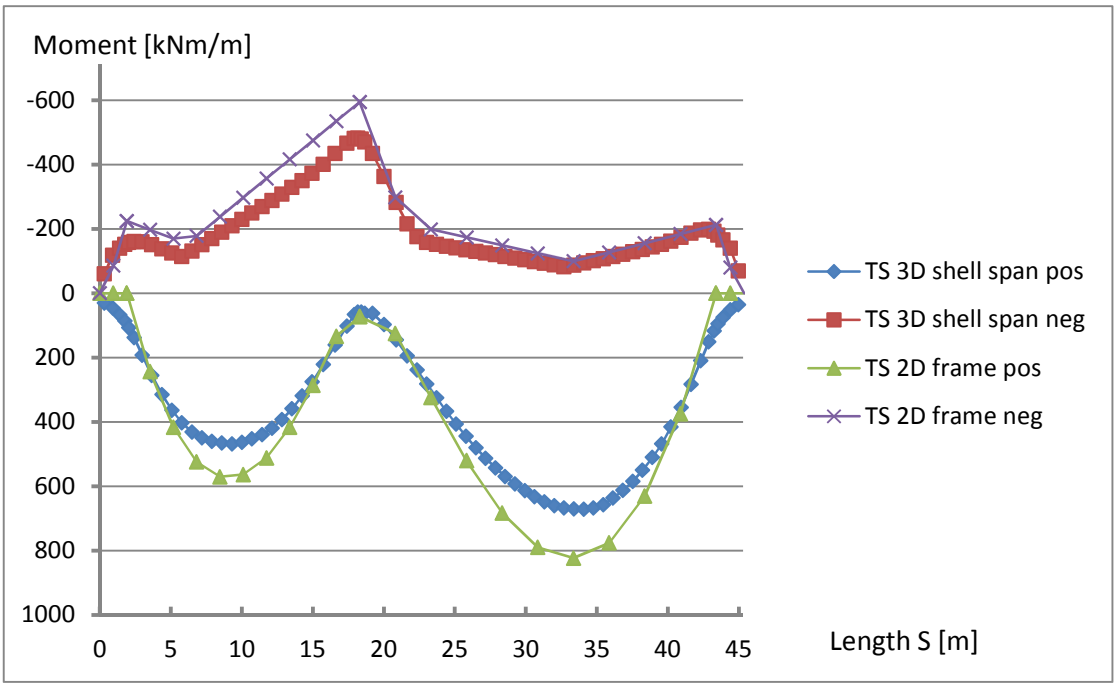


*Figure C.15 – Illustration of the bending moment distribution in span due to traffic load TS*

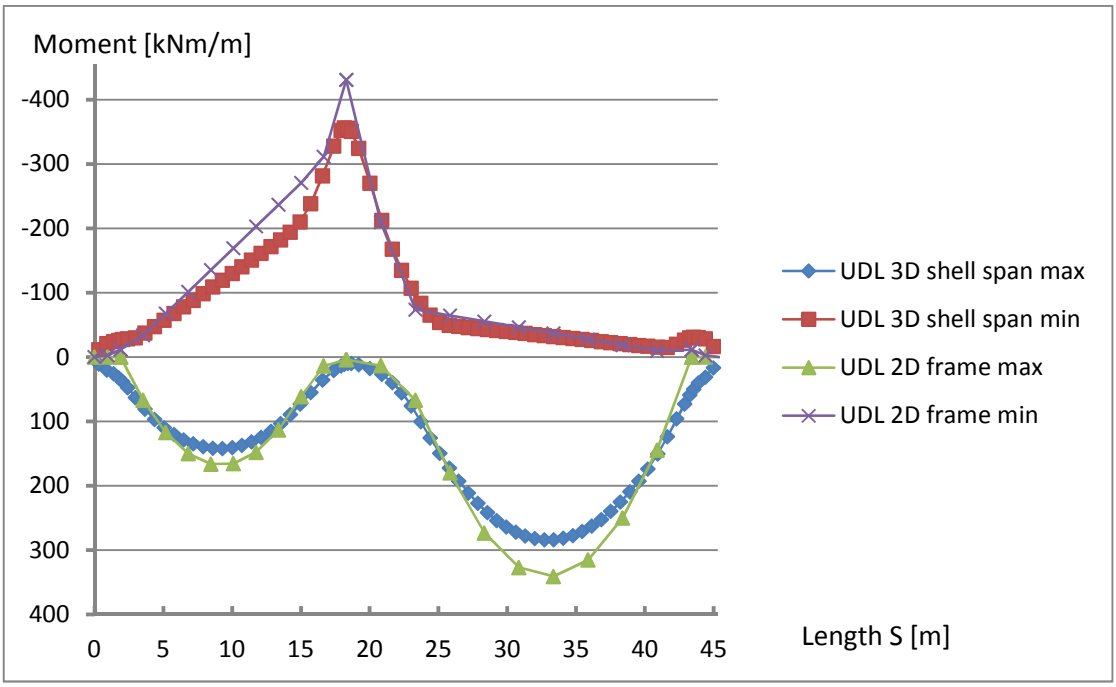


*Figure C.16 – Illustration of the bending moment distribution in span due to traffic load UDL*

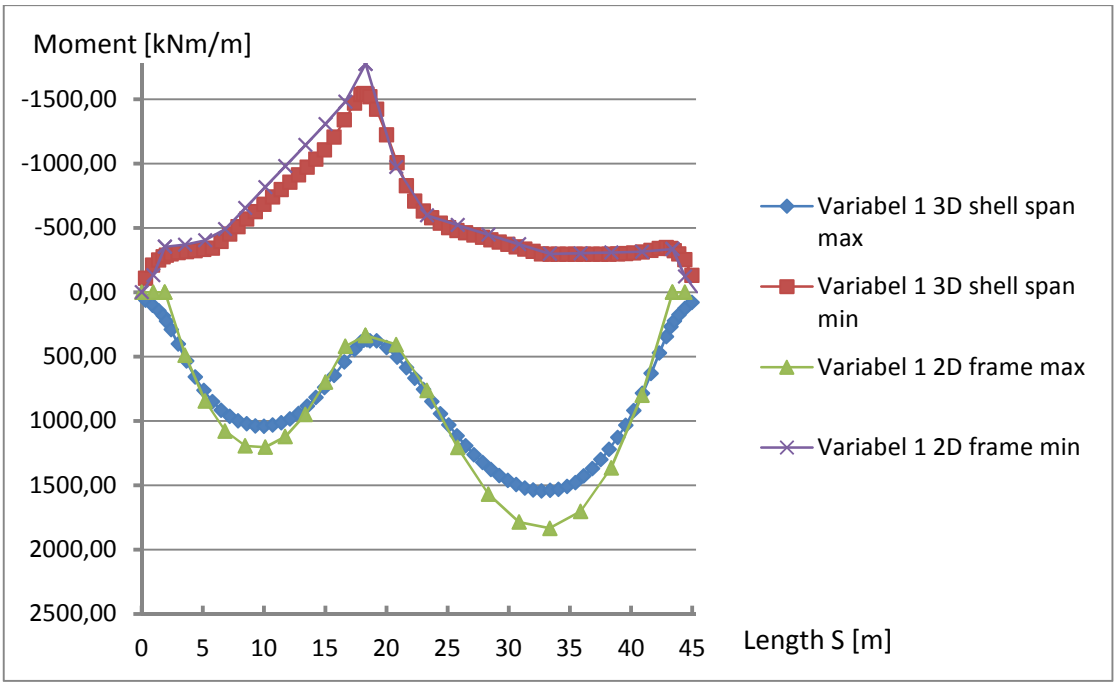


*Figure C.17 – Illustration of the bending moment distribution in span due to variable load 1*

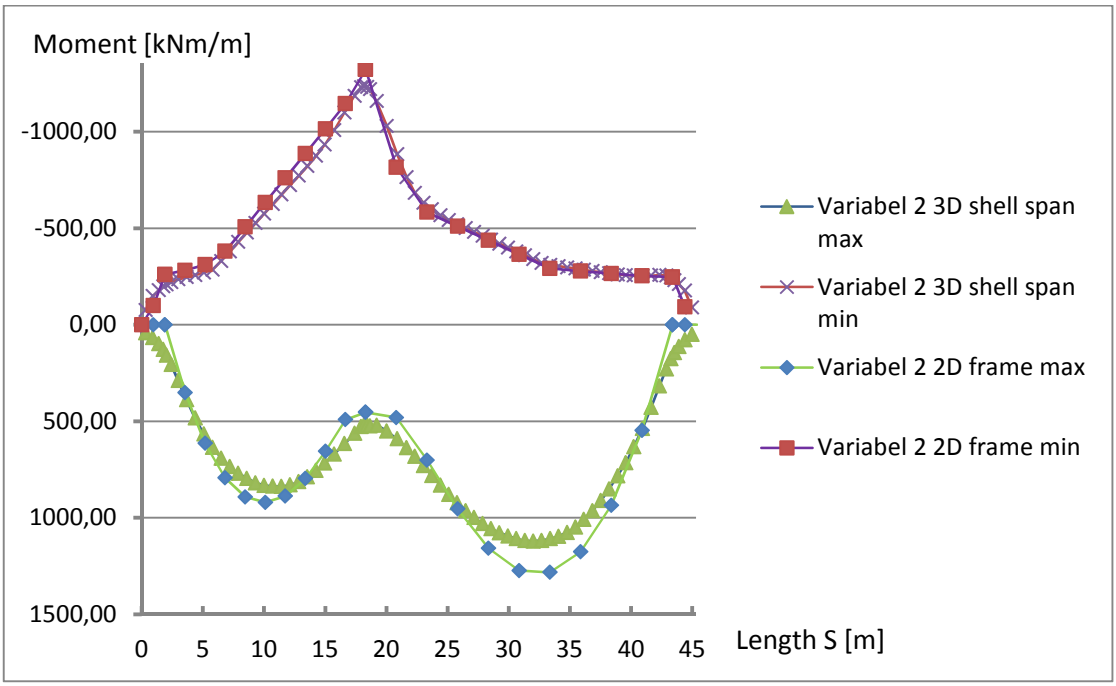


*Figure C.18 – Illustration of the bending moment distribution in span due to variable load 2*

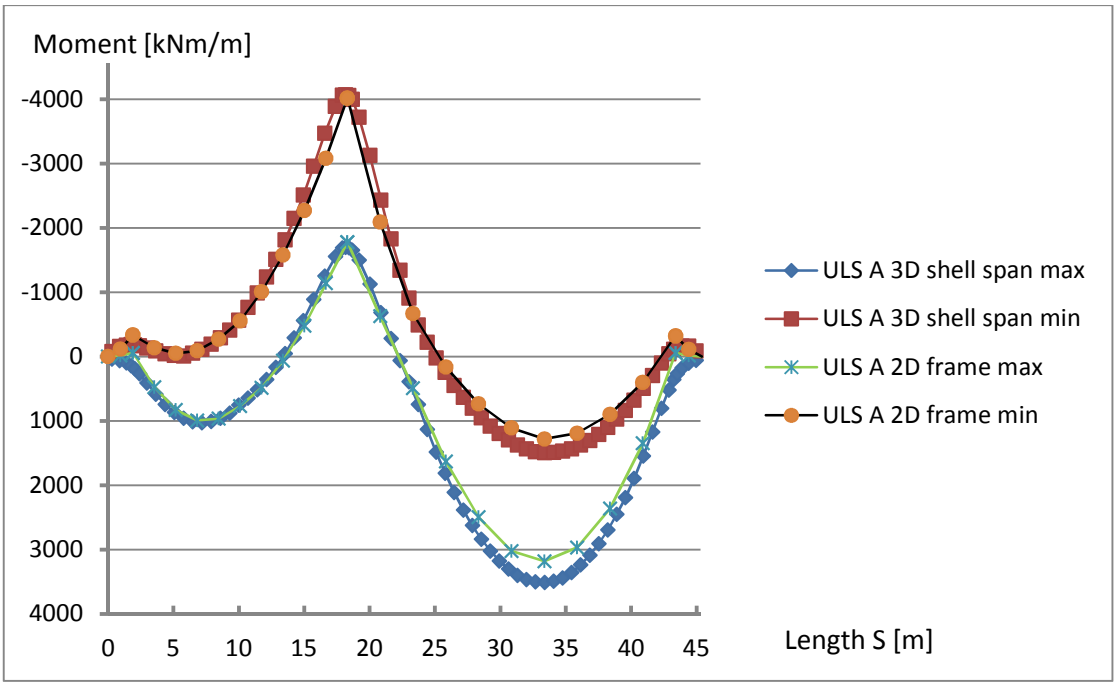


*Figure C.19 – Illustration of the bending moment distribution in span after load combination for ULS A*

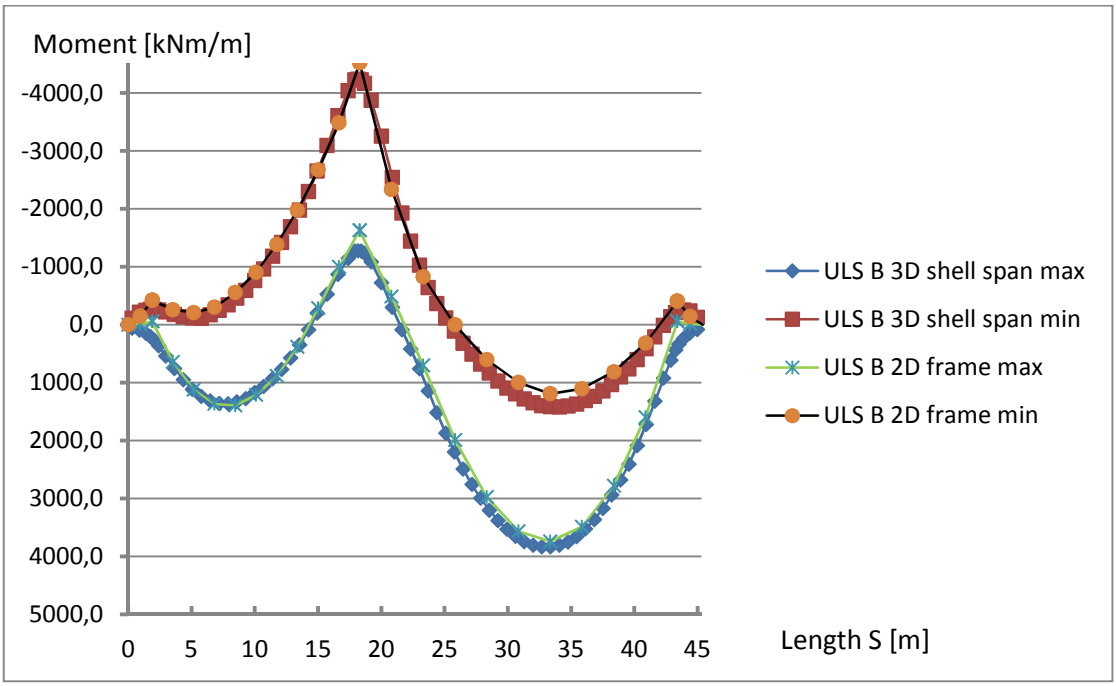


*Figure C.20 – Illustration of the bending moment distribution in span after load combinationfor ULSB*

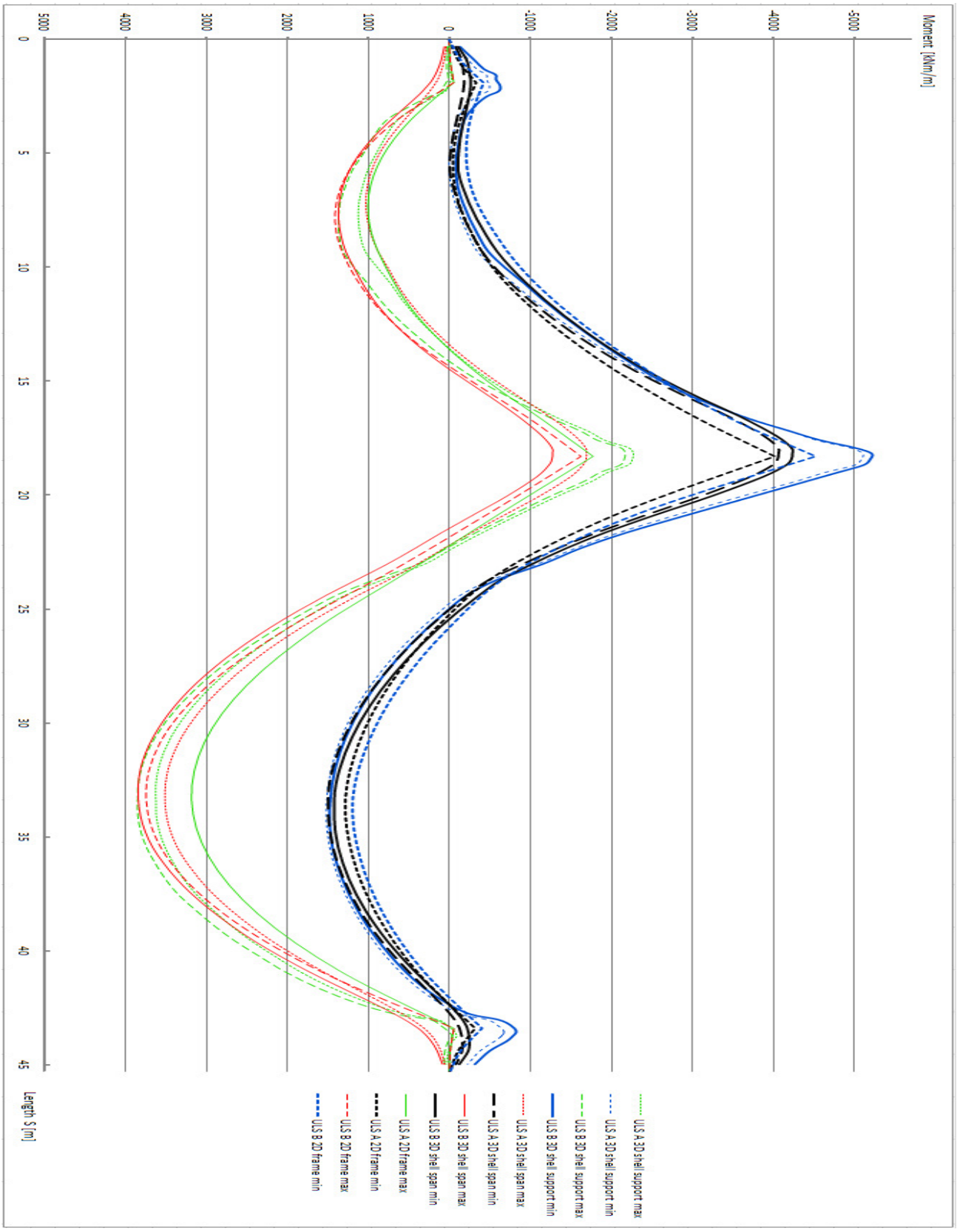


*Figure C.21 – Illustration of the bending moment distribution for ULS A and ULS B in span and over support for 3D shell- and 2D frame models.*

## *Frame Slab-bridge*

The values are extracted from two strips, middle strip and end strip; see Figure C.22

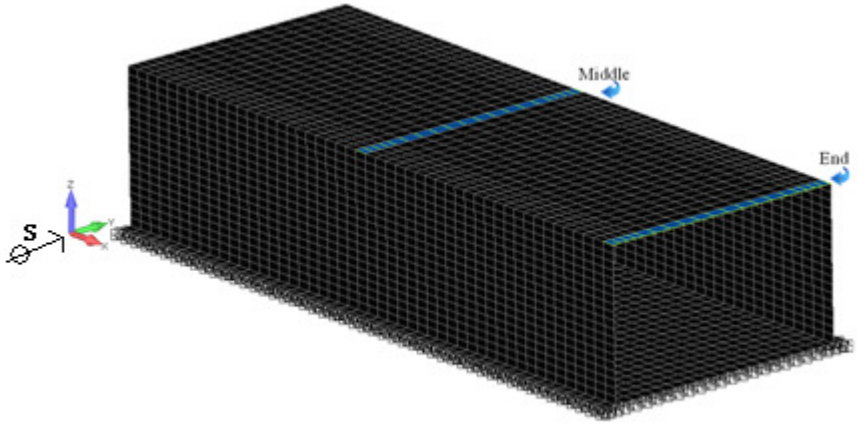


*Figure C.22 – Illustration of the location of the middle- and end strip*

*Table C.2 – Partial factors*

Partial factors

Safety class: 2

| | | | | | | | | ULS-A | | | | SLS |
|---|---|---|---|---|---|---|---|---|---|---|---|---|
| | Lastfall | | Load coefficient | | | | | ULS-A | | ULS-B | | SLS-QP |
| | Permanenta laster | | sup | inf | Y.G.jsup | Y.G.jinf | ξ | max | min | max | min | |
| 1 | EG | Self-weight | 1 | 1 | 1.35 | 1 | 0.89 | 1.23 | 1 | 1.09 | 1 | 1 |
| 2 | BEL | Pavement | 1.1 | 0.9 | 1.35 | 1 | 0.89 | 1.35 | 0.9 | 1.2 | 0.9 | 0.75 |
| 3 | JORD | Earth pressure | 1 | 1 | 1.1 | 1 | 1 | 1 | 1 | 1 | 1 | 0.75 |
| 4 | KRYMP | Shrinkage | 1 | 1 | 1.35 | 1 | 0.89 | 1.23 | 1 | 1.09 | 1 | 1 |
| | Variabla laster | | k | Ψ.0 | Ψ.1 | Ψ.2 | Y.Q | | | | | |
| 5 | TS | Traffic loads | k | 0.75 | 0.75 | 0 | 1.5 | 1.02 | 1.02 | 1.37 | 1 | 0 |
| 6 | UDL | Traffic loads | k | 0.4 | 0.4 | 0 | 1.5 | 0.55 | 0.55 | 1.37 | 0.6 | 0 |
| 7 | TEMP | Thermal actions | k | 0.6 | 0.6 | 0.5 | 1.5 | 0.82 | 0.82 | 1.37 | 0.8 | 0.5 |

# Middle strip

| s [m] | Selfweight total [kNm/m] | | Earth pressure [kNm/m] | | Pavement [kNm/m] | |
|---|---|---|---|---|---|---|
| | max | min | pos | neg | pos | neg |
| 0.16 | 0 | -63.6487 | 0 | -2.1884 | 0 | -19.8198 |
| 0.49 | 0 | -45.0342 | 0 | -2.1875 | 0 | -14.8538 |
| 0.81 | 0 | -28.2874 | 0 | -2.18548 | 0 | -10.2663 |
| 1.14 | 0 | -13.2778 | 0 | -2.18352 | 0 | -6.05867 |
| 1.56 | 3.72275 | 0 | 0 | -2.18156 | 0 | -1.20655 |
| 2.13 | 22.9053 | 0 | 0 | -2.17964 | 4.32535 | 0 |
| 2.74 | 39.1607 | 0 | 0 | -2.17808 | 9.02204 | 0 |
| 3.35 | 50.7458 | 0 | 0 | -2.17693 | 12.3748 | 0 |
| 3.96 | 57.6617 | 0 | 0 | -2.17629 | 14.3841 | 0 |
| 4.58 | 59.9092 | 0 | 0 | -2.17641 | 15.0503 | 0 |
| 5.19 | 57.4884 | 0 | 0 | -2.17748 | 14.3739 | 0 |
| 5.8 | 50.3987 | 0 | 0 | -2.17916 | 12.3551 | 0 |
| 6.41 | 38.6388 | 0 | 0 | -2.18135 | 8.99283 | 0 |
| 7.02 | 22.2069 | 0 | 0 | -2.18393 | 4.28665 | 0 |
| 7.59 | 2.86544 | 0 | 0 | -2.18681 | 0 | -1.25368 |
| 8.01 | 0 | -14.2497 | 0 | -2.18948 | 0 | -6.11267 |
| 8.34 | 0 | -29.3549 | 0 | -2.19198 | 0 | -10.3256 |
| 8.66 | 0 | -46.1974 | 0 | -2.19453 | 0 | -14.9184 |
| 8.99 | 0 | -64.9052 | 0 | -2.19598 | 0 | -19.8896 |

| s [m] | Shrinkage [kNm/m] | | TS [kNm/m] | | UDL [kNm/m] | |
|---|---|---|---|---|---|---|
| | pos | neg | max | min | max | min |
| 0.16 | 3.09576 | 0 | 8.71903 | -124.398 | 1.55725 | -26.5289 |
| 0.49 | 3.06185 | 0 | 28.6235 | -115.458 | 4.00887 | -25.6147 |
| 0.81 | 3.00201 | 0 | 36.5664 | -95.0636 | 5.97117 | -21.1152 |
| 1.14 | 2.94729 | 0 | 49.8638 | -73.9273 | 6.94482 | -15.6028 |
| 1.56 | 2.89433 | 0 | 58.0251 | -49.2102 | 8.32266 | -9.82528 |
| 2.13 | 2.84353 | 0 | 73.3323 | -25.5918 | 11.0011 | -5.10688 |
| 2.74 | 2.80291 | 0 | 91.9426 | -11.2022 | 14.247 | -2.40291 |
| 3.35 | 2.77168 | 0 | 105.11 | -3.18683 | 16.3329 | -0.6344 |
| 3.96 | 2.75021 | 0 | 112.976 | -1.88835 | 17.4525 | -0.27968 |
| 4.58 | 2.73957 | 0 | 115.317 | -1.57693 | 17.6619 | -0.24407 |
| 5.19 | 2.74568 | 0 | 112.109 | -1.88098 | 17.4359 | -0.28238 |
| 5.8 | 2.76222 | 0 | 103.447 | -3.20545 | 16.3007 | -0.64755 |
| 6.41 | 2.78856 | 0 | 90.3325 | -11.3984 | 14.2662 | -2.49403 |
| 7.02 | 2.82446 | 0 | 73.894 | -25.6514 | 10.9621 | -5.13589 |
| 7.59 | 2.87121 | 0 | 58.6894 | -49.2905 | 8.28994 | -9.85688 |
| 8.01 | 2.92154 | 0 | 47.3307 | -73.9699 | 6.91342 | -15.6328 |
| 8.34 | 2.97468 | 0 | 36.8898 | -94.9181 | 5.93846 | -21.1414 |
| 8.66 | 3.03331 | 0 | 19.5157 | -115.711 | 4.00701 | -25.6745 |
| 8.99 | 3.0659 | 0 | 7.32356 | -124.991 | 1.55012 | -26.5786 |

| s [m] | EXP [kNm/m] | | CON [kNm/m] | | Temp differance [kNm/m] | |
|---|---|---|---|---|---|---|
| | pos | neg | pos | neg | max | min |
| 0.16 | 0 | -26.2823 | 30.8137 | 0 | 30.81 | -26.28 |
| 0.49 | 0 | -26.0902 | 30.5885 | 0 | 30.59 | -26.09 |
| 0.81 | 0 | -25.6874 | 30.1162 | 0 | 30.12 | -25.69 |
| 1.14 | 0 | -25.3185 | 29.6838 | 0 | 29.68 | -25.32 |
| 1.56 | 0 | -24.9749 | 29.2809 | 0 | 29.28 | -24.97 |
| 2.13 | 0 | -24.6635 | 28.9158 | 0 | 28.92 | -24.66 |
| 2.74 | 0 | -24.4253 | 28.6366 | 0 | 28.64 | -24.43 |
| 3.35 | 0 | -24.2445 | 28.4246 | 0 | 28.42 | -24.24 |
| 3.96 | 0 | -24.1231 | 28.2823 | 0 | 28.28 | -24.12 |
| 4.58 | 0 | -24.0667 | 28.2162 | 0 | 28.22 | -24.07 |
| 5.19 | 0 | -24.1289 | 28.289 | 0 | 28.29 | -24.13 |
| 5.8 | 0 | -24.259 | 28.4415 | 0 | 28.44 | -24.26 |
| 6.41 | 0 | -24.45 | 28.6655 | 0 | 28.67 | -24.45 |
| 7.02 | 0 | -24.7005 | 28.9592 | 0 | 28.96 | -24.70 |
| 7.59 | 0 | -25.0255 | 29.3403 | 0 | 29.34 | -25.03 |
| 8.01 | 0 | -25.3808 | 29.7568 | 0 | 29.76 | -25.38 |
| 8.34 | 0 | -25.7597 | 30.201 | 0 | 30.20 | -25.76 |
| 8.66 | 0 | -26.1739 | 30.6866 | 0 | 30.69 | -26.17 |
| 8.99 | 0 | -26.3782 | 30.9262 | 0 | 30.93 | -26.38 |

| s [m] | Heat [kNm/m] | | Cool [kNm/m] | | Temp gradient [kNm/m] | |
|---|---|---|---|---|---|---|
| | pos | neg | pos | neg | max | min |
| 0.16 | 27.8474 | 0 | 0 | -29.7015 | 27.85 | -29.70 |
| 0.49 | 27.8245 | 0 | 0 | -29.677 | 27.82 | -29.68 |
| 0.81 | 27.7479 | 0 | 0 | -29.5953 | 27.75 | -29.60 |
| 1.14 | 27.6694 | 0 | 0 | -29.5116 | 27.67 | -29.51 |
| 1.56 | 27.5873 | 0 | 0 | -29.424 | 27.59 | -29.42 |
| 2.13 | 27.5019 | 0 | 0 | -29.3329 | 27.50 | -29.33 |
| 2.74 | 27.4234 | 0 | 0 | -29.2493 | 27.42 | -29.25 |
| 3.35 | 27.3529 | 0 | 0 | -29.174 | 27.35 | -29.17 |
| 3.96 | 27.2993 | 0 | 0 | -29.1168 | 27.30 | -29.12 |
| 4.58 | 27.2705 | 0 | 0 | -29.0862 | 27.27 | -29.09 |
| 5.19 | 27.2979 | 0 | 0 | -29.1153 | 27.30 | -29.12 |
| 5.8 | 27.3502 | 0 | 0 | -29.1711 | 27.35 | -29.17 |
| 6.41 | 27.4193 | 0 | 0 | -29.2449 | 27.42 | -29.24 |
| 7.02 | 27.4964 | 0 | 0 | -29.3271 | 27.50 | -29.33 |
| 7.59 | 27.5806 | 0 | 0 | -29.4169 | 27.58 | -29.42 |
| 8.01 | 27.6618 | 0 | 0 | -29.5035 | 27.66 | -29.50 |
| 8.34 | 27.7396 | 0 | 0 | -29.5865 | 27.74 | -29.59 |
| 8.66 | 27.8155 | 0 | 0 | -29.6674 | 27.82 | -29.67 |
| 8.99 | 27.8377 | 0 | 0 | -29.6911 | 27.84 | -29.69 |

| s [m] | Variabel 1 [kNm/m] | | Variabel 2 [kNm/m] | |
|---|---|---|---|---|
| | max | min | max | min |
| 0.16 | 90.12 | -218.17 | 62.18061 | -252.677 |
| 0.49 | 111.43 | -208.26 | 92.60501 | -238.999 |
| 0.81 | 119.86 | -184.32 | 105.725 | -204.497 |
| 1.14 | 133.25 | -159.10 | 124.8574 | -167.617 |
| 1.56 | 141.67 | -130.12 | 137.5284 | -125.486 |
| 2.13 | 158.14 | -102.89 | 161.7993 | -86.3342 |
| 2.74 | 178.42 | -86.28 | 191.449 | -62.6522 |
| 3.35 | 192.61 | -76.78 | 212.1143 | -49.0383 |
| 3.96 | 200.98 | -75.02 | 224.264 | -46.6269 |
| 4.58 | 203.35 | -74.56 | 227.6802 | -46.0801 |
| 5.19 | 200.09 | -75.02 | 223.0578 | -46.624 |
| 5.8 | 190.92 | -76.82 | 209.8035 | -49.0913 |
| 6.41 | 176.82 | -86.56 | 189.2898 | -63.0624 |
| 7.02 | 158.75 | -103.01 | 162.5464 | -86.4812 |
| 7.59 | 142.40 | -130.28 | 138.4368 | -125.675 |
| 8.01 | 130.74 | -159.24 | 121.3977 | -167.761 |
| 8.34 | 120.27 | -184.27 | 106.186 | -204.385 |
| 8.66 | 102.26 | -208.65 | 80.19783 | -239.488 |
| 8.99 | 88.83 | -218.92 | 60.34334 | -253.627 |

| s [m] | ULS A [kNm/m] | | ULS B [kNm/m] | | SLS-QP [kNm/m] | |
|---|---|---|---|---|---|---|
| | max | min | max | min | max | min |
| 0.16 | -22.0151 | -291.521 | 9.8 | -344.9 | -51.0422 | -113.102 |
| 0.49 | 22.47546 | -252.155 | 54.2 | -305.0 | -27.6197 | -89.4122 |
| 0.81 | 52.01036 | -201.747 | 83.4 | -246.8 | -6.61964 | -67.8342 |
| 1.14 | 84.42139 | -152.695 | 115.6 | -188.6 | 12.28742 | -48.3892 |
| 1.56 | 115.2665 | -97.3987 | 145.6 | -127.1 | 33.84463 | -26.3194 |
| 2.13 | 162.4427 | -45.7275 | 192.9 | -75.4 | 58.28303 | -1.40228 |
| 2.74 | 209.2034 | -8.85565 | 245.8 | -38.4 | 79.01565 | 19.71188 |
| 3.35 | 242.2884 | 15.07521 | 283.1 | -14.3 | 93.78103 | 34.77865 |
| 3.96 | 261.9602 | 25.44465 | 305.2 | -3.8 | 102.5868 | 43.79363 |
| 4.58 | 268.036 | 28.68954 | 311.9 | -0.5 | 105.4424 | 46.75074 |
| 5.19 | 260.8374 | 25.25896 | 303.8 | -4.0 | 102.4014 | 43.60709 |
| 5.8 | 240.1187 | 14.66296 | 280.4 | -14.7 | 93.41187 | 34.40438 |
| 6.41 | 206.8897 | -9.68835 | 243.1 | -39.2 | 78.46259 | 19.14817 |
| 7.02 | 162.0862 | -46.5864 | 192.8 | -76.3 | 57.54581 | -2.1582 |
| 7.59 | 114.8388 | -98.483 | 145.3 | -128.2 | 32.94342 | -27.2495 |
| 8.01 | 80.81586 | -154.1 | 112.0 | -189.9 | 11.26847 | -49.4466 |
| 8.34 | 51.22398 | -203.092 | 82.7 | -248.0 | -7.73552 | -68.9976 |
| 8.66 | 11.99407 | -254.06 | 43.7 | -306.9 | -28.8314 | -90.6823 |
| 8.99 | -24.7218 | -293.9 | 7.2 | -347.4 | -52.347 | -114.476 |

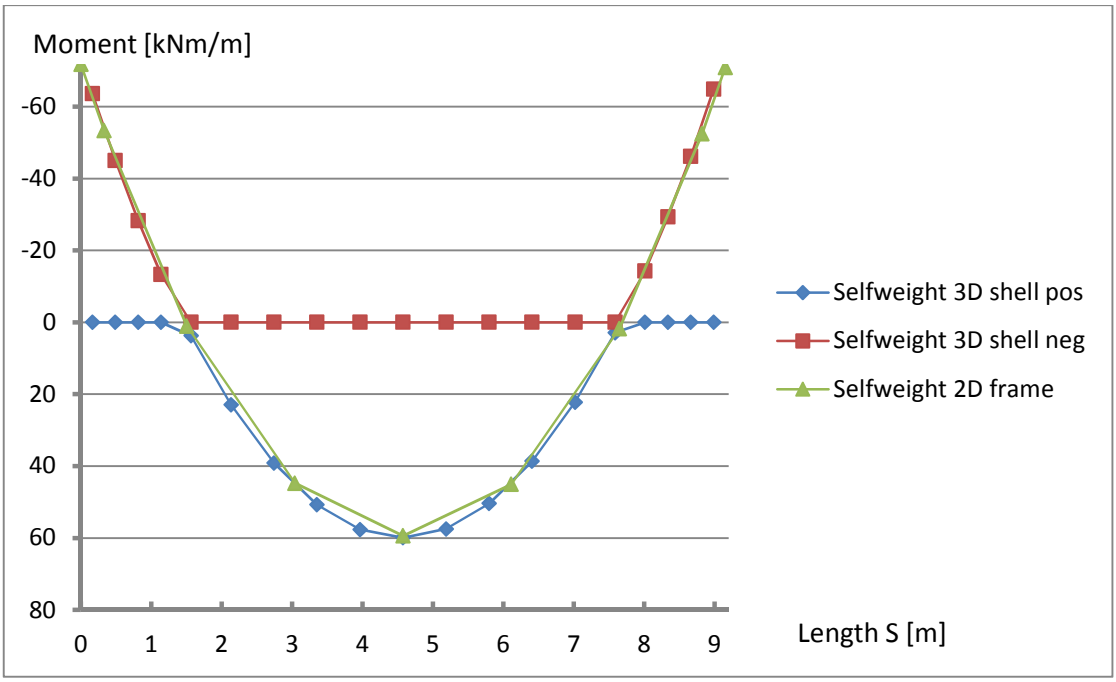


*Figure C.23 – Illustration of the bending moment distribution in the middle strip due to self weight*

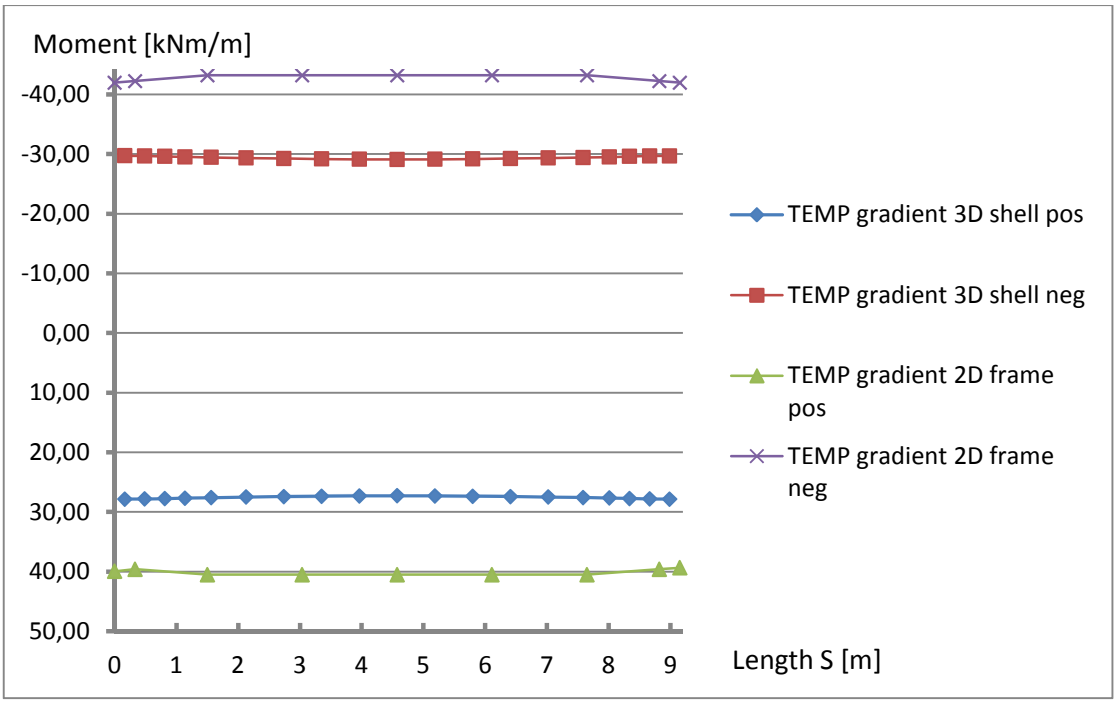


*Figure C.24 – Illustration of the bending moment distribution in the middle strip due to temperature gradient*

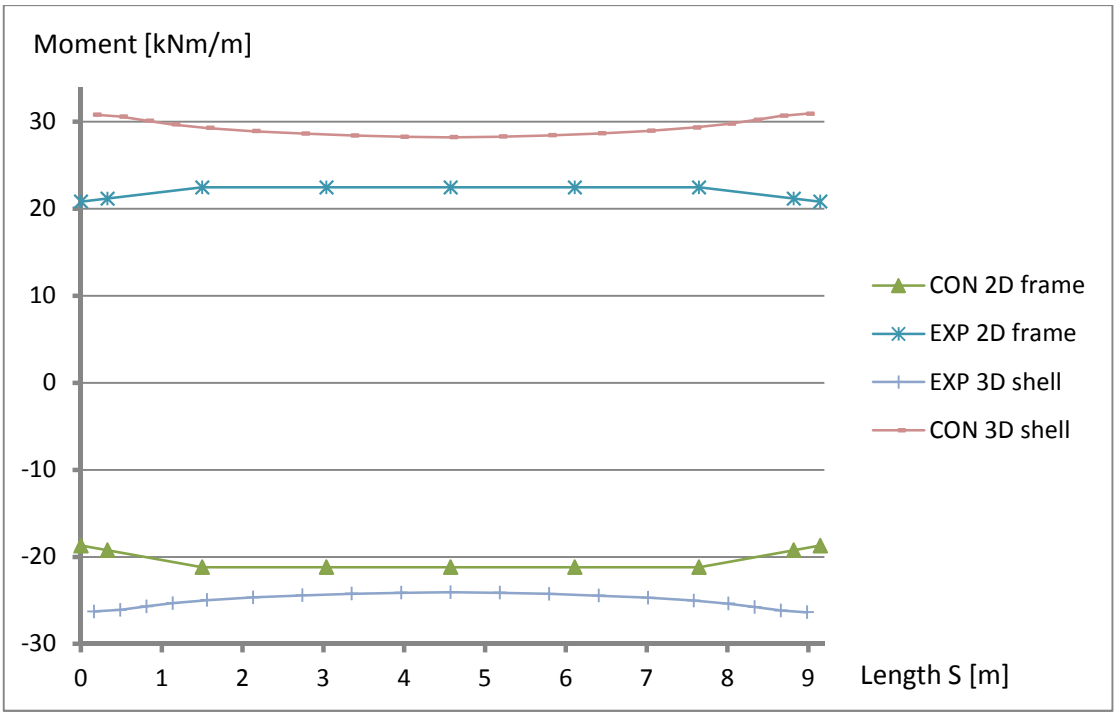


*Figure C.25 – Illustration of the bending moment distribution in the middle strip due to temperature difference*

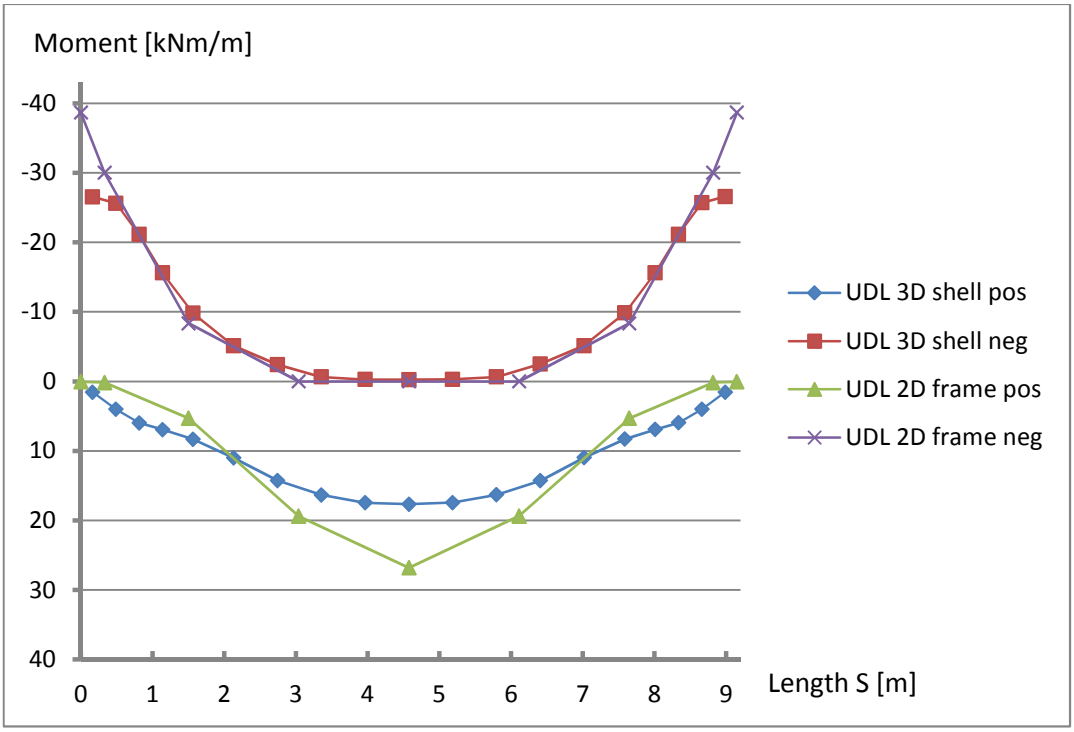


*Figure C.26 – Illustration of the bending moment distribution in the middle strip due to ULD traffic load*

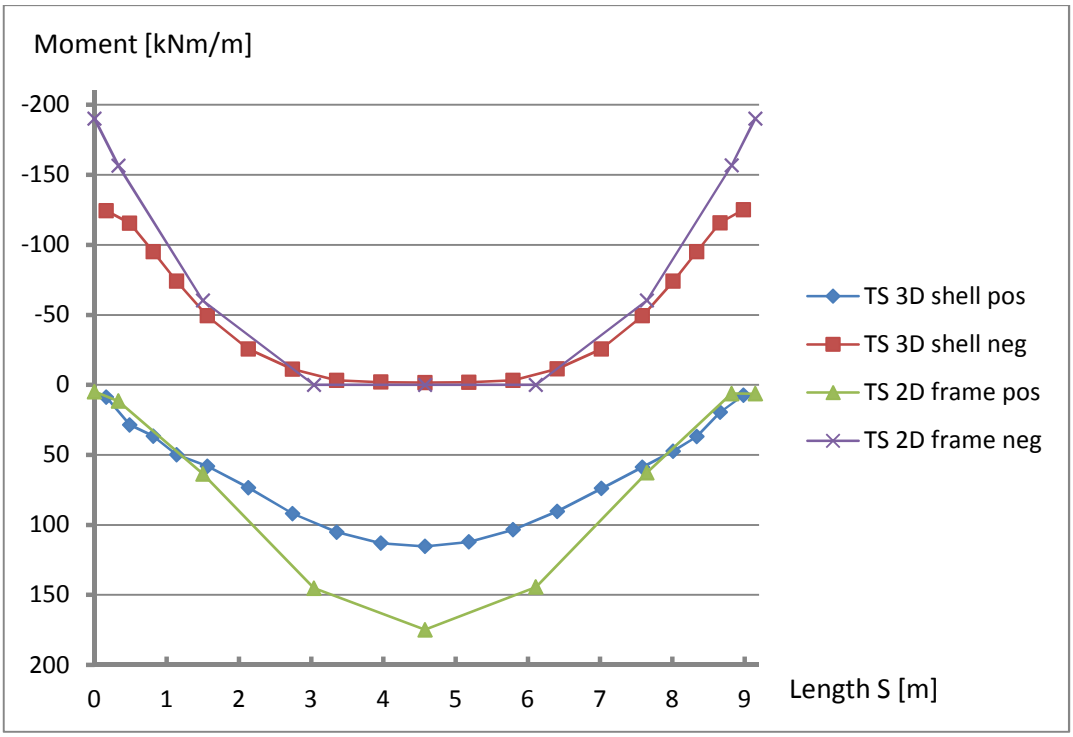


*Figure C.27 – Illustration of the bending moment distribution in the middle strip due to TS traffic load*

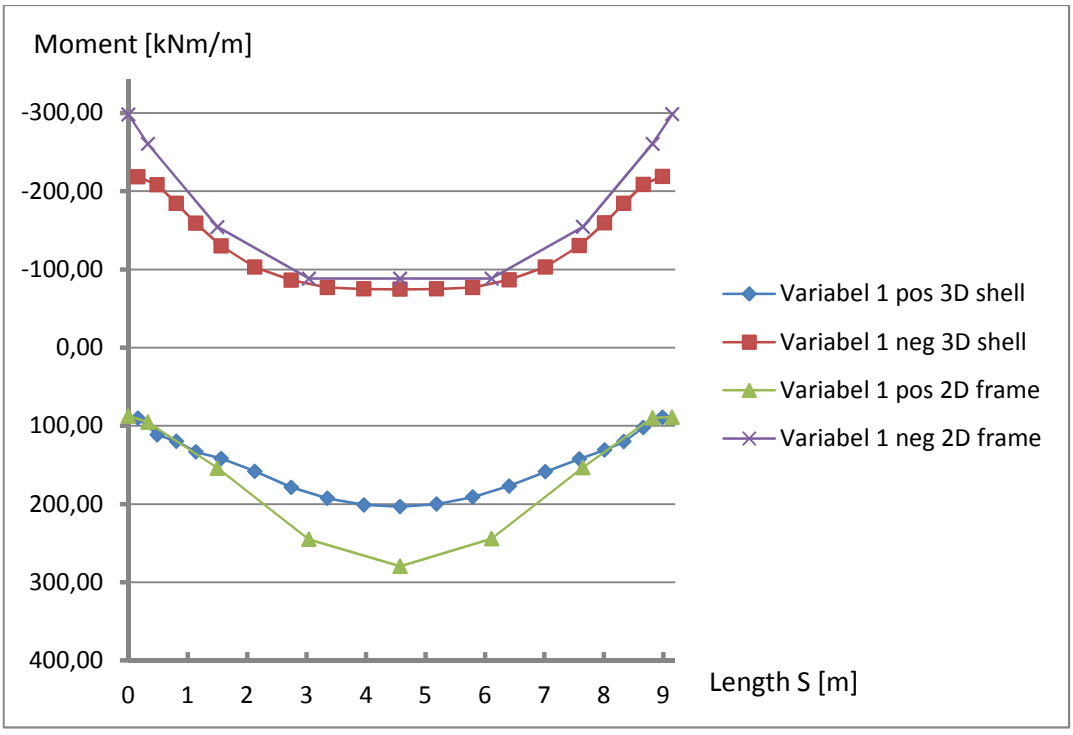


*Figure C.28 – Illustration of the bending moment distribution in the middle strip due to variable load 1*

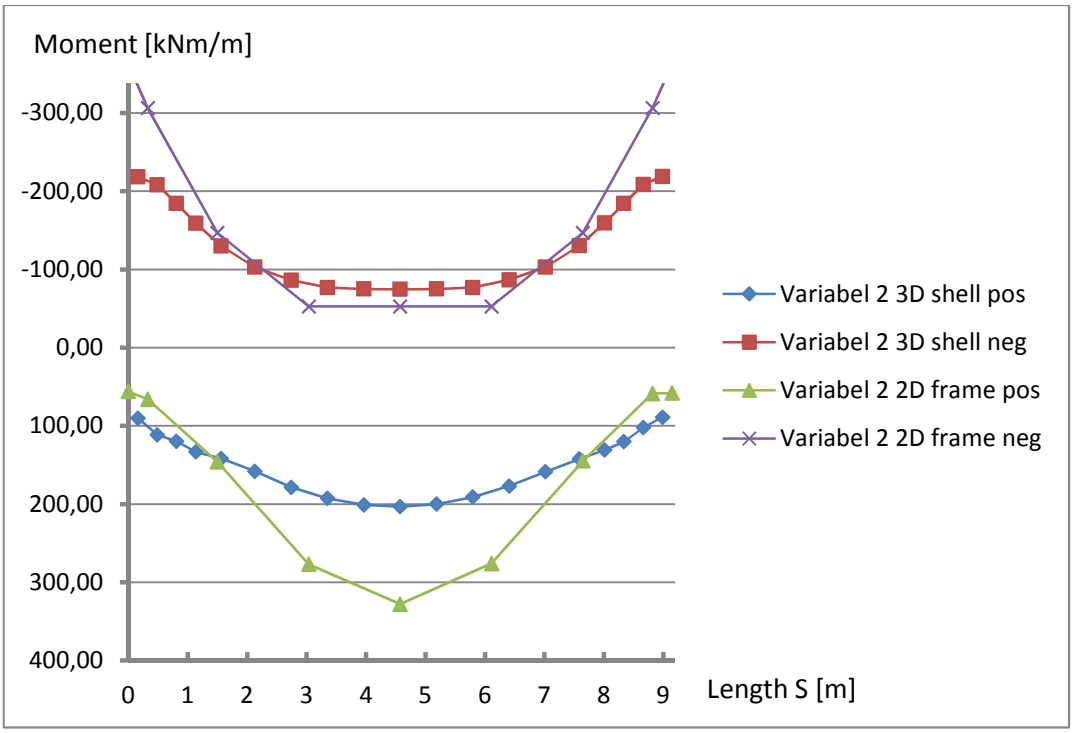


*Figure C.29 – Illustration of the bending moment distribution in the middle strip due to variable load 2*

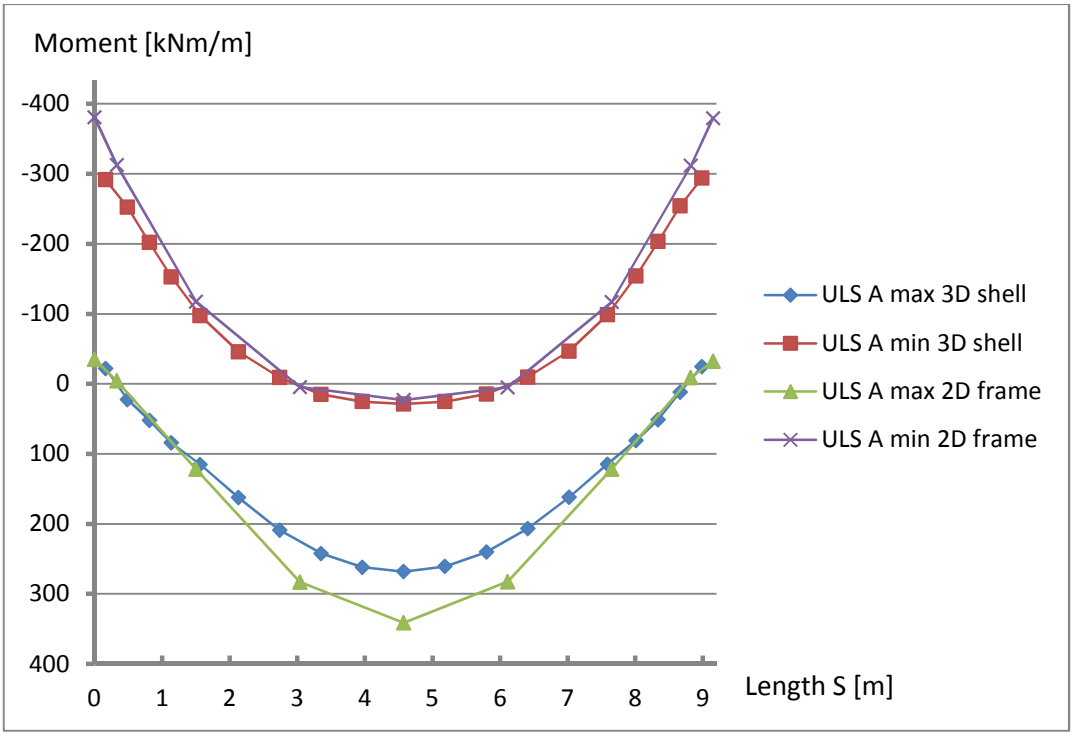


*Figure C.30 – Illustration of the bending moment distribution in the middle strip due to load combination ULS A*

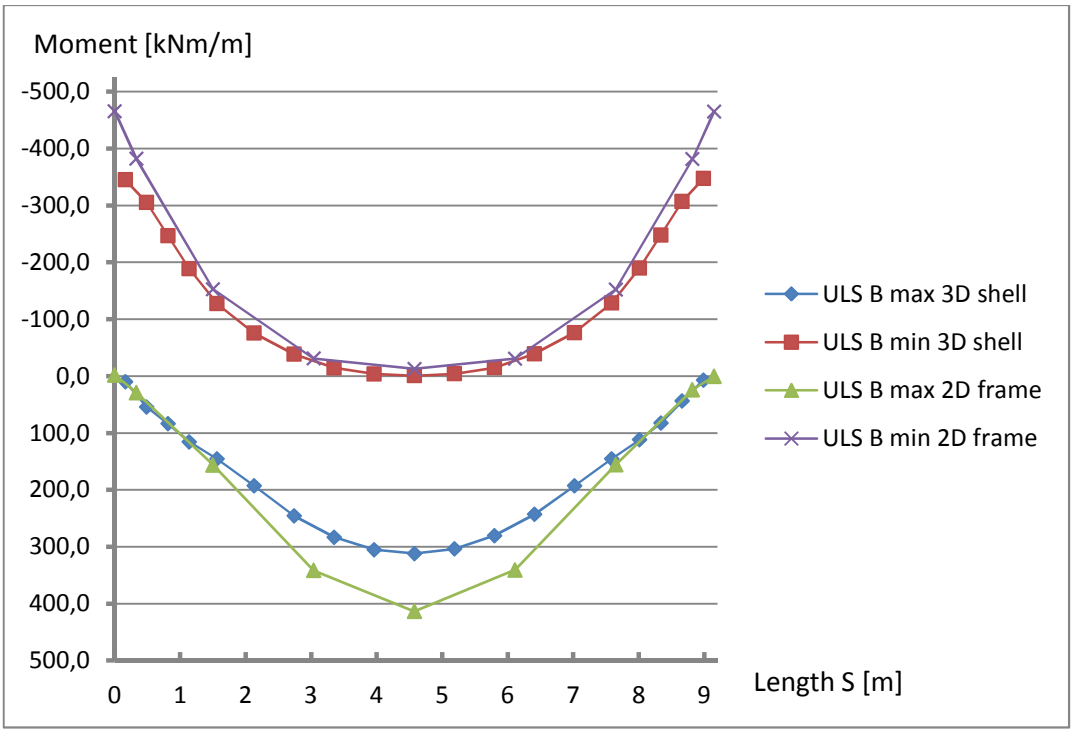


*Figure C.31 – Illustration of the bending moment distribution in the middle strip due to load combination ULS B*

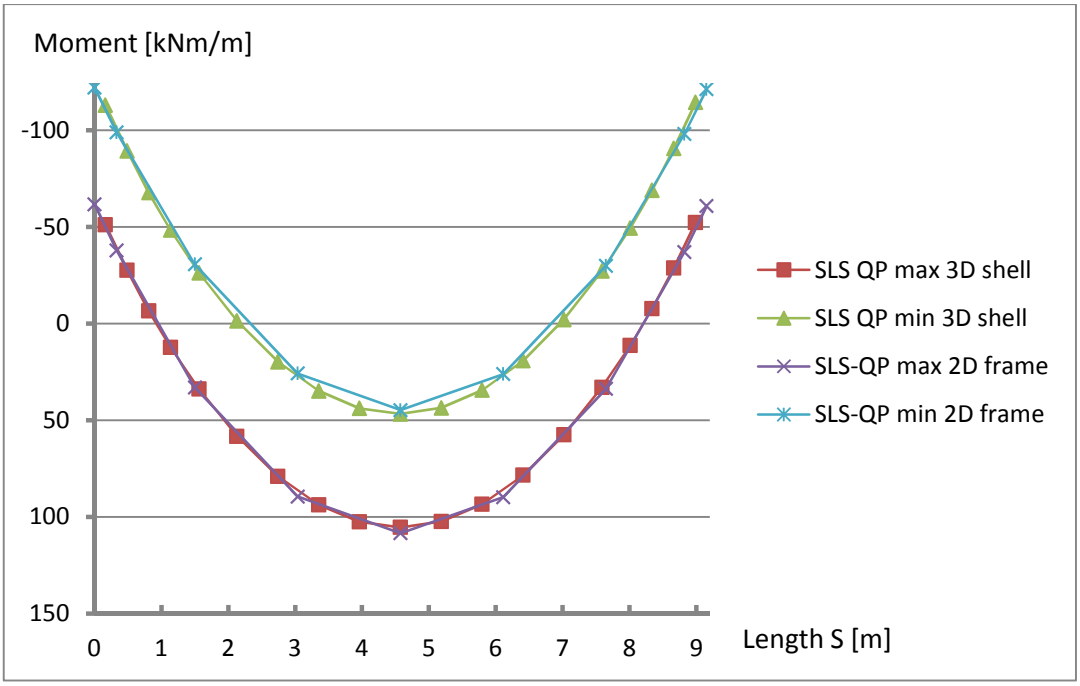


*Figure C.32 – Illustration of the bending moment distribution in the middle strip due to load combination SLS-Quasi permanent*

# End strip

| s [m] | Selfweight total [kNm/m] | | Earth pressure [kNm/m] | | Pavement [kNm/m] | |
|---|---|---|---|---|---|---|
| | max | min | pos | neg | pos | neg |
| 0.16 | 0 | -57.7215 | 0 | -2.85663 | 0 | -18.8063 |
| 0.49 | 0 | -44.8829 | 0 | -2.89282 | 0 | -15.1182 |
| 0.81 | 0 | -31.5753 | 0 | -2.62559 | 0 | -11.2883 |
| 1.14 | 0 | -18.091 | 0 | -2.45969 | 0 | -7.4365 |
| 1.56 | 8.12115 | -1.01209 | 0 | -2.38019 | 0 | -2.58415 |
| 2.13 | 27.8554 | 0 | 0 | -2.34519 | 5.29288 | 0 |
| 2.74 | 44.4335 | 0 | 0 | -2.33144 | 10.1397 | 0 |
| 3.35 | 55.5396 | 0 | 0 | -2.30838 | 13.4107 | 0 |
| 3.96 | 61.5201 | 0 | 0 | -2.28296 | 15.1993 | 0 |
| 4.58 | 62.5741 | 0 | 0 | -2.2562 | 15.5552 | 0 |
| 5.19 | 61.3717 | 0 | 0 | -2.28384 | 15.191 | 0 |
| 5.8 | 55.2078 | 0 | 0 | -2.31044 | 13.3924 | 0 |
| 6.41 | 43.9168 | 0 | 0 | -2.3347 | 10.1113 | 0 |
| 7.02 | 27.1552 | 0 | 0 | -2.34964 | 5.2546 | 0 |
| 7.59 | 7.25401 | -1.83836 | 0 | -2.3857 | 0 | -2.62891 |
| 8.01 | 0 | -19.0001 | 0 | -2.4659 | 0 | -7.48578 |
| 8.34 | 0 | -32.542 | 0 | -2.63219 | 0 | -11.3409 |
| 8.66 | 0 | -45.8983 | 0 | -2.89961 | 0 | -15.1736 |
| 8.99 | 0 | -58.7639 | 0 | -2.86322 | 0 | -18.8634 |

| s [m] | Shrinkage [kNm/m] | | TS [kNm/m] | | UDL [kNm/m] | |
|---|---|---|---|---|---|---|
| | pos | neg | max | min | max | min |
| 0.16 | 1.28079 | 0 | 29.7928 | -169.555 | 4.30563 | -34.0288 |
| 0.49 | 1.40214 | 0 | 41.6829 | -155.996 | 5.41202 | -30.2604 |
| 0.81 | 1.6945 | 0 | 55.1353 | -136.439 | 6.84273 | -25.5795 |
| 1.14 | 2.00154 | 0 | 68.2213 | -113.82 | 8.38641 | -20.403 |
| 1.56 | 2.24575 | 0 | 83.4882 | -82.3739 | 10.6864 | -14.1554 |
| 2.13 | 2.47295 | 0 | 105.81 | -47.9794 | 14.3201 | -7.98175 |
| 2.74 | 2.62791 | 0 | 129.871 | -24.1652 | 18.0959 | -3.82099 |
| 3.35 | 2.69025 | 0 | 145.838 | -10.869 | 20.8041 | -1.39715 |
| 3.96 | 2.69521 | 0 | 154.759 | -5.66818 | 22.0348 | -0.71798 |
| 4.58 | 2.65952 | 0 | 158.496 | -2.55113 | 22.112 | -0.599 |
| 5.19 | 2.68916 | 0 | 154.328 | -5.90241 | 22.051 | -0.75363 |
| 5.8 | 2.69248 | 0 | 148.304 | -10.8429 | 20.8558 | -1.41612 |
| 6.41 | 2.64075 | 0 | 133.3 | -24.2731 | 18.1601 | -3.80952 |
| 7.02 | 2.50043 | 0 | 109.464 | -47.4942 | 14.3754 | -7.94144 |
| 7.59 | 2.29109 | 0 | 87.7622 | -81.9914 | 10.7146 | -14.0651 |
| 8.01 | 2.06383 | 0 | 65.0702 | -113.064 | 8.39846 | -20.2683 |
| 8.34 | 1.77464 | 0 | 57.8358 | -134.972 | 6.8246 | -25.4037 |
| 8.66 | 1.49305 | 0 | 33.203 | -154.905 | 5.36328 | -30.0445 |
| 8.99 | 1.39064 | 0 | 25.9527 | -167.926 | 4.10258 | -33.7798 |

| s [m] | EXP [kNm/m] | | CON [kNm/m] | | Temp differance [kNm/m] | |
|---|---|---|---|---|---|---|
| | pos | neg | pos | neg | max | min |
| 0.16 | 11.72 | -8.85559 | 10.3824 | -13.7363 | 22.10 | -22.59 |
| 0.49 | 4.36 | -22.571 | 26.4625 | -5.11098 | 30.82 | -27.68 |
| 0.81 | 0.00 | -21.5035 | 25.211 | 0 | 25.21 | -21.50 |
| 1.14 | 0.00 | -20.8845 | 24.4852 | 0 | 24.49 | -20.88 |
| 1.56 | 0.00 | -21.8651 | 25.6349 | 0 | 25.63 | -21.87 |
| 2.13 | 0.00 | -23.7043 | 27.7912 | 0 | 27.79 | -23.70 |
| 2.74 | 0.00 | -24.8465 | 29.1304 | 0 | 29.13 | -24.85 |
| 3.35 | 0.00 | -24.862 | 29.1486 | 0 | 29.15 | -24.86 |
| 3.96 | 0.00 | -24.3144 | 28.5066 | 0 | 28.51 | -24.31 |
| 4.58 | 0.00 | -23.4251 | 27.4639 | 0 | 27.46 | -23.43 |
| 5.19 | 0.00 | -24.3152 | 28.5074 | 0 | 28.51 | -24.32 |
| 5.8 | 0.00 | -24.8365 | 29.1187 | 0 | 29.12 | -24.84 |
| 6.41 | 0.00 | -24.7914 | 29.0658 | 0 | 29.07 | -24.79 |
| 7.02 | 0.00 | -23.6145 | 27.686 | 0 | 27.69 | -23.61 |
| 7.59 | 0.00 | -21.7397 | 25.4879 | 0 | 25.49 | -21.74 |
| 8.01 | 0.00 | -20.7314 | 24.3057 | 0 | 24.31 | -20.73 |
| 8.34 | 0.00 | -21.328 | 25.0052 | 0 | 25.01 | -21.33 |
| 8.66 | 4.54 | -22.3717 | 26.2289 | -5.32521 | 30.77 | -27.70 |
| 8.99 | 11.909 | -8.64551 | 10.1361 | -13.9623 | 22.0451 | -22.6078 |

| s [m] | Heat [kNm/m] | | Cool [kNm/m] | | Temp gradient [kNm/m] | |
|---|---|---|---|---|---|---|
| | pos | neg | pos | neg | max | min |
| 0.16 | 15.9732 | -13.9467 | 14.8753 | -17.0367 | 30.85 | -30.98 |
| 0.49 | 34.305 | -5.21977 | 5.56729 | -36.589 | 39.87 | -41.81 |
| 0.81 | 31.2999 | 0 | 0 | -33.3838 | 31.30 | -33.38 |
| 1.14 | 29.2398 | 0 | 0 | -31.1866 | 29.24 | -31.19 |
| 1.56 | 29.6853 | 0 | 0 | -31.6617 | 29.69 | -31.66 |
| 2.13 | 31.5412 | 0 | 0 | -33.6412 | 31.54 | -33.64 |
| 2.74 | 32.6536 | 0 | 0 | -34.8277 | 32.65 | -34.83 |
| 3.35 | 32.3348 | 0 | 0 | -34.4877 | 32.33 | -34.49 |
| 3.96 | 31.3519 | 0 | 0 | -33.4393 | 31.35 | -33.44 |
| 4.58 | 29.9683 | 0 | 0 | -31.9636 | 29.97 | -31.96 |
| 5.19 | 31.3508 | 0 | 0 | -33.4381 | 31.35 | -33.44 |
| 5.8 | 32.3333 | 0 | 0 | -34.486 | 32.33 | -34.49 |
| 6.41 | 32.6518 | 0 | 0 | -34.8257 | 32.65 | -34.83 |
| 7.02 | 31.5394 | 0 | 0 | -33.6392 | 31.54 | -33.64 |
| 7.59 | 29.6837 | 0 | 0 | -31.66 | 29.68 | -31.66 |
| 8.01 | 29.2386 | 0 | 0 | -31.1853 | 29.24 | -31.19 |
| 8.34 | 31.2994 | 0 | 0 | -33.3833 | 31.30 | -33.38 |
| 8.66 | 34.3058 | -5.21935 | 5.56685 | -36.5899 | 39.87 | -41.81 |
| 8.99 | 15.9752 | -13.9453 | 14.8737 | -17.0389 | 30.8489 | -30.9842 |

| s [m] | Variabel 1 [kNm/m] | | Variabel 2 [kNm/m] | |
|---|---|---|---|---|
| | max | min | max | min |
| 0.16 | 105.29 | -265.06 | 90.13155 | -322.842 |
| 0.49 | 142.34 | -270.96 | 122.4892 | -312.154 |
| 0.81 | 137.42 | -228.43 | 131.2488 | -266.973 |
| 1.14 | 147.80 | -198.66 | 149.0071 | -226.584 |
| 1.56 | 166.82 | -165.14 | 174.3818 | -176.137 |
| 2.13 | 197.09 | -131.89 | 213.2308 | -123.69 |
| 2.74 | 227.07 | -108.50 | 253.3775 | -87.2739 |
| 3.35 | 244.43 | -93.16 | 278.7161 | -65.4714 |
| 3.96 | 251.98 | -85.30 | 291.2915 | -56.1071 |
| 4.58 | 252.51 | -78.81 | 294.5274 | -49.7344 |
| 5.19 | 251.55 | -85.56 | 290.723 | -56.4765 |
| 5.8 | 246.93 | -93.11 | 282.1396 | -65.4393 |
| 6.41 | 230.51 | -108.53 | 258.1088 | -87.3592 |
| 7.02 | 200.70 | -131.25 | 218.2248 | -122.895 |
| 7.59 | 171.00 | -164.52 | 180.1539 | -175.385 |
| 8.01 | 144.35 | -197.60 | 144.5584 | -225.237 |
| 8.34 | 139.88 | -226.60 | 134.7545 | -264.578 |
| 8.66 | 133.60 | -269.75 | 110.7636 | -310.376 |

| s [m] | ULS A [kNm/m] | | ULS B [kNm/m] | | SLS-QP [kNm/m] | |
|---|---|---|---|---|---|---|
| | max | min | max | min | max | min |
| 0.16 | 13.08363 | -317.764 | 42.0 | -395.9 | -48.7734 | -105.458 |
| 0.49 | 57.1125 | -293.479 | 95.8 | -366.2 | -23.2519 | -96.9161 |
| 0.81 | 77.54862 | -236.666 | 108.4 | -301.2 | -12.9137 | -72.2764 |
| 1.14 | 110.55 | -181.759 | 141.0 | -237.1 | 3.33654 | -53.4078 |
| 1.56 | 144.4434 | -131.201 | 181.0 | -171.3 | 34.43076 | -24.0236 |
| 2.13 | 206.5589 | -67.6055 | 250.3 | -99.1 | 65.28743 | 2.716638 |
| 2.74 | 262.3267 | -21.8272 | 314.5 | -54.6 | 88.09311 | 22.98752 |
| 3.35 | 298.0322 | 7.469534 | 356.0 | -25.2 | 102.3823 | 37.54417 |
| 3.96 | 316.2782 | 22.07725 | 377.2 | -9.7 | 109.3439 | 46.13033 |
| 4.58 | 319.9026 | 28.62676 | 382.0 | -1.8 | 109.5049 | 48.7428 |
| 5.19 | 315.6452 | 21.65626 | 376.5 | -10.1 | 109.181 | 45.97317 |
| 5.8 | 300.1181 | 7.159926 | 359.0 | -25.5 | 102.0187 | 37.20612 |
| 6.41 | 265.1438 | -22.4168 | 318.7 | -55.2 | 87.52765 | 22.46853 |
| 7.02 | 207.5067 | -69.986 | 252.7 | -101.2 | 64.52293 | 2.02072 |
| 7.59 | 128.6398 | -154.915 | 166.8 | -192.1 | 32.66363 | -25.7024 |
| 8.01 | 75.69049 | -219.579 | 105.1 | -270.1 | 2.3501 | -54.2937 |
| 8.34 | 52.36133 | -269.129 | 83.1 | -329.1 | -13.956 | -73.2127 |
| 8.66 | 21.26134 | -325.693 | 59.9 | -394.0 | -24.257 | -97.9997 |

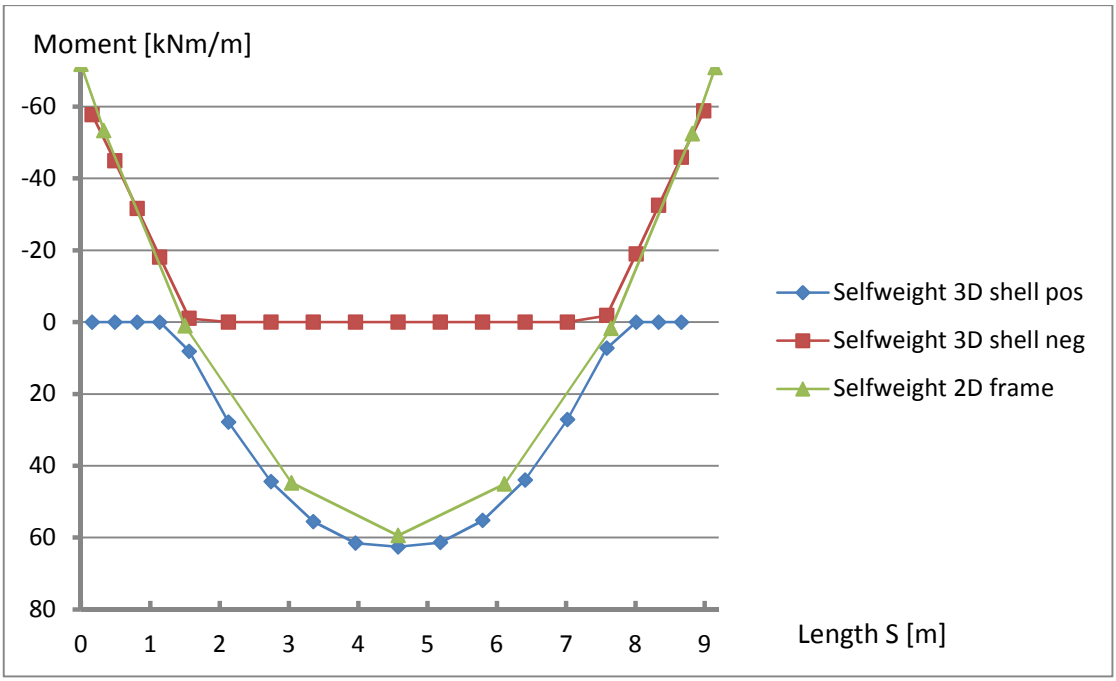


*Figure C.33 – Illustration of the bending moment distribution in the end strip due to self weight*

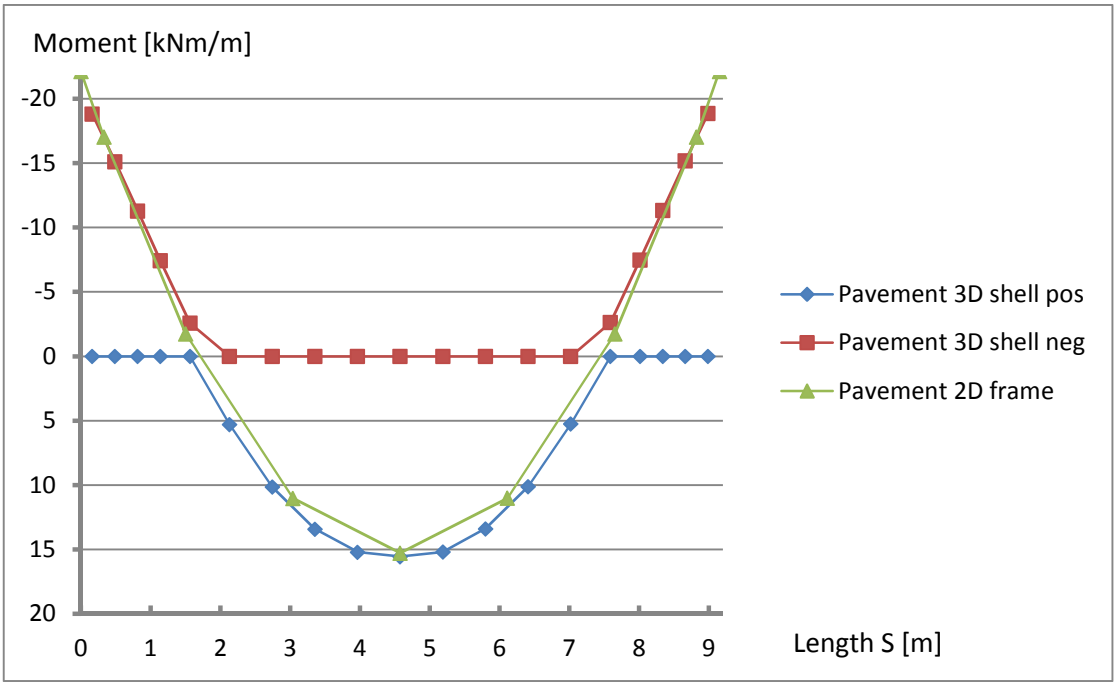


*Figure C.34 – Illustration of the bending moment distribution in the end strip due to pavement*

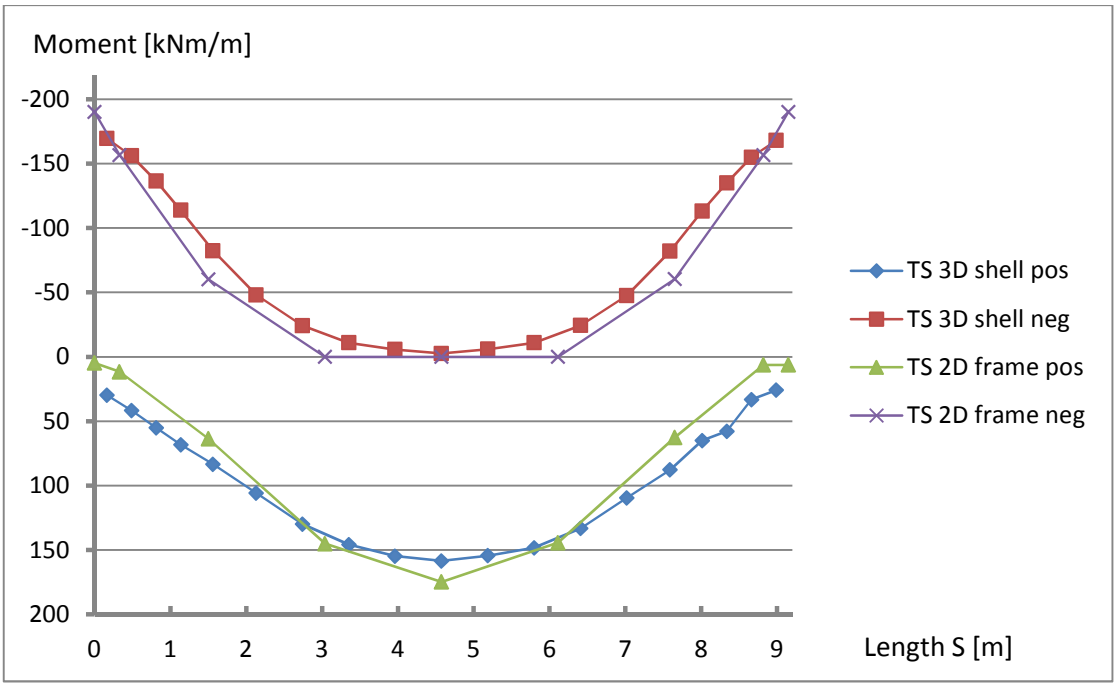


*Figure C.35 – Illustration of the bending moment distribution in the end strip due to TS traffic load*

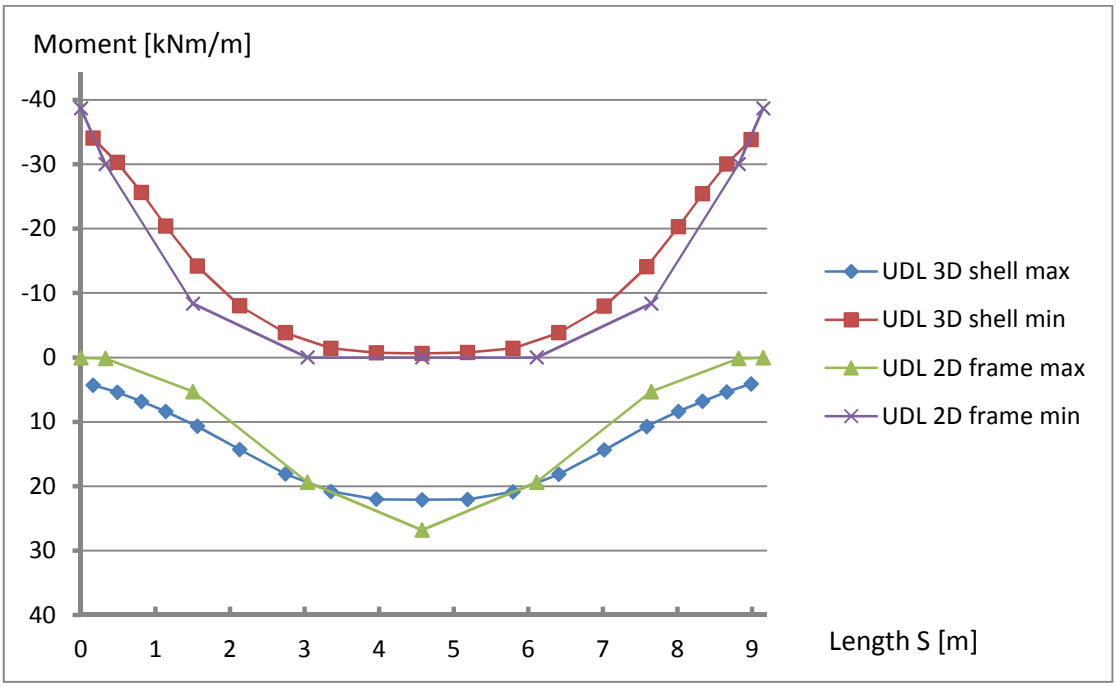


*Figure C.36 – Illustration of the bending moment distribution in the end strip due to UDL traffic load*

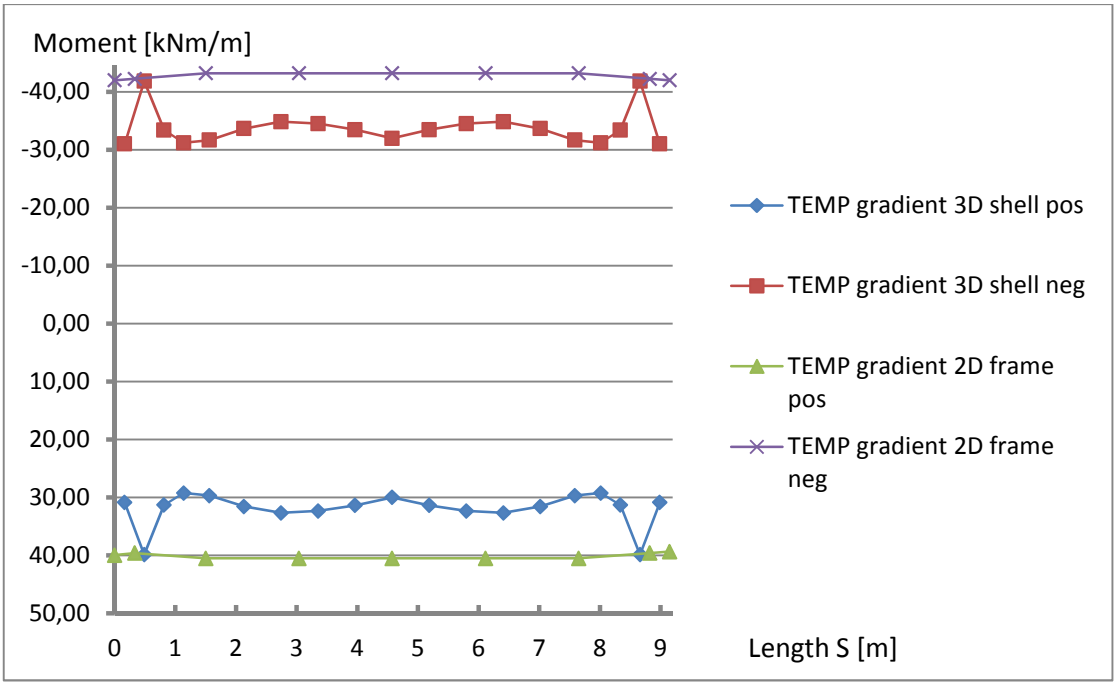


*Figure C.37 – Illustration of the bending moment distribution in the end strip due to temperature gradient*

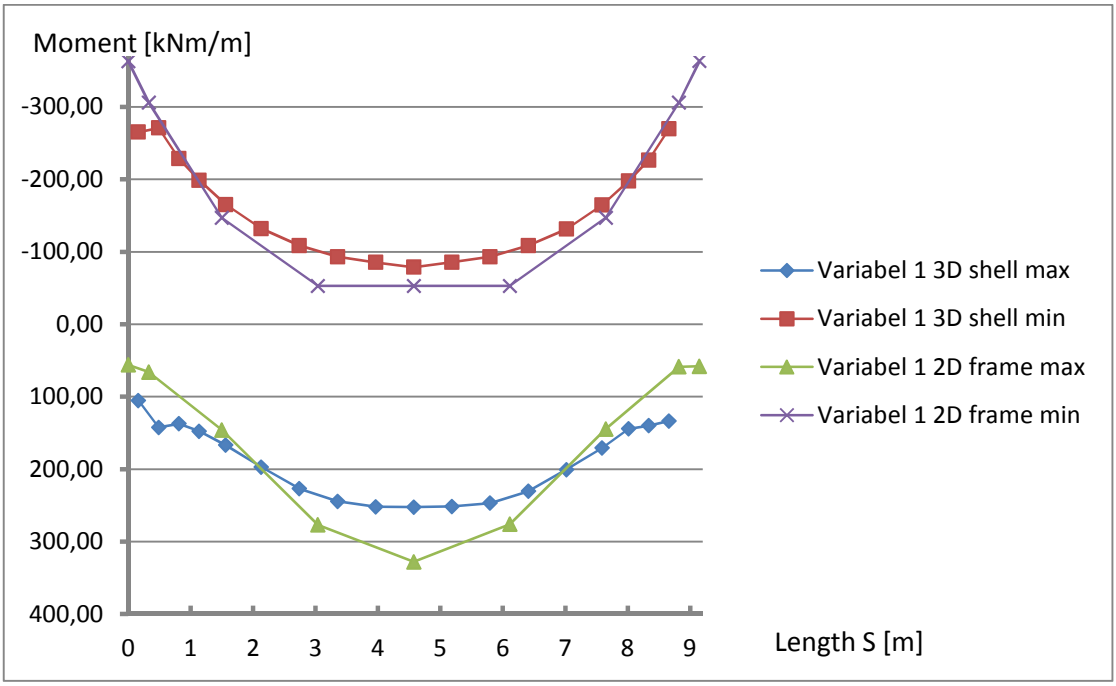


*Figure C.38 – Illustration of the bending moment distribution in the end strip due to variable load 1*

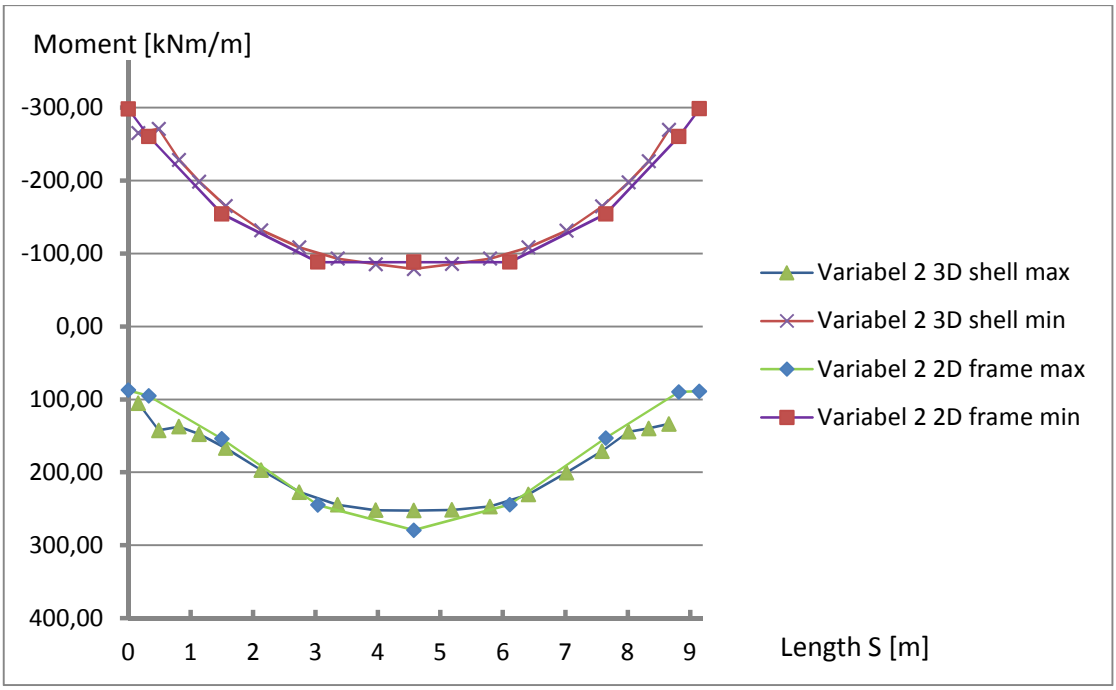


*Figure C.39 – Illustration of the bending moment distribution in the end strip due to variable load 2*

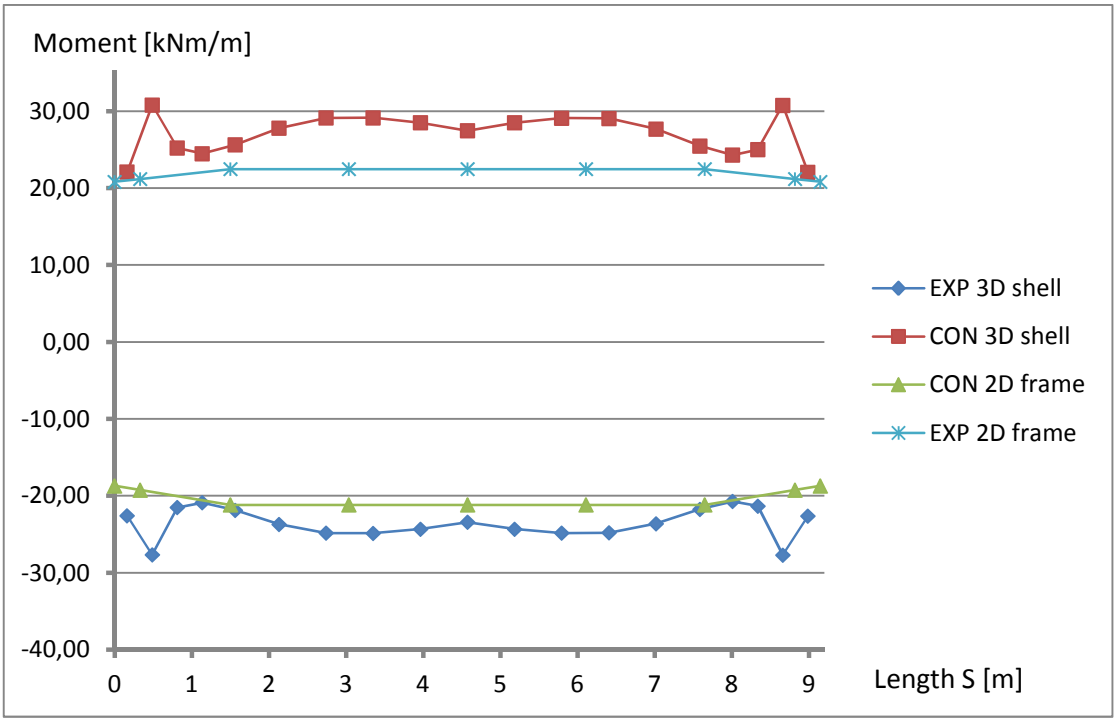


*Figure C.40 – Illustration of the bending moment distribution in the end strip due to temperature difference*

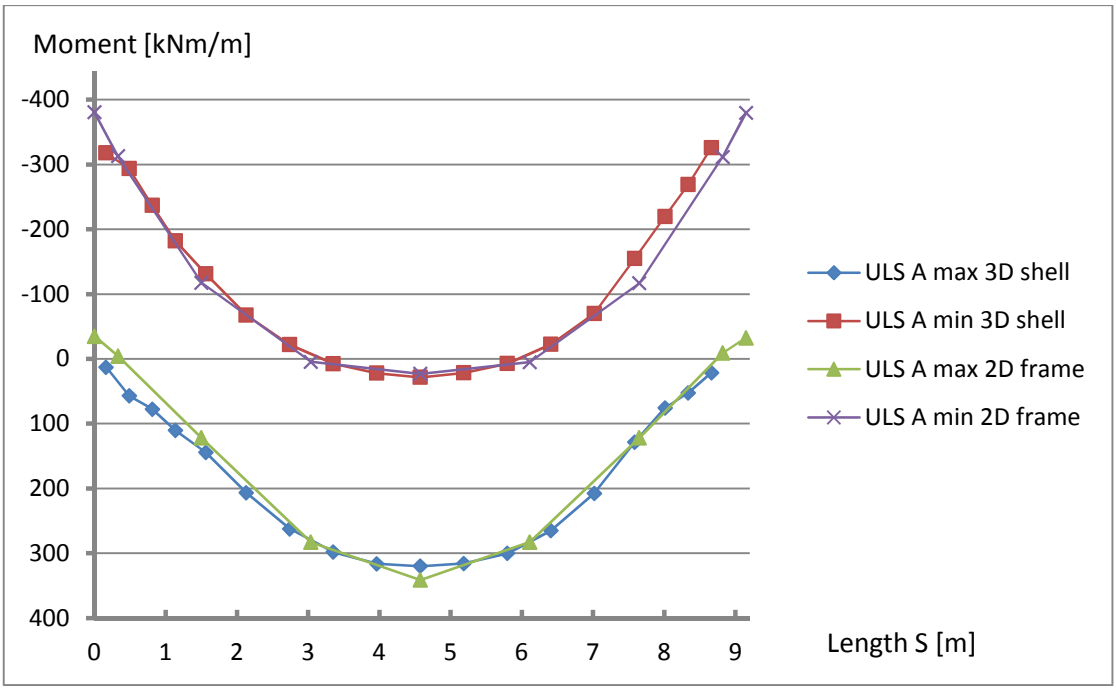


*Figure C.41 – Illustration of the bending moment distribution in the end strip due to load combination ULS A*

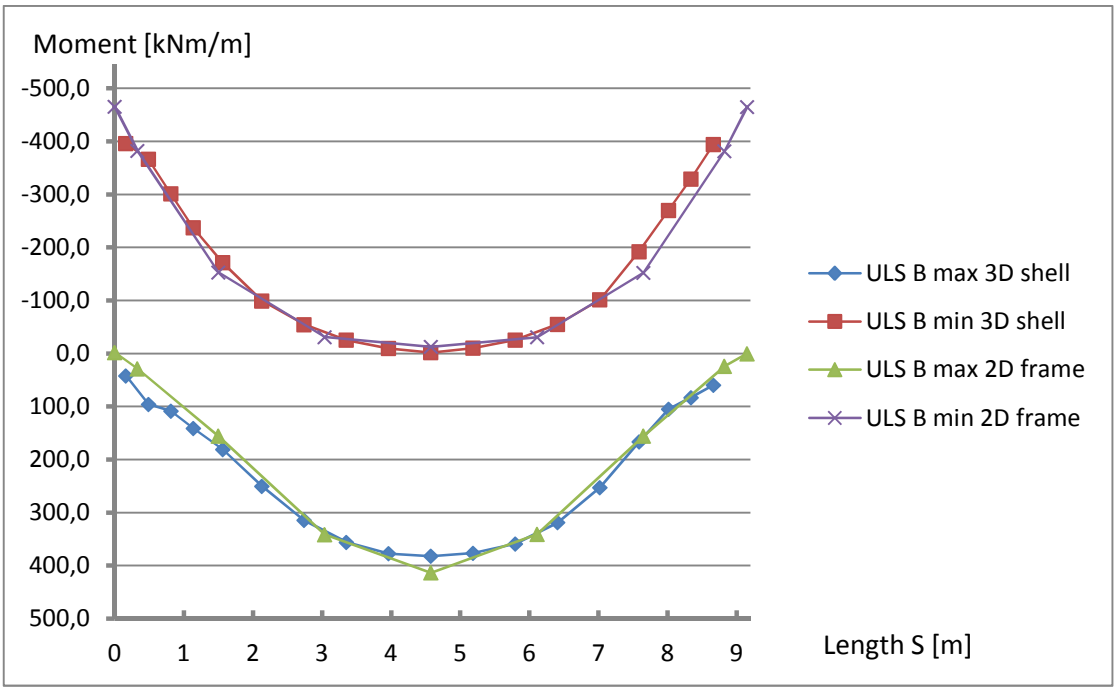


*Figure C.42 – Illustration of the bending moment distribution in the end strip due to load combination ULS B*

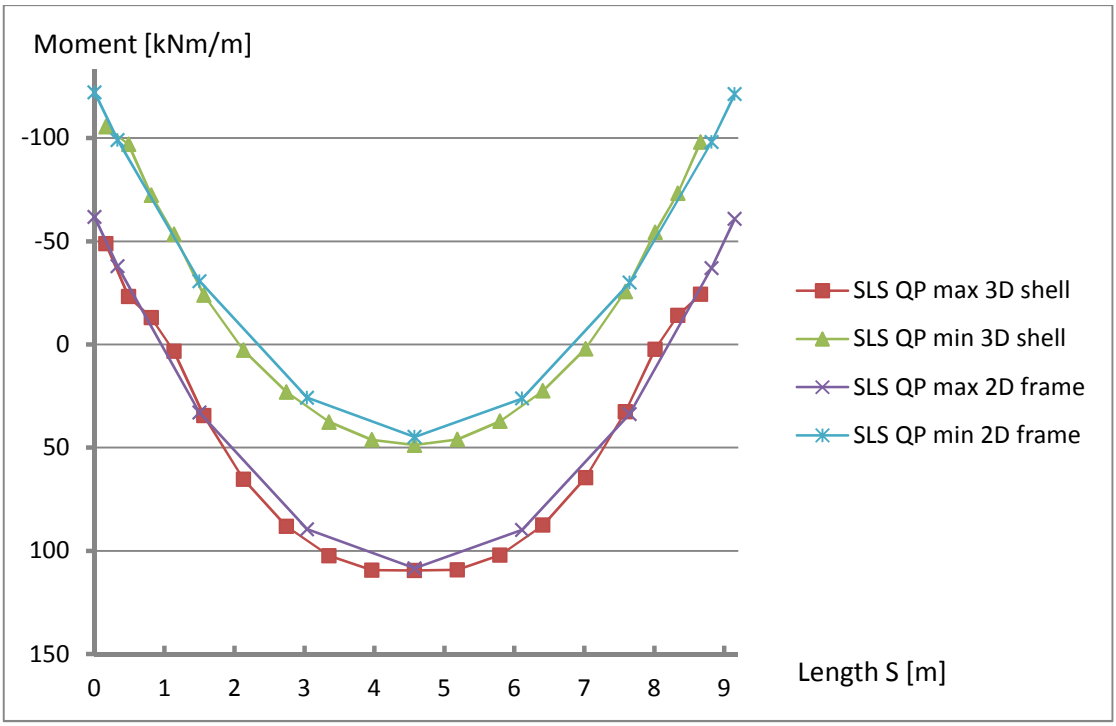


*Figure C.43 – Illustration of the bending moment distribution in the end strip due to load combination SLS-Quasi permanent*

# 2D frame analysis of slab bridge

| s | Selfweight total | Pavement | UDL | | Support disp | |
|---|---|---|---|---|---|---|
| [m] | [kNm/m] | [kNm/m] | [kNm/m] | | [kNm/m] | |
| | | | max | min | max | min |
| 0 | 0 | 0 | 0 | 0 | 0 | 0 |
| 0.95 | -13.03 | -1.62 | 0 | -2.84 | 0 | 0 |
| 1.9 | -52.12 | -6.5 | 0 | -11.37 | 0 | 0 |
| 1.9 | -52.12 | -6.5 | 0 | -11.37 | 0 | 0 |
| 3.54 | 107.48 | 13.4 | 67 | -33.82 | 13.45 | -13.45 |
| 5.18 | 189.42 | 23.62 | 117.06 | -67.65 | 26.89 | -26.89 |
| 6.82 | 193.69 | 24.15 | 150.17 | -101.47 | 40.34 | -40.34 |
| 8.46 | 120.3 | 15 | 166.33 | -135.29 | 53.78 | -53.78 |
| 10.1 | -30.75 | -3.83 | 165.54 | -169.11 | 67.23 | -67.23 |
| 11.74 | -259.46 | -32.35 | 147.81 | -202.93 | 80.67 | -80.67 |
| 13.38 | -565.83 | -70.55 | 113.13 | -236.76 | 94.12 | -94.12 |
| 15.02 | -949.87 | -118.43 | 61.51 | -270.58 | 107.56 | -107.56 |
| 16.66 | -1411.57 | -175.99 | 13.89 | -311.41 | 121.01 | -121.01 |
| 18.3 | -1950.93 | -243.23 | 3.88 | -430.67 | 134.46 | -134.46 |
| 18.3 | -1950.93 | -243.23 | 3.88 | -430.67 | 134.46 | -134.46 |
| 20.81 | -942.43 | -117.5 | 13.32 | -209.39 | 121.01 | -121.01 |
| 23.32 | -115.84 | -14.44 | 67.07 | -73.96 | 107.56 | -107.56 |
| 25.83 | 528.83 | 65.93 | 179.76 | -64.71 | 94.12 | -94.12 |
| 28.34 | 991.58 | 123.63 | 273.18 | -55.47 | 80.67 | -80.67 |
| 30.85 | 1272.42 | 158.64 | 326.91 | -46.22 | 67.23 | -67.23 |
| 33.36 | 1371.34 | 170.97 | 340.93 | -36.98 | 53.78 | -53.78 |
| 35.87 | 1288.35 | 160.63 | 315.25 | -27.73 | 40.34 | -40.34 |
| 38.38 | 1023.45 | 127.6 | 249.87 | -18.49 | 26.89 | -26.89 |
| 40.89 | 576.62 | 71.89 | 144.78 | -9.85 | 13.45 | -13.45 |
| 43.4 | -52.12 | -6.5 | 0 | -11.37 | 0 | 0 |
| 43.4 | -52.11 | -6.5 | 0 | -11.37 | 0 | 0 |
| 44.4 | -13.03 | -1.62 | 0 | -2.84 | 0 | 0 |
| 45.4 | 0 | 0 | 0 | 0 | 0 | 0 |

| s | Temp gradient | | TS | | Variabel 1 | |
|---|---|---|---|---|---|---|
| [m] | [kNm/m] | | [kNm/m] | | [kNm/m] | |
| | max | min | max | min | max | min |
| 0 | 0 | 0 | 0 | 0 | 0 | 0 |
| 0.95 | 0 | 0 | 0 | -85.5 | 0 | -132.51 |
| 1.9 | 0 | 0 | 0 | -224.1 | 0 | -353.21 |
| 1.9 | 0 | 0 | 0 | -224.1 | 0 | -353.21 |
| 3.54 | 40.95 | -43.67 | 243.73 | -196.81 | 488.21 | -369.53 |
| 5.18 | 81.89 | -87.34 | 416.45 | -169.51 | 844.48 | -402.9 |
| 6.82 | 122.84 | -131.01 | 524.09 | -178.19 | 1077.71 | -490.23 |
| 8.46 | 163.78 | -174.69 | 570.6 | -237.58 | 1193.84 | -653.64 |
| 10.1 | 204.73 | -218.36 | 563.32 | -296.98 | 1203.85 | -817.05 |
| 11.74 | 245.67 | -262.03 | 511.6 | -356.38 | 1121.77 | -980.46 |
| 13.38 | 286.62 | -305.7 | 416.25 | -415.77 | 948.84 | -1143.87 |
| 15.02 | 327.56 | -349.37 | 286.62 | -475.17 | 699.08 | -1307.28 |
| 16.66 | 368.51 | -393.04 | 134 | -534.56 | 420.83 | -1481.21 |
| 18.3 | 409.46 | -436.72 | 72.72 | -593.96 | 336.01 | -1772.78 |
| 18.3 | 409.46 | -436.72 | 72.72 | -593.96 | 336.01 | -1772.78 |
| 20.81 | 368.51 | -393.04 | 124.84 | -297.78 | 406.23 | -973 |
| 23.32 | 327.56 | -349.37 | 323.89 | -198.5 | 763.33 | -597.35 |
| 25.83 | 286.62 | -305.7 | 520.32 | -173.69 | 1204.89 | -522.68 |
| 28.34 | 245.67 | -262.03 | 683.57 | -148.87 | 1567.8 | -448.01 |
| 30.85 | 204.73 | -218.36 | 789.88 | -124.06 | 1785.73 | -373.34 |
| 33.36 | 163.78 | -174.69 | 822.97 | -99.25 | 1834.29 | -298.67 |
| 35.87 | 122.84 | -131.01 | 775.75 | -126.86 | 1702.82 | -302.65 |
| 38.38 | 81.89 | -87.34 | 630.32 | -155.38 | 1364.5 | -307.96 |
| 40.89 | 40.94 | -43.67 | 374.33 | -183.89 | 800.78 | -314.18 |
| 43.4 | 0 | 0 | 0 | -212.4 | 0 | -335.66 |
| 43.4 | 0 | 0 | 0 | -212.4 | 0 | -335.66 |
| 44.4 | 0 | 0 | 0 | -79.65 | 0 | -123.74 |
| 45.4 | 0 | 0 | 0 | 0 | 0 | 0 |

| s | Variabel 2 | | ULS A | | ULS B | |
|---|---|---|---|---|---|---|
| [m] | [kNm/m] | | [kNm/m] | | [kNm/m] | |
| | max | min | max | min | max | min |
| 0 | 0 | 0 | 0 | 0 | 0 | 0 |
| 0.95 | 0 | -98.32 | -14.49 | -116.8 | -14.49 | -150.29 |
| 1.9 | 0 | -260.06 | -57.97 | -333.96 | -57.97 | -424.33 |
| 1.9 | 0 | -260.06 | -57.97 | -333.96 | -57.97 | -424.33 |
| 3.54 | 352.47 | -281.99 | 475.48 | -137.34 | 643.75 | -258.86 |
| 5.18 | 614.52 | -310.74 | 830.48 | -49.85 | 1120.7 | -209.98 |
| 6.82 | 792.87 | -380.15 | 991.65 | -89.39 | 1368.64 | -301.43 |
| 8.46 | 891.98 | -506.86 | 963.46 | -272.61 | 1393.5 | -555.34 |
| 10.1 | 920.13 | -633.58 | 767.21 | -555.24 | 1214.02 | -903.38 |
| 11.74 | 887.9 | -760.29 | 484.31 | -1008.09 | 886.45 | -1387.76 |
| 13.38 | 796.2 | -887.01 | 64.72 | -1580.21 | 381.64 | -1978.11 |
| 15.02 | 655.6 | -1013.72 | -481 | -2271.6 | -286.38 | -2674.44 |
| 16.66 | 491.41 | -1144.65 | -1138.84 | -3082.69 | -998.68 | -3487.26 |
| 18.3 | 453.01 | -1322.62 | -1777.58 | -4017.75 | -1628.08 | -4523.7 |
| 18.3 | 453.01 | -1322.62 | -1777.58 | -4017.75 | -1628.08 | -4523.7 |
| 20.81 | 480.72 | -815.86 | -627.45 | -2088.51 | -487.59 | -2338.87 |
| 23.32 | 701.05 | -583.12 | 489.06 | -666.3 | 705.48 | -826.42 |
| 25.83 | 953.77 | -510.23 | 1627.79 | 160.82 | 1988.63 | 3.37 |
| 28.34 | 1157.45 | -437.34 | 2497.57 | 736.55 | 2974.13 | 601.59 |
| 30.85 | 1272.96 | -364.45 | 3021.24 | 1109.95 | 3566.41 | 997.48 |
| 33.36 | 1281.92 | -291.56 | 3180.42 | 1281.02 | 3741.09 | 1191.05 |
| 35.87 | 1176.3 | -277.91 | 2967.07 | 1190.52 | 3487.49 | 1103.65 |
| 38.38 | 935.88 | -265.28 | 2360.99 | 896.69 | 2778.81 | 812.57 |
| 40.89 | 546.71 | -253.01 | 1348.22 | 400.48 | 1596.5 | 318.27 |
| 43.4 | 0 | -246.84 | -57.96 | -320.73 | -57.96 | -406.77 |
| 43.4 | 0 | -246.84 | -57.96 | -320.73 | -57.96 | -406.77 |
| 44.4 | 0 | -91.71 | -14.49 | -110.18 | -14.49 | -141.52 |
| 45.4 | 0 | 0 | 0 | 0 | 0 | 0 |

# 2D frame analysis of frame slab bridge

| s | Selfweight total | Pavement | Shrinkage | UDL | |
|---|---|---|---|---|---|
| [m] | [kNm/m] | [kNm/m] | [kNm/m] | [kNm/m] | |
| | | | | max | min |
| 0 | -71.77 | -22.12 | 2.07 | 0.05 | -38.67 |
| 0.3294 | -53.37 | -17.02 | 2.11 | 0.16 | -30 |
| 1.5006 | 1.03 | -1.74 | 2.24 | 5.3 | -8.36 |
| 3.0378 | 44.73 | 11.03 | 2.24 | 19.38 | 0 |
| 4.575 | 59.41 | 15.28 | 2.24 | 26.81 | 0 |
| 6.1122 | 45.06 | 11.02 | 2.24 | 19.37 | 0 |
| 7.6494 | 1.72 | -1.74 | 2.24 | 5.3 | -8.36 |
| 8.8206 | -52.47 | -17.02 | 2.11 | 0.16 | -30 |
| 9.15 | -70.88 | -22.12 | 2.07 | 0.05 | -38.67 |

| s | Temp differance | | Temp gradient | | TS | |
|---|---|---|---|---|---|---|
| [m] | [kNm/m] | | [kNm/m] | | [kNm/m] | |
| | max | min | max | min | max | min |
| 0 | 60.18 | -60.68 | 39.95 | -41.97 | 4.76 | -190.04 |
| 0.3294 | 60.79 | -61.48 | 39.6 | -42.24 | 11.58 | -156.63 |
| 1.5006 | 62.98 | -64.38 | 40.51 | -43.2 | 63.5 | -60.22 |
| 3.0378 | 62.98 | -64.38 | 40.51 | -43.2 | 145.09 | 0 |
| 4.575 | 62.98 | -64.38 | 40.51 | -43.2 | 174.82 | 0 |
| 6.1122 | 62.98 | -64.38 | 40.51 | -43.2 | 144.37 | 0 |
| 7.6494 | 62.98 | -64.38 | 40.51 | -43.2 | 62.63 | -60.32 |
| 8.8206 | 60.78 | -61.48 | 39.6 | -42.24 | 6.21 | -156.64 |
| 9.15 | 60.18 | -60.68 | 39.35 | -41.97 | 6.23 | -190.21 |

| s | Variabel 1 | | Variabel 2 | | ULS A | |
|---|---|---|---|---|---|---|
| [m] | [kNm/m] | | [kNm/m] | | [kNm/m] | |
| | max | min | max | min | max | min |
| 0 | 55.93 | -363.09 | 87.32 | -298.24 | -34.91 | -380.47 |
| 0.3294 | 65.93 | -306.1 | 95.18 | -260.5 | -4.35 | -312.71 |
| 1.5006 | 145.91 | -146.75 | 153.97 | -154.23 | 121.78 | -117.39 |
| 3.0378 | 276.97 | -52.79 | 244.93 | -88.2 | 282.95 | 4.62 |
| 4.575 | 327.87 | -52.79 | 279.34 | -88.2 | 341.15 | 23.12 |
| 6.1122 | 275.97 | -52.79 | 244.2 | -88.2 | 282.62 | 4.94 |
| 7.6494 | 144.72 | -146.88 | 153.08 | -154.33 | 121.75 | -116.79 |
| 8.8206 | 58.58 | -306.12 | 89.7 | -260.51 | -8.92 | -311.61 |
| 9.15 | 57.95 | -363.32 | 88.82 | -298.41 | -32.52 | -379.54 |

| s | ULS B | | SLS-QP | |
|---|---|---|---|---|
| [m] | [kNm/m] | | [kNm/m] | |
| | max | min | max | min |
| 0 | -2.1 | -465.62 | -61.74 | -122.16 |
| 0.3294 | 28.79 | -382.4 | -37.89 | -99.02 |
| 1.5006 | 155.96 | -152.85 | 33.01 | -30.67 |
| 3.0378 | 341.4 | -31.11 | 89.49 | 25.81 |
| 4.575 | 413.4 | -12.61 | 108.41 | 44.73 |
| 6.1122 | 340.76 | -30.78 | 89.81 | 26.13 |
| 7.6494 | 155.83 | -152.26 | 33.71 | -29.97 |
| 8.8206 | 24.21 | -381.43 | -36.99 | -98.12 |
| 9.15 | 0.29 | -464.87 | -60.84 | -121.27 |

# Appendix D – Point load evaluation

**Method 1**

**Slab Frame Bridge (Element nr 218)**

**Mx bending moment:**

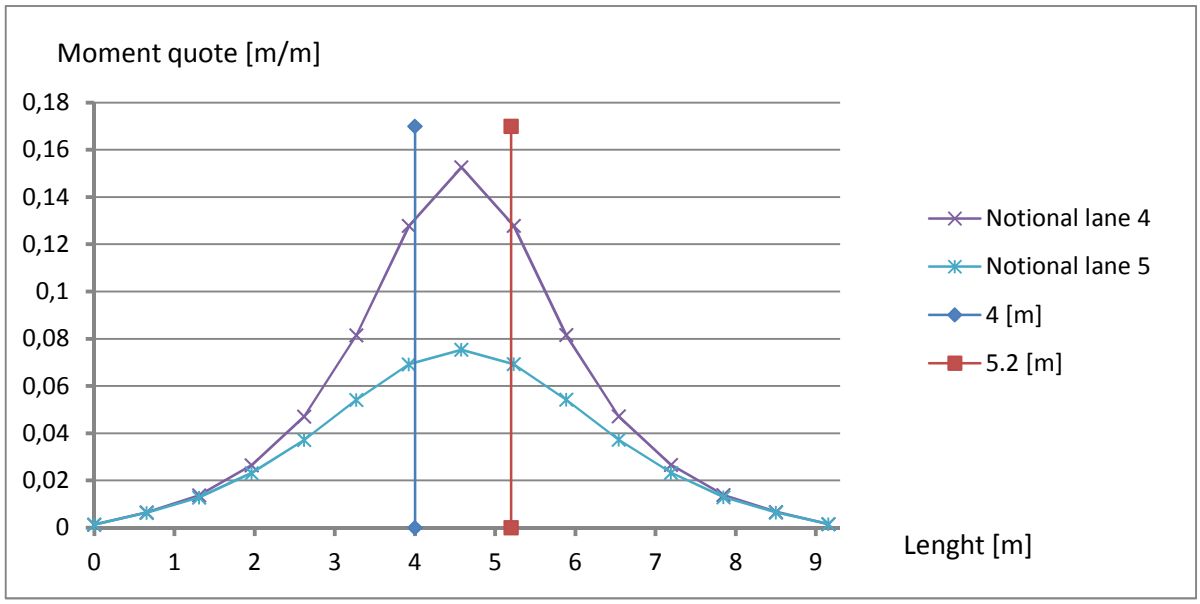


*Figure D.1 - Mx for notional lane 4 and 5 for the critical group 1 and critical load position at 4 and 5.2 m*

Notional lane 4 (from Figure D.1)

$m_{x.4} := 0.133 \frac{m}{m}$

Notional lane 5 (from Figure D.1)

$m_{x.5} := 0.07 \frac{m}{m}$

$M_{x.4} := F_1 \cdot (m_{x.4} 2) = 71.82\,kN \cdot \frac{m}{m}$

$M_{x.5} := F_2 \cdot (m_{x.5} 2) = 25.2\,kN \cdot \frac{m}{m}$

$M_{x.tot.2} := M_{x.4} + M_{x.5} = 97.02\,kN \cdot \frac{m}{m}$

**Mxy torsional moment:**

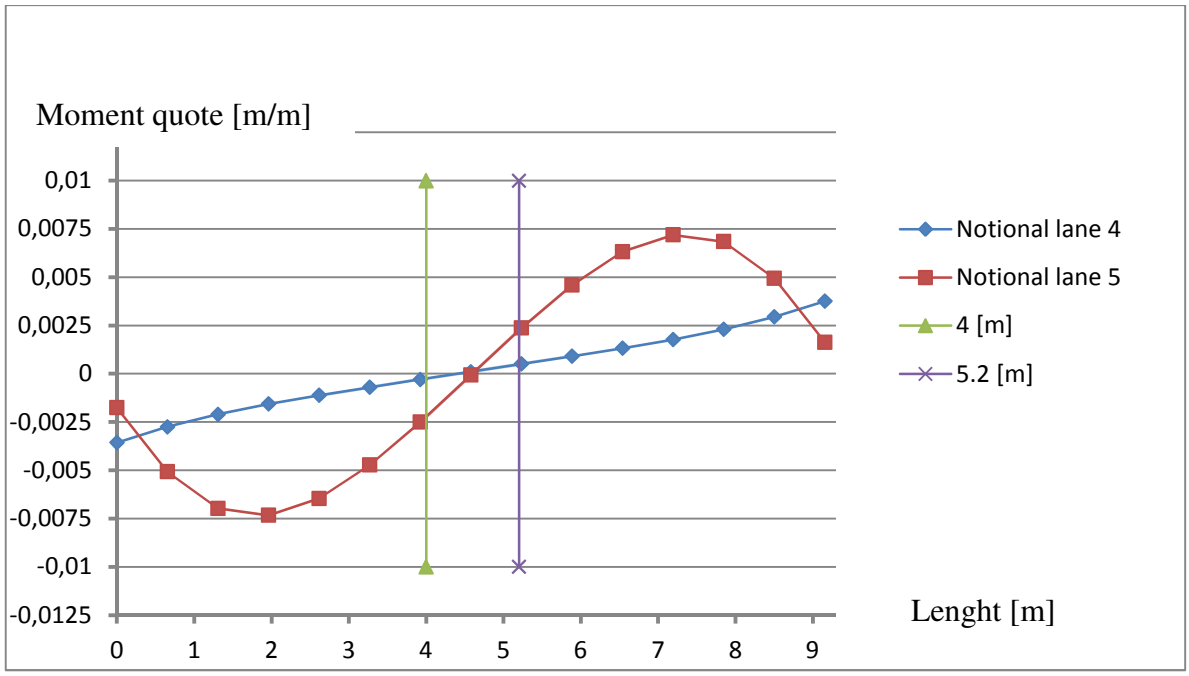


*Figure D.2 - Mxy for notional lane 4 and 5 for the critical group 1 and critical load position at 4 and 5.2 m*

Notional lane 4 (from Figure D.2)

$$m_{x.y.4.a} := 0.0025 \frac{m}{m}$$

$$m_{x.y.4.b} := 0.002 \frac{m}{m}$$

Notional lane 5 (from Figure D.2)

$$m_{x.y.5.a} := 0.00023 \frac{m}{m}$$

$$m_{x.y.5.b} := 0.0002 \frac{m}{m}$$

$$M_{x.y.4} := F_1 \cdot \left(m_{x.y.4.a} - m_{x.y.4.b}\right) = 0.135\,kN \cdot \frac{m}{m}$$

$$M_{x.y.5} := F_2 \cdot \left(m_{x.y.5.a} - m_{x.y.5.b}\right) = 5.4 \times 10^{-3} \cdot kN \cdot \frac{m}{m}$$

$$M_{x.y.tot.2} := M_{x.y.4} + M_{x.y.5} = 0.14\,kN \cdot \frac{m}{m}$$

Mx +Mxy:

$$M_{x.xy} := M_{x.tot.2} + M_{x.y.tot.2} = 97.16\,kN \cdot \frac{m}{m}$$

**Slab Frame Bridge (Element nr 245)**

**Mx bending moment:**

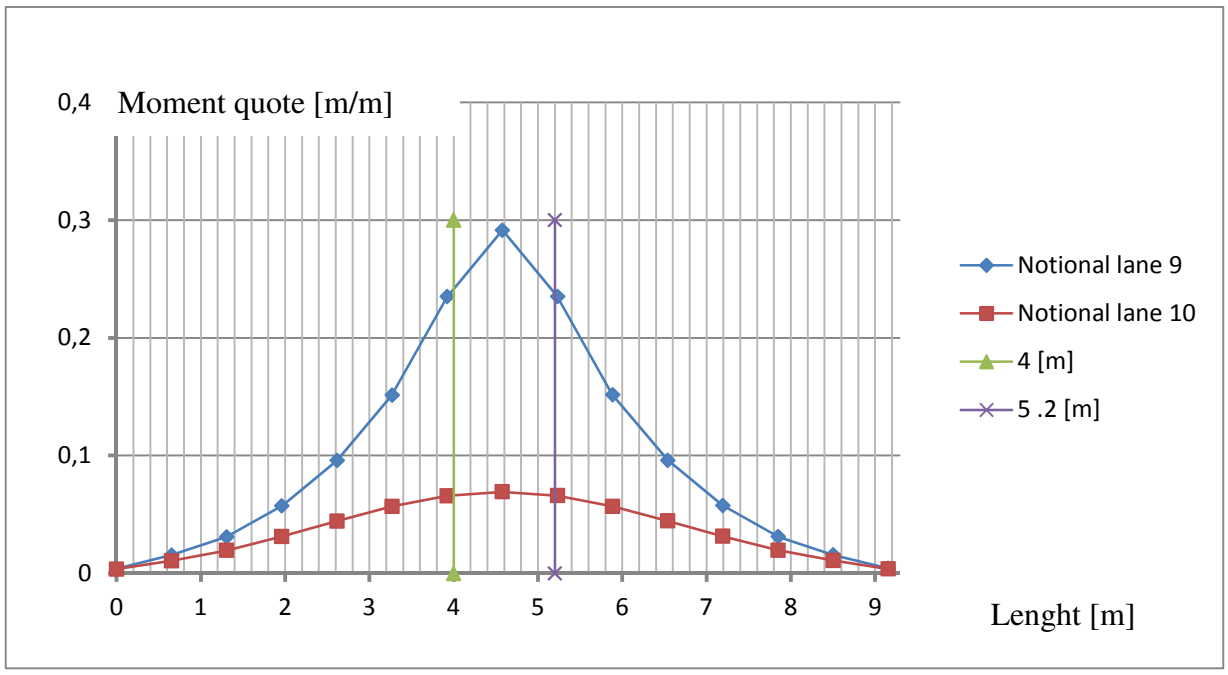


*FigureD.3 - Mx for notional lane 9 and 10 for the critical group 2 and critical load position at 4 and 5.2 m*

Notional lane 9 (from Figure D.3)

$m_{x.10.a.b} := 0.243 \frac{m}{m}$

Notional lane 10 ( from Figure D.3)

$m_{x.11.a} := 0.067 \frac{m}{m}$

$m_{x.11.b} := 0.069 \frac{m}{m}$

$M_{x.10} := F_1 \cdot \left(m_{x.10.a.b} 2\right) = 131.22 kN \cdot \frac{m}{m}$

$M_{x.11} := F_2 \cdot \left(m_{x.11.a} + m_{x.11.b}\right) = 24.48 kN \cdot \frac{m}{m}$

$M_{x.tot.1} := M_{x.10} + M_{x.11} = 155.7 kN \cdot \frac{m}{m}$

**Mxy torsional moment:**

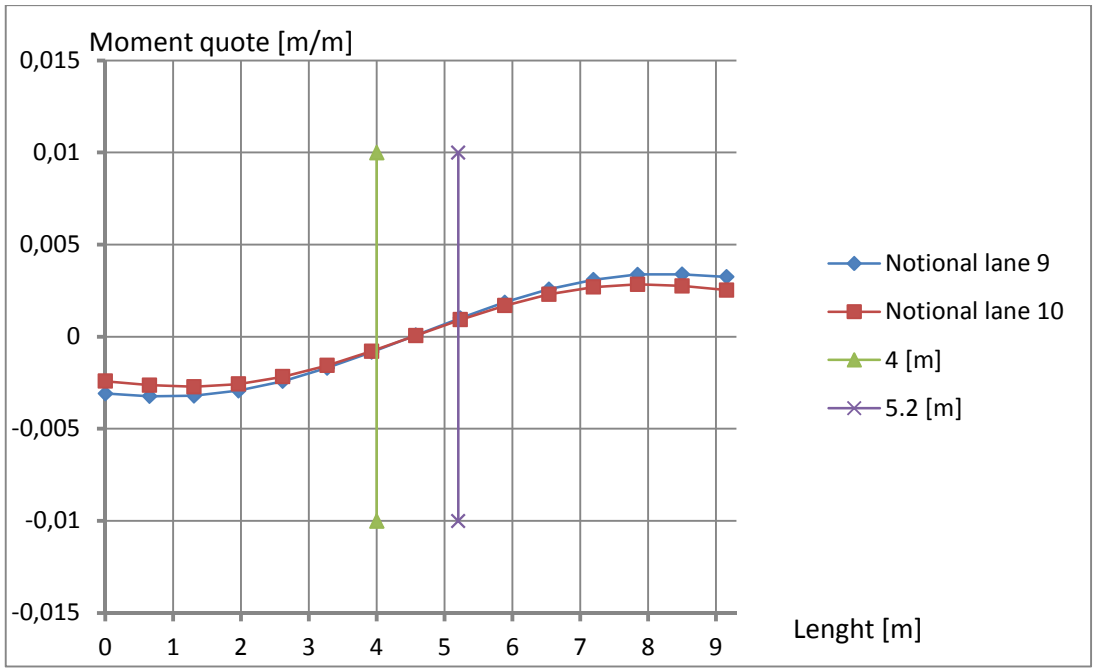


*Figure D. 4 - Mxy for notional lane 9 and 5.2 for the critical group 2 and critical load position at 4 and 5.2 m*

Notional lane 9 (from Figure D.4)

$$m_{x.y.9.a} := 0.001 \frac{m}{m}$$

$$m_{x.y.9.b} := 0.0006 \frac{m}{m}$$

Notional lane 10 ( from Figure D.4)

$$m_{x.y.10.a} := 0.001 \cdot \frac{m}{m}$$

$$m_{x.y.10.b} := 0.00006 \frac{m}{m}$$

$$M_{x.y.9} := F_1 \cdot \left(m_{x.y.9.a} - m_{x.y.9.b}\right) = 0.108\,kN \cdot \frac{m}{m}$$

$$M_{x.y.10} := F_2 \cdot \left(m_{x.y.10.a} - m_{x.y.10.b}\right) = 0.169\,kN \cdot \frac{m}{m}$$

$$M_{x.ytot.1} := M_{x.y.9} + M_{x.y.10} = 0.277\,kN \cdot \frac{m}{m}$$

Mx +Mxy:

$$M_{x.xy} := M_{x.tot.1} + M_{x.ytot.1} = 155.977\,kN \cdot \frac{m}{m}$$

**Slab Bridge (Element nr 260)**

**Mx bending moment:**

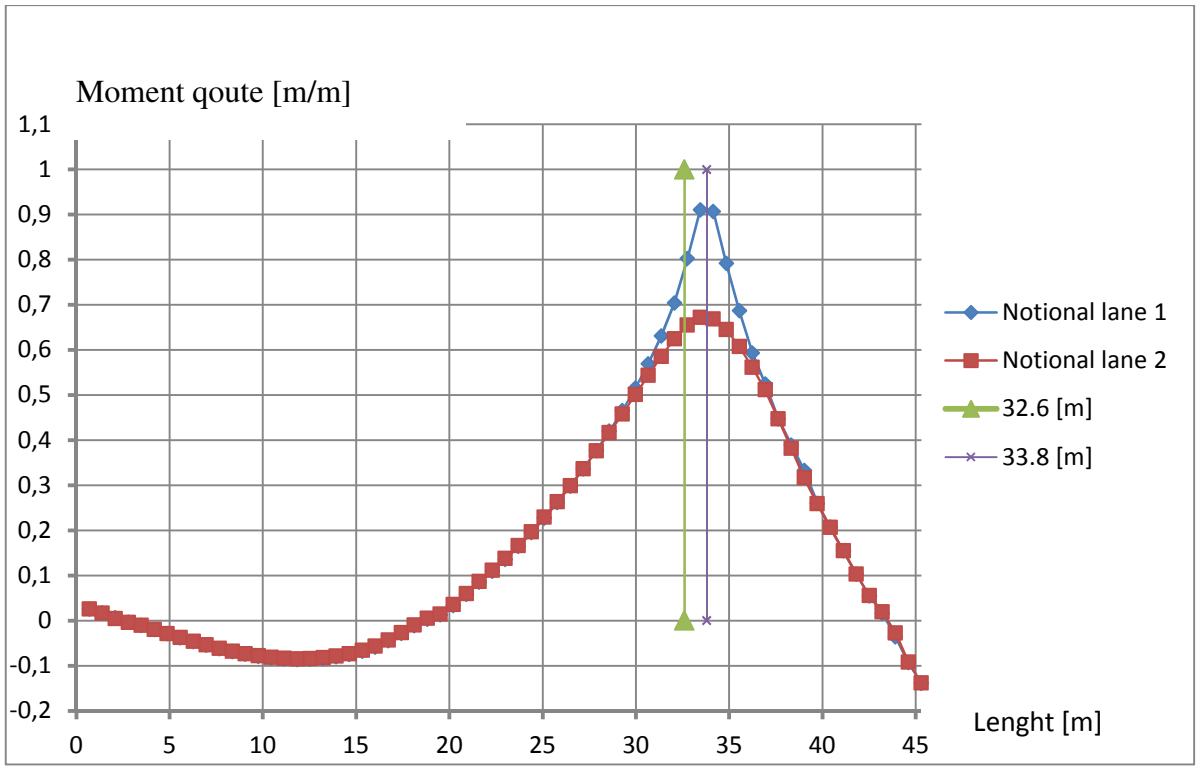


*Figure D.5 - Mx for notional lane 1 and 2 for the critical group 2 and critical load position at 32.6 and 33.8 m*

Notional lane 1 ( from Figure D.5)

$m_{x.1.a} := 0.817 \frac{m}{m}$

$m_{x.1.b} := 0.92 \frac{m}{m}$

Notional lane 2 ( from Figure D.5)

$m_{x.2.a} := 0.655 \frac{m}{m}$

$m_{x.2.b} := 0.681 \cdot \frac{m}{m}$

$M_{x.1} := F_1 \cdot (m_{x.1.a} + m_{x.1.b}) = 468.99 kN \cdot \frac{m}{m}$

$M_{x.2} := F_2 \cdot (m_{x.2.a} + m_{x.2.b}) = 240.48 kN \cdot \frac{m}{m}$

$M_{x.tot.3} := M_{x.1} + M_{x.2} = 709.47 kN \cdot \frac{m}{m}$

**Mxy torsional moment:**

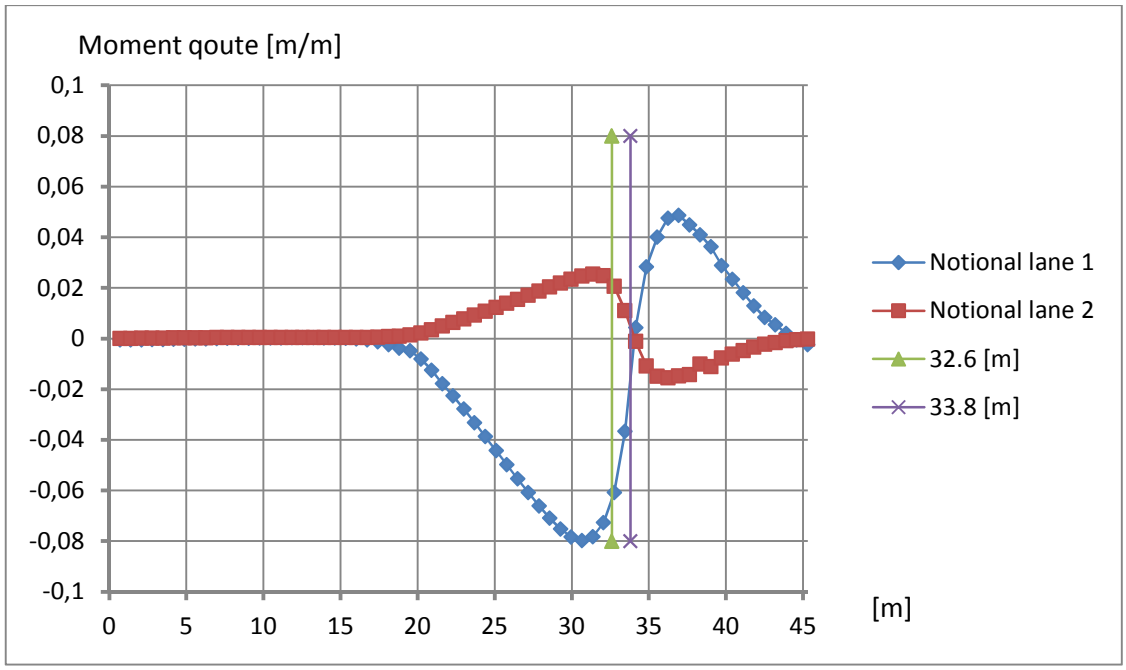


*Figure D.6 - Mxy for notional lane 1 and 2 for the critical group 2 and critical load position at 32.6 and 33.8 m*

Notional lane 1 ( from Figure D.6)

$m_{x.y.1.a} := 0.065 \frac{m}{m}$

$m_{x.y.1.b} := 0.016 \frac{m}{m}$

Notional lane 2 ( from Figure D.6)

$m_{x.y.2.a} := 0.021 \cdot \frac{m}{m}$

$m_{x.y.2.b} := 0.002 \frac{m}{m}$

$M_{x.y.1} := F_1 \cdot \left(m_{x.y.1.a} + m_{x.y.1.b}\right) = 21.87\,kN \cdot \frac{m}{m}$

$M_{x.y.2} := F_2 \cdot \left(m_{x.y.2.a} + m_{x.y.2.b}\right) = 4.14\,kN \cdot \frac{m}{m}$

$M_{x.y.tot.3} := M_{x.y.1} - M_{x.y.2} = 17.73\,kN \cdot \frac{m}{m}$

Mx +Mxy:

$M_{x.3} := M_{x.tot.3} + M_{x.y.tot.3} = 727.2\,kN \cdot \frac{m}{m}$

**Slab Bridge (element nr 388)**

**Mx bending moment:**

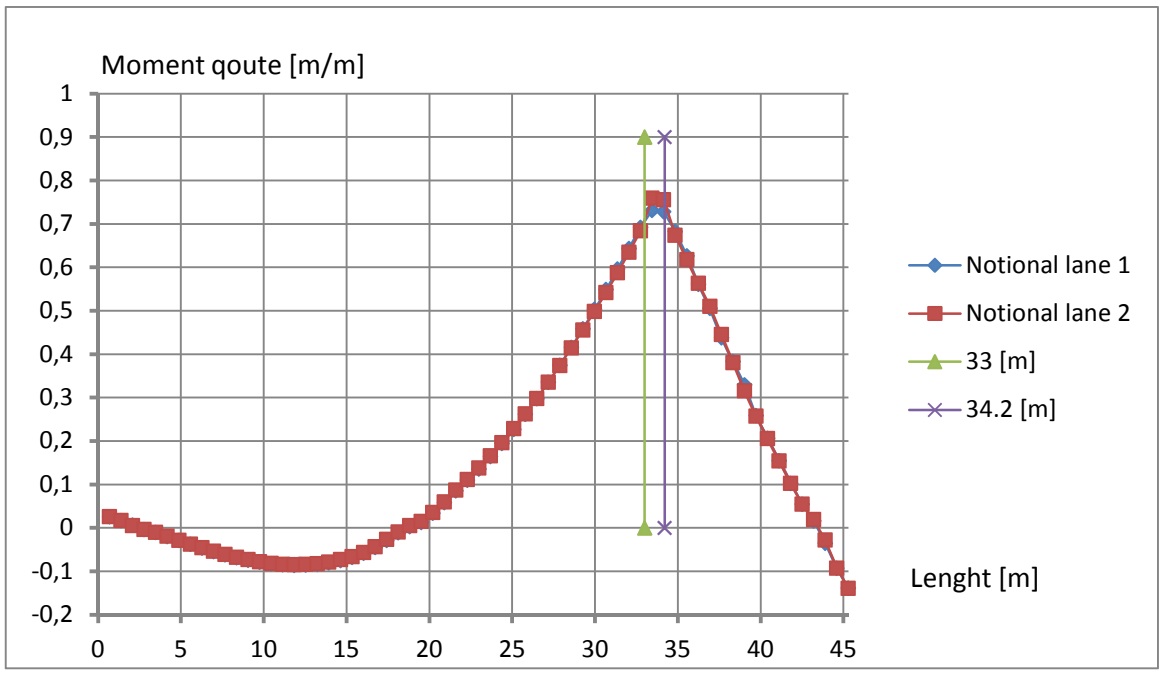


*Figure D.7 - Mx for notional lane 1 and 2 for the critical group 1 and critical load position at 33 and 34.2 m*

Notional lane 1 ( from Figure D.7)

$m_{x.1.a.4} := 0.756 \frac{m}{m}$

$m_{x.1.b.4} := 0.71 \frac{m}{m}$

Notional lane 2 ( from Figure D.7)

$m_{x.2.a.4} := 0.71 \cdot \frac{m}{m}$

$m_{x.2.b.4} := 0.724 \frac{m}{m}$

$M_{x.1.m} := F_1 \cdot (m_{x.1.a.4} + m_{x.1.b.4}) = 395.82 kN \cdot \frac{m}{m}$

$M_{x.2.m} := F_2 \cdot (m_{x.2.a.4} + m_{x.2.b.4}) = 258.12 kN \cdot \frac{m}{m}$

$M_{x.tot.4} := M_{x.1.m} + M_{x.2.m} = 653.94 kN \cdot \frac{m}{m}$

**Mxy torsional moment:**

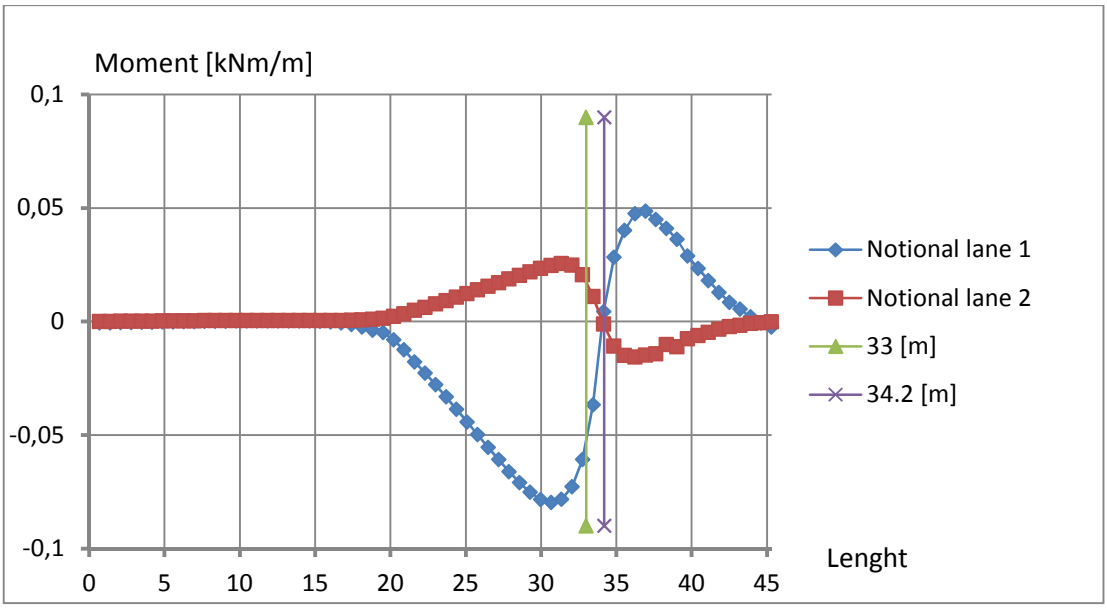


*Figure D.8 - Mx for notional lane 1 and 2 for the critical group 2 and critical load position at 33 and 34.2 m*

Notional lane 1 ( from Figure D.8)

$m_{x.y.1.a.4} := 0.018 \frac{m}{m}$

$m_{x.y.1.b.4} := 0.002 \frac{m}{m}$

Notional lane 2 ( from Figure D.8)

$m_{x.y.2.a.4} := 0.055 \frac{m}{m}$

$m_{x.y.2.b.4} := 0.0 \frac{m}{m}$

$M_{x.y.2.4} := F_2 \cdot \left(m_{x.y.2.a.4} + m_{x.y.2.b.4}\right) = 9.9 \, kN \cdot \frac{m}{m}$

$M_{x.y.tot.4} := M_{x.y.1.4} + M_{x.y.2.4} = 5.58 \, kN \cdot \frac{m}{m}$

**Mx +Mxy:**

$M_{x.y.1.4} := -F_1 \cdot \left(m_{x.y.1.a.4} - m_{x.y.1.b.4}\right) = -4.32 \, kN \cdot \frac{m}{m}$

$M_{x..4} := M_{x.tot.4} + M_{x.y.tot.4} = 659.52 \, kN \cdot \frac{m}{m}$

**Method 2**

**Slab Frame Bridge (Element nr 245)**

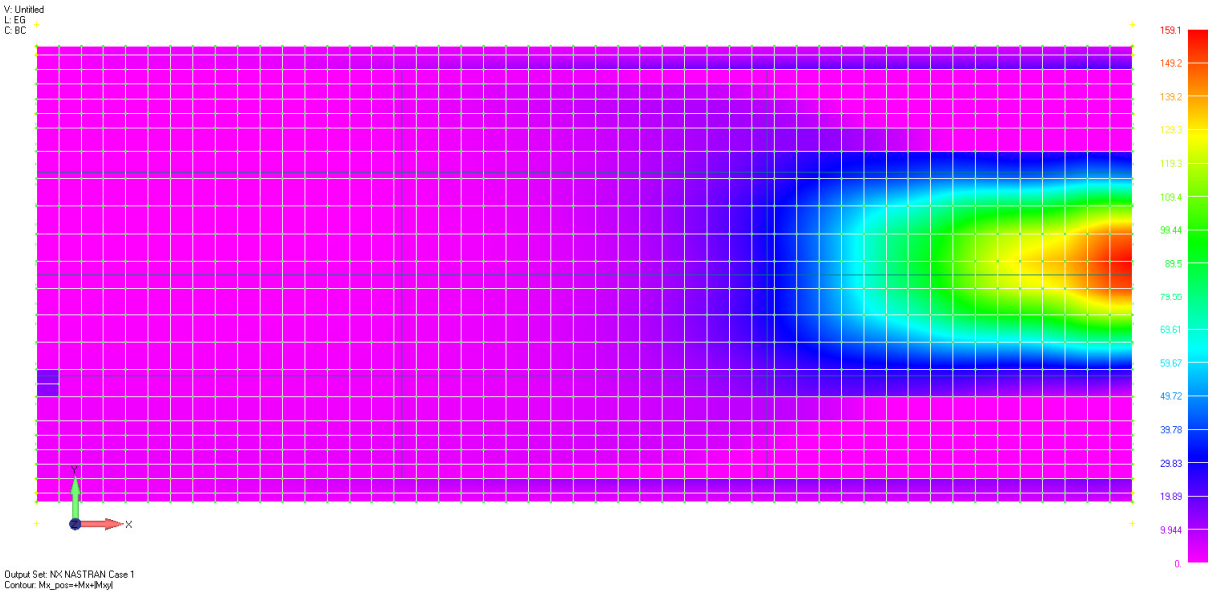


*Figure D.9 - Element nr 245 is critical with 159.1 [kNm/m]*

**Slab Frame Bridge (Element nr 218)**

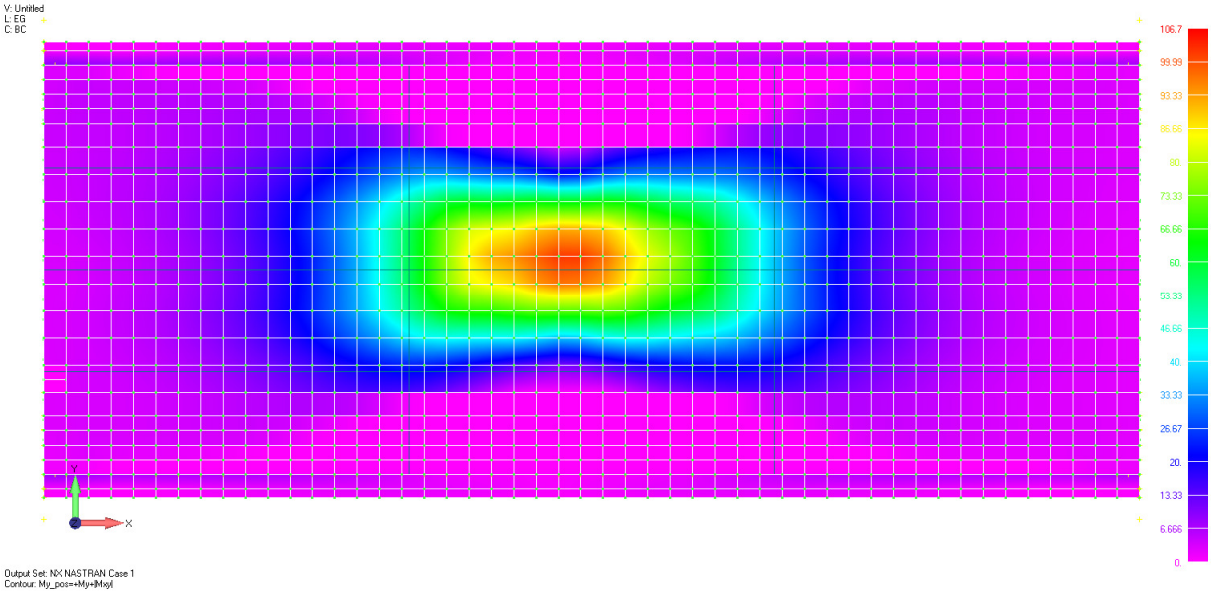


*Figure D.10 – Element nr 218 is critical with 96.2 [kNm/m]*

**Slab Bridge (Element nr 388)**

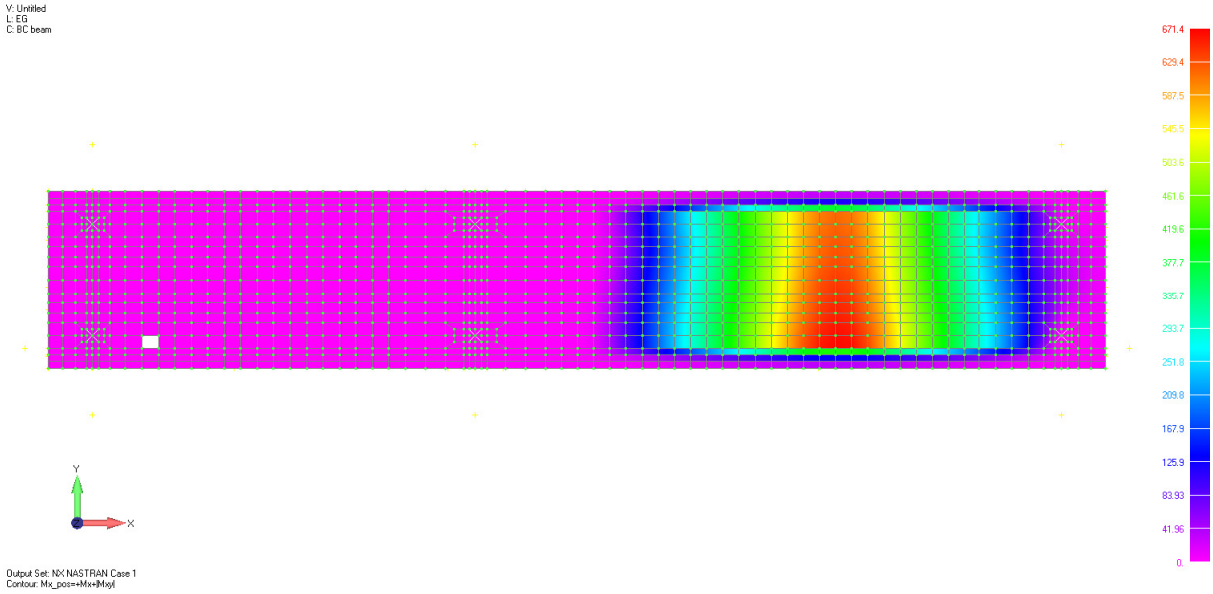


*Figure D.11 – Element nr 245 is critical with 643 [kNm/m]*

**Slab Bridge (Element nr 260)**

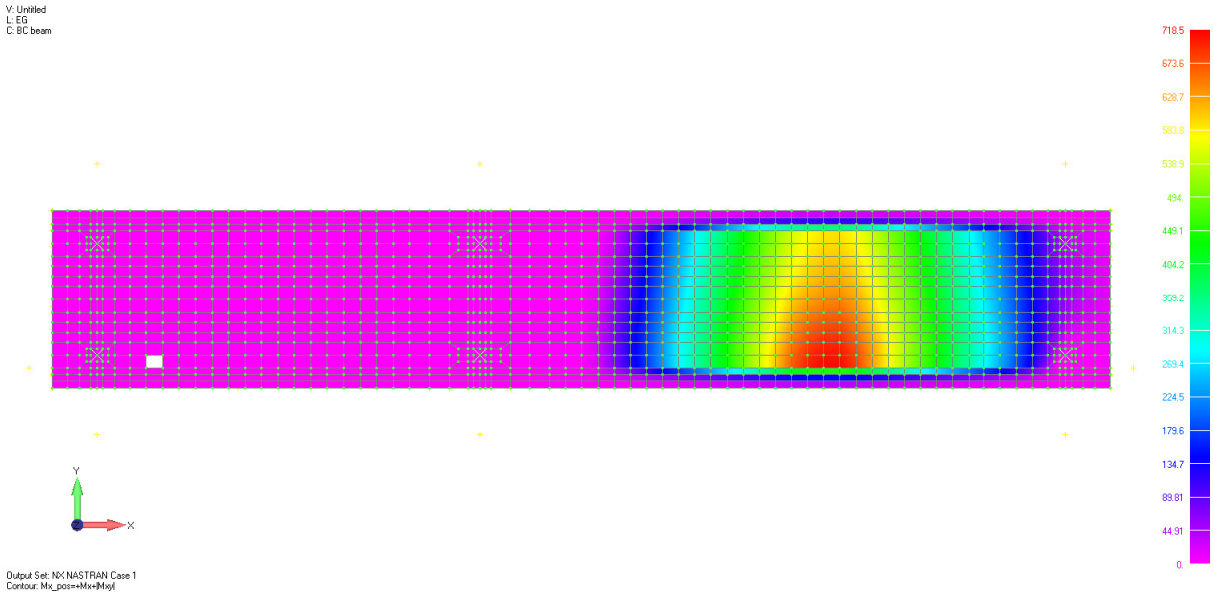


*Figure D.12 – Element nr 245 is critical with 718.5 [kNm/m]*

# Appendix E – Input for 2D frame analysis

# Slab bridge

The 2D frame model is modeled with the same material data as the 3D shell model see chapter 3.1

s= Element length

f= Distance from central line from lower edge

H=Height

K= Konstant (10)

I= Second moment of inertia

A= Area

Element 102

| s | f | H | K*I | K*A |
|---|---|---|---|---|
| m | m | m | m | m |
| 0 | -0.596 | 1.192 | 1.411 | 11.92 |
| 1.9 | -0.596 | 1.192 | 1.411 | 11.92 |

Element 203

| s | f | H | K*I | K*A |
|---|---|---|---|---|
| m | m | m | m | m |
| 0 | -0.596 | 1.192 | 1.411 | 11.92 |
| 13.9 | -0.596 | 1.192 | 1.411 | 11.92 |
| 15.9 | -0.796 | 1.592 | 3.362 | 15.92 |
| 16.4 | -0.796 | 1.592 | 3.362 | 15.92 |

Element 304

| s | f | H | K*I | K*A |
|---|---|---|---|---|
| m | m | m | m | m |
| 0 | -0.796 | 1.592 | 3.362 | 15.92 |
| 0.5 | -0.796 | 1.592 | 3.362 | 15.92 |
| 2.5 | -0.596 | 1.192 | 1.411 | 11.92 |
| 25.1 | -0.596 | 1.192 | 1.411 | 11.92 |

Element 405

| s | f | H | K*I | K*A |
|---|---|---|---|---|
| m | m | m | m | m |
| 0 | -0.596 | 1.192 | 1.411 | 11.92 |
| 2 | -0.596 | 1.192 | 1.411 | 11.92 |

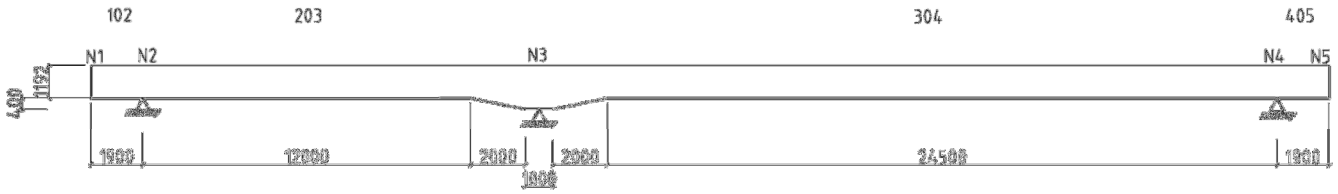


*Figure E.1 - Beam model used in the 2D analyses for the slab bridge.*

# Frame slab Bridge

The 2D frame model is modeled with the same material data as the 3D shell model see chapter 3.2

| Punkt | Y | Z |
|---|---|---|
| 1 | 0 | 5.46 |
| 2 | 9.8 | 5.46 |
| 30 | 0 | 0 |
| 40 | 9.8 | 0 |
| 31 | 1.633 | 0 |
| 32 | 3.267 | 0 |
| 33 | 4.9 | 0 |
| 34 | 6.533 | 0 |
| 35 | 9.8 | 0 |

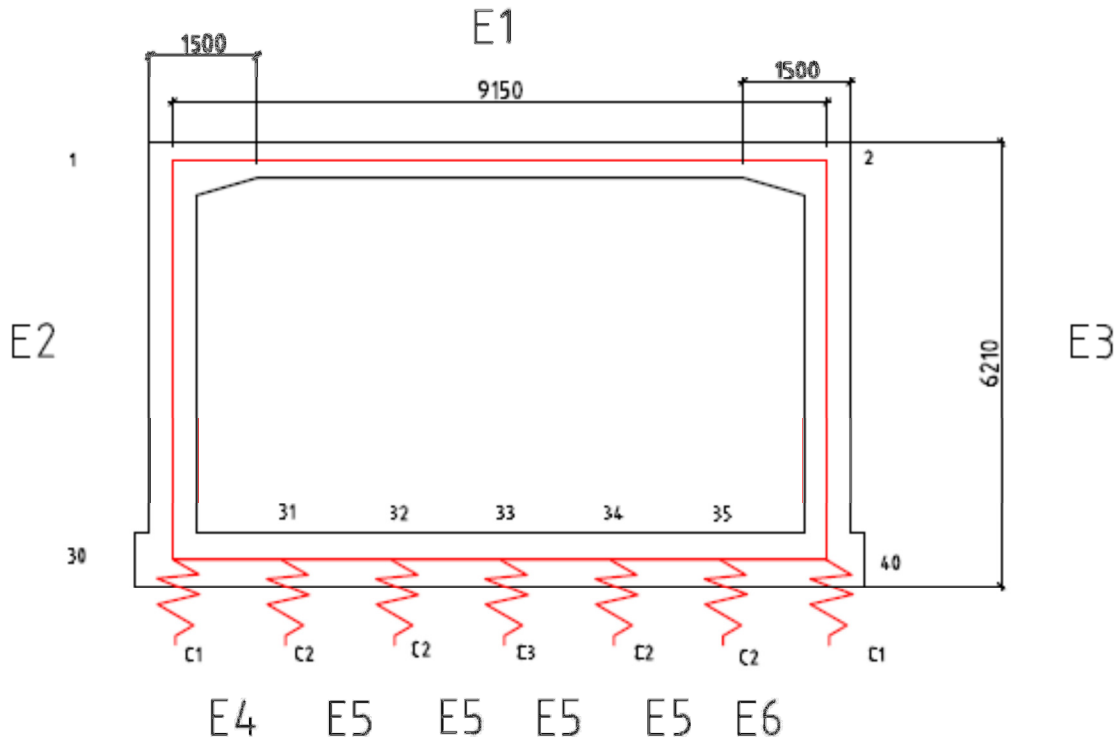


*Figure.E.2 - Beam model used in the 2D analyses for the frame slab bridge*

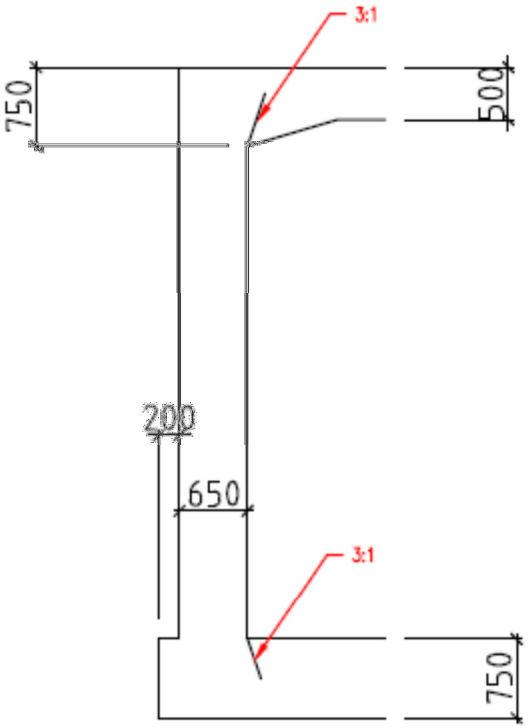


*Figure.E.3 - Adjusting with for the frame slabwale*

s= Element length

f= Distance from central line from lower edge

H=Height

K= Konstant (10)

I= Second moment of inertia

A= Area

Element 1

| s | f | H | K*I | K*A |
|---|---|---|---|---|
| m | m | m | m | m |
| 0 | -0.375 | 0.75 | 0.352 | 7.5 |
| 1.5 | -0.25 | 0.5 | 0.104 | 5 |
| 8.3 | -0.25 | 0.5 | 0.104 | 5 |
| 9.8 | -0.375 | 0.75 | 0.352 | 7.5 |

Element 2

| s | f | H | K*I | K*A |
|---|---|---|---|---|
| m | m | m | m | m |
| 0 | -0.167 | 0.983 | 0.7925 | 9.83 |
| 0.5 | 0 | 0.65 | 0.229 | 6.5 |
| 5.085 | 0 | 0.65 | 0.229 | 6.5 |
| 5.46 | -0.125 | 0.775 | 0.388 | 0.75 |

Element 3

| s | f | H | K*I | K*A |
|---|---|---|---|---|
| m | m | m | m | m |
| 0 | -0.167 | 0.983 | 0.7925 | 9.83 |
| 0.5 | 0 | 0.65 | 0.229 | 6.5 |
| 5.085 | 0 | 0.65 | 0.229 | 6.5 |
| 5.46 | -0.125 | 0.775 | 0.388 | 0.75 |

Element 4

| s | f | H | K*I | K*A |
|---|---|---|---|---|
| m | m | m | m | m |
| 0 | 0.108 | 0.858 | 0.527 | 8.58 |
| 0.325 | 0 | 0.75 | 0.352 | 7.5 |
| 1.633 | 0 | 0.75 | 0.352 | 7.5 |

Element 5

| s | f | H | K*I | K*A |
|---|---|---|---|---|
| m | m | m | m | m |
| 0 | 0 | 0.75 | 0.352 | 7.5 |
| 1.633 | 0 | 0.75 | 0.352 | 7.5 |

Element 6

| s | f | H | K*I | K*A |
|---|---|---|---|---|
| m | m | m | m | m |
| 0 | 0 | 0.75 | 0.352 | 7.5 |
| 1.308 | 0 | 0.75 | 0.352 | 7.5 |
| 1.633 | 0.108 | 0.858 | 0.527 | 8.58 |

# Appendix F - Drawings of slab- and slab frame bridge

# Appendix G - Calculation of reinforcement amount

# Space for picture

Replace this square with a picture illustrating the content of the report. This picture should be “floating over the text”, in order not to change the position of the title below (clic on Format: Object: Layout, and chose “In front of text”)

## Instructions for use of this template

Replace the yellow marked text with your own title, name etc on the first nine pages. Replace only the text and not the return-signs, comment marks [mp1] etc. Update all field in the document by choosing Edit: Select All (Ctrl A) and then clicking the F9-button. (The footers need to be marked separately and updated with the F9-button.) Write your report using the formats and according to the instructions in this template. When it is completed, update the table of contents.

The report is intended to be printed double-sided.

]